Faculty of Engineering

Department of Civil Engineering

The Tensile Stiffness of a Novel Anchored Blind-bolt Component for Moment-resisting Connections to Concrete-filled Hollow Sections

by

Theodoros Pitrakkos

A thesis submitted to the University of Nottingham

for the degree of Doctor of Philosophy

June 2012

Materials, Mechanics and Structures Division

Centre for Structural Engineering and Construction (CSEC) Group

Abstract

The use of hollow section columns in steel construction is presently hindered by the lack of adequate connection technologies. Due to access constraints, standard bolting techniques are difficult to achieve, if not impossible without welding. As an alternative to welding, blind-bolting techniques were developed to provide desirable bolted configurations, allowing hollow column frames to be erected in the same way as open profile column frames. But the current blind-bolting techniques are restricted to the construction of simple connections because of their difficulties in achieving sufficient tensile stiffness.

More recently, a novel anchored blind-bolt, labelled the Extended Hollo-bolt (*EHB*), has been developed at the University of Nottingham; as a modification of the standard Hollo-bolt. For the proposed connection technology, its potential in providing moment-resistance has been assessed successfully. However, the existing data related to the performance of this novel connector in tension is insufficient to permit its design. This work investigates the performance of the *EHB* blind-bolt under tension loading and focuses on determining, and modelling the stiffness of this novel technology in such a way to enable its application within the component method approach.

An extensive experimental programme was devised to collect sufficient component characteristic data to enable the development of an *EHB* component model. This covered data deals with the overall response of the connector and the individual responses of its contributing elements. A total of 51 experimental pull-out tests and 20 pre-load tests have been performed.

The force-displacement behaviour of the investigated joint component was determined under monotonic pull-out testing, where remote video gauge techniques have been adopted to capture the full non-linear response of the component, alongside traditional techniques to confirm the reliability of the data. The test matrix varies the grade and size of the component's internal bolt, the strength of concrete, and the depth of its mechanical anchorage. From the pull-out tests it was identified that the *EHB* component can ultimately develop the full

tensile capacity of its internal bolt. This ultimate failure mode is confirmed for the range of parameters that was covered in this study. Increasing concrete strength had the most enhancing effect on the response of the component.

A secondary programme was related to the measurement of pre-load that is induced in the internal bolt of the *EHB* component at its tightening stage; where pre-load was monitored over a five day period. The test matrix varies the grade and size of its internal bolt, and also considers various bolt batches. It was concluded that the relative level of component pre-load to ultimate strength increased only in the case where higher bolt grades were used.

To model the tension behaviour of the *EHB* component, a mechanical model was developed that is based on an assembly of the component's different sources of deformation. The component model employs idealised springs with tetra-linear characteristics for the elongation of its internal bolt element, and springs with tri-linear characteristics for the slip of its expanding sleeves and mechanical anchorage elements. By comparing the predictions of the component model with relevant experimental data, the component model has been shown to be capable of describing the *EHB* component response with reasonable accuracy; capturing its tensile stiffness and its yielding trend. The accuracy of the component model has also been assessed in exclusion of pre-load effects. It was found that if the level of pre-load is excluded from the assembly process, this can have highly undesirable effects on the predictions of the component's response. The findings of the supplementary pre-load testing programme assisted greatly in the accuracy of the component model by providing the necessary levels of pre-load.

The proposed component model has demonstrated that the behaviour of the *EHB* component can be modelled by the component method approach; by employing idealised models for the behaviour of its contributing elements. The validated component model is considered to simulate the tension behaviour of the novel anchored blind-bolt with sufficient fidelity that it can be considered as a benchmark for further studies.

List of Contents

List of Tables

List of Figures

List of Notation

Roman symbols

d_3	minor diameter of external thread
d_b	bolt (or bar) diameter
d_{emb}	embedded depth or effective embedment
d_h	major end anchor head diameter
f_c'	cylinder compressive strength of concrete
f_{cu}	concrete compressive strength measured on cubes
$f_{cu\ ,\ 28\ days}$	28-day concrete compressive strength measured on cubes
f_{ub}	ultimate stress
f_y	specified yield strength
f_{yb}	yield stress
k	stiffness
k_b	stiffness related to bolt elongation element in *EHB* component
k^e	initial elastic stiffness
k_{EHB}	stiffness of individual *EHB* component
k_{HB}	stiffness related to expanding sleeves element in *EHB* component
k_i	component stiffness coefficient
k_M	stiffness related to mechanical anchorage and bond element in *EHB* component
k_{nc}	factor of 15.5 for cast-in situ headed anchor bolts
$k_{norm}{}^e$	normalised initial stiffness of element (or mechanism)
k^p	post-limit stiffness
k_x^e	initial stiffness of element (or mechanism)
k_x^p	post-limit stiffness of element (or mechanism)
k_x^u	ultimate stiffness of element (or mechanism)
l_{dt}	development length in tension of headed deformed bars
t_{bh}	thickness of hexagon bolt head
t_h	thickness of circular or square shaped end anchor head
t_{HBc}	depth of the *HB* (or *EHB*) cone
t_n	thickness of metric hexagon nut
z	lever arm

Capital roman symbols

A_b	bolt (or bar) area based on d_b
A_{brg}	net bearing area of the anchor head
A_{emb}	embedded surface area
A_g	gross bearing area
A_s	effective cross sectional area
$A_{s,net}$	net tensile stress area
$A_{s,nom}$	nominal tensile stress area
E	Young's modulus of elasticity
E_b	Young's modulus of elasticity (tension bolt model)
F	tensile Force
F_p	pre-load
$F_{p,\ 2h}$	pre-load (after 2 hours in tightening)
$F_{p,\ ini}$	initial pre-load
$F_{p,\ res}$	residual pre-load
$F_{Rd\ i}$	component resistance
$F_{test,\ max}$	maximum force achieved in correspondent pull-out test
F^u	component ultimate capacity
F^y	component yield capacity
H	thickness of the collar of the *HB* (or *EHB*) blind-bolt
K	nut factor (dimensionless)
L	length of bolt shank
L_b	effective length (or bolt elongation length)
M	moment
M_p	beam plastic moment capacity
M_{Rd}	joint resistance
N	axial load (or number of specimens)
N_{cb}	nominal concrete breakout strength in tension of a single anchor
N_{pn}	nominal pullout strength in tension of a single anchor
N_{sa}	nominal strength of a single anchor in tension as governed by the steel strength
P	pull-out strength
$P_{(ACI)}$	pull-out strength for cracked concrete (using f_c')
$P_{(CEN)}$	pull-out strength for cracked concrete (using f_{cu})
$P_{predicted}$	predicted pull-out strength of type *M* (modified equation)
P_{test}	experimental pull-out strength of type *M* (at δ_{slip}=0.3mm)
R^2	coefficient of determination
R_m	tensile strength

$R_{p0,2}$	stress at 0.2% non-proportional elongation
$S_{j,ini}$	joint initial stiffness
T	tightening torque
V	shear load
W	clamping thickness

Greek symbols

δ	displacement (or deformation)
δ_b	bolt elongation
δ_{Cd}	deformation capacity
δ_{global}	global displacement
δ_{slip}	slip
ε	strain
ε_p	pre-strain in the bolt
ε_{yb}	yield strain
λ	component ductility index
λ_{Actual}	experimental ultimate *EHB* component ductility index
λ_{Model}	*EHB* component model ductility index
μ	mean value
μ^p	strain hardening coefficient for post-limit stiffness
μ^u	strain hardening coefficient for ultimate stiffness
σ	stress (or standard deviation)
σ_p	pre-stress in the bolt
τ	bond stress
ϕ	rotation
ϕ_{cd}	rotation capacity of joints
ϕ_{Ed}	design rotation capacity
$\psi_{c,P}$	modification factor
ψ_e	development length modification factor based on reinforcement coating

Capital Greek symbols

Δ^u	component collapse displacement
Δ^y	component yield displacement

Abbreviations

ACI	American Concrete Institute
CCD	Concrete Capacity Design
CI	Confidence Interval
EC3	Eurocode Design Code 3
EHB	Extended Hollo-bolt
HB	Hollo-bolt
LC	Load cell
RC	Reinforced Concrete
RHS	Rectangular Hollow Section
RMH	Reverse Mechanism Hollo-bolt
SHS	Square Hollow Section
VG	Video Gauge

Trademarks

Hollo-bolt is a trademark of Lindapter International, UK.

Video Gauge is a trademark of Imetrum Limited, UK.

Acknowledgements

I would like to express profound gratitude to my advisor, Dr Walid Tizani, for his invaluable support, guidance, supervision and enthusiasm throughout this research work.

The assistance provided in the laboratory to carry out the experimental work is gratefully acknowledged. Specifically, I wish to acknowledge the following members of staff: Gordon Hardy, the Director of Facilities, Michael Langford, the chief technician, Balbir Loyla, Damien Goy, Jim Bellis, Nigel Rook, and Thomas Buss, the technicians of the laboratory.

I would like to express my thanks towards the sponsors of this project, the Engineering and Physical Sciences Research Council (EPSRC).

The author is also thankful for the support of TATA Steel (previously Corus Tubes) and Lindapter International. Profound gratitude is expressed to the following individuals: Trevor Mustard and Andrew Orton, of TATA Steel, and Neil Gill, of Lindapter International.

On a more personal note, I would like to thank my father, Pantelis Pitrakkos, for providing moral support throughout the duration of this project.

Declaration

I hereby declare that, except where specific reference has been made to the work of others, I am the sole author of this thesis. The work presented herein was performed at the University of Nottingham, under the direction of my supervisor, between October 2008 and June 2012. This thesis has not been submitted to any institution other than the University of Nottingham, in consideration for the degree of Doctor of Philosophy.

Theodoros Pitrakkos, MEng

1 Introduction

The majority of structures which incorporate a steelwork frame usually consist of open section profiles for both the beam and column members. The dominance of the profile as a beam member results from the favourable disposition of the section's mass to the extreme fibres of the beam which is suited to developing efficient bending resistance. On the other hand, an open profile column which is subject to compression, due to its asymmetrical properties, a buckling failure is exhibited about its minor axis. For this reason, it is generally accepted that hollow section columns are structurally more efficient when compared to the equivalent open profile due to their symmetrical properties. Hollow sections can achieve a constant external dimension for all weights of a given size, which enables them to achieve standardisation of architectural and structural details. Although many advantages have been reported of the combination of an open section beam connected to a hollow section column, one of the remaining areas of difficulty regarding the use of structural hollow sections is that of bolting to the face of the section; to tighten a standard bolt and nut is difficult, if not impossible.

Over the years, various alternatives have been used for connections to hollow sections. Current practice usually involves the welding of fittings to the column to provide adequate access for site bolting (Figure 1.1). On occasions, the beam has been seen to be directly site welded to the column face. However, there is a reluctance to utilise welding due to the cost implications involved, as well as the concerns over the actual making and inspection of the weld. Consequently, structural hollow sections are not used as extensively as they should. Since the popularity of steel framed buildings is partly attributed to the ease with which steel members can be pre-fabricated and erected, the use of hollow sections as columns will not be as popular as open sections until a method is developed that allows hollow column frames to be erected in the same way as open profile frames.

Modern advances in bolting technology have developed a system that overcomes the complexities involved in the construction of connections between open and hollow sections; blind-bolting systems. The term blind relates to the ability of

forming a connection with a fastener which can be tightened from one side only. Commercially available examples of blind-bolting technology include the Flow-drill, the Huck (HSBB & BOM), the AJAX one-side, and the Lindapter Hollo-bolt. Hence an alternative to welding has been established, but the performance of blind-bolting systems in comparison with that of standard bolting is in question. At present, the use of blind-bolt systems is restricted to shear-resisting joints (SCI/BCSA 2002) whereas rigid behaviour may be achieved by fully welded connections (CEN 2005).

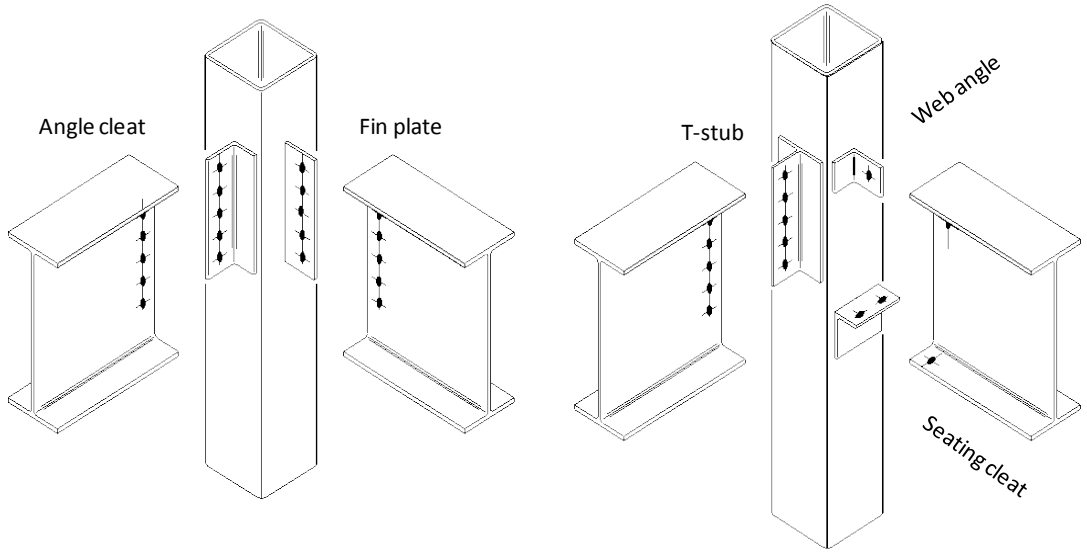

Figure 1.1 Current methods of connections between open and hollow sections

Research conducted in the field of composite structural steelwork connections at the University of Nottingham has identified a blind-fastened configuration that may resist the predominant tensile loads expected in moment-resisting construction. The configuration involves a fastener labelled the Extended Hollo-bolt (*EHB*), which was developed as an experimental modification of the commercially available Lindapter Hollo-bolt (*HB*). The *EHB* blind-bolt is designed specifically for use in connections to concrete-filled hollow sections and its potential in moment-resistance has been assessed successfully (Al-Mughairi et al. 2009). However, the available data is insufficient to permit design of the proposed connection.

Current state-of-the-art models for steel and composite joints are based on the component method. With the aim of extending the principles of the component method for this novel connection, it is found that application rules are not available for two basic components. These components relate to: (1) the behaviour of the connector in tension, and (2) the bending resistance of the tube face on which the connection is established. Having determined the response for both of these components, this will allow for the development of a mechanical model to predict the moment-rotation characteristics for the proposed connection technology. It is the purpose of this thesis to focus on the tension behaviour of the novel connector.

1.1 Justification of ongoing research

Blind-bolts have been developed to provide construction-efficient bolted connections between open and hollow section members. Up to date there is no viable bolted moment-resisting configuration for joints between open and hollow sections. The development of a blind-bolted moment-resisting connection can certainly promote the use of hollow sections as columns in multi-storey steel construction. Such connections will offer many advantages, from the execution point of view, and the ease of design. Structural advantages will arise in the design as lateral stability may be provided by means of moment connections, thus eliminating the current needs for structural bracing and various forms of welding. Consequently, a cost effective solution to current practice should result.

1.2 Aim & objectives

The aim of this research is to investigate, whether the response of a salient component, of a moment-resisting blind-bolted connection, can be modelled in such a way, to allow the component to be used in the characterisation of such structural joints within the context of the component method. This component is labelled as the “Bolts (*EHB*) in tension”.

The hypothesis of the thesis is that the tension behaviour of the investigative joint component can be modelled, on the basis of an assembly of the response of the

individual mechanisms (or elements) that contribute to its overall deformability curve.

The objectives of the research are:

- Evaluate the load transfer mechanism of the *EHB* component.
- Determine the full non-linear, tension force-displacement response of the *EHB* component in consideration of the principal parameters affecting the response; namely, internal bolt grade, concrete infill strength, embedded depth of mechanical anchorage, and internal bolt diameter size.
- Determine the force-displacement relationships of the individual mechanisms (or elements) that contribute to the deformability of the *EHB* component, in consideration of the main parameters affecting their behaviour.
- Propose a model for the tension behaviour of the *EHB* component that is based on an assembly of the response of its individual mechanisms (or elements), in view of predicting the component's strength, stiffness, and ductility.
- Evaluate the proposed model and compare its predictions with experimental data.

1.3 Objectives and methodology

A review of existing knowledge in the field of structural steelwork connections directed the project towards an experimentally based investigation. Extensive experimental work was employed in this research programme as a method of evaluating and quantifying the tensile behaviour of the *EHB* component and that of its individual elements. Due to the novelty involved in the investigative component, in terms of its structural system and unique geometry, an experimental programme was required to quantify its response.

A review of literature related to similar structural systems with the *EHB* anchored blind-bolt component allowed for the identification of the primary parameters that may affect the tension behaviour of the component. Similarly, an experimental plan was devised as a method of measuring the effects on the tensile response of the component and its elements when a variation in parameters is considered.

Mechanical modelling and basic spring theory was used in this project as a method of modelling the tension behaviour of the *EHB* component. A semi-empirical mechanical model was developed, with springs of linear characteristics, whose assembly predictions were evaluated with experimental data that was obtained throughout this research work.

To satisfy the objectives of the research, the relevant literature and current state-of-the-art models for steel joints were reviewed. These models are based on the so-called "component method", which is widely recognised now as a general procedure for joint characterisation in the scientific community and in the European design codes. Although full-scale experimental testing is naturally the most reliable method to describe, and study accordingly the rotational behaviour of joints, it is time consuming, expensive, and cannot be considered as a design tool. Due to the complex interaction between the investigative joint components, a component based approach is essential towards the first development of design rules for the proposed connection. For these reasons, a component based approach has been adopted in this investigation. It is revealed that one of the limiting factors in extending the principles of the component method for the proposed connection technology is the unknown tensile behaviour of the fastener. It is the purpose of this work to investigate this unknown behaviour at a component level of sophistication. To evaluate the behaviour of the *EHB* component, the component is decomposed into individual mechanisms (or elements) to identify the mechanics that contribute to its deformability curve. The approach of this study will thus contribute to the research community and design field of moment-resisting joints utilising blind-bolted connections to structural hollow sections.

1.4 Thesis structure

The literature review of this thesis is found in Chapter 2. The aim of the Chapter is to review the current knowledge in order to conclude on the area in which a lack of knowledge exists, which in turn will lead to the research proposals of this study. The review commences with the basics of this research field. The mechanism of the Lindapter Hollo-bolt (*HB*) is presented, and existing knowledge with regard to its

performance is reviewed. A historical overview of research at the University of Nottingham is summarised to demonstrate how the ongoing research reached the development of the Extended Hollo-bolt (*EHB*) blind-bolt. The principles of the component method are outlined, and an assessment of extending the method for blind-bolted (*EHB*) connections between open and concrete filled rectangular hollow sections is reported.

It is the purpose of Chapter 3 to conclude on the research methodology in order to carry out quantitative analysis of the joint component that is under investigation. To understand the mechanics of the *EHB* anchored blind-bolt component, in Chapter 3, the component is decomposed into its individual mechanisms and focus is given to relevant publications. Due to the similarities in behaviour, literature related to the bond and anchorage of concrete steel reinforcement is reviewed. The key parameters that may affect the response of the *EHB* component are identified, and sufficient information is collected to devise an adequate testing programme to evaluate the component. Additionally, the development of an improved component end anchor head, and qualitative testing of the anchorage mechanism of the component is reported.

Chapter 4 involves a detailed description of the testing programme completed in the duration of this research work. The experimental work is mainly divided into three programmes: measurements of the pre-load induced in the *EHB* component; measurements of full component and individual mechanism force-displacement relationships by means of monotonic tensile pull-out tests; and relevant material property testing. The Chapter details the test matrix, the experimental set-ups, and instrumentation involved.

Chapter 5 presents the raw experimental results. The results of the pull-out and pre-load testing programme are demonstrated, the results are discussed, and key observations with regard to failure modes are outlined. Focus is given to the evaluation of the load transfer mechanism of the *EHB* component - with respect to the behaviour of its individual elements - and the component's full, non-linear, global force-displacement relationship is quantified with respect to the main parameters affecting the response. Moreover, parameter variation effects are

investigated in reflection with the response of the individual elements of the component, and the reliability level of the test results is addressed.

Chapter 6 presents the detailed analysis of the experimental data related to the principal pre-load and pull-out test results, where regression analysis and statistical tools are used to quantify the integrity of the analysis. In the course of the analysis, the development of the individual element models which comprise the *EHB* component is demonstrated. It is the purpose of the Chapter to propose: (a) a model related to the force-bolt elongation (F-δ_b) response of the component's internal bolt, and (b) models related to the force-slip (F-δ_{slip}) response of the expanding sleeves, and mechanical anchorage elements of the component.

In Chapter 7, a mechanical model is proposed to predict the tension response of the investigative joint component. The characteristics of the elements that are involved in the equivalent spring model are described, and their assembly procedure is outlined for evaluation of the component model. The predictions of the component model are compared with experimental data, and regression analysis is performed to quantify the goodness of fit. Additionally, the *EHB* component is classified in terms of ductility in accordance with current classification systems, and the component model is also incorporated within an equivalent tension T-stub model for assessment.

In conclusion, Chapter 8 summarises the key findings of the thesis and recommendations for future research are suggested.

2 Literature review

A review of published information follows in order to report the existing knowledge in this field. The review includes the basics of this research area, it presents in detail the commercially available Lindapter "Hollo-bolt (*HB*)" and it summarises information with regard to its performance. The key findings of ongoing research carried out at the University of Nottingham are addressed, with a focus on the development of the "Extended Hollo-bolt (*EHB*)" and its potential application for use in moment-resisting joints. The principles of the component method and their application in the design of structural joints are demonstrated. Lastly, an assessment of potentially extending the method for joints comprised of *EHB* connections to concrete filled hollow sections is discussed. It is the purpose of this Chapter to establish any gaps that are present in the existing knowledge, thereby permitting determination of the necessary issues that require further investigation.

2.1 Beam-to-column joints

Some terms used throughout this thesis are defined in this section, prepared in agreement to Eurocode 3 (CEN 2005). Figure 2.1 shows the main parts of a beam-to-column joint. A joint is the zone where two or more members are interconnected and a connection is defined as the location at which two or more elements meet. Single sided joints consist of one connection and double sided joints consist of two connections. The principal structural requirement of a connection is that it be capable of safely transferring load from the supported members to the supporting member. A component is a part of a joint that makes a contribution to one or more of its structural properties (e.g. bolts & end-plates). It is well known that the structural properties of joints are of major influence on the strength, stiffness and stability of the whole structure. Hence a good understanding of the behaviour of joints is essential. In consideration of moment-resisting joints, as an example, a bolted end-plate connection would transmit moment by coupling tension in the bolts with compression at the opposite flange. Note that in such a

joint, it is the bolt row furthest from the compression flange that will attract the most tension.

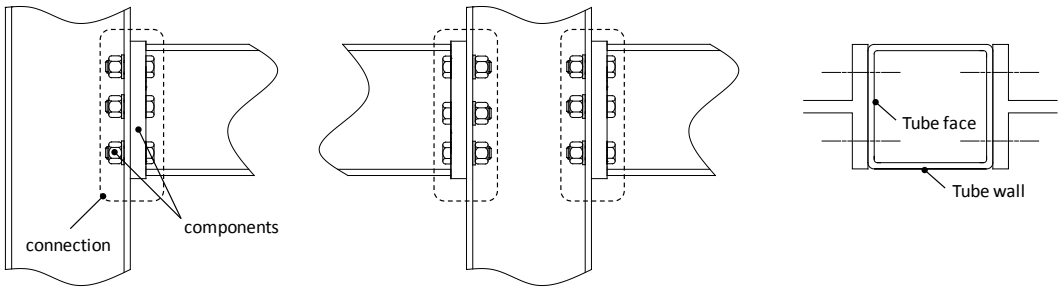

(a) Single-sided joint (b) Double-sided joint (c) Cross section

Figure 2.1 Parts of a beam-to-column joint configuration

Other terms used in this thesis are defined as follows: “tube face” is the side of the hollow section at which a connection has been constructed; “tube walls” refer to the lateral sides of the hollow section, at which no connection has been constructed. Square hollow section may sometimes be abbreviated as *SHS*.

2.1.1 Joint characteristics

The characteristics of a joint can be best understood by considering its rotation under load. Rotation is the actual change in angle (ϕ) which takes place as shown in Figure 2.2. Steel joints exhibit a behaviour that ranges from very rigid to extremely flexible. Obviously deformability varies in accordance with the applied loading. As measured in experiments, the corresponding moment-rotation (M-ϕ) curves are clearly non-linear, a typical feature of joint behaviour. However there are different possible ways to idealise a joint M-ϕ characteristic curve without significant loss of accuracy. The choice of one of them is dependent upon the type of global frame analysis.

In design terms, this means that the properties of joints to be evaluated depend on the type of global frame analysis and design process which is followed by the designer; for instance:

- For an elastic analysis combined with an elastic verification of the member sections and joints, the stiffness and the elastic resistance of the joints should be derived.
- For an elastic analysis combined with a plastic verification of the most heavily loaded member section or joint, the stiffness and the plastic resistance are required.
- For a rigid-plastic analysis, only the plastic resistance and the rotation capacity of the joints will have to be evaluated.

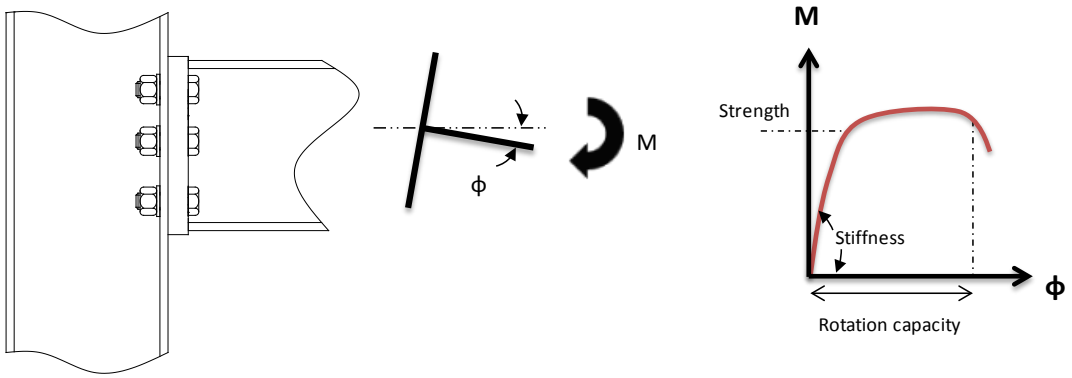

Figure 2.2 Moment - rotation of a joint

2.1.2 Joint classification

Joints can be classified in three ways as illustrated in Figure 2.3. These are by:

- Strength (Moment resistance).
- Rotational stiffness.
- Rotation capacity (Ductility).

The strength classification simply consists of comparing the joint design moment resistance to “full-strength” and “pinned” boundaries (Figure 2.3a). The boundaries adopted in Eurocode 3 (CEN 2005) seem to be well accepted at the international level.

The stiffness classification into rigid, semi-rigid and pinned joints is performed by comparing the design joint stiffness to two stiffness boundaries (Figure 2.3b). For sake of simplicity, the stiffness boundaries are usually derived so as to allow a direct comparison with the initial joint stiffness, whatever the type of joint idealization

that is used afterwards in the analysis. The limits which are set in Eurocode 3 (CEN 2005) are defined in various ways and may change depending on whether or not the frame is braced. Different stiffness boundaries have been suggested by some authors. They mainly differ by the criteria used as a basis for classification and the level of the sophistication in their expression (Jaspart 2000).

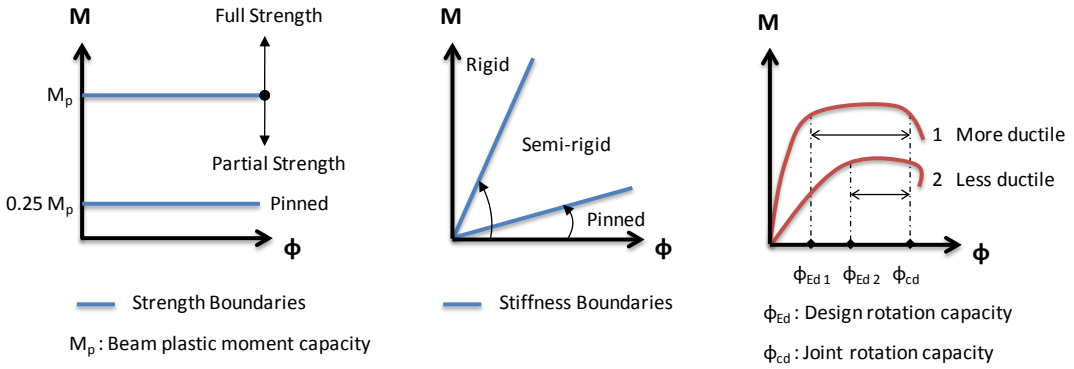

(a) Strength classification (b) Stiffness classification (c) Ductility

Figure 2.3 Joint classification

Few studies have been devoted to the evaluation of the rotation capacity (ϕ_{cd}) of joints. This is clearly illustrated in Eurocode 3 (CEN 2005) where only a limited amount of information is given. It is the subject of ongoing research to establish criteria to distinguish between "ductile", "semi-ductile" and "brittle" joints (Da Silva et al. 2002; Kuhlmann et al. 1998). To illustrate the definition of ductility, a simple plot is shown in Figure 2.3c.

2.2 The Lindapter 5 piece Hollo-bolt *(HB)*

The Hollo-bolt (*HB*) incorporates a sleeve with four equidistant slots around a standard bolt, a collar and a threaded mild steel cone (Figure 2.4). Upon tightening of the bolt head, the cone rides along the shank of the bolt resulting in a flaring of the steel legs. The steel sleeves undergo significant plastic deformation, and the four flared legs therefore clamp against the inside of the hole, holding the two plies together. The *M16* and *M20 HB* which are the most commonly used sizes for structural applications feature a collapse mechanism that maximizes the clamping

force. This is achieved by placing a rubber washer that has been designed to compress between the expanding sleeve and collar (Lindapter 2009). A blind-bolted connection between an open section beam and a hollow section column utilising the *HB* is presented in Figure 2.5.

Figure 2.4 The Lindapter 5 piece Hollo-bolt *(HB)*

Figure 2.5 Application of *HB* for connections to hollow sections

The installation of the *HB* is a relatively simple process (Figure 2.6). The fastener is inserted through the connecting element and steelwork (e.g. end-plate and hollow section), the *HB* collar is then griped with an open ended spanner, and finally a torque wrench - set at the recommended torque by Lindapter (2009) - is used to complete the tightening process.

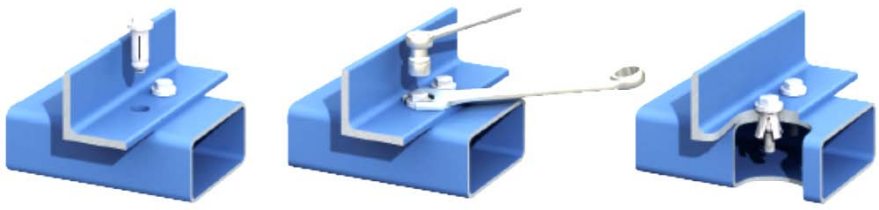

Figure 2.6 Hollo-bolt installation

2.2.1 Application of *HB* in joints between open and hollow sections

The existing knowledge with regard to the behaviour of the *HB* is complete as far as transfer of vertical shear is considered. Occhi (1995) and Banks (1997) primarily

studied the behaviour of the *HB* when subjected to direct shear. Hollo-bolts have a shear capacity slightly higher than that for ordinary bolting, since the body of the fastener provides resistance as well as the bolt shank. In effect, the updated version of SCI/BSCA (2002) has included guidance for the design of pinned joints with the use of the *HB* system. This publication has enhanced the confidence of designers, and the practicality of the *HB* system has furthermore increased the popularity of using such a system in practice today.

When designing for pinned joints, although the theoretical definition of a pinned joint implies transfer of vertical shear only, due to the need to satisfy structural integrity criteria, tensile resistance is also an issue. The design checks in SCI/BCSA (2002) are associated with the structural integrity requirements of BS 5950 (2000b), whereby beam-to-column connections must be able to resist lateral tying forces unless these forces are resisted by other means within the construction framework e.g. the floor slabs. When carrying out the full design procedure, this additional check should be made and will only be of significance when the tie force is greater than the shear force on the beam. To ensure that disproportionate collapse will not occur, a basic value of 75kN tying force requirement is reported in BS 5950. The behaviour of the *HB* when subjected to direct tension is very different from that observed with standard bolts. Therefore, several investigations have been carried out to determine also the tensile resistance of the *HB* in order to assess its feasibility in satisfying structural integrity criteria. A summary of the experimental results is found in Yeomans (1998). The individual tensile tests identified two different failure modes when the *HB* is connected to hollow section members, both being dependent upon the thickness of the hollow element. For a thickness of up to 8mm, excessive deformation of the tube face during loading led to the whole insert being pulled out of the section, whereas for a thickness of 8mm and above, a shear failure of the flared legs of the fastener against the side of the hole was observed. Evidently, the *HB* has been found adequate for pinned joints with a capacity that withstands predominantly shear load and the limited tensile loads arising from structural integrity requirements.

2.2.2 Behaviour of the *HB* when subjected to direct tension

To extend the application of the *HB* from pinned joints to moment-resisting joints, it is necessary to develop detailed knowledge with regard to its tensile behaviour. This is because when considering bolted moment-resisting joints, the bolt row furthest from the compression zone tends to attract tension so as to transfer the moment. In addition to strength that is considered for pinned joints to satisfy structural integrity, axial stiffness and ductility is of major importance in moment connections. The characteristics of the *HB* in direct tension have been examined by previous investigators by means of individual and group tensile tests. The internal bolts within the *HB* system employed in the earlier investigations were of grade 8.8. The bolt grade designation system relates to the mechanical properties of standard bolts and is based on two numbers, e.g. 8.8. The first number is the minimum ultimate tensile stress of the bolt material divided by 100, whereas the second number is the ratio of the Proof (yield) stress and the ultimate tensile stress.

As discussed previously, the tensile failure mechanism of the *HB* was found to be dependent upon the thickness of the connected element. In order to study the full tensile behaviour of the *HB* as a single component, more recently Elghazouli et al. (2009) have performed further direct tension tests. The aim of the tests was to establish the initial stiffness and yield strength of the *HB* for modelling purposes, while the objective was to determine the effect of using an internal bolt of higher grade. The experimental set-up is shown in Figure 2.7. Based on the load-deformation relationship, a comparison was drawn between grade 8.8 and 10.9 setscrews. The typical tensile behaviour of an *M16 HB* may be represented by that shown in Figure 2.8 for the two studied setscrew grades. It was concluded that when a grade of 10.9 was employed, the elastic stiffness was maintained to a much higher load and the failure displacement was reduced but no significant effect was seen for the ultimate strength or initial stiffness. As Lindapter International recommends a higher tightening torque for higher bolt grade setscrews, it is in fact the effect of the initial tightening torque which affected the behaviour in these tests. The higher torque permitted in grade 10.9 Hollo-bolts results in significant improvement in its axial stiffness in comparison with grade 8.8, at the expense of

some reduction in local ductility. This is directly reflected in a more favorable performance on the overall connection level, depending on the relative stiffness of other connection components (Elghazouli et al. 2009).

Figure 2.7 Set-up for direct tension tests on Hollo-bolts (Elghazouli et al. 2009)

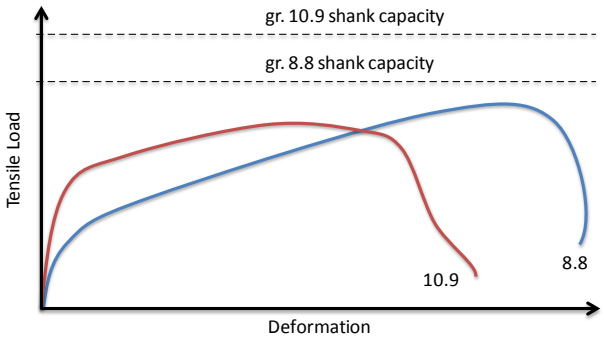

Figure 2.8 Load-deformation relationship for M16 Hollo-bolts (Elghazouli et al. 2009)

2.3 Review of research at the University of Nottingham

Since 1998, research at the University of Nottingham is aiming to devise and validate a blind-bolted moment-resisting connection to hollow sections. The objectives involve the development of an appropriate fastener and connection configuration that would enable the construction of such a connection. This section has been prepared to review the work carried out up to date with the intention to report on the areas in which a lack of knowledge exists.

The first stage of the research commenced with extensive testing of the *HB* so as to test its feasibility for application in moment-resisting joints. The benchmark of stiffness required to be achieved was that of a standard bolt. Equivalent T-stub to T-stub and T-stub to SHS experiments were performed by Barnett (2001). The tests were designed in such a manner so as to investigate the behaviour of the fastener alone (Figure 2.9a), and then test its feasibility by an arrangement that represents the tension region of a moment resisting connection (Figure 2.9b).

It was concluded that the *HB* did not possess sufficient stiffness due to inadequate clamping action, exhibiting a pull-out failure mode with shearing off of the sleeve

legs, as also observed by Yeomans (1998). At this stage it was felt that a modified version could overcome the issue. Hence the so-called Reverse Mechanism Hollo-bolt (*RMH*) was developed, an evolution of the *HB* which was rigorously tested and investigated by Barnett (2001).

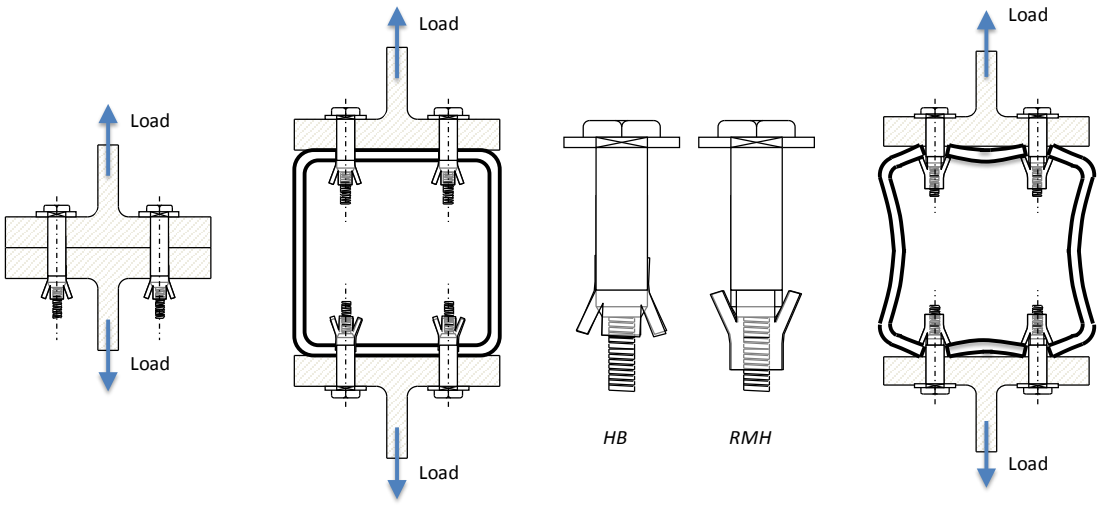

(a) T-stub to T-stub (b) T-stub to SHS (c) Types of fasteners tested (d) Face Flexibility

Figure 2.9 Tensile testing

The principal difference between the *HB* and the *RMH* was the inverted sleeve clamping action, designed as such to increase the clamping forces between plies (Figure 2.9c). It was found that the *RMH* possessed a higher stiffness and axial tensile capacity than the standard *HB* by overcoming the clamping inadequacy. The *RMH* behaved in the same manner as an equivalent sized standard bolt in terms of stiffness and capacity. However, in contrast with the *HB* configuration, the capacity of connections assembled with the *RMH* was seen to be greatly affected by the tube face flexibility (Figure 2.9d).

2.3.1 Exploration of concrete infill effect

Since the flexibility of the tube limited the performance of the type of connection under investigation, it was necessary to devise a practical system that could reduce such deformations. To achieve this, a concrete infill was applied to the hollow section in order to act as a local stiffener. Tizani et al. (2003) reported that the infill enhanced the connection performance since it allowed for the full tensile capacity

of the fasteners to be developed by resisting the deformation of the tube walls. The strength of the concrete infill did not seem to have a major influence on the stiffness of the connection, but it was observed that once the ultimate capacity of the filled sections was reached, the load dropped to that resisted by the unfilled section. T-stub to SHS tensile test results are depicted in Figure 2.10 to illustrate the effect of applying the concrete infill when the *RMH* was utilised as a connector.

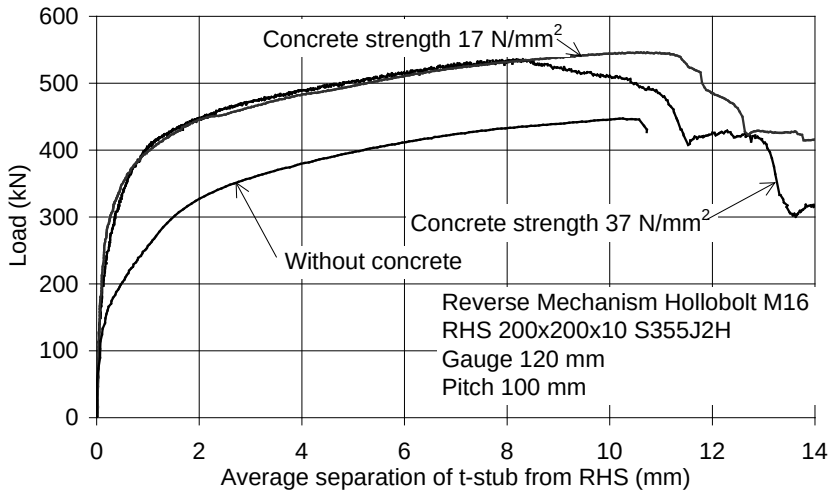

Figure 2.10 *RMH* connection: Concrete infill & strength effect (Tizani et al. 2003)

Analysis led to the conclusion that the *RMH* may at best exhibit semi-rigid connection behaviour when the infill exists, whereas the *HB* did not possess enough stiffness either with or without the infill. Although the stiffness provided by the *RMH* was satisfactory towards the development of a moment-resisting joint, due to the fact that it required custom sleeves with every increase of 5mm in clamping, its application was limited as a connector to *SHS*. The range of application was not wide enough to satisfy the requirements as a product in the construction industry. Therefore, investigations commenced to devise another blind-fastener that took into consideration the benefits arising from a concrete infill to the tube, in view of achieving moment-resisting behaviour.

2.3.2 The Extended Hollo-bolt (*EHB*)

The Extended Hollo-bolt (*EHB*) is another modification of the Lindapter Hollo-bolt, devised at the University of Nottingham specifically for connections to concrete

filled SHS (Figure 2.11). The primary difference with the standard *HB* is that the shank length is longer, and that it involves an anchorage mechanism. Designed in a practical manner, a standard hexagon nut that fits through the bolt hole is attached at its end in order to anchor the fastener in the concrete. It is anticipated that the longer threaded shank additionally improves the behaviour of the fastener by enhancing bond characteristics between the shank and the concrete infill. It is worthwhile noting however that the total possible shank length is limited to the SHS size, and the size of the end anchor is limited to the diameter of the bolt hole.

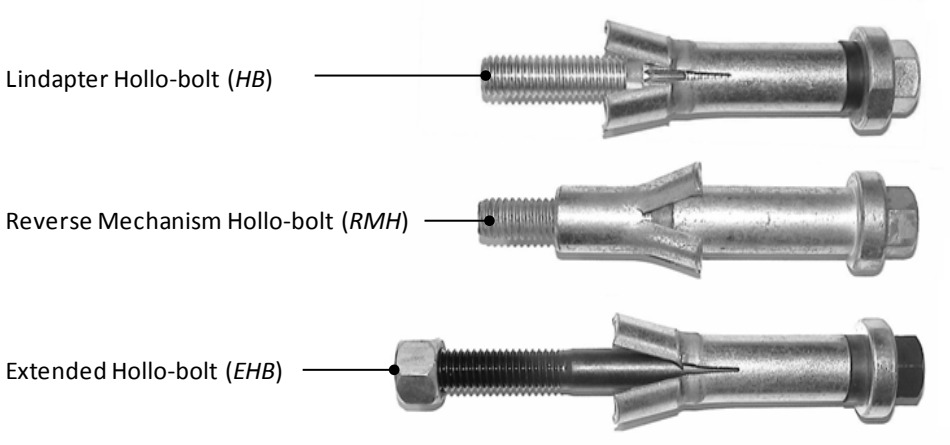

Figure 2.11 Lindapter Hollo-bolt modifications

Exploratory tests by Ellison (2003) investigated the performance of the *EHB* in comparison with the *RMH* and the *HB* by means of T-stub to concrete filled SHS tensile tests. Standard bolts were tested to provide a benchmark behaviour required to be achieved by the blind-bolt. The *RMH* and *EHB* connections displayed very similar stiffness characteristics to those of the standard bolt whereas the *HB* exhibited lower stiffness. The standard *HB* connection demonstrated much larger initial deformations. This indicates that the extra bond and anchorage provided by the longer shank and anchor nut helped to limit the amount of initial deformation, hence the increased stiffness. A further study by Pitrakkos (2008) demonstrated that the required level of stiffness could be reached when setscrews of grade 10.9 are employed within the *EHB* system, rather than the standard grade 8.8 used by Ellison (2003) (Figure 2.12).

So far, exploratory tests involved a testing arrangement that represented the tension region of a moment-resisting joint. To test the feasibility of the *EHB* for application in moment-resisting joints between open and concrete filled hollow sections, a series of full-scale moment connection tests were performed by Al-Mughairi et al. (2009). Specimens were subject to monotonic loading conditions, and based on their moment-rotation responses, a parametric study and connection classification was carried out.

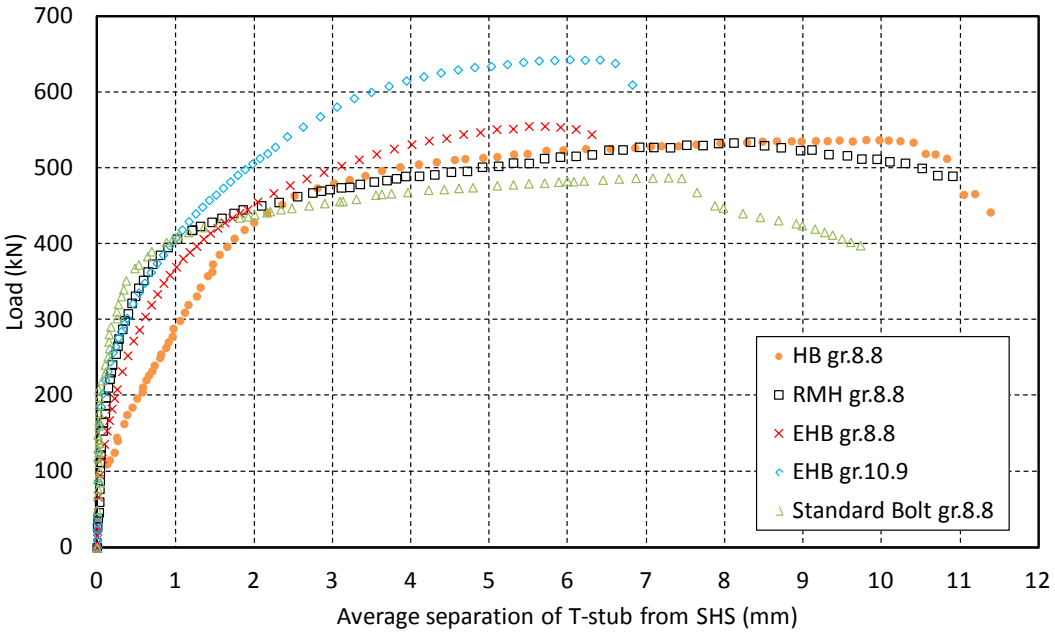

Figure 2.12 T-stub to concrete filled SHS results (Ellison 2003; Pitrakkos 2008)

The test set-up employed by Al-Mughairi represented an exterior beam-to-column joint of a structural steel frame, as depicted in Figure 2.13. A summary of the test results and parameters investigated are shown in Table 2.1, where “bolt pitch” is the vertical distance between the centreline of two bolt rows. All samples failed by bolt fracture, as designed for, in order to assess the efficiency of using such a blind-bolt. No evident bolt pull-out was observed in the tests, which implies that the anchorage provided by the *EHB* was not overcome. The tests have indicated that at least a semi-rigid behaviour is achievable according to the classification system in EC3 (CEN 2005). Hence, the use of the *EHB* for such connections is satisfactory in

providing a moment-resisting joint. This justifies the continuation of research on the proposed type of structural joint. Furthermore, it was found that the thickness of the tube has an influence on the connection behaviour however did not dominate. As expected, the use of an extended endplate in relation to a flush endplate showed to greatly improve the connection characteristics. In contrast, the strength of the concrete infill and a longer bolt pitch showed to not influence significantly the behaviour of the joint.

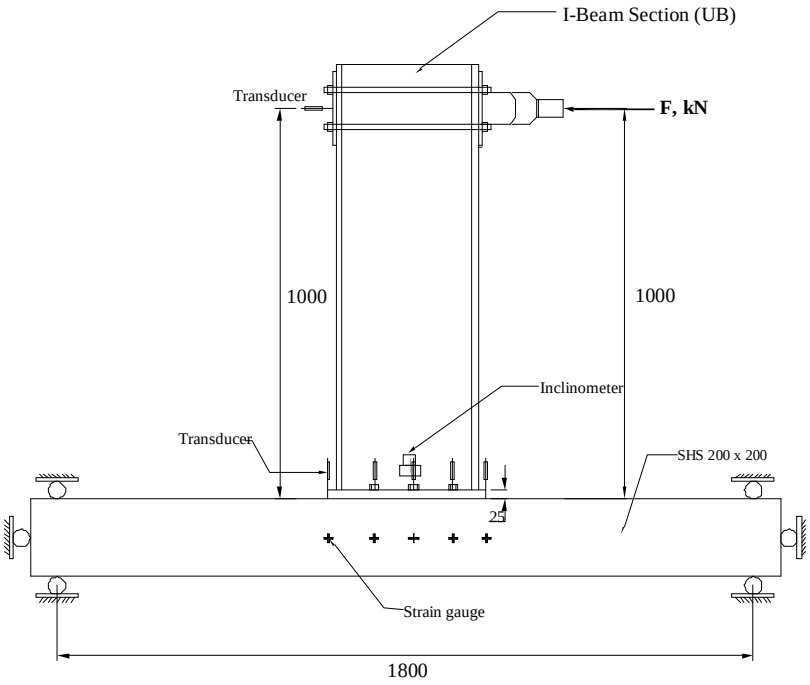

Figure 2.13 Moment connection test set-up (Al-Mughairi et al. 2009)

Table 2.1 Summary of moment connection tests (Al-Mughairi et al. 2009)

Test No.	Column Section (width x thick)	Concrete Strength (N/mm2)	Endplate Type (all 25mm)	Bolt Pitch (mm)	Connecting UKB size (all S355)	Initial Stiffness (kNm/mRad)	Ultimate Moment (kNm)
1	SHS 200x12.5	40	Flush	100	356x171x67	58	186
2	SHS 200x10	45	Flush	140	457x152x52	45	208
3	SHS 200x10	41	Extended	100	356x171x67	53	292
4	SHS 200x8	39	Flush	140	457x152x52	33	217
5	SHS 200x8	40	Flush	100	356x171x67	29	186
6	SHS 200x12.5	42	Flush	140	457x152x52	65	220
7	SHS 200x10	40	Flush	100	356x171x67	32	190
8	SHS 200x10	60	Flush	100	356x171x67	43	190

When the behaviour of joints are considered as a whole, it is possible to classify the overall joint in terms of strength, stiffness and rotation capacity, however it is difficult to interpret the results as a design tool. Although the previous work has demonstrated the potential of the modified blind-bolt in moment resistance, the data is insufficient to permit design of the proposed type of joint. Based on the key findings of ongoing research at the University of Nottingham, the use of the *EHB* in moment-resisting joints is the subject of detailed investigation and focus of this thesis. The research proposal to facilitate the furthering of understanding is outlined upon a review of the current state-of-the-art models for steel joints.

2.4 The Component Method

The behaviour of steel joints is complex due to a multitude of phenomena such as material and geometrical non-linearity. Apart from experimental testing, three modelling options are practically available in view of estimating the overall M-ϕ response of structural joints. These are analytical or empirical models, mechanical models that are based on the so-called component method, and advanced finite element models. Analytical and empirical models usually feature simple analytical expressions for the calculation of the response and thus they offer the advantage of ease of use, at the cost however of reduced reliability, which is not easily scalable to cases of joint designs other than those used for their calibration. On the contrary, advanced finite element models can be considered very reliable for the simulation of the complex, non-linear joint response, however their use for practical design purposes remains limited, due to the high computational cost they involve and the sophisticated preparation process they require. Mechanical models lie between the two previous modelling practices, both with respect to computational complexity and reliability.

Nowadays, the component method is widely accepted as the practical approach in predicting the behaviour of steel joints (Da Silva 2008). Existing design rules have in fact been converted into a component format. The Eurocode 3 design approach consists of this so-called component method that provides procedures for the

evaluation of the rotational behaviour of joints, thus allowing the specification of the corresponding moment-rotation curve or the associated properties (CEN 2005).

Given the complexity of steel joints, the development of the component method, and the prediction of the behaviour of steel joints in general, heavily relied on the results of a large number of experimental research programmes carried out at a number of research institutes. The component method entails the use of relatively simple mechanical models, whereby the joint is simulated by an appropriate choice of rigid links and spring components. Wales & Rossow (1983) effectively introduced the component-based approach when they developed a mechanical model for double web cleat connections, in which the joint was idealised as two rigid bars connected by a homogeneous continuum of independent non-linear springs (Figure 2.14). Since then, mechanical models have been developed by several researchers to predict moment-rotation curves for a wide range of joints. For steel and composite joints connecting members with open sections, a great amount of work has been accomplished which led to the publication of design tables of standardised joints and simple design sheets [SCI/BCSA (2002) (1995a) (1995b) (1998)].

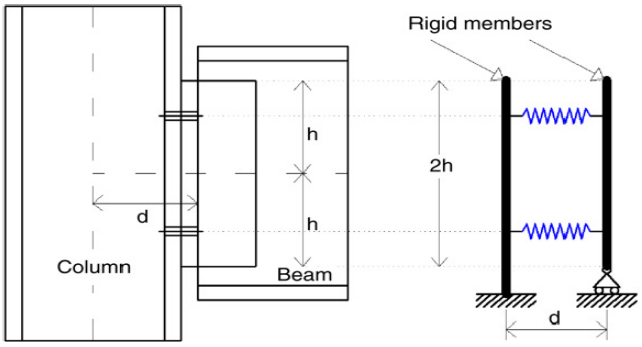

Figure 2.14 Connection and mechanical model for web cleat connections (Wales et al. 1983)

2.4.1 Principles of the method

The component based unified design approach is a quite powerful tool for the evaluation of the stiffness and/or resistance properties of structural steel and composite joints under several loading situations. In experimental tests, a joint is generally considered as a whole and is studied accordingly; the originality of the

component method is to consider any joint as a set of “individual basic components”. The application of the component method requires the following three steps:

1. Identification of the active components for the studied joint.
2. Evaluation of the mechanical characteristics of each individual basic component (initial stiffness, design resistance - or the whole deformability curve).
3. Assembly of the components in view of the evaluation of the mechanical characteristics of the whole joint (initial stiffness, design resistance - or the whole M-ϕ curve).

To demonstrate the principles of the component method and conclude on its limitations, a typical joint with a bolted end-plate connection subject to bending (M), shear (V) and axial (N) loading is presented (Figure 2.15). The information has been extracted from a guide commonly used by engineers today for the design of structural steelwork moment-resisting connections. Identification - step 1 - is the process of decomposing a joint in different components. Typical components for bolted steel joints are shown in Table 2.2. Each of these basic components possesses its own level of strength and stiffness in tension, compression or shear - characterized by a non-linear force-deformation curve. For simplicity, within the component method, any non-linear behaviour is normally simplified to a bi-linear or tri-linear relationship. The coexistence of several components within the same joint element - for instance, the column web which is simultaneously subjected to compression (or tension) and shear - can obviously lead to stress interactions that are likely to decrease the strength and the stiffness of each individual basic component; this interaction affects the shape of the deformability curve of the related components but does not call the principles of the component method into question again (COST 1997). Lastly, to determine the properties of the whole joint, the mechanical properties of the components are combined. The “assembly” is based on a distribution of the internal forces within the joint. As a matter of fact, the external loads applied to the joint distribute, at each loading step, between the individual components according to the instantaneous stiffness and resistance of

each component (Jaspart 2000). However, to obtain a safe estimate of joint resistance, this distribution has at least to satisfy the following basic requirements:

- The internal forces must be in equilibrium with the external forces applied to the joint.
- The internal forces have never to exceed the resistance of the components.
- The maximum deformation capacity of the components has never to be exceeded.

For stiffness calculation, the elastic distribution of internal forces in the joint is requested to fulfil one more condition, the compatibility of displacements amongst the constitutive components.

Table 2.2 Basic components of a joint with a bolted end-plate connection (SCI/BCSA 1995a)

Zone	Ref	Component
Tension	a	Bolt tension
	b	End plate bending
	c	Column flange bending
	d	Beam web tension
	e	Column web tension
	f	Flange to end plate weld
	g	Web to end plate weld
Horizontal shear	h	Column web panel shear
Compression	j	Beam flange compression
	k	Beam flange weld
	l	Column web compression
	m	Column web buckling
Vertical shear	n	Web to end plate weld
	p	Bolt shear
	q	Bolt bearing (plate or flange)

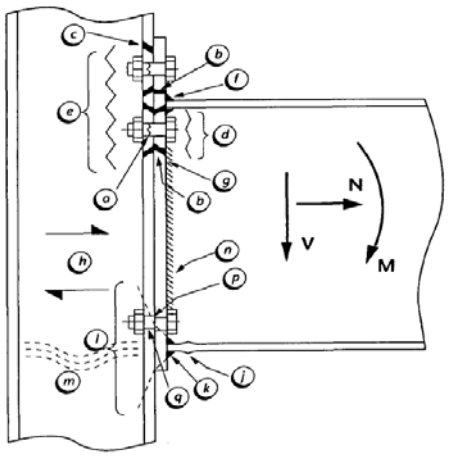

Figure 2.15 Bolted end-plate connection

The application of the method is schematically shown in Figure 2.16 for a single-sided joint with a welded connection. The particular type of joint has been selected for illustration purposes because a small number of components are required to be checked against. Relevant equations used to predict the rotational stiffness and moment resistance of the joint are listed at appropriate steps in accordance to Eurocode 3. These equations have been derived based on the assumption that the

internal forces (*F*), act at a lever arm (*z*), equal to the depth of the connected beam minus the thickness of the beam flange.

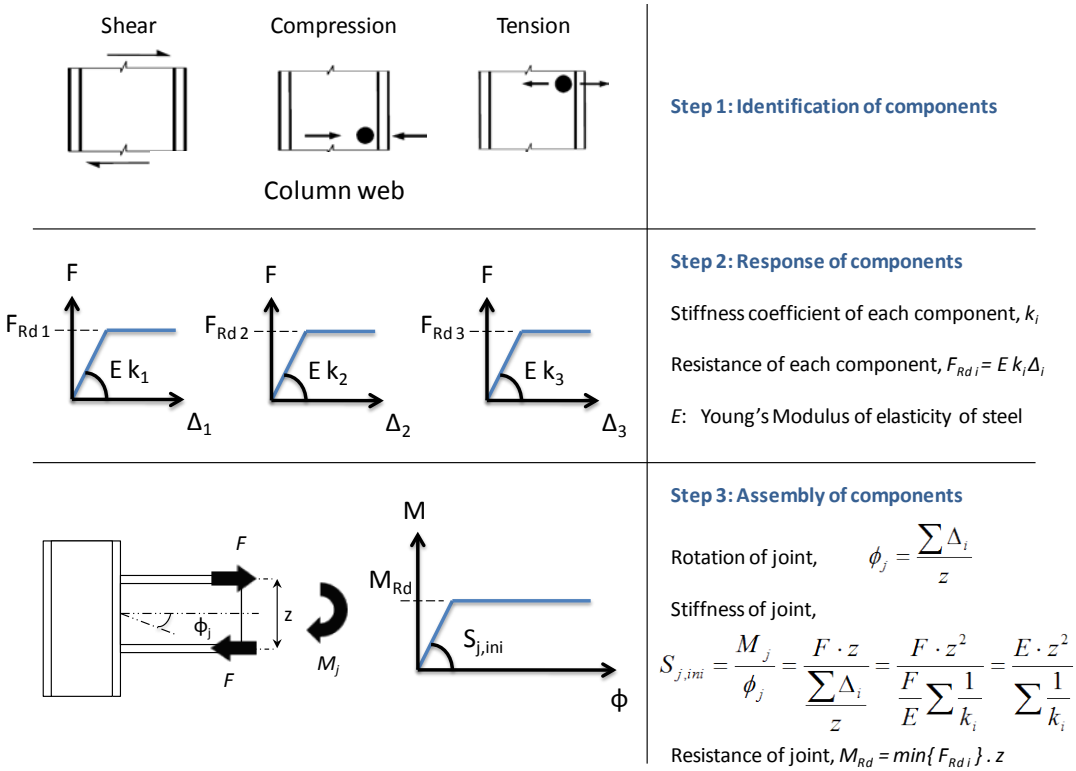

Figure 2.16 Component method for welded connection (bi-linear approach)

2.4.2 Limitations of the method

The analysis and design of joints within the framework of the component method requires the knowledge of the behaviour of all relevant components. Thus, the only limitations to its use may be expressed as follows:

- Design rules for the evaluation of the rotational stiffness, design resistance and rotation capacity would not be available for some or all the constitutive individual components.
- These rules would have a limited range of application.
- An appropriate assembly procedure would not be available.

2.4.3 Joints with connections to hollow sections

Up to date, application rules given in Eurocode 3 (CEN 2005) for evaluation of the properties of beam-to-column joints, are provided, as long as open sections (hot-rolled H or I) or built-up welded profiles are employed for the connected members. No component based guidance is specified for moment-resisting joints between open and tubular sections utilising bolted connections. This is because the behaviour of some salient components related to such joints is yet to be fully characterised. Consequently, in practice it is common to provide fully welded connections or complex configurations that stiffen the joint in order to achieve moment resistance. To overcome these issues, researchers have attempted to extend the use of the component method to joints in tubular construction (Jaspart et al. 2001). Its extension was reported to appear as promising because of lack of accurate knowledge regarding only one component. The survey carried out by Jaspart et al. (2001) involved a single-sided joint comprised of an open section connected to a concrete-filled rectangular hollow section by means of the stud technique. The stud technique consists in welding with the help of a special gun a threaded stud on the face of the section on which the connection is to be realised. Since few years, the same authors have been investigating the perspective of devising design rules for joints between members of tubular and open profiles utilising the stud technique. As mentioned earlier, further investigations were required for only one component, labelled as the column face in bending. In result, a paper was published as a "first practical implementation" of the component method for such joints (Weynand et al. 2006). Although this publication outlines a design philosophy, the effects of a concrete-infill have been disregarded in relation to the investigation by Jaspart (2001) and there are still vital steps to cross. Furthermore, the range of applicability is limited when the type of connector is to be considered. Hence the successful application of the component method to joints between tubular and open sections is yet to be fully validated. Derivation of design formulae for still-unknown components is required, which in turn need to be validated against extensive experimental work. Either new additional components

need to be considered, or the range of validity of some components must be extended.

2.4.4 Justification of component based approach for this study

The component method is widely recognised now as a general procedure for joint characterisation in the scientific community and in the European design codes. Aforementioned, for joints between members with open sections, a huge work has been achieved within the framework of the component method, which led to the publication of design tables of standardised joints. From a design, construction, and economic point of view, efficient joints are those that require minimum effort in terms of detailing, fabrication and erection. Such benefits arise from joint standardisation. And so, for mixed open/hollow sections joints, such an effort will have to be achieved too.

Although some work has been carried out by others in this specific research area, literature based on a component approach for such joints is limited. Most researchers consider and study the behaviour of the full joint rather than performing detailed investigations on basic components. Therefore it is felt that a component based approach is in fact necessary as a first step towards the development of appropriate rules for the design of moment-resisting joints utilising blind-bolted connections to concrete filled hollow sections. A wider implementation of this method would lead to simplifications in view of the standardisation and hence it would help to facilitate the daily work of designers.

2.5 Extension of component method for blind-bolted (*EHB*) joints

Hereafter, the application of the component method on the particular type of joint involved in this study is discussed, so as to extend its application to such types. The relevant components are identified and those which require further investigation or not are reported.

2.5.1 Identification of relevant components

Depicted in Figure 2.17 is a single-sided joint between an open section beam and a concrete-filled square hollow section column with a blind-bolted flush end-plate connection, with one row of Extended Hollo-Bolts in tension, and one row in compression. The internal force distribution is based upon guidance given in EC3 (CEN 2005), where it can be assumed that if the lever arm (*z*) is sufficiently large, the compressive and tensile stress zones will not interact. The lever arm may therefore be expressed as the distance from the centre of compression (being that in line with the mid-thickness of the compression beam flange) to the bolt-row in tension. The identification has been based on the following assumptions:

- The compression on the beam side is regarded as being carried entirely by the flange, thus no need to consider the component beam web in compression, except for when large moments combine with axial load as the compression zone will then spread up into the beam web (SCI/BCSA 1995a).
- The presence of the concrete-infill stiffens the zones to such an extent that the failure mechanism can neglect the following components: Bolts in shear, column face in compression, lateral column faces in compression or tension and any punching shear failure around the bolt heads in compression.
- The weld components (signed *f, g, k, &* n in Table 2.2) do not contribute to the rotational stiffness of the joint (CEN 2005). However, their resistance must be checked against the existing rules available in EC3 Part 1-8.

The identified relevant components for the particular joint are summarised in Table 2.3. The availability of appropriate rules to determine their mechanical properties within EC3 is also reported in the same table. As stated earlier, the application of the component method requires an understanding of the stiffness and resistance of each constitutive component in order to establish the whole joint behaviour. From Table 2.3 it is clear that the extension of the component method for the studied joint is limited due to unknown behaviour of two components, labelled as the "Bolts (*EHB*) in tension" - (X) and the "Column face in bending" - (Y).

With regard to component (Y), extensive studies are found in the literature (Gomes et al. 1996; Neves et al. 1996; 2004a; 2004b; Silva et al. 2003). However, the range

of validity of the published material is limited. Still there is not an accurate method that can predict the stiffness or resistance of this component due to the complexities involved, and the wide range of validity required. It is the subject of current research at the University of Nottingham to attempt to derive design formulae for this component, when the *EHB* is used as a connector. The response of this component is out of the scope of this work, therefore detailed information with respect to its known so far behaviour is not reported. In addition, it should be noted that the interaction of the connector with the yielding of the tube face is also a failure mode which requires attention, but is also out of the scope of this project.

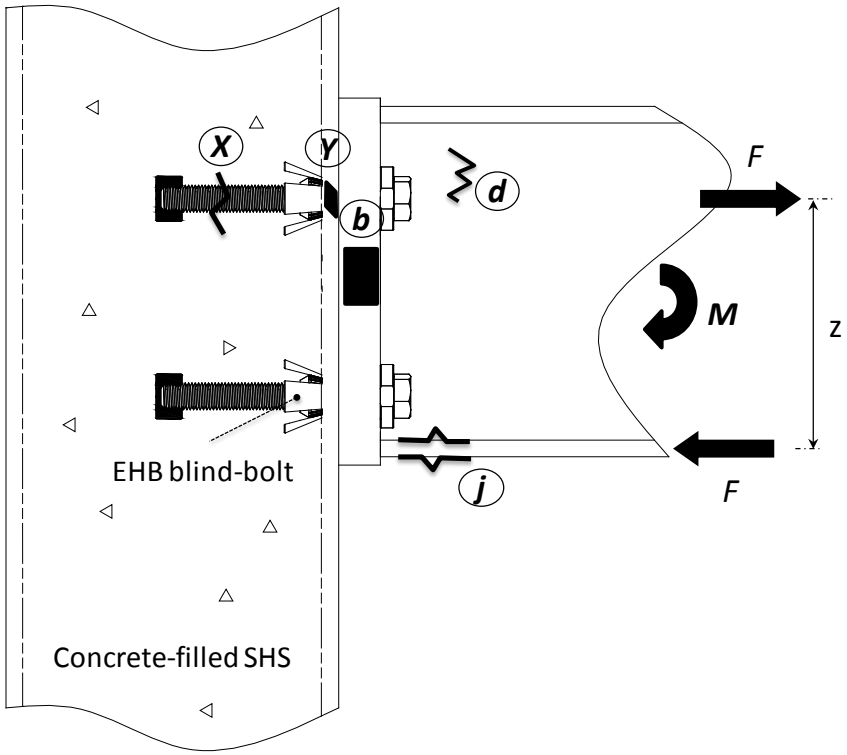

Figure 2.17 Basic components of investigative joint

Table 2.3 Relevant components & availability of evaluation rules

Zone	Ref	Component	Availability in EC3: Part 1-8	Contribution to rotational stiffness
Tension	X	Bolts (*EHB*) in tension	NO	YES
	Y	Column face in bending	NO	YES
	b	End plate in bending	YES	YES
	d	Beam web tension	YES	NO
Compression	j	Beam flange compression	YES	NO

Opposing the work of Jaspart (2001), which reported uncertainties regarding the behaviour of only the column face in bending, an additional component (X) is introduced. This is because the survey carried out by Jaspart employed the stud technique, in which no contact exists between the threaded studs and the concrete-infill as the studs are welded directly to the column face; hence the rules to evaluate the component "Bolts in tension" could be applied accordingly to those existing in EC3 for a standard bolt. Employing the stud technique however is generally not considered as a practical solution, because the studs are in fact prone to damage during delivery of the member to site and the tensile capacity of the bolts is limited to the weld capacity. In the particular joint configuration of this study, the blind-bolt is in direct contact with the concrete-infill, and obviously due to its unique geometry and mechanical properties, the rules of EC3 are not applicable. It is the focus of this thesis to evaluate the component "Bolts (*EHB*) in tension".

2.5.2 Evaluation of unknown component (X) - Bolts (*EHB*) in tension

To evaluate the initial stiffness of a joint, only the elastic stiffness of each basic component is required. To evaluate the ductility of a joint, knowledge of the full non-linear force–deformation response of each component is required. The evaluation process of available components in EC3 (CEN 2005) is limited to derivations of strength (design resistance) and initial stiffness. This is because of lack of documented data for the post-limit response of components.

The actual response of a generic component is characterised by a non-linear force-deformation curve, typified in Figure 2.18 (a). This non-linear behaviour may be characterised by a bi-linear or even a tri-linear curve. The idealisation in Figure 2.18 (b) neglects any strain hardening effects, in contrast with Figure 2.18 (c) which takes these effects into account. k^e, k^p, F^y, F^u, Δ^y and Δ^u denote the initial elastic stiffness, the post-limit stiffness, the component yield capacity, the component ultimate capacity, the yield displacement and the collapse displacement of the component, respectively. Post limit-stiffness is defined as in Equation 2-1, where μ^p is the strain hardening coefficient for post-limit stiffness (Del Savio et al. 2009). This

coefficient may be obtained for each constitutive component, based on trial and error values for a best fit to any experimental results. Currently, no reliable estimates of the post-limit stiffness of the various components are available in the literature, the usual practice being to consider a plastic plateau for ductile components. Additionally, no estimates are available for the collapse displacement of the components.

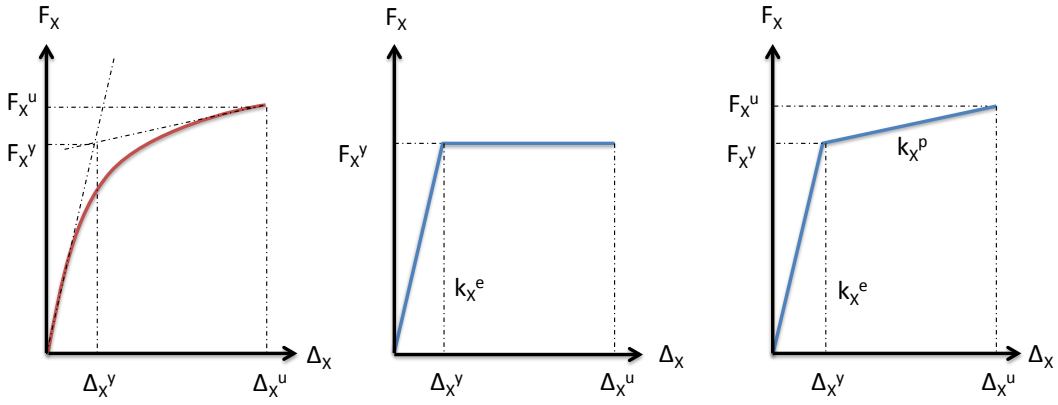

(a) Typical behaviour (actual)

(b) Bi-linear approximation (elastic-perfectly plastic approach)

(c) Bi-linear approximation (post-limit stiffness)

Figure 2.18 Generic component response

$$k^p = \mu^p k^e \qquad \textbf{Equation 2-1}$$

Based on the work by Kuhlmann et al. (1998), to evaluate ductility in the context of the component method, Da Silva at al. (2002) classified components into three main groups depending on the collapse to yield displacement ratio:

- Components with high ductility, Figure 2.19 (a)
- Components with limited ductility, Figure 2.19 (b) and
- Components with brittle failure, Figure 2.19 (c).

Standard bolts in tension are classified as brittle because they exhibit a linear force-deformation response up to failure. It is anticipated however that component (X)

may be considered to exhibit behaviour somewhere between brittle and limited ductility. But because the behaviour of the component strongly depends upon the adequacy of its anchorage mechanism, only a quantitative evaluation of the component's full force-deformation curve will allow for further conclusions.

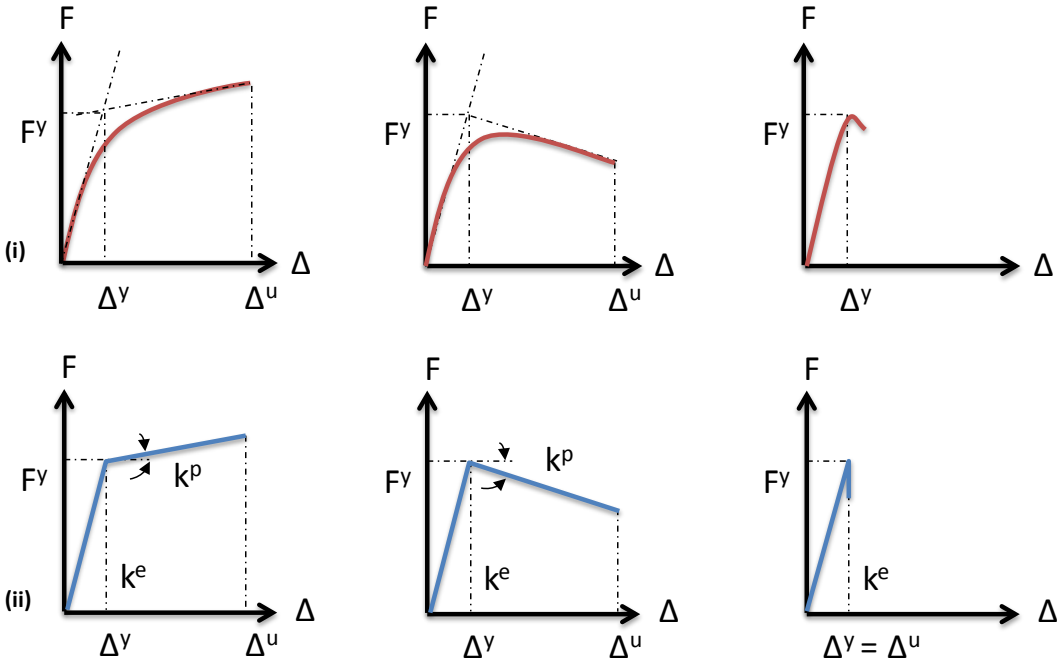

(a) High ductility (b) Limited ductility (c) Brittle failure

Figure 2.19 Constitutive laws of joint components: (i) actual behaviour, (ii) bi-linear

Given that small variations of the post-limit stiffness (in particular for a critical component) may result in large variations of the maximum rotation of a joint, Gervasio et al. (2004) assessed the influence of the various component properties on the available ductility of the joint. It was concluded that a change in failure mode may occur from the combination of two random variables, leading to failure of the stronger (in statistical sense) component. This aspect is crucial in steel joints because a brittle component like the bolts or the welds may become critical, leading to unexpected brittle failure of the joint. Current Eurocode specifications (CEN 2005) do not consider this possibility. In fact, by assuming that the post-limit stiffness of all components is zero, in clear contrast with the real stable behaviour

of ductile components, such as the end-plate in bending, brittle components may reach their collapse loads for smaller rotations. The safe use of the semi-rigid concept completely depends on a clear understanding of these aspects. The abovementioned clearly outlines the necessity to classify component (X) in terms of ductility and to measure its post-limit stiffness in addition to its resistance and initial stiffness.

2.6 Concluding remarks

The key findings of the literature review of this thesis are summarised as below:

- Convenient and practical connections between open and hollow section profiles can be achieved by utilising the Lindapter Hollo-bolt (*HB*) as a blind fastener. However, in design, the safe use of this system is restricted to transfer of vertical shear and limited tensile loads arising from structural integrity requirements. Investigations have tested the feasibility of using the *HB* for construction of moment-resisting joints. The results were unsatisfactory, reporting a complex mechanism between the fastener and the hollow section.
- Researchers at the University of Nottingham have devised an experimental modification of the commercially available *HB*, labelled as the Extended Hollo-bolt (*EHB*). The novel blind-bolting system was developed for application in concrete-filled hollow sections in view of resisting the predominant, tensile loads expected in moment-resisting construction. Rigorous opposite T-stub testing and full-scale moment connection tests have indicated that when the *EHB* is used as a connector for joints between open and concrete filled hollow sections, semi-rigid to rigid connection behaviour is achievable.
- Current state-of-the-art models for steel joints are based on the so-called component method. An assessment of potentially extending the principles of the method, for joints comprised between open and concrete filled hollow sections, utilising *EHB* blind-bolted connections, has revealed that insufficient knowledge exists with respect to two basic components. The unknown components are identified and labelled as the “Bolts (*EHB*) in tension”, and the “column face in bending”.

2.6.1 Areas in which a lack of knowledge exists

It has been stated that the construction of connections to hollow section columns still face a large challenge despite the rigorous research and innovative solutions that have been assessed throughout the years. Up to date, a viable bolted moment resisting configuration for such joints does not exist in practice. Ongoing research at the University of Nottingham has identified such a configuration; however, a full understanding of the behaviour of the proposed connection is yet to be developed due to the complex interaction among its components. This complex interaction has not allowed for a quantitative analysis of the parameters that affect the response of its basic components. Previous studies have not considered the joint at a component level of sophistication. Consequently, the available data is insufficient to permit design of the proposed novel connection technology. As a first step towards the development of appropriate design rules for the proposed type of joint configuration, it is felt that there is a need for a component based approach study.

For successful extension of the principles of the component method for the particular joint considered in this study, there is a lack of knowledge which requires attention. The response of a salient component that is located in the tension region of the connection is unknown; the tensile behaviour of the novel *EHB* blind bolts. The “Bolts (*EHB*) in tension” component requires classification in terms of resistance, stiffness and ductility for safe application in semi-rigid joints. It is apparent that because the *EHB* fastener was developed at the University of Nottingham, as a modification to the existing *HB*, not much related data will be found in the literature. However, even for the non-modified standard *HB* available on the market, no study has been carried out elsewhere, at a component level, in consideration of a concrete-filled tube.

2.6.2 Proposals to facilitate the furthering of understanding

Steel joints may present a wide range of geometries, with different number of bolt rows and connecting parts. Because of this variety of configurations, joint models may range from a simple three-component model, to a complex *n*-component model. For this study, it is felt that a component based approach, where basic joint components are investigated separately, will facilitate the understanding that is necessary to provide some form of design recommendations for the investigative type of joint.

The tensile behaviour of the *EHB* anchored blind-bolt has been identified as a component which requires further investigation. It is proposed to investigate the load transfer mechanism of the component, and to measure its initial stiffness, resistance, ductility, and post-limit stiffness response in consideration of the main parameters affecting its behaviour. To achieve this, the component will be decomposed into individual mechanisms that contribute to its overall deformability, and the response of these individual mechanisms will be measured with the aid of laboratory work. The importance of decomposing the component and investigating accordingly its individual mechanisms is signified if an adaptable model is required for development. To design for an adequate testing programme, it is however necessary to review relevant information with respect to the mechanics of the component. And so, a secondary review is found in the following Chapter of the thesis, and the outcomes are expected to assist the design of the testing programme, particularly with respect to the testing arrangement and design of test matrix that will involve the key parameters expected to affect the components response.

Based on the findings of the experimental work, it is expected to be able to develop a simplified mechanical model for the component which can be evaluated against actual full component experimental data.

3 Mechanisms of *EHB* anchored blind-bolt

The following Chapter of the thesis identifies the active mechanisms of the *EHB* anchored blind-bolt component and relevant work is reviewed to conclude on the research methodology. Due to the similarities in behaviour, a background of studies on reinforced concrete (RC) elements - fastenings and headed reinforcement - are reviewed and pertinent code provisions are discussed to provide guidance in designing and preparing for the experimental phase of this work. Moreover, the development of a modified end anchor head, and qualitative testing of the anchorage mechanism of the *EHB* component is covered.

3.1 Decomposition of component "Bolts *(EHB)* in tension"

To characterize the response of the *EHB* blind-bolt component, it is required to develop detailed knowledge relating its tensile behaviour. However, investigating merely the overall behaviour of the component is not sufficient to develop a model for design. It is necessary to understand and to be able to model the individual mechanisms that contribute to the overall deformability of the component in view of developing an "adaptable" model. A decomposition of the component identifies three individual mechanisms as sources of deformability, depicted in Figure 3.1.

Mechanism 1 - internal bolt shank elongation - is a source of deformability that is directly related to the material properties of the bolt shank. This mechanism also involves a level of pre-load that is induced due to the applied tightening torque. The expanding sleeves mechanism, signed 2 in Figure 3.1, represents the sleeves of the fastener that were plastically deformed at the tightening stage of the component, which further interacts with the concrete infill. Mechanism 2 provides resistance to pull-out due to direct contact with the tube face, at the surface level of the concrete infill. The bond and anchorage mechanism, signed 3 in Figure 3.1, arises from bond resistance developed by interaction of bolt threads with concrete, and head bearing stress acting on the concrete in front of the end anchor head. The manner in which these individual mechanisms interact in order to transfer a tensile load is not well understood. Therefore, to understand the load transfer mechanism

of the component, it is essential to develop knowledge with respect to its individual mechanisms.

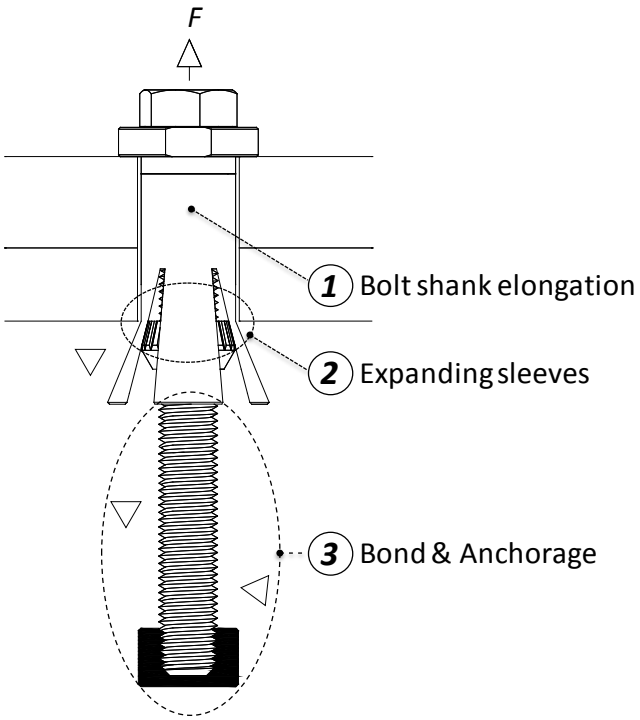

Figure 3.1 Component mechanisms

Literature with respect to standard bolting pre-load and a more detailed discussion regarding the mechanics of mechanism 3 follows. The confinement level given to the concrete infill by the tube walls will be considered in addition to other factors that are expected to influence the behaviour of the component.

3.2 Pre-load in component

The main purpose of bolts is to clamp joint members together. Specifically, in tensile joints, bolts should clamp the joint members together with enough force to prevent them from separating. The clamping force between joint members can significantly affect the characteristics of a moment resisting joint, as separation will occur once the tensile load that is applied to the joint overcomes the clamping force. At a component level, this force can affect the initial stiffness of the component as it resists plate separation. The clamping force a bolt exerts on the

joint is usually called or equated to the so-called pre-load in the bolt (Figure 3.2). As will be discussed below, some effects are known to modify pre-load in bolts.

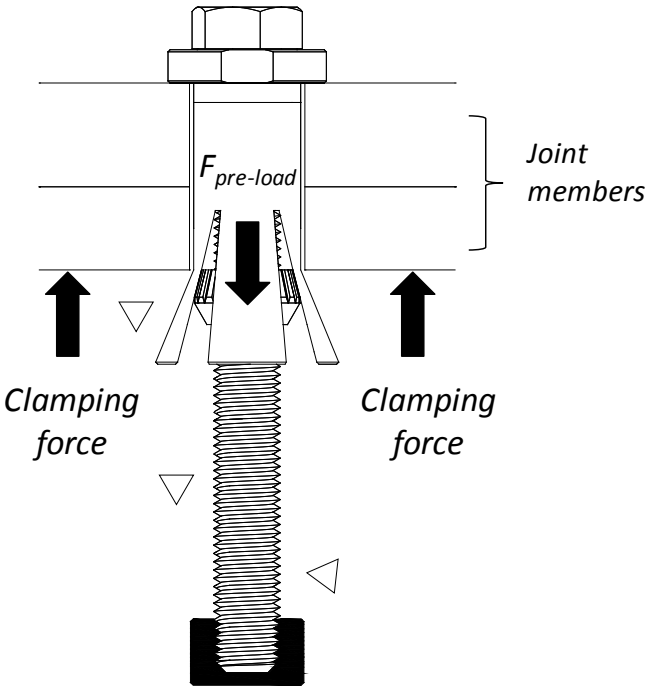

Figure 3.2 Component pre-load & clamping force

3.2.1 Torque versus pre-load

Torque control is nowadays accepted as an adequate method that can inform the user of when a bolt has reached the required pre-load for use in a particular joint. Predicting the amount of pre-load achieved when a bolt is tightened has been the subject of extensive research. With respect to standard bolting, a huge amount of work has been accomplished which has resulted in the derivation of theoretical equations that may predict the relationship between pre-load and tightening torque (Bickford 2008). Equation 3-1, sometimes referred to as the "short form equation", involves a general-purpose, experimental constant *K*, which says that ''when a torque is experimentally applied to a fastener, and the actual achieved pre-load is measured, it is discovered that the ratio between them can be defined by a constant and its nominal diameter".

$$T = F_p \, K \, d_b \qquad \text{Equation 3-1}$$

where

T : Tightening Torque (Nm)

F_p : Pre-load (kN)

d_b : Bolt nominal diameter (mm)

K : nut factor (dimensionless)

The advantage of using a nut factor is that it summarizes anything and everything that has affected the relationship between torque and pre-load in an experiment e.g. friction, torsion, bending, plastic deformation of threads, and any other factor that may or may not have anticipated. The drawback of *K*, however, is that it can only be determined experimentally, and experience shows that it really has to be determined for each new application for accurate representation. Typical values of *K* range from 0.15 to 0.25 for application in structural joints, dependent upon the type of material of joint members.

In the contrary, data relating pre-load to tightening torque in the *HB* or *EHB* assembly is limited. Due to the different load transfer mechanism between standard and *HB* blind-bolting, it is not sufficient to employ data based on standard bolting. In the *HB* assembly, as the threaded cone of the fastener approaches the inner ply, the expanding sleeves lock into the clearance hole, and subsequent tightening of the bolt head results in the sleeves attempting to open the clearance hole, i.e. a large proportion of the bolt pre-load is distributed into the inner plate and is not used in clamping the joint members together. Because of such losses, it is expected that the magnitude of pre-load developed in a *HB* assembly is lower than that of a standard bolt, at an equivalent tightening torque.

3.2.2 Effects on pre-load

At the tightening stage of a fastener, hole misalignments, undersized holes, press-fit fasteners, etc. are relatively common factors in the bolting world that may affect pre-load. For example, Figure 3.3 demonstrates an undersized hole which results in

pre-load losses due to frictional and embedment constraints between the sides of the bolt and the walls of the hole.

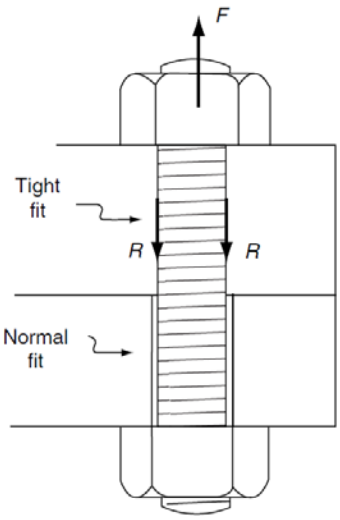

Figure 3.3 Effects of hole interference (Bickford 2008)

3.2.3 Pre-load relaxation

After bolts are initially tightened, short term relaxation occurs which is mostly attributed to a process called embedment. Embedment principally involves poor thread engagement, non perpendicular bolt heads, bent joint members, or elastic recovery of components. The factors that cause and contribute to relaxation are many and hard to predict. Although attempts have been made to write equations for the amount of relaxation to expect (Bickford 2008), in most cases the amount must be determined experimentally. In general, fasteners relax rapidly following initial tightening, and then relax at a slower rate, following the pattern shown in Figure 3.4. It is thus common to define pre-load created in an individual fastener when it is first tightened as the "initial" pre-load, and final pre-load in bolts as "residual".

The aforementioned suggests that the pre-load relaxation of the *EHB* component requires attention, by experimental means, in order to measure its residual pre-load for incorporation into an adaptable model. An attempt to derive appropriate values of the nut factor *K* can be utilised on the basis of repetitive testing in view of predicting the pre-load of the component. Moreover, the experimental set-up

should eliminate effects due to under or oversized holes to avoid measurements of pre-load that involve significant losses. Standard measurement techniques that are normally used to measure the pre-load of bolts are outlined below. The advantages and disadvantages of each technique are discussed in consideration of employing the data towards the development of the *EHB* component model.

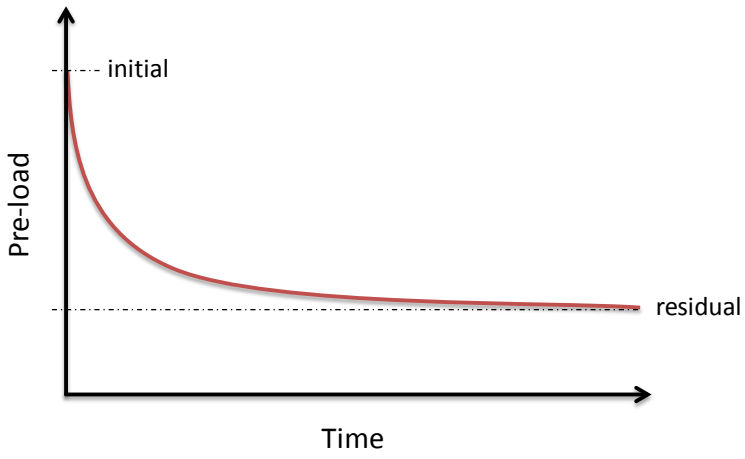

Figure 3.4 Pre-load relaxation with time

3.2.4 Pre-load measurement techniques

The traditional methods employed to measure pre-load of fasteners are principally divided into two approaches; via bolt stretch control (indirect) and direct measurements. Stretch control involves the measurement of change in length of the bolt due to the tension induced at tightening. This bolt elongation can easily be translated into pre-load with the use of Hooke's Law, assuming that the bolt still lies within its elastic region. Such changes in length are typically measured with the use of strain gauged bolts, or ultrasonic measurements. Where gauges are used, they are placed either below the bolt head, or at the front location of the end nut, as these surface locations are the primary locations at which the tensile stress is distributed over the effective grip length. Despite the quality and accuracy of ultrasonic measurements, unfortunately special equipment is required in the set-up and thus not as frequently used as gauged bolts.

Direct methods typically involve the use of a load cell that can measure the compressive clamping force between joint members. Such an approach requires less time for setting-up and does not require any modifications to the geometry of the fastener (to allow for installation of gauges) in comparison with gauged bolts.

The principal difference between a strain gauge and load cell approach is that strain gauges can provide additional data e.g. a value of actual change in bolt length, whereas the latter provides a value of pre-load alone. But merits arise from both approaches. The load cell approach can eliminate effects due to temperature changes or installation errors which gauges are well known to be prone to, however cannot measure the actual change in length of the bolt. On the other hand, it is fast, and easy to set-up, whereas strain gauges are expensive, time consuming, and require modifications on the bolt's geometry for installation purposes. Taking into account the above, this study will approach the pre-load measurement of the *EHB* component by using both techniques, direct and indirect, and a comparison between the different measurements will be carried out for further conclusions.

3.3 The mechanics of bond

The usefulness of reinforced concrete as a structural material depends on the strength and permanency of the bond between the concrete and the reinforcing steel, and for this reason bond resistance has received much attention from engineers and experimenters.

Bond refers to the interaction between reinforcing steel and the surrounding concrete that allows for transfer of tensile stress from the steel into the concrete. Bond is the mechanism that allows for anchorage of straight reinforcing bars and influences many other important features of structural concrete such as crack control and section stiffness. Figure 3.5 shows a straight bar embedded into a block of concrete. When the bond stress is sufficient to resist design tensile loads in the bar, then the bar is "developed" and the embedment necessary for anchorage of the fully stressed reinforcing bar is referred to as its development length.

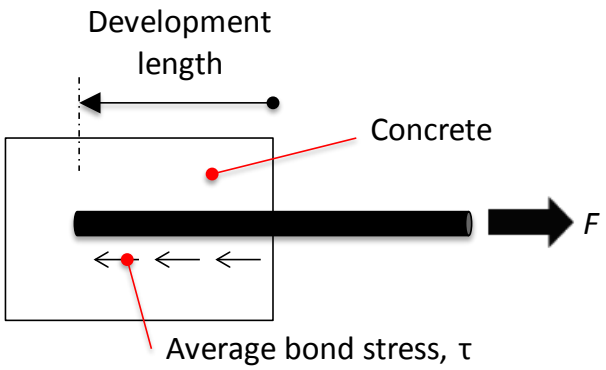

Figure 3.5 Simple concept of bond stress

It is said that Thaddeus Hyatt made tests to determine the bond between concrete and iron bars as early as 1876. During the past century numerous bond tests have been reported (Abrams 1913; Eligehausen et al. 1982). In general, all tests indicated that if a bar embedded in concrete is subjected to a tensile stress sufficient to overcome the bond resistance and withdraw the bar, certain relations exist between the amount of movement of the bar and the bond stresses developed.

3.3.1 Bond stress versus slip

The relationship between bond stress and the relative slippage between a steel bar and concrete, is of fundamental importance in predicting the complex interaction between the two materials. A statistically acceptable, average “local bond” versus “local slip” relationship is available in the CEB-FIP Model code 1990. For monotonic loading, the bond stresses between concrete and reinforcing bar can be determined as a function of the relative displacement, with a path as shown in Figure 3.6. The first curved part refers to the stage in which the ribs penetrate into the mortar matrix, characterised by local crushing. The horizontal level occurs only for confined concrete, referring to advanced crushing and shearing off of the concrete between the ribs. The decreasing branch refers to the reduction of bond resistance due to the occurrence of splitting cracks along the bars (CEB 1993).

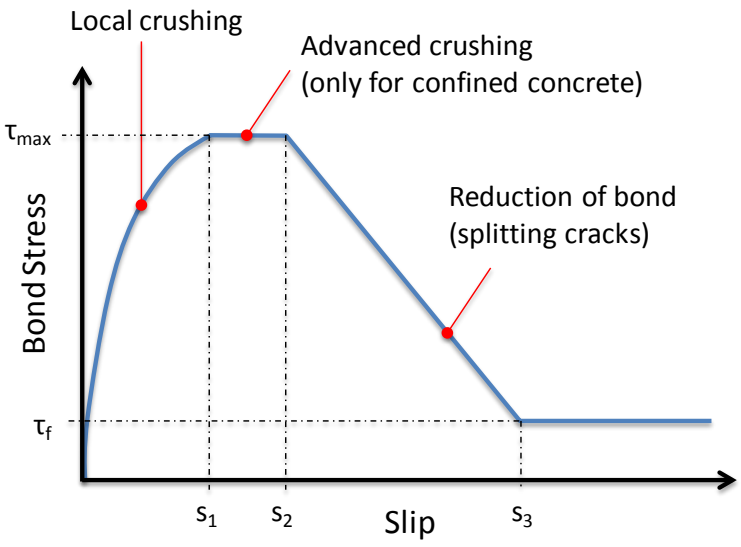

Figure 3.6 Bond stress-slip relationship

The typical testing arrangement that is used to evaluate bond properties is the so called pull-out test (Figure 3.7). The recommendations set out by RILEM/CEB/FIP (1983) are widely accepted and treated as the local bond law, however a survey of published literature on bond shows a bewildering variety of test methods and forms of test specimen (Cairns et al. 2003; Shima et al. 1987).

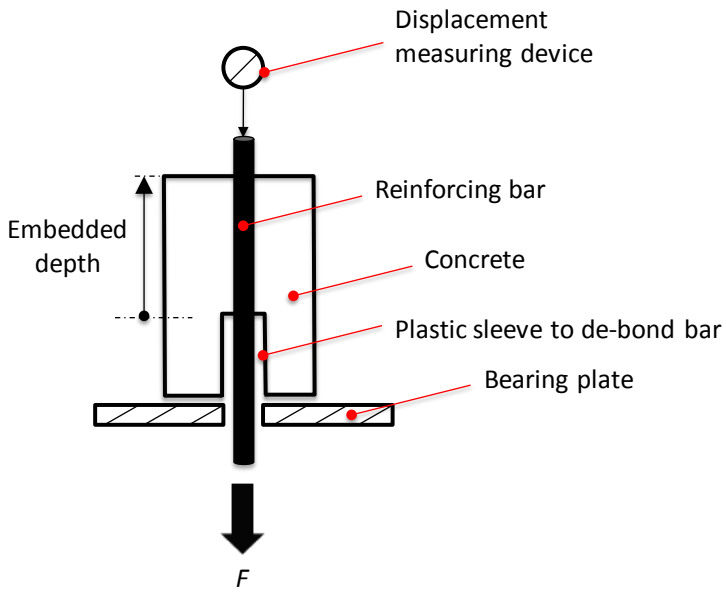

Figure 3.7 Pull-out test set-up

In the pull-out test, a bar is incorporated in a concrete block along a defined length, and is strained at one end by a tensile force, while the other end remains unstressed. The relation between the tensile force and the relative displacement (slip) between steel and concrete is measured. The specimen is loaded progressively up to bond failure or the splitting of the concrete block, hence the relation between tensile force and slip. Tests may be carried out under load control (N/sec) however, to detect descending branches, tests should be carried out under displacement control (mm/s) (Fabbrocino et al. 2005). The embedded depth is used to evaluate the bond stress, which is normally calculated assuming a constant distribution of stress along the rebar, as per Equation 3-2 where τ , F , A_{emb} , d_{emb} , and d_b is the bond stress, tensile force, embedded surface area of the rebar, embedded depth of the rebar, and diameter of the rebar, respectively.

$$\tau = \frac{F}{A_{emb}} = \frac{F}{\pi \ d_{emb} \ d_b} \qquad \text{Equation 3-2}$$

With the use of pull-out tests, many researchers have studied the influence that different parameters have on bond behaviour, relating to the stress conditions normally encountered at beam ends. The key findings of recent studies that are considered to be relevant to this research work are summarised below. The results refer to pull-out tests under monotonic loading conditions, and the review is expected to reveal the key parameters that may influence the bond mechanism of the *EHB* component.

3.3.2 Effect of level of concrete confinement

Confinement of concrete results in a modification of the effective stress-strain relationship; higher strength and higher critical strains are achieved (CEN 2004). In reinforced concrete members, confinement can be generated by adequately closed links or cross-ties, which reach the plastic condition due to lateral extension of the concrete. Experiments indicate that the confinement effect offered by a steel tube also increases the ductility of the concrete core in a square or rectangular concrete

filled steel tube beam-column (Liang 2009). A general stress-strain curve depicted in Figure 3.8 illustrates the material behaviour of confined and unconfined concrete.

Bond tests by Eligehausen et al. (1982) demonstrated that with increased confinement, maximum bond resistance and ultimate frictional bond resistance are increased. The influence of increased concrete confinement on bond has been found significant also in improving ductility, especially after reaching the maximum bond strength (Alavi-Fard et al. 2004). With respect to the failure mechanism, it was found that unconfined specimens fail by concrete splitting, whereas confined specimens tend to lead to pull-out failures, allowing bond to develop, attributed purely to the different material behaviour.

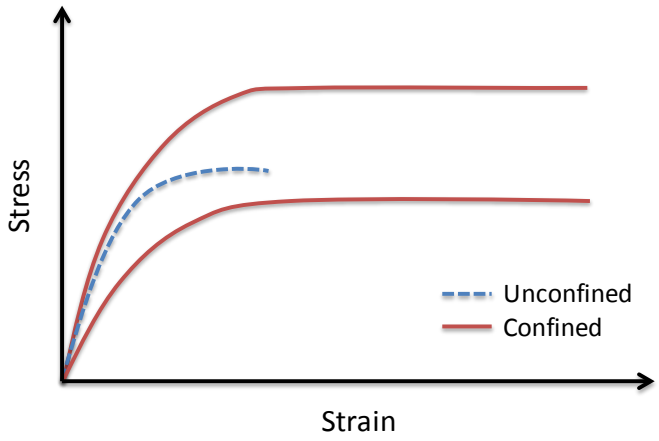

Figure 3.8 Stress-strain relationship for confined & unconfined concrete

The *EHB* blind-bolt component is anchored in confined concrete, provided by the structural steel hollow section that encloses the concrete infill. The aforesaid clearly emphasizes the importance of maintaining this level of confinement within the experimental set-up of this investigation. The testing set-up should represent the actual conditions that the structural component is subject to in real conditions. This is representative, and will also eliminate any premature splitting concrete failures in consideration of evaluating mechanism 3.

3.3.3 Effect of bar type

Two main types of steel bars are used to reinforce concrete, plain round and deformed bars. Deformed bars relate the most to this study because of their similar geometry; the steel bar having ribs along its length and the bolt having threads along its shank. Tests report that bond resistance of plain rebars is much lower than that of deformed rebars (Kankam 2003; Mo et al. 1996). In general, bond resistance between concrete and plain round bars develops initially due to adhesion and then due to sliding resistance between the steel and concrete. Conversely, the average bond stress developed by ribbed bars is primarily due to bearing of the ribs against concrete. Since plain rebars have no deformations, it is expected that no bearing component of the bond in plain rebars exist. Thus, lower bond strength is expected for plain rebars. This justifies the use of a fully threaded shank within the *EHB* system; to improve the bond characteristics of the component.

3.3.4 Effect of bar size

Several investigations have been carried out to determine the effect on bond resistance for different bar diameters, most being in good agreement. An extensive experimental programme by Eligehausen et al. (1982) concluded that the maximum bond resistance decreased slightly with the increasing bar diameter. However, the frictional bond resistance was not influenced significantly by the different bar diameter. Other test specimens showed that a smaller bar diameter develops the greatest average bond stress at all values of slip (Kankam 2003). More recently, Alavi-Fard et al. (2004) investigated such an influence in consideration of embedment in high strength concrete (70 - 95MPa). Tests once again indicated that bond resistance was higher for the specimens with smaller bar diameter than for the large one. Hence a justification to investigate different bolt sizes in consideration of mechanism 3 of the *EHB* component in this study.

3.3.5 Effect of concrete compressive strength

The bond resistance of a reinforcing steel bar is known to be related to the compressive strength of concrete. Codes state that design bond stress is

proportional to the square root of the compressive strength (BSI 1997). Tests have shown that bond properties between steel bars and concrete are improved by increasing the compressive strength of the concrete (Dancygier et al. 2009; Kankam 2003; Mo et al. 1996). The strength of concrete is expected to become significant once bearing stresses due to the wedging of the bar lugs are generated.

The bond stress-slip curve of high strength concrete has been characterised by a sharp drop of the stress at the beginning of the descending portion of the bond stress-slip curve. The behaviour of high strength concrete has been found as brittle in comparison with normal strength concrete. Nevertheless, bond resistance in high strength concrete has been found greater than the corresponding one in normal strength concrete (Alavi-Fard et al. 2004).

Similarly, Ahmed et al. (2007) reported that when the compressive strength of concrete is increased, bond resistance increases and relative slippage between steel and concrete decreases for the same embedded length and same bar diameter. This decrease in slippage was attributed to increased compressive strength of concrete keys which offer greater bearing resistance against slippage. The necessity of including concrete compressive strength as a parameter in this study has been clearly justified by the aforementioned.

3.3.6 Effect of embedded depth

Ahmed at el. (2007) compared bond conditions generated between deformed bars and concrete, in high strength concrete and normal strength concrete. In high strength concrete, it was found that by increasing the embedment depth of the bar, slippage also increases. This was not the case however when embedded in normal strength concrete.

3.3.7 Effect of loading rate

The bond stress-slip relationship is known to be influenced by the rate of slip increase (Eligehausen et al. 1982). The investigation of Mo et al. (1996) found that loading rates (N/s) applied in pull-out tests have insignificant influence on the maximum bond stress however the failure slip increases with increased loading

rate. Alavi-Fard et al. (2004) reported that for tests carried out under different displacement rates (mm/s), the bond stress-slip curve patterns were similar, however slips increased with increasing rate. The maximum bond strength was again seen to not be affected. More recently, Ožbolt et al. (2006) reported that in static analysis, the failure mode of bond is independent of the loading rate.

3.4 Mechanical anchorage

So far some literature about bond between concrete and reinforcing steel has been reviewed. The contribution of mechanism 3 however is also comprised of a bearing (anchorage) mechanism. Because of the similarities in mechanics, it thus seems pertinent to review relevant published design guidance and existing equations for anchors used in concrete. The findings of topics related to anchorage of headed reinforcement are also presented.

3.4.1 Design of fastenings to concrete

The demand for more flexibility in the planning, design, and strengthening of concrete structures has resulted in an increased use of metallic anchoring systems. The behaviour of fastenings to concrete has received much attention, and the work is well documented in the form of state-or-the-art reports and design guides. The most advanced knowledge regarding anchorage to concrete is embodied in the CEB (1994; 1997) publication, and in Appendix D of ACI 318 (ACI 2008b). Fastenings must be designed for all load directions taking into account different failure modes. The mechanical anchorage of the *EHB* component in tension can be related to cast-in situ anchors such as headed bolts subject to tension. Shear as well as combined tension and shear loading is out of the scope of this research, therefore the following review is limited to tensile loading. Depending on the concrete strength, the embedment depth, the edge distance, and the steel strength of the anchor, cast-in mechanical anchors under tension loading exhibit different failure modes. Generally five failure types were experimentally identified, depicted in Figure 3.9, each with very different load-displacement patterns.

Ductile failures are failure by yielding of the fastening device or system fastened to the concrete before any breakout of concrete occurs. Under conditions that the steel material is sufficiently ductile and the length of the fastener over which inelastic steel strains appear is large enough, and assuming that the concrete base material does not fail, a ductile steel failure will occur. The design against steel failure is rather straightforward, where the nominal strength of a fastener in tension is evaluated by calculations based on the properties of the fastener material and the physical dimensions of the fastener, as in Equation 3-3 where N_{sa} is the steel strength, A_s is the effective cross sectional area, and f_{ub} is the ultimate stress, in consideration of a single fastener.

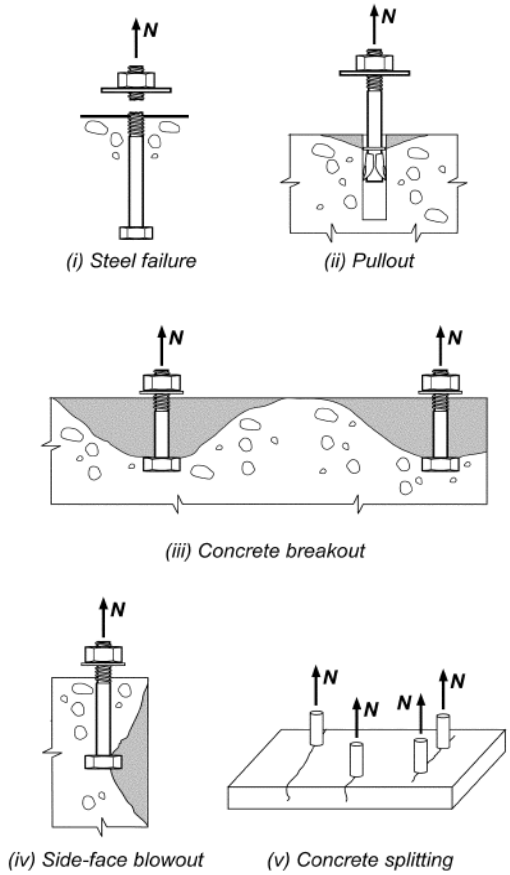

Figure 3.9 Tensile loading failure modes for anchors (ACI 2008b)

$$N_{sa} = A_s f_{ub} \qquad \textbf{Equation 3-3}$$

Pullout failure is characterised by crushing of concrete above the anchor head, followed by the formation of a shallow concrete cone as the head of the anchor approaches the concrete surface. Currently, there is no established procedure to determine theoretically the ultimate load expected of fastenings in the pullout type of failure. The pullout strength (N_{pn}) in tension of a single headed bolt is however recommended to not exceed a value that corresponds to the load at which crushing of the concrete occurs due to bearing of the anchor head, calculated as in Equation 3-4, where $\psi_{c,P}$ is a modification factor taken as 1.0 for cracked concrete at service load levels or 1.4 for un-cracked, A_{brg} is the net bearing area of the anchor head, and f_c' is the cylinder compressive strength of concrete (ACI 2008b). Local crushing of the concrete greatly reduces the stiffness of the connection, and generally will be the beginning of a pullout failure.

$$N_{pn} = \psi_{c,P}\, N_p = \psi_{c,P}\, 8\, A_{brg}\, f_c' \qquad \textbf{Equation 3-4}$$

Brittle failures are failure by concrete breakout or splitting of the structural concrete member before yielding of the fastener or fastened element. For non ductile fasteners and cases where the concrete capacity is less than the fastener device capacity, a brittle failure will occur. It is not yet possible to determine theoretically the failure load to be expected in the splitting type of failure, but splitting failure due to loading can be avoided by providing splitting reinforcement, and by complying with minimum values for edge distances, spacing, and member depth. Similarly, verification of blow-out failure is not required by specifying minimum edge distance in all directions.

Concrete breakout failure though is a very important practical design case, because many fasteners are made such that a concrete failure will occur before yielding of steel. Two major design methods are available for the common case of concrete breakout failure; the American Concrete Institute (ACI) 349 cone method (ACI 2008a), and the concrete capacity design (CCD) method (Fuchs et al. 1995).

The cone method was developed by Cannon et al. (1981) on the basis of very limited test data, that was later incorporated in ACI 349. Figure 3.10 (a) shows concrete breakout for single anchors under tension, idealised according to ACI 349. ACI Committee 349 is concerned with nuclear-related structures, and because of concern with nuclear safety, the philosophy of ACI 349 is to design ductile fastenings. To obtain a limit to guard against brittle concrete failure, the cone model was incorporated. The method assumes a concrete cone, with an angle of 45^{o} between failure surface and anchor axis, and constant concrete tensile stress acting on the projected area of the failure cone. For a single anchor unlimited by edge influences or overlapping cones, under tension loading, the concrete capacity N_{cb}, is calculated as in Equation 3-5, where f_{cu}, d_{emb}, and d_h is the concrete compressive strength measured on cubes, the effective embedment, and major anchor head diameter, respectively.

$$N_{cb} = 0.96\sqrt{f_{cu}}\, d_{emb}^2 \left(1 + \frac{d_h}{d_{emb}}\right) \qquad \textbf{Equation 3-5}$$

According to the CCD method that was mainly developed at the University of Stuttgart, the concrete capacity of a single fastening is determined assuming an inclination of about 35^{o}, and a four sided pyramid shaped failure surface rather than a coned shape, as shown in Figure 3.10 (b). This corresponded to widespread observations that the horizontal extent of the failure surface is about three times the effective embedment, d_{emb}. Fuchs et al. (1995) proposed Equation 3-6 to predict concrete capacity, where a factor k_{nc} is recommended at 15.5 in consideration of cast-in situ headed anchor bolts.

$$N_{cb} = k_{nc}\sqrt{f_{cu}}\, d_{emb}^{1.5} \qquad \textbf{Equation 3-6}$$

Comparison of the failure loads predicted by both, ACI 349 and CCD methods with the results of extensive testing performed over the last decade indicates that, the

CCD method is able to predict concrete breakout strength with consistent accuracy in different design situations, while the ACI 349 cone method may yield conservative results in certain conditions, and may be unconservative in other applications (Eligehausen et al. 1998). This discrepancy was attributed to the fact that the cone method assumes the failure load to be proportional to a failure area that increases with the square of the embedment depth, whereas the CCD method takes size effect into account and assumes that the failure load is proportional to the embedment depth to the 1.5 power. The design guide published by CEB (1997), the ACI 318 code for structural concrete (ACI 2008b), and the European Standard draft for development guide of fastenings (CEN/TS 2009) are all based on the CCD method.

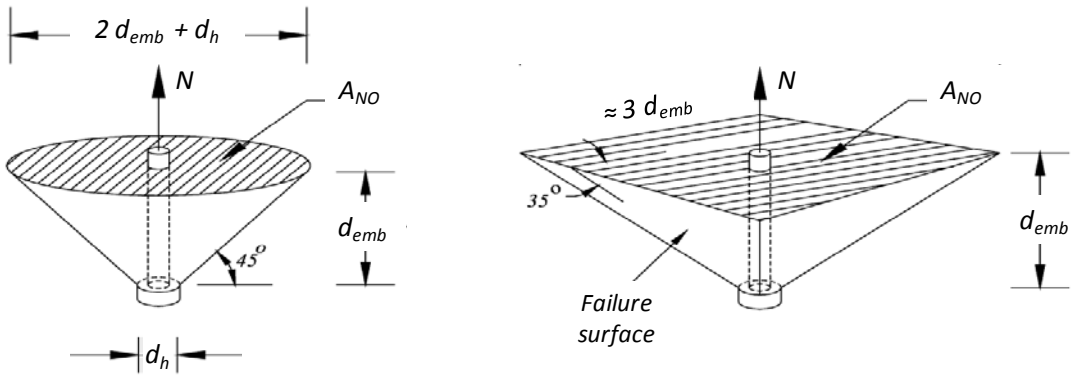

(a) (b)

Figure 3.10 (a) cone model, (b) idealised failure pyramid according to CCD

3.4.2 Use of headed reinforcement in beam-column joints

Another structural component that is implemented in reinforced concrete (*RC*) structures and that can be related to the mechanical anchorage of the *EHB* component is headed reinforcement. This section discusses the current state-of-the-art of headed bar technology, available research is reviewed, and code provisions are outlined.

Headed reinforcing bars principally evolved from headed stud anchors in view of developing an alternative to conventional hooked rebars for anchorage to concrete.

Research mostly initiated with interest for application in *RC* structures that involve large rebar sizes, which can be difficult to bend to form end hooks, as well as to reduce reinforcement in congested zones, particularly where joints form, that complicates concrete placement/compaction and makes construction difficult. Experimentalists identified the obvious advantages if headed rebars could replace standard hooks, however extensive testing was required to demonstrate the feasibility of using headed bars within *RC* joints. Headed bars are created by the attachment of a plate or nut to the end of a reinforcing bar to provide a large bearing area that can help anchor the tensile force in the bar. The tensile force in the bar can be anchored by a combination of bearing on the ribs and on the head, as illustrated in Figure 3.11.

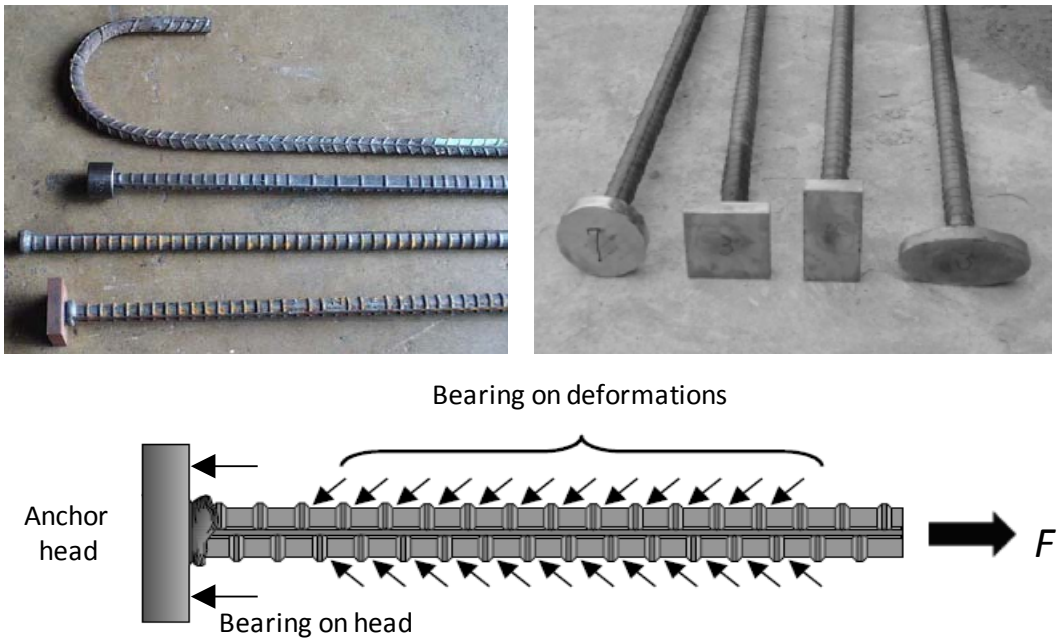

Figure 3.11 Headed rebar anchorage (Park et al. 2003; Thompson et al. 2002)

The Electric Railway Improvement Company (ERICO) and Headed Reinforcement Corp (HRC) are currently the primary suppliers of headed bars. The products of *ERICO* and *HRC* differentiate by means of the shape of the anchor head, and the attachment technique among anchor head and rebar. The principal differences between the mechanical anchorage of the *EHB* component and that of headed

reinforcement are the bolt threads in contrast with a deformed rebar; the level of concrete confinement offered by tube walls in contrary with concrete base materials with/without transverse reinforcement; free edge effects; the amount bearing area provided by the end anchor heads; and possible embedment depths - known to affect concrete breakout strength - which are limited (if not fixed) by the size of the hollow section with regards to the *EHB* component.

The available research on headed bars can be separated into two categories; application studies (Chun et al. 2007; Chun et al. 2009; Wallace 1998) and general behaviour studies. For the most part, the general studies entail research on development length or anchorage capacity, as well as investigations of the mechanics of the headed bars under idealised conditions. Only some of the research that was deemed to study general behavioural trends is reviewed in more detail within this section.

Twenty-one shallow and 123 deep embedment headed bar pullout tests were conducted by DeVries et al. (1999) in view of proposing comprehensive design recommendations for the use of headed bars in a wide range of applications. Shallow embedment tests were somewhat arbitrarily distinguished from deep embedment tests by having a ratio of embedment depth to bar clear cover less than 5. Among these tests, the primary variables were concrete strength, embedment depth and edge distances. Also studied were the effects of transverse reinforcement, development length, and head size. DeVries et al. (1999) determined that the primary variables upon which a design should be based were edge distance, net head bearing area, and the concrete compressive strength.

A total of 48 pull-out tests were performed by Choi at el. (2002) to evaluate pullout strengths and load-displacement behaviours of headed bars in comparison with hooked bars. Test variables included concrete strengths, reinforcing bar diameters, embedment depths, edge conditions, column reinforcement, and single versus multiple bar pullout. The net areas (A_{brg}) and thickness of the heads were $3A_b$ and $1d_b$ respectively. The results revealed that the heads effectively provided the pullout resistances of the deformed bars in tension (bar yield prior to failure), and

that the load-displacement behaviours were similar between the 90^{o} hooks and the headed reinforcement.

Park et el. (2003) conducted pull-out tests to investigate the influence of the shape and thickness of the head on the pullout behaviour of bars anchored in this way. As anticipated, it was found that for an identical diameter of reinforcing bar, by increasing the net area of the anchor head, ultimate capacity is enhanced but increasing thickness is not directly associated with ultimate capacity.

The Texas Department of Transportation funded a program to study the feasibility of using headed reinforcement in bridge structures (Thompson et al. 2006; Thompson et al. 2005). With respect to the mechanics of headed anchorage, it was found that the anchorage of headed bars was mobilised in two stages; in the first stage anchorage was carried almost entirely by bond stress, which peaked as the first stage ended. In the second stage, as bond began to deteriorate, stress in the bar was transferred to the anchor head. Throughout the second stage, bond declined and head bearing increased. The second stage ended with yielding of the bar or bearing failure of the concrete at the head. The capacity of headed bars was found to be comprised of peak bearing capacity plus some contribution from reduced bond along the bar between the head and the point of peak bar stress.

Further pull-out tests by Thomas et al. (2010) were conducted with test variables involving the head size, shape, and head attaching technique (welding versus threading). The results revealed that all types of heads and head-attaching techniques performed almost equally well with equivalent hooked bars, demonstrating that small-headed bars ($A_{brg}/A_b < 4$) can be effectively anchored in exterior beam-column joints.

Authors have stated that headed bar anchorage behaves as hooked bar anchorage. Despite the increased use of headed reinforcement, there had been no design provisions dealing with headed bars until 2008. The effort of ongoing research in the field of headed bars has now been formulated into design codes. Current specifications for the dimensions of headed bars, manufacture technology and qualifying testing (quality control) are found in ASTM A970 (2009). Most recently, ACI published building code requirements (ACI 2008b) defining the development of

headed and mechanically deformed bars in tension (Section 12.6). The recommended development length l_{dt} is the length of embedded reinforcement that is required to develop the design strength of reinforcement at a critical section, as in Equation 3-7, where ψ_e is a modification factor taken as 1.2 for epoxy-coated reinforcement and 1.0 for other cases, f_y is the specified yield strength of the reinforcing bar, d_b is the bar diameter, and f_c' is the cylinder compressive strength of concrete.

$$l_{dt} = \frac{0.19\,\psi_e\,f_y\,d_b}{\sqrt{f_c}'} \qquad \text{Equation 3-7}$$

Equation 3-7 results in a development length of approximately 80% of that required for hooked bars by ACI 318-08. Although it has been observed that the head size influences anchorage capacity, Equation 3-7 is not a function of the head size. Rather, it is indirectly accounted for as one of the minimum requirements in ACI 318-08, where acceptable criteria for material, geometrical, and reinforcing properties (for example, head size, clear cover, and spacing) are set forth. A minimum ratio of A_{brg}/A_b = 4 is specified and the concrete material is restricted to normal weight mixes. Experimental research has demonstrated that headed bars with head sizes of a ratio less than 4 can ensure anchorage both in the elastic and inelastic deformation ranges, but their performance is not accurately represented by Equation 3-7. ACI 318-08 does permit the use of headed bars with ratios of A_{brg}/A_b < 4 however adequacy of anchorage should be determined by testing and the results must be approved by building official. The geometrical properties of the end anchor nut of the *EHB* component falls within the category of ratios less than 4.

3.5 Modified *EHB* component end anchor head

The current mechanical anchorage system of the *EHB* component employs a standard bolting hexagon nut (Figure 3.12). The subject of this section involves a closer examination of this system, and modifications that can be easily accommodated in its design are identified which could allow for practical and

performance enhancements. Firstly, to install the current system, the blind-bolt along with the hexagon nut attached at its end is inserted through the clearance bolt hole, the bolt is tightened to the recommended torque, and thereafter concrete is casted within the hollow section. Previous investigations that were performed at the University of Nottingham (reported in section 2.3) recommend the application of a bonding adhesive (lock tight glue) between the threaded bolt and nut to ensure that the hexagon nut remains in its original position, unaffected by concrete placement and vibration induced in its compaction process. The application of such an adhesive is indeed required because without it, the standard nut can freely ride along or off the threaded shank, during or even prior to the placement of the concrete infill, that could result in highly undesirable anchorage characteristics for the component.

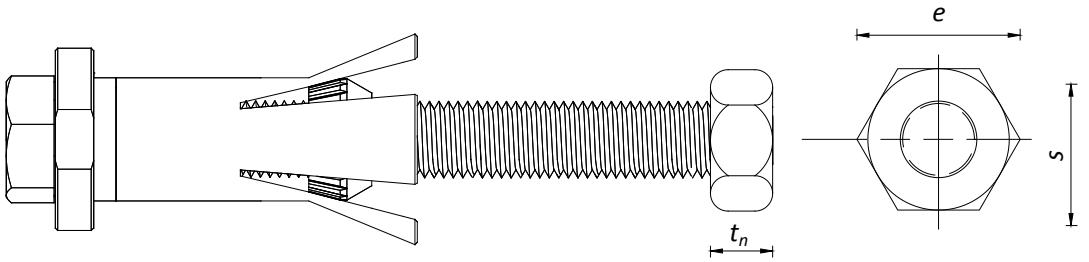

Figure 3.12 *EHB* current mechanical anchorage system using standard hexagon nut

Secondly, in reference to the design of fastenings in concrete (section 3.4.1) and in particular to Equation 3-4, it has been stated that the pullout resistance of such mechanical anchorage systems is directly proportional to the net bearing area (A_{brg}) provided at the contact interface between concrete and end anchor head. By increasing A_{brg}, the load required to crush local concrete in front of the anchor head also increases. This suggests that if it is possible to increase the bearing area of that provided by the current system, improvements in the anchorage behaviour of the *EHB* component may be achieved.

To enhance the practicality, safe usage and performance of the *EHB* component, it is felt that there is a need for a revised, easily adaptable end anchor head. In consideration of the installation procedure, possible performance enhancements with increased bearing area, and understanding that the current system could

involve undesirable movements of its anchorage hexagon nut, a modified end anchor head is proposed herein for employment in the *EHB* component.

3.5.1 Head shape

The shape and size of the *EHB* component end anchor head is governed by the clearance bolt hole. To determine the type of shape that could provide the maximum net bearing area, different shapes were investigated in consideration of their unrestricted insertion through the clearance bolt hole (Figure 3.13). The clearance hole involves a 2mm construction tolerance with respect to the outer sleeve diameter of the *EHB*, giving 28 and 35mm for the *EHB16* and *EHB20*, respectively. In consideration of 16 and 20mm *EHB* bolt sizes, Table 3.1 summarises the values used to compare the current hexagon head shape with the square and circular shapes in view of identifying/quantifying the maximum achievable A_{brg} among them; d_b is the bolt diameter, d_h is the major diameter of the circular head, t_h is the thickness of the circular/square head, t_n is the thickness of the hexagon nut, A_g is the gross bearing area (represented by whole head shape area), A_b is the bolt cross sectional area taken as $A_b = \pi\ d_b^2 / 4$, and the net bearing area is calculated by subtracting the area A_b from the gross bearing area, i.e. $A_{brg} = A_g - A_b$.

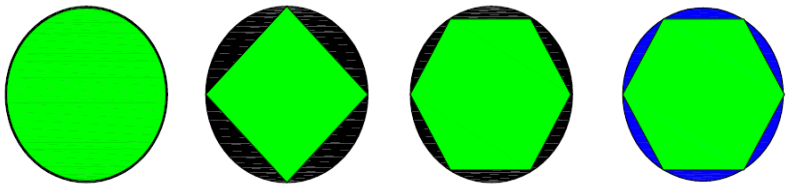

(a) (b) (c) (d)

Figure 3.13 Possible head shapes (a) circular, (b) square, (c) hexagon, (d) hexagon vs circular

As expected, it is found that the maximum ratio of A_{brg} to A_b is achieved when a circular shape is employed. This ratio is increased by 0.5 in comparison with that of the current hexagon, which according to Equation 3-4 could correspond to a 30% increase in pullout resistance. The space required to accommodate a circular head in the *EHB* system is readily available within the clearance hole, and currently this

space is not being utilised as it should. It is therefore proposed to modify and replace the current hexagon nut with a circular shaped anchor head for the *EHB* component, which is to be employed throughout this research work.

Table 3.1 Determination of maximum A_{brg} under different head shapes

Head shape	d_b (mm)	d_h (mm)	t_h (mm)	t_n (mm)	Width across flats , e (mm)	Width across corners , s (mm)	A_g (mm^2)	A_{brg}/A_b
Hexagon	16	N/A	N/A	13*	24.0*	27.7*	498	1.5
Circular	16	27.5	16	N/A	N/A	N/A	594	2.0
Square	16	N/A	16	N/A	19.8	28.0	392	1.0
Hexagon	20	N/A	N/A	16*	30.0*	34.6*	778	1.5
Circular	20	34.5	20	N/A	N/A	N/A	935	2.0
Square	20	N/A	20	N/A	24.7	35.0	613	1.0

*: Values of t_n , e & s for hexagon nut were extracted from BS 3692:2001 (BSI 2001a).

3.5.2 Head thickness and attaching technique

Having selected the shape of the revised end anchor head, it remains to decide on the thickness of the head, and the attaching technique between threaded bolt and head in consideration of eliminating the free sliding along the shank. With respect to headed reinforcement, ASTM A970 (2009) permits the use of threaded head-to-bar connections since 2004, in addition to welded or forged connections as depicted in Figure 3.14. Such techniques would not be practical to adopt for the connection of that required in the *EHB* system due to the complexities involved in their manufacture process. It is proposed to maintain the current threaded technique that does not require any modifications to the geometry of the threaded bolt, such as tapering the shank to form a connection, or obstructions. To overcome the issue of free sliding in a practical manner, the circular head can easily involve a solid extension at its end that restricts such movements. With a total head thickness of $1d_b$, it is possible to provide a thread engagement length equal to that which a standard hexagon nut would provide, while the remainder thickness is used to form the solid end (Figure 3.15). This corresponds to a solid extension of 3 and 4mm for 16 and 20mm *EHB* systems, respectively. The coarse pitch thread profile and mechanical properties of the modified head should conform to BS 3692:2001,

sized as summarised in Table 3.1. The manufactured circular head prototype is shown in Figure 3.16 in comparison with the standard hexagon nut.

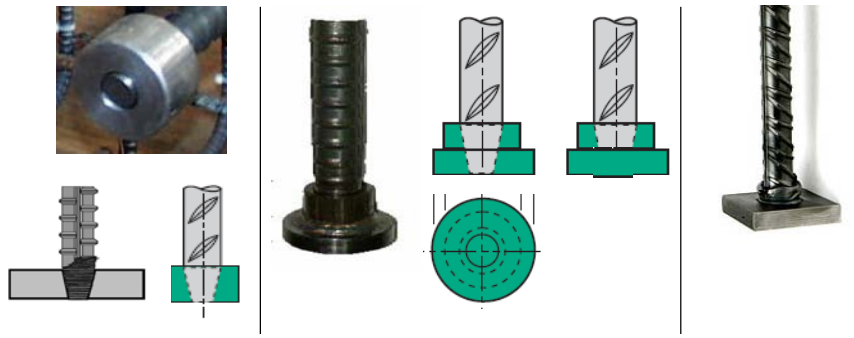

(a) Tapered thread (no obstructions)

(b) Tapered / flush thread (with obstruction)

(c) Forged (friction welded)

Figure 3.14 Headed reinforcement: common head-to-bar connections

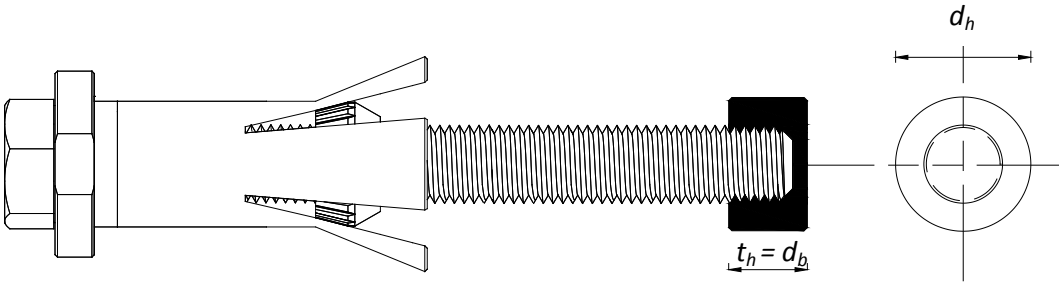

Figure 3.15 Modified circular end anchor head

Figure 3.16 *EHB* anchor head prototype in comparison with current system

3.5.3 Thread stripping strength

The amount of tension created in a bolt depends not only on the strength of its body, but also on the shear strength of its threads. When designing a standard bolting nut it is required to ensure that the thread engagement length will be great enough to allow the strength of the bolt to develop. Such requirements can be verified by performing thread strip tensile experiments. The testing carried out to verify the adequacy of the proposed anchor head prototype is reported herein.

The fixture and setup of the test specimens as well as the test results are shown in Figure 3.17. The tested circular head was hand tightened at the fixed end (BSI 2005), and the tensile load was applied at 5mm/min up to failure within a Zwick 1484, 200kN capacity testing rig. To ensure that the load was applied axially, and to reduce occurrences of off-center loading and undesired bending moments, a 3-bolt loading frame was employed. The results reveal that the proposed attaching technique between the prototype circular head and the threaded bolt is adequate in developing the required stresses for application in concrete anchorage as the threaded connection may develop safely the yield strength of the bolt prior to any thread stripping.

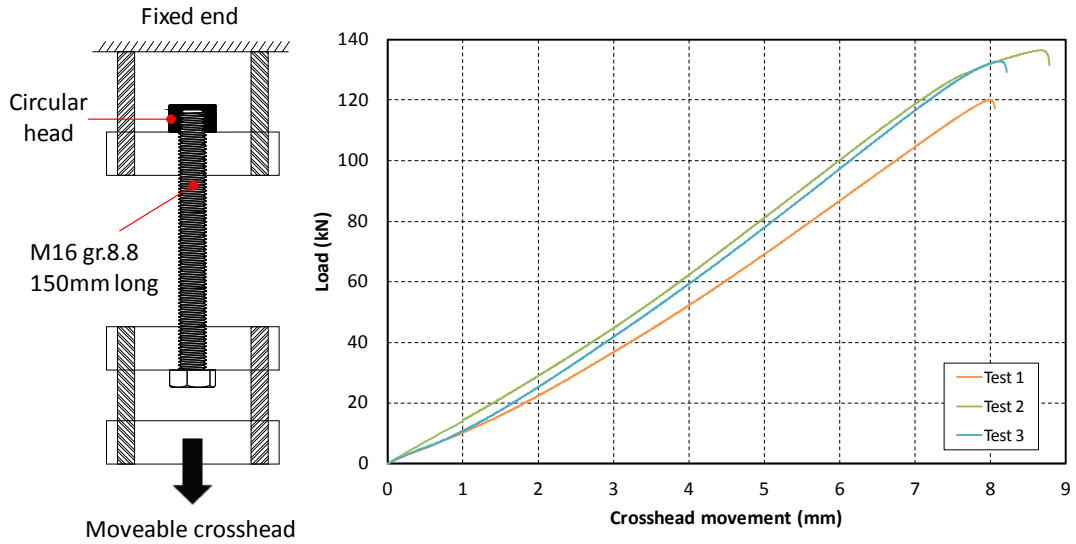

Figure 3.17 Modified circular anchor head thread strength testing

3.6 Qualitative testing of *EHB* bond & anchorage mechanism

This section discusses the results of exploratory testing which assisted towards the development of the research methodology of this work. With a focus on the evaluation of the bond and anchorage mechanism of the *EHB* component, the influence of the level of concrete confinement provided in the proposed testing set-up is reported. Additionally, the contribution of the end anchor head with respect to the bond and anchorage mechanism is presented.

3.6.1 Exploratory pull-out testing

To investigate merely the behaviour of the bond and anchorage mechanism of the *EHB* component, several exploratory pull-out tests were performed. The principal aim of the tests was to establish a suitable, adequate experimental arrangement that can be adopted in the quantitative testing part of this research. The objectives of the exploratory programme involve qualitative analysis of the effect of level of concrete confinement present in the testing set-up, and evaluation of the contribution of the component's end anchor head.

Test specimen details are summarised in Table 3.2 and the various configurations are schematically illustrated in Figure 3.18. To investigate concrete confinement, pull-out tests were performed on fasteners that were embedded in reinforced concrete blocks (unconfined specimens), and on fasteners that were casted within a concrete-filled tube (confined specimens). Because the exploratory work was concerned with the evaluation of the component's bond and anchorage mechanism alone, the test set-up was designed in a manner so that the expanding sleeves mechanism was eliminated. This was achieved by providing a larger bolt hole (95mm) than that specified for the particular size of blind-bolt (28mm). Specimens were assembled by first tightening together a circular plate and loading ring with the *EHB*. The 95mm clearance diameter would facilitate this pre-tightened assembly, which was then clamped to the tube or concrete block formwork, and concrete was poured into the sections. Such an arrangement enforces the applied load to be resisted by the concrete embedded elements only, while having the expanding sleeves also in contact with the concrete infill. For reliability, two

specimens were tested on the same day, for each test, and the compressive strength of concrete (f_{cu}) on the day of testing is reported in Table 3.2, as determined by water cured cubes.

Table 3.2 Test specimen details

Specimen index	d_b (mm)	Shank length (mm)	Bolt grade	f_{cu} (N/mm^2)	Remarks
EHB16-150-8.8-C40-U	16	150	8.8	41.5	Unconfined
EHB16-150-8.8-C40-C	16	150	8.8	42.0	Confined
HB16-150-8.8-C40-C	16	150	8.8	38.8	Confined
HB16-100-8.8-C40-C	16	100	8.8	39.7	Confined

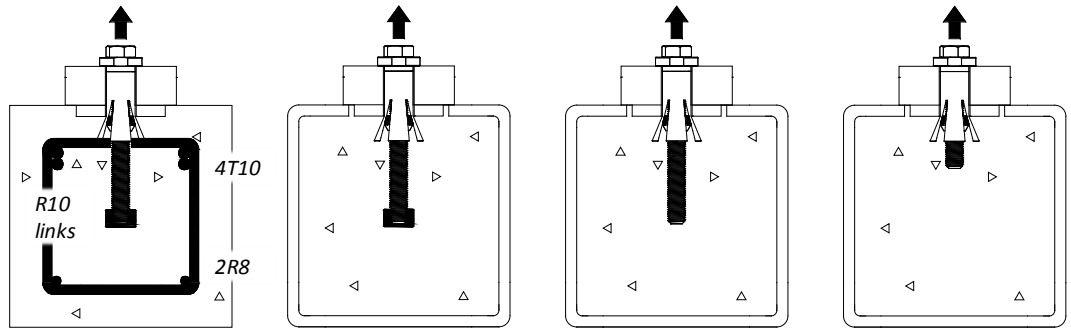

Figure 3.18 Cross sections of exploratory pull-out test specimens

The exploratory pull-out test set-up is shown in Figure 3.19. All samples were 500mm long and the set-up considers any additional resistance that may be provided by the reaction frame; the latter being satisfied by placing the frames at specified distances upon guidance given in BS 5080-1:1993 (BSI 1993). Tensile loading was applied monotonically, in displacement control at a rate of 0.0015mm/s, and the global displacement of the fastener was measured by placing a linear potentiometer directly on the component's bolt head.

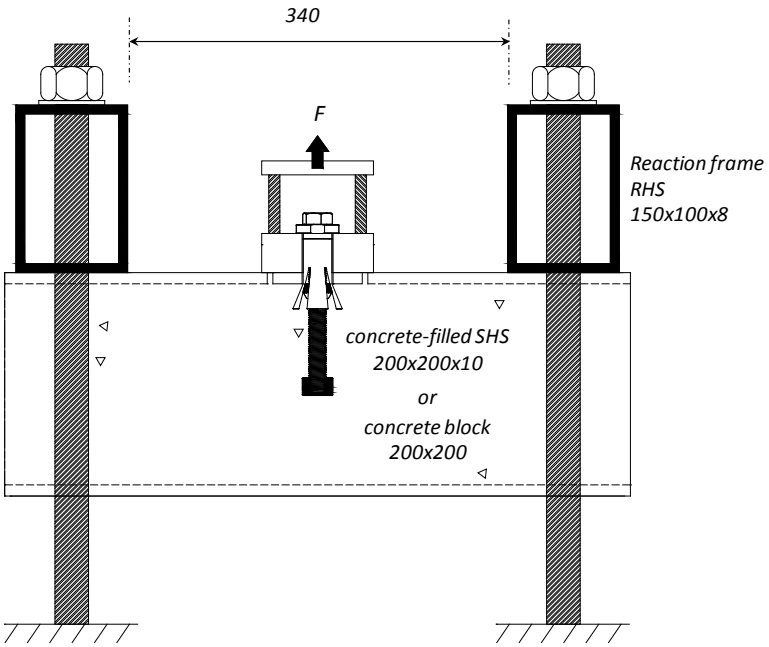

Figure 3.19 Exploratory pull-out test set-up

3.6.2 Effect of level of concrete confinement

The effect of level of concrete confinement present in the pull-out test sample is investigated by comparing unconfined with confined specimens. Unconfined relates to reinforced concrete blocks (specimen signed as EHB16-150-8.8-C40-U), whereas confined refers to concrete filled tubes (specimen signed as EHB16-150-8.8-C40-C) due to the high confinement offered by the tube walls to the concrete infill. The steel cage reinforcement in the unconfined specimens was designed in accordance to BS 8110-1:1997 (BSI 1997) - see Appendix A for detailed design and drawings.

The significant influence that the level of concrete confinement has on the force-displacement relationship is demonstrated in Figure 3.20. The results are the average of two tests that were found to be in good agreement. When the component was tested in confined concrete, significant improvements are observed. Up to 30kN, confinement does not affect much the behaviour; actually very similar characteristics are noticed with the non-confined components. Surpassing this load, the stiffness of the confined component was maintained. In contrast, the stiffness of the non-confined component decreased. The capacity and ductility characteristics are seen to be greatly influenced by confining the infill. A

closer examination of the failure surface of the specimens (Figure 3.21) indicates that the anchorage mechanism in the unconfined set-up did not fully develop due to concrete premature splitting and breakout. On the other hand, the confined specimens allowed the anchorage to develop, without exhibiting evident surface cracking. This justifies the importance of providing concrete confinement in the pull-out test set-up in consideration of evaluating the bond and anchorage mechanism. This confinement is required to eliminate premature splitting cracks in order to allow anchorage to develop for experimental measurements.

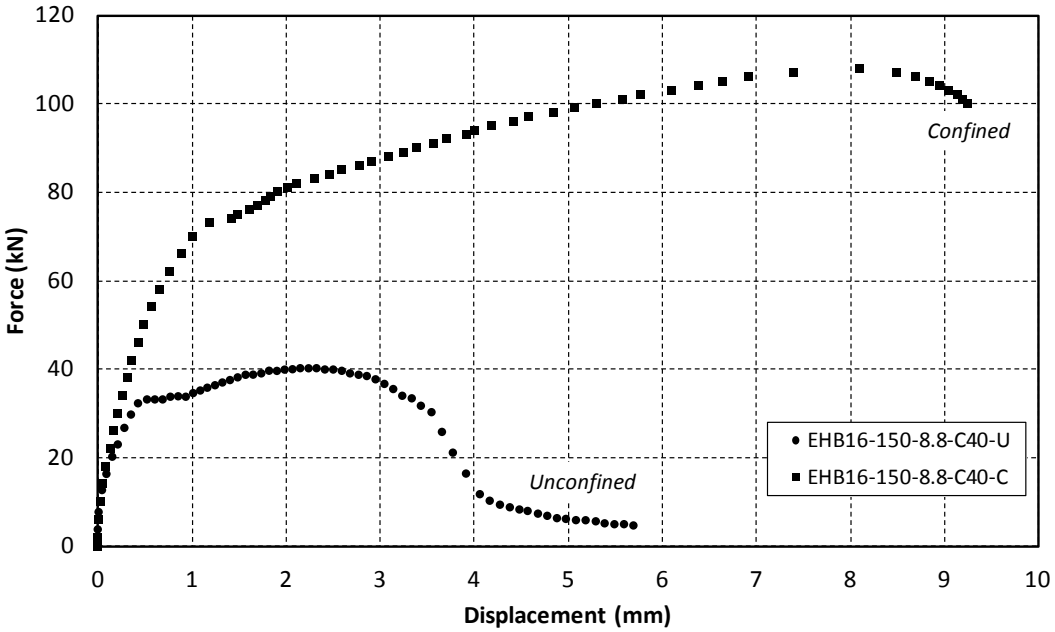

Figure 3.20 Effect of level of concrete confinement

(a) (b)

Figure 3.21 Specimens after testing (a) unconfined, (b) confined

3.6.3 Contribution of end anchor head

To evaluate the contribution of the end anchor head of the *EHB* component, tests were performed on fasteners with and without end anchor heads under confined concrete conditions. The *EHB* is compared with the commercially available *HB* of a standard and extended shank length to conclude on the contribution provided by the end head. These tests will indicate whether bond or mechanical anchorage is the principal contributor towards the mechanism's performance.

The pull-out test results are shown in Figure 3.22. It is found that the least resistance and ductility is provided by that of the *HB* assembly, with a standard shank length of 100mm. When the shank length is extended, the performance is slightly enhanced due to the increased bond resistance provided by the additional threaded length that is in contact with the concrete infill. However, the magnitude of improved performance by increasing bond is not comparable to that observed by the *EHB* which involves an anchor head. This demonstrates that the end anchor head is the main contributor in the load transfer within the bond and anchorage mechanism. It is thus proposed to measure bond and anchorage simultaneously for quantitative analysis of pull-out test results, rather than individual measurements.

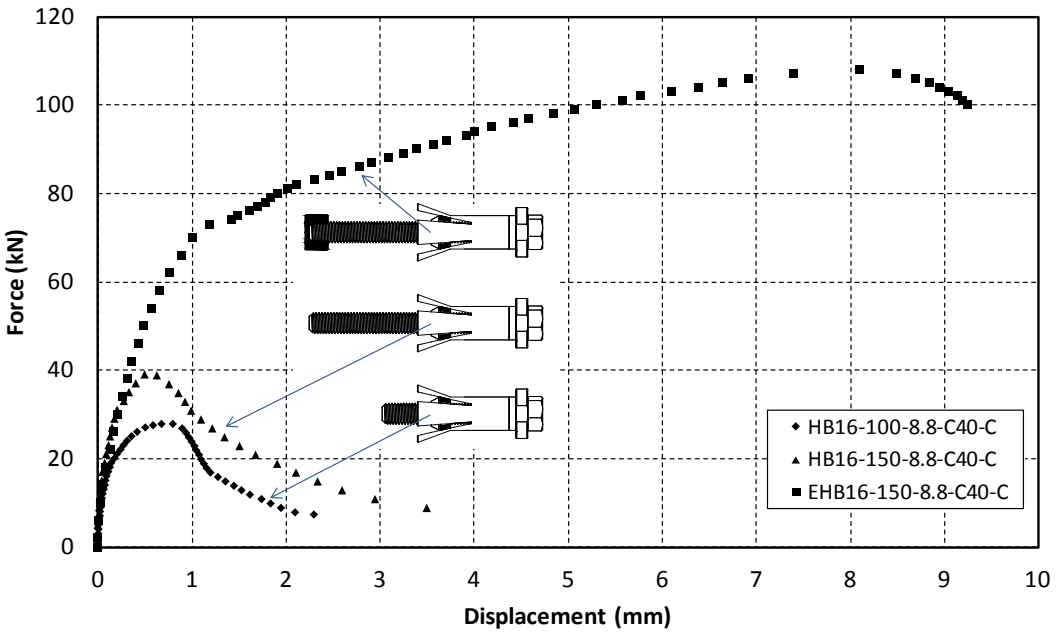

Figure 3.22 Contribution of end anchor head

3.7 Concluding remarks

This Chapter has concentrated on the elements that contribute to the overall deformability curve of the component "Bolts (*EHB*) in tension". Three individual mechanisms have been identified as those which contribute to the overall deformability, namely bolt elongation, expanding sleeves, and bond and anchorage. To identify the key parameters that may affect the response of the component in consideration of its individual mechanisms, relevant literature and existing knowledge was reviewed. On the basis of research and design publications, the review presented information about the pre-load that exists in the bolt elongation mechanism, and focus was given to bond and anchorage characteristics between reinforcing steel bars and concrete. Moreover, the general design procedure of fastenings to concrete under tension loading, and research in the field of headed reinforcement for application in beam-column joints was demonstrated. Such systems were reviewed as they carry similar mechanisms with the *EHB* component, when a particular type of loading is considered. The concluding remarks of the Chapter are summarised as follows:

Pre-load in blind-bolt system

- Bolt hole interferences and relaxation effects result in bolt pre-load losses.
- Relaxation of pre-loaded joints occurs over lifetime, but relaxation rates are much lower after twenty four hours of tightening. Short term relaxation can be monitored sufficiently over a period of five days in order to establish the residual pre-load in standard bolts.
- The effective length of the bolt which incurs elongation when tightening a bolt to induce a pre-load is dependent upon the total grip length in between the bolt head and end nut.
- The ratio between tightening torque and pre-load can be defined by a constant and the nominal diameter of the bolt. Data relating pre-load and tightening torque in the *HB* or *EHB* assembly is limited.
- Pre-load can be measured via direct and indirect techniques. Direct involve measurements of the actual clamping force, whereas indirect involve the translation of bolt elongation into bolt pre-load.

Bond stress-slip pull-out tests

- A review of published material on pull-out tests under monotonic loading conditions reveals that there is a lack of standardization in preparing test specimens when evaluating steel and concrete bond properties.
- Studies dedicated to investigate the effects that several parameters have on the bond-slip relationship between steel reinforcement and concrete revealed that those which affect most the bond resistance are: the size of the rebar, the compressive strength of concrete, the level of concrete confinement provided in the test, and the embedded length of the rebar.

Fastenings to concrete

- The basis for current, general anchorage provisions of embedded anchors subject to tension loading was reviewed. Relevant failure modes signify the importance of concrete confinement via its ability to resist concrete breakout and premature splitting failures.
- Equations are available to predict limits that guard against different failure modes, however they do not relate to stiffness characteristics. There is a scarce of equations that predict stiffness characteristics of fastenings to concrete due to the complexities involved in such measurements. Nevertheless, the available equations are primarily functions of the compressive strength of concrete and embedment length. This signifies that such parameters may also affect the response of the *EHB* component, and should thus be considered in its test matrix.

Headed steel reinforcement

- For applications of anchorage in concrete, headed bars are found to behave as hooked bars with embedment lengths of 75% of that required for a standard hook. Headed bars with geometrical properties of $A_{brg}/A_b < 4$ can be effectively anchored which is a category that the *EHB* component falls within. This demonstrates the efficient design of the *EHB* anchored blind-bolt component which adopts a headed anchor to represent its mechanical anchorage.

- Published material relating to stiffness characteristics of headed reinforcement is scarce. The available data is mostly related to ultimate anchorage capacities or pullout strengths.
- The capacity of headed bars was found to be comprised of peak bearing capacity plus some contribution from reduced bond along the bar between the head and the point of peak bar stress.

Modified *EHB* end anchor head

- For practical and structural reasons, a modified end anchor head is proposed for application in the mechanical anchorage system of the *EHB* component. It is proposed to replace the existing standard hexagon nut with a modified closed end circular head. The modified anchor overcomes the possibility of having the standard nut sliding off or along the shank during installation or casting of concrete. Structurally, the proposed anchor provides additional bearing area towards the resistance against pull-out, which according to the design of fastenings in concrete could increase the pull-out strength capacity of the fastener.

Qualitative testing

- Exploratory pull-out tests were performed on *EHB* components under confined and unconfined concrete conditions. It is found that concrete confinement is required in the pull out test set-up in order to eliminate premature splitting or breakout failures. It is undesirable to have such premature failure modes dominating against anchorage development when anchorage characteristics are being assessed.
- A preliminary investigation of the tensile behaviour of the bond and anchorage mechanism of the *EHB* component revealed that the mechanical anchorage (end anchor head) is the main contributor in resisting pull-out, while bond provides a minimal contribution. Based on this finding it is recommended to measure bond and mechanical anchorage simultaneously, within a suitable confined concrete arrangement rather than individual measurements of bond resistance.

3.8 Research methodology

In order to develop an adaptable model that is able to predict the response of the component "Bolts (*EHB*) in tension", based on an assembly of the individual elements that contribute to its overall deformability, it is necessary to develop knowledge in the force-displacement performance of those elements. An evaluation of their behaviour can provide guidelines towards an appropriate mechanical modelling assembly procedure, and also give an insight to the load transfer mechanism of the component. The component model is to be classified in terms of initial stiffness, resistance, post-limit stiffness and ductility. Such knowledge may be determined by means of quantitative analysis of experimental work; tensile pull-out tests of the *EHB* component and its individual elements, in consideration of parameters that may affect their response, as identified by in the literature.

A series of tests are proposed to be carried out that involve measurements of the bond/anchorage response alone, and measurements of the response of the expanding sleeves alone (Figure 3.23). Finally, by testing the full *EHB* component itself, which in theory is comprised of the two aforementioned mechanisms, the manner in which these elements interact can be identified. The test results will form the basis for the development of the adaptable component model.

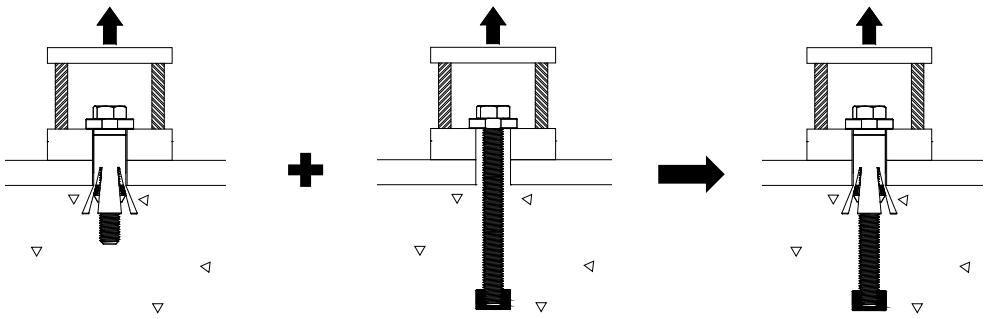

Figure 3.23 Objectives methodology

4 Experimental work

This Chapter involves a detailed description of the testing programme completed in the duration of this research work. The programme is principally divided into three different categories of testing; monotonic tensile pull-out testing, bolt pre-load testing, and relevant material property testing. The Chapter outlines the objectives of the testing, describes the test setups, and details the instrumentation that was employed throughout the testing. Moreover, the design of the pull-out test setup is discussed in consideration of the quantitative analysis of the tensile behaviour of the *EHB* anchored blind-bolt component. Actual (measured) material properties, specimen preparations, and loading procedures are also reported on. In addition, reliability of test results is also addressed.

4.1 Monotonic tensile pull-out testing

A tensile pull-out test is a common test that is performed to evaluate the stiffness, strength and ductility of fastenings in concrete. A total of 51 pull-out test specimens with varying parameters were tested in the course of the project. Being the principal programme of the three categories of testing, the pull-out test results form the basis for quantitative analysis of data relating to the force-displacement response of the *EHB* anchored blind-bolt component.

The aim of the pull-out testing is to evaluate the load transfer mechanism of the *EHB* component, and to determine its global force-displacement response when subject to pure tension loading. The objectives of the testing programme are:

- Design for a suitable and adequate pull-out testing arrangement.
- Determine the response of the individual elements that contribute to the overall deformability of the *EHB* component, in consideration of the primary parameters affecting their behaviour.

4.1.1 Test matrix

The experimental programme that was developed to investigate the tensile behaviour of the *EHB* component is summarised in Table 4.1, with each tested type of fastener or element schematically demonstrated as in Figure 4.1. Type *HB* represents the expanding sleeves mechanism of the *EHB* component, in which the testing principally involves the commercially available Lindapter Hollo-bolt, in consideration of concrete-filled and un-filled sections. Type *M* represents the bond and anchorage mechanism of the *EHB* component, in which the testing involves a standard size, fully threaded bolt, with an end anchor head that is embedded in concrete. Type *EHB* represents the full component that is under investigation.

The parameters that vary in the test matrix are: the bolt diameter, d_b (*16 & 20mm*); the grade of the bolts (*8.8 & 10.9*); the grade of the concrete infill (*C40 & C60*); and the embedded depth, d_{emb} (*4.0 - 6.5*d_b). In this study, d_{emb} is defined as the length measured along the bolt, from the bearing face of the end anchor head, to the surface level of the concrete member in which the bolt is anchored (Figure 4.1). The selection of such parameters was established based on the findings of the literature review, which demonstrated that they are the most likely parameters to affect the tensile response of the component.

The use of bolts of the same batch could provide consistent mechanical properties, which would be ideal for application throughout the experimental programme. This could reduce the level of variability in the testing, however it was somehow very difficult to achieve this as the project evolved. Atypical bolt shank lengths were required, particularly in the case of the grade 8.8, 16mm bolt diameter specimens. For this reason, different bolt batches are identified in the test matrix, labelled as *A, B, C, D, E, & F* in order to distinguish between them for comparison against benchmark specimens. The actual (measured) material properties for the various bolt batches and concrete mixes are reported in section 4.3. With regard to reliability of test results, a minimum of two identically prepared specimens were tested, and two independent displacement measurement techniques were adopted throughout the experimental programme to increase the level of reliability.

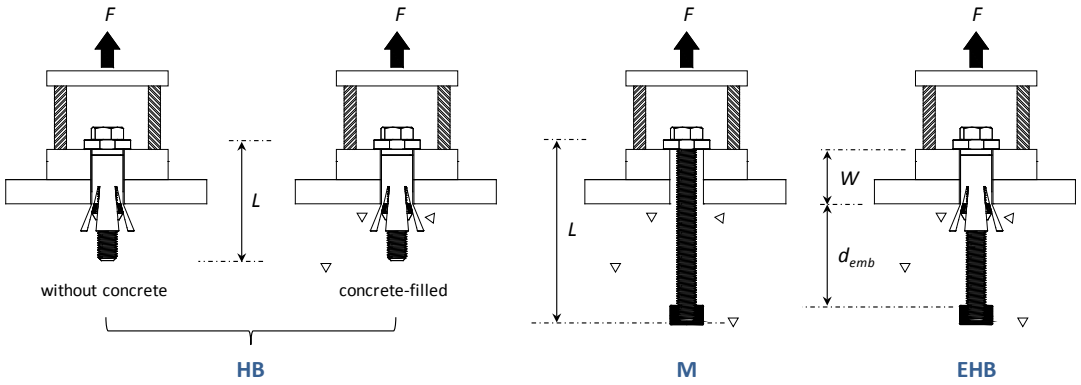

Figure 4.1 Types of fasteners / elements tested

Table 4.1 Test matrix

Specimen index *	d_b (mm)	Shank length, L (mm)	Bolt grade / Batch	Concrete grade	d_{emb} (mm)	d_{emb}/d_b
Type of fastener : HB (without concrete)						
HB16-100-8.8D-0-1	16	100	8.8 / D	n/a	n/a	n/a
HB16-100-8.8D-0-2	16	100	8.8 / D	n/a	n/a	n/a
HB16-100-8.8D-0-3	16	100	8.8 / D	n/a	n/a	n/a
Type of fastener : HB (concrete-filled)						
HB16-100-8.8A-C40-1	16	100	8.8 / A	C40	n/a	n/a
HB16-100-8.8A-C40-2	16	100	8.8 / A	C40	n/a	n/a
HB16-100-8.8A-C40-3	16	100	8.8 / A	C40	n/a	n/a
HB16-100-8.8A-C40-4	16	100	8.8 / A	C40	n/a	n/a
HB16-100-8.8C-C40-1	16	100	8.8 / C	C40	n/a	n/a
HB16-100-8.8C-C40-2	16	100	8.8 / C	C40	n/a	n/a
HB16-100-8.8D-C40-1	16	100	8.8 / D	C40	n/a	n/a
HB16-100-8.8D-C40-2	16	100	8.8 / D	C40	n/a	n/a
HB16-100-8.8D-C40-3	16	100	8.8 / D	C40	n/a	n/a
HB16-100-8.8D-C60-1	16	100	8.8 / D	C60	n/a	n/a
HB16-100-8.8D-C60-2	16	100	8.8 / D	C60	n/a	n/a
HB16-100-10.9E-C40-1	16	100	10.9 / E	C40	n/a	n/a
HB16-100-10.9E-C40-2	16	100	10.9 / E	C40	n/a	n/a
HB20-120-8.8F-C40-1	20	120	8.8 / F	C40	n/a	n/a
HB20-120-8.8F-C40-2	20	120	8.8 / F	C40	n/a	n/a
Type of fastener : M						
M16-150-8.8A-C40-1	16	150	8.8 / A	C40	84	5.3
M16-150-8.8A-C40-2	16	150	8.8 / A	C40	84	5.3
M16-150-8.8D-C40-1	16	150	8.8 / D	C40	84	5.3
M16-150-8.8D-C40-2	16	150	8.8 / D	C40	84	5.3
M16-150-8.8D-C40-3	16	150	8.8 / D	C40	84	5.3
M16-150-8.8D-C60-1	16	150	8.8 / D	C60	84	5.3
M16-150-8.8D-C60-2	16	150	8.8 / D	C60	84	5.3
M16-150-10.9E-C40-1	16	150	10.9 / E	C40	84	5.3
M16-150-10.9E-C40-2	16	150	10.9 / E	C40	84	5.3
M20-150-8.8F-C40-1	20	150	8.8 / F	C40	79	4.0
M20-150-8.8F-C40-2	20	150	8.8 / F	C40	79	4.0

Table 4.1 *(continued)*

Specimen index *	d_b (mm)	Shank length, L (mm)	Bolt grade / Batch	Concrete grade	d_{emb} (mm)	d_{emb}/d_b
M16-130-8.8C-C40-1	16	130	8.8 / C	C40	64	4.0
M16-130-8.8C-C40-2	16	130	8.8 / C	C40	64	4.0
M16-170-8.8B-C40-1	16	170	8.8 / B	C40	104	6.5
M16-170-8.8B-C40-2	16	170	8.8 / B	C40	104	6.5
Type of fastener : EHB						
EHB16-150-8.8A-C40-1	16	150	8.8 / A	C40	84	5.3
EHB16-150-8.8C-C40-1	16	150	8.8 / C	C40	84	5.3
EHB16-150-8.8D-C40-1	16	150	8.8 / D	C40	84	5.3
EHB16-150-8.8D-C40-2	16	150	8.8 / D	C40	84	5.3
EHB16-150-8.8D-C40-3	16	150	8.8 / D	C40	84	5.3
EHB16-150-8.8D-C60-1	16	150	8.8 / D	C60	84	5.3
EHB16-150-8.8D-C60-2	16	150	8.8 / D	C60	84	5.3
EHB16-150-10.9E-C40-1	16	150	10.9 / E	C40	84	5.3
EHB16-150-10.9E-C40-2	16	150	10.9 / E	C40	84	5.3
EHB20-150-8.8F-C40-1	20	150	8.8 / F	C40	79	4.0
EHB20-150-8.8F-C40-2	20	150	8.8 / F	C40	79	4.0
EHB16-130-8.8C-C40-1	16	130	8.8 / C	C40	64	4.0
EHB16-130-8.8C-C40-2	16	130	8.8 / C	C40	64	4.0
EHB16-170-8.8B-C40-1	16	170	8.8 / B	C40	104	6.5
EHB16-170-8.8B-C40-2	16	170	8.8 / B	C40	104	6.5
Strain gauged bolts test series [§]						
HB16-100-8.8D-C40-4	16	100	8.8 / D	C40	n/a	n/a
M16-150-8.8D-C40-4	16	150	8.8 / D	C40	84	5.3
EHB16-150-8.8D-C40-4	16	150	8.8 / D	C40	84	5.3

* ①-②-③-④-⑤ : ① *type of fastener (HB, M, or EHB) & bolt shank diameter,* d_b *;*
② *bolt shank length, L ;* ③ *bolt shank grade & designation of bolt batch (A, B, C, D, E, or F) ;*
④ *grade of concrete infill ;* ⑤ *number of specimen;*
§ *: Refer to section 4.1.4;*
n/a: not applicable or not available.

4.1.2 Test set-up & instrumentation

The pull-out test arrangement is presented in Figure 4.2. The setup involves a re-usable steel box assembly that simulates a rectangular hollow section (*RHS*), comprised of flat plates which are bolted to parallel flange channel sections. Rather than employing a standard *RHS* section in the pull-out test setup, the bolted steel box assembly was principally selected for two reasons; in contrast with an *RHS* section, it allows for an easy access to visually inspect tested specimens by simply unbolting its sections, and secondly, it significantly reduces the amount of material resources required to complete the programme as it may be re-used throughout

the testing for the preparation of all specimens. Furthermore, the design of the setup considers confinement of the concrete member with respect to that provided by an *RHS* section, as the concrete infill remains under confined conditions by its enclosure within the steel box. Such active confinement is important in the pull-out test setup because it eliminates premature splitting failures and allows the concrete components as well as the fastener to develop.

Reaction forces are provided by an *RHS* frame, and a single bolt pull-out arrangement is adopted. With reference to the design of fastenings to concrete (section 3.4.1), the reaction frame has been placed at a specified distance to allow for free concrete cone formation, in consideration of a possible pyramid shaped failure surface (Figure 4.3). The test matrix was used to identify the maximum value of d_{emb} in order to: (a) specify the location of the *RHS* frame, (b) specify the overall dimensions of the steel box rig so that the possible formation of a pull-out cone is not influenced by boundary conditions. The single bolt test setup is implemented in order to monitor the behaviour of the fastening system under consistent load distribution conditions, in contrast with a scenario of having additional testing bolts where an even load distribution among test bolts cannot be guaranteed.

To facilitate an investigation of the response of the fastening systems alone, a rigid top plate (20mm thick) is employed at the loaded end of the test setup. The thickness of the plate is determined in order to eliminate the influence of the bending of the plate under the anticipated loading. The elastic bending of the plate is calculated to be negligible. To eliminate prying effects, a circular loading plate (25mm thick) combined with a 3-bolt system is employed for application in the loading frame of the setup. Hence the overall clamping thickness, *W* is determined as 45mm; herein defined as the sum of the thicknesses of the rigid top plate and circular loading plate. This requires that all *HB* and *EHB* fasteners within the test matrix are to be of Size 2, according to the Lindapter manufacturer brochure. Importantly, the clamping thickness of bolted joints is known to be related to the effective length of which bolt elongation occurs. Therefore, for consistency, the clamping thickness was maintained at a value of 45mm throughout the experimental programme.

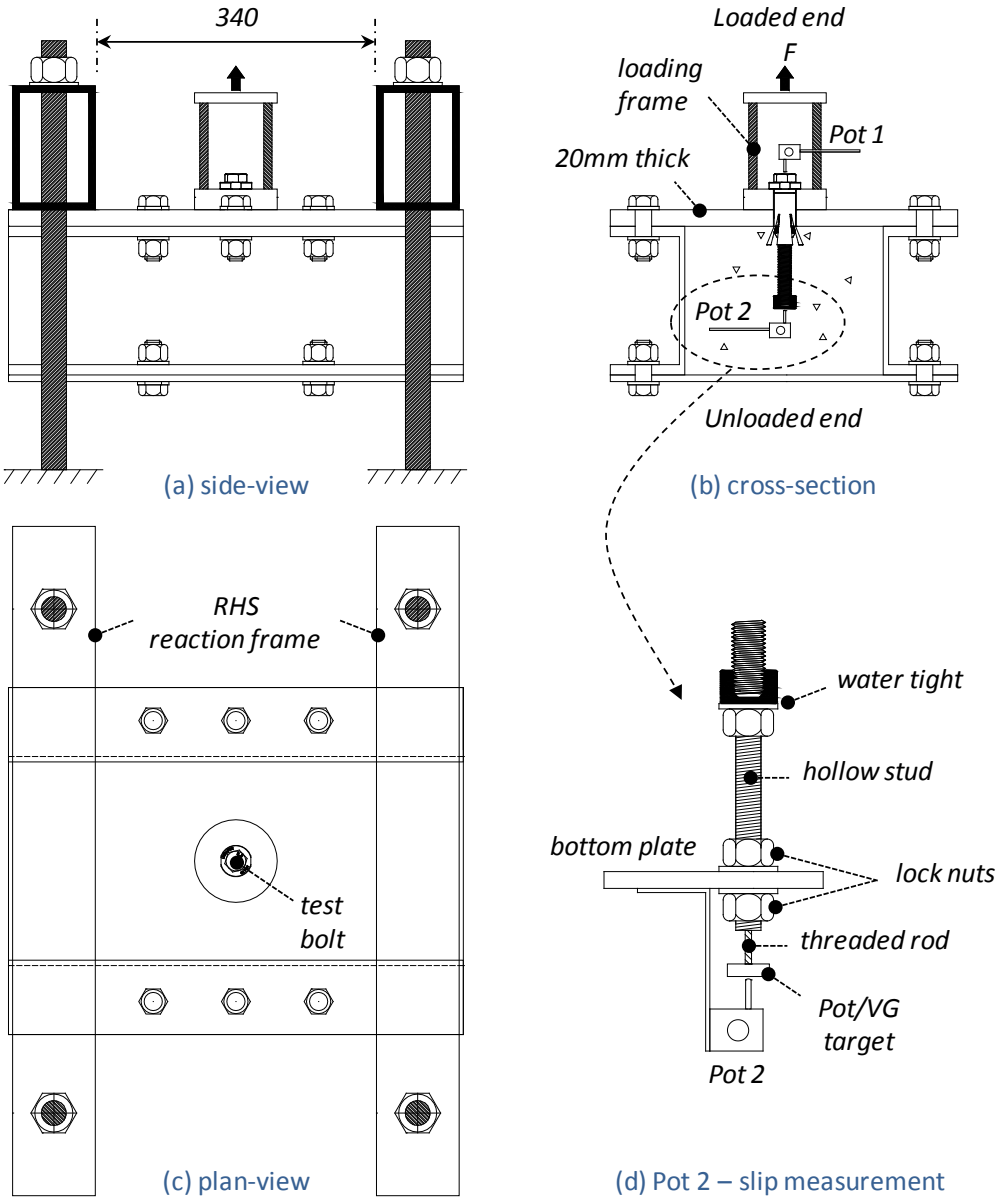

Figure 4.2 Pull-out test setup

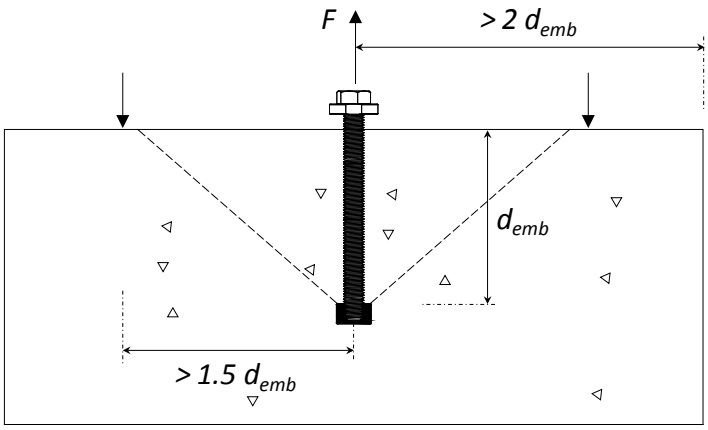

Figure 4.3 Clear distance to reaction forces and boundary conditions

The preparation of all specimens commenced with the tightening of the bolts that held together the sections of which the re-usable steelwork rig was comprised of; such bolts were pre-loaded by applying a tightening torque of 410Nm, in a diagonal sequence. Once the rig was built up, the test bolt (type *HB*, *M* or *EHB*) was inserted through the clearance bolt hole that is located in the centre of the top plate. All test bolts - except those of type *M* - were pre-loaded by applying a specified tightening torque, as recommended by Lindapter International. Type *HB16*/*EHB16* of grade 8.8 was tightened at 190Nm, whereas type *HB16*/*EHB16* of grade 10.9 and type *HB20*/*EHB20* of grade 8.8 were tightened at 300Nm. All bolts were tightened with the use of a handheld torque wrench. The next stage of preparation involved the fixing of necessary arrangements which would allow for measurements of displacement at the unloaded end of the specimens, as detailed in Figure 4.2 (d). To gain access to the unloaded end of the test bolts in the presence of the concrete infill during the test, a threaded rod was inserted through a hollow stud, and was attached to the end anchor head (for type *M* & *EHB*) or to the termination point of the bolt shank (for type *HB*) prior to any concrete casting. The interaction between the target rod and the concrete infill was thus eliminated as the rod was protected within the hollow stud, and with the assistance of lock nuts, the whole arrangement was rigidly held into position. Attaching a target to the end of the rod, which in turn was attached to each test bolt, made it possible to measure displacement at that point of interest. Once the unloaded end targets were in position, all specimens were then allowed at least 24 hours prior to casting of concrete to allow for relaxation effects. Upon the 24 hours, the specimens were ready for concrete casting. Although specimens were tested in the horizontal, all specimens were concrete-filled while in the vertical position, reflecting the actual condition in which a hollow section column would be filled with concrete on site. A standard vibrating poker was used to compact the concrete-filled sections, and all specimens were room temperature cured for a minimum of 7 days.

With regard to the application of the tension loading, all specimens were tested under monotonic loading conditions, with the load being applied in displacement control, at a rate of 0.0015mm/s up to failure. An actual sample ready for testing is

depicted in Figure 4.4. During the test, standard linear potentiometers record displacements at the loaded and unloaded ends of the test bolt. Unloaded end displacements represent the slip of the test bolt, δ_{slip}, whereas loaded end displacements represent the global displacement of the test bolt, δ_{global}. The global displacement of each test bolt is measured by positioning a linear potentiometer directly onto the head of the test bolt, captured by *Pot 1* in the test setup. The global displacement is thus comprised of slip (δ_{slip}), plus elongation of the bolt shank, δ_b. The slip at the unloaded ends is captured by *Pot 2*. The following equation may thus be expressed with reference to the labels of the instrumentation employed in the pull-out test setup.

$$\delta_{global} = \delta_{slip} + \delta_b \qquad \text{Equation 4-1}$$

Further information and detailed drawings relating to the design of the pull-out test setup may be found in Appendix B.

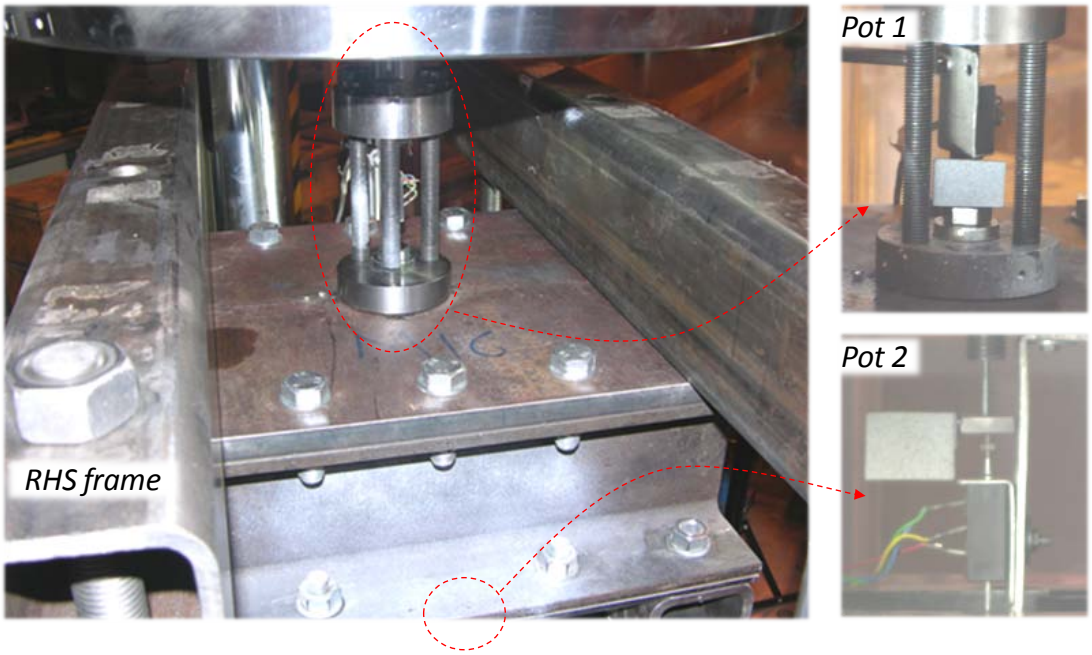

Figure 4.4 Pull-out test specimen ready for testing

4.1.3 Video gauge (*VG*) instrumentation

In addition to the standard linear potentiometers labelled as *Pot 1* and *Pot 2*, the Imetrum Video Gauge (*VG*) instrument is introduced in the pull-out test setup for measurement of 2D displacement, depicted in Figure 4.5 (a). Imetrum's *VG* is a high-resolution, monochrome digital camera which has the ability to measure the (x,y) displacement of a target relative to its initial position. The system is point based, with each user-defined target point being tracked in images in real time. The *VG* analyses video images and therefore all measurements are made in pixels. To convert from pixels to real units, such as millimetres, it is necessary to calculate a conversion factor to go from pixels to real units. This requires measuring a distance between two points both in the image (pixels) and in the real world (millimetres). The number of millimetres per pixel is then derived by dividing these two values.

The *VG* does not require targets to have a specific shape or appearance. However, some targets result in higher tracking resolution and certain types of target are better suited to particular applications. For application in the pull-out test which requires precise measurements, an ideal target should contain light and dark areas, as well as all the shades of grey in between. To achieve this, a speckle pattern was applied at the locations of interest in the test setup. The speckle pattern involves spraying with a very light dusting of white spray paint followed by a very light dusting of black spray paint. The process creates a target with many light, dark and grey areas resulting in very precise tracking of the target.

Achieving the best lighting at the locations of interest in the test is also another factor for optimum results when employing the *VG* instrument technology. Shadows and highlights tend to move across the surface of an object as the object moves relative to the light source. As the *VG* tracks what it sees in the image, these moving shadows/highlights will interfere with tracking the target. For this reason, a fluorescent lamp is used to give a cool diffuse light which evenly illuminates the test object such that there are no shadow edges or highlights on the target markings.

Three primary locations are identified as those required to be monitored during the pull-out test in order to measure the required displacements using the *VG*. These points are shown as crosshairs within the targets on the image of the specimen

presented in Figure 4.5 (b). The first target, *T1*, is located on the head of the test bolt, at the loaded end of the specimen; *T2* is positioned on the channel section web and at the unloaded end of the specimen, *T3* is placed on an offset target. The reference height for each of these targets is that of the height at which the *VG* camera is mounted. Since the *VG* remains stationary during loading, the 2D displacement measurements of the targets set out may involve vertical movements due to an uplift of the specimen; an issue which does not exist for the linear pots due to the manner in which they are attached to the test specimen. It is considered that the newly introduced target *T2* accounts for this, whose purpose is to monitor such movements, in view of modifying if necessary, the global displacement, δ_{global}, measured by *T1*, and the slip, δ_{slip}, measured by *T3*. If displacements at *T2* are found negligible, then *T1* and *T2* are treated alike with the linear pots in the analysis. Similarly, bolt elongation, δ_b may be expressed by the difference between *T1* and *T3*. In the testing, the *VG* instrument measured the position of the aforementioned targets in real-time, at a frequency of 15Hz.

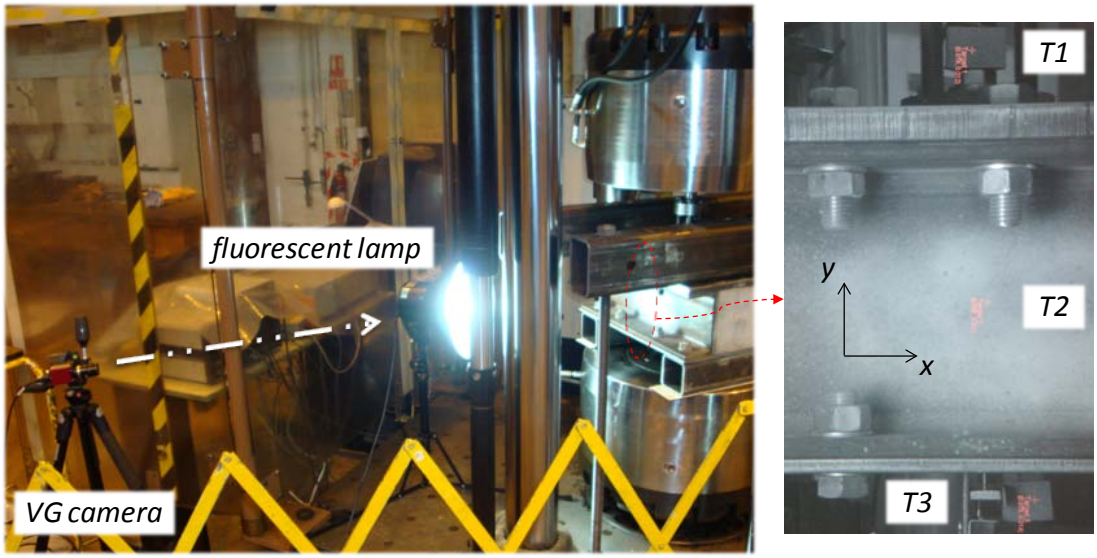

(a) (b)

Figure 4.5 (a) Imetrum Video Gauge, (b) Pull-out test *VG* targets for 2D displacements

In the pull-out testing programme, the key benefit that arises from the employment of the *VG* instrument is that it may capture the full force-displacement response of

the pullout specimens (including descending branches). In contrast, the data that is generated by the linear potentiometers is limited upon ultimate capacity, in particular with regard to that which is measured at the loaded end of the specimen. This is attributed to the fact that it is necessary to prematurely remove the instrumentation that's on the head of the test bolt, signed as *Pot 1* in order to guard it against possible shot-fire bolt failures in the case where pull-out specimens may exhibit a bolt shank failure. Nevertheless, adopting the *VG* technique enhances the reliability of the experimental results by allowing for a direct comparison of displacement measurements among two independent measuring techniques.

4.1.4 Strain gauged bolts test series

Another type of instrumentation that was employed within the pull-out test setup is strain gauges. The bolts of one test series were instrumented with strain gauges on their surface at specified locations. With reference to Table 4.1, the unique specimen indexes of these specimens are signed as *EHB16-150-8.8D-C40-4*, *M16-150-8.8D-C40-4*, and *HB16-100-8.8D-C40-4*; representing the full anchored blind-bolt component, its bond and anchorage mechanism, and its expanding sleeves mechanism, respectively. The parameters involved in the series are in agreement with those of the benchmark of the overall test matrix. The aim of the strain gauged bolts test series is to investigate the load transfer mechanism of the full *EHB* component. The objectives of the testing are: determine the stress profile of the component as well as that of its assumed individual elements; identify their interaction; and assess their contribution.

Strain gauges are used on the surface of the bolt to provide information on the development of force in the bolt. The development of force in the bolt of the *EHB* component is primarily attributed to its mechanical anchorage and its expanding sleeves element. The instrumentation will measure the stress profile along the bolt, allowing for an assessment of the distribution along its length. Developing such knowledge can demonstrate the engagement and evolution of the component's individual elements. Therefore, the positioning of the gauges should be selected such that their location will allow for distinguishing between the forces developed

in the bolt due to development of mechanical anchorage and expanding sleeves. The arrangement of the strain gauges is shown in Figure 4.6. Staggered to minimise continuous disruption of bond properties, the gauges are spaced at $1d_b$, with the first gauge applied at $1d_b$ from the face of the end anchor head. The gauge that is closest to the end anchor head can determine the development of forces due to mechanical anchorage resistance. Those along the shank are to represent the development of bond resistance, and with regard to the resistance provided by the expanding sleeves element, a gauge that is positioned at the contact area of the sleeves and connecting member is used; at $5d_b$ which also represents the pre-load in the bolt at its tightening stage.

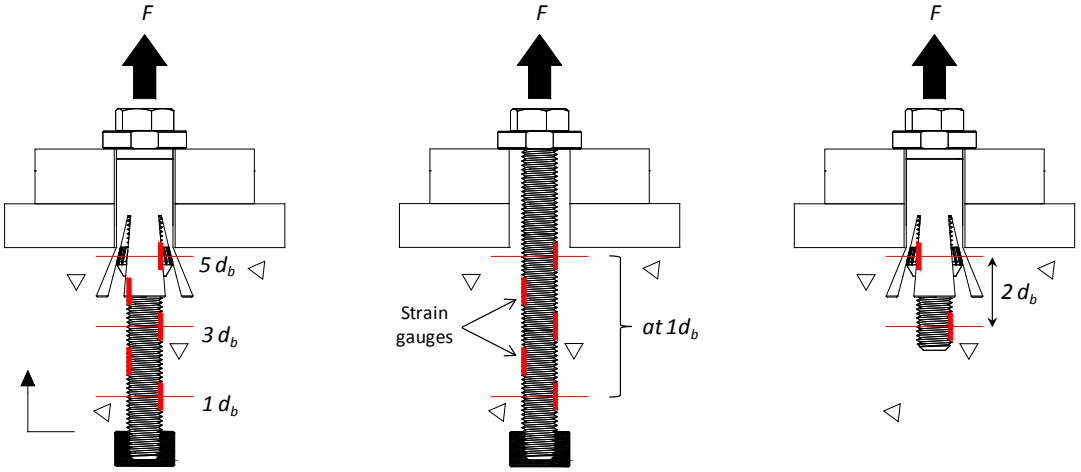

Full component *(Type EHB)*

Bond & Anchorage - *Mechanism 3* *(Type M)*

Expanding sleeves - *Mechanism 2* *(Type HB)*

Figure 4.6 Strain gauged bolts test series: position of gauges

The procedure involved in the installation of the gauges is shown in Figure 4.7. The wiring of the strain gauges is installed through diagonal inserts and a central hole, designed as such to avoid the possibility of damage due to shearing of wires against hardened concrete with the application of tensile load. The application of the protective coating was flush with respect to the external thread diameter of the bolt in order to allow for the threaded cone of the blind-bolt to ride along its shank during tightening. Nevertheless, the flush level of the coating ensures a minimum effect on bond properties. The actual instrumented bolts of the test series are presented in Figure 4.8 prior to any tightening.

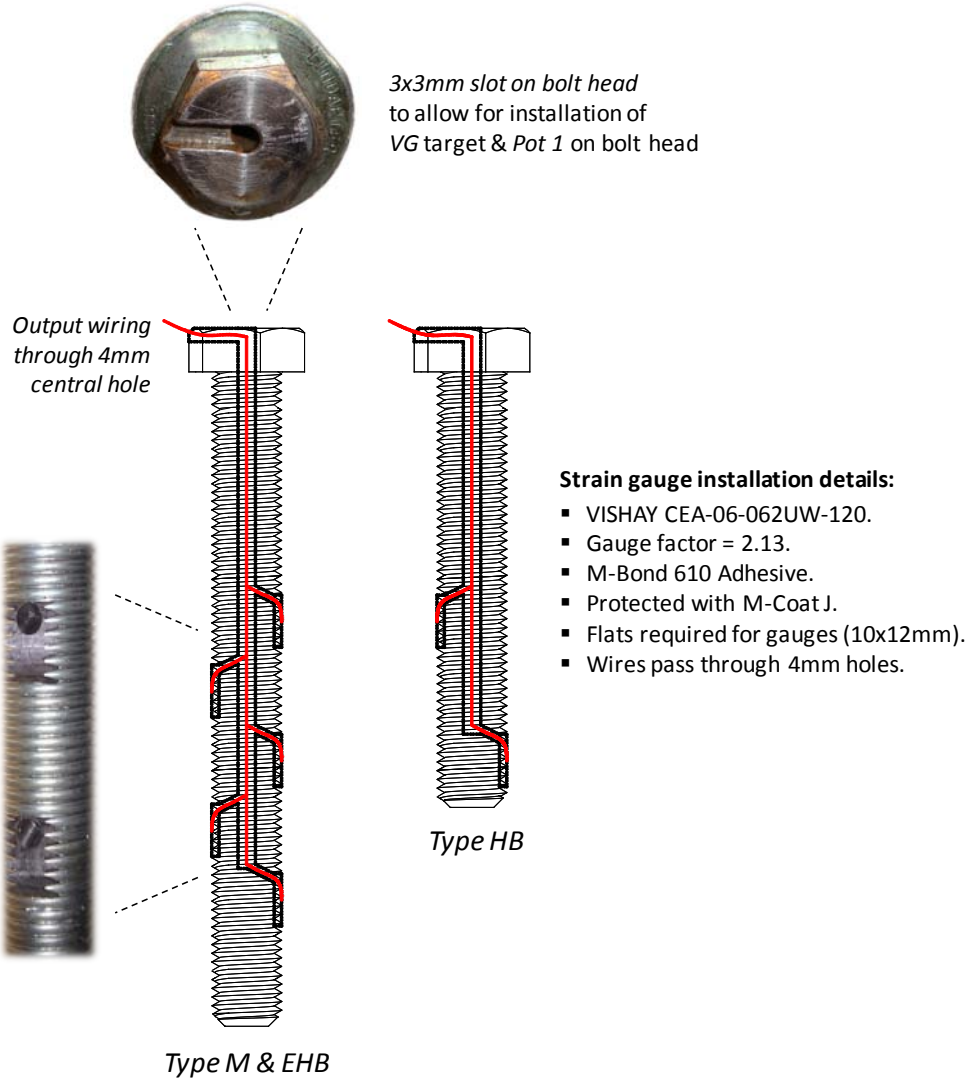

Figure 4.7 Strain gauged bolts test series: installation of gauges

Figure 4.8 Instrumented bolts: fully assembled ready for tightening / testing

4.2 Pre-load in blind-bolt testing

This section relates to the pre-load testing programme that was performed to determine the range of pre-load that is induced in the bolt of the *EHB* component at its tightening stage. It is known that the level of bolt pre-load can significantly affect the stiffness of bolted joints, therefore the range of that induced in the *EHB* is of significant importance towards the investigation of its response. Herein, the pre-load test setup and instrumentation is presented in detail. The aim of the testing is to measure the pre-load induced in the *EHB* blind-bolt, and the objectives involve an evaluation of the pre-load condition over a sustained period of time, allowing for relaxation effects.

The theoretical expression that exists to calculate pre-load in bolts is a function of tightening torque and bolt diameter. It is thus important to realise the scale effects with regard to an increased tightening torque, in the case of a larger bolt diameter and higher bolt grade. A total of 20 pre-load measurements were carried out with all measured separate from the pull-out test specimens. The details of the specimens are outlined in Table 4.2; prepared in conjunction of the overall test matrix of this research programme. The varying parameters involve different bolt sizes, d_b (*16 & 20mm*); different bolt grades (*8.8 & 10.9*); and different bolt batches.

The testing arrangement is shown in Figure 4.9. The tightening torque in all specimens was applied with the use of a handheld torque wrench set at the specified torque. Two different measurement techniques were adopted; indirect measurements with the use of strain gauged bolts, and direct measurements with the use of a compression load cell. In both methods, readings of pre-load were taken during and after tightening of the bolts, at appropriate time intervals. The initial pre-load was taken as that which was achieved once the tightening torque was reached. Residual pre-load was taken as that available after allowing 5 days for relaxation effects. In the test setup, the clearance bolt hole that was bored on the face of the *SHS* section involved a typical construction tolerance of 2mm for both, 16 and 20mm bolt diameter fasteners; resulting in a clearance diameter of 28 and 35mm for *HB16* and *HB20*, respectively, to eliminate hole interference effects which can result in pre-load losses. Moreover, with reference to the pull-out test

setup, for consistency, the same construction tolerance, tightening torque, and clamping thickness (*W=45mm*) applied to the equivalent pre-load specimens; the latter to ensure an identical effective length over which bolt elongation, δ_b occurs.

Table 4.2 Details of pre-load testing specimens

Specimen index *	d_b (mm)	Shank length, L (mm)	Bolt grade / Batch	Tightening torque (Nm)	Method	$A_{s,net}$ (mm^2)
HB16-100-8.8G-M1-1	16	100	8.8 / G	190	3 at 120°	144
HB16-100-8.8G-M1-2	16	100	8.8 / G	190	3 at 120°	144
HB16-100-8.8G-M1-3	16	100	8.8 / G	190	3 at 120°	144
HB16-100-8.8G-M2-1	16	100	8.8 / G	190	central gauge	144
HB16-100-8.8G-M2-2	16	100	8.8 / G	190	central gauge	144
HB16-100-8.8G-M2-3	16	100	8.8 / G	190	central gauge	144
HB16-150-8.8A-M3-1	16	150	8.8 / A	190	LC	157
HB16-150-8.8A-M3-2	16	150	8.8 / A	190	LC	157
HB16-150-8.8A-M3-3	16	150	8.8 / A	190	LC	157
HB16-150-8.8C-M3-1	16	150	8.8 / C	190	LC	157
HB16-150-8.8C-M3-2	16	150	8.8 / C	190	LC	157
HB16-150-8.8C-M3-3	16	150	8.8 / C	190	LC	157
HB16-150-8.8D-M3-1	16	150	8.8 / D	190	LC	157
HB16-150-8.8D-M3-2	16	150	8.8 / D	190	LC	157
HB16-150-8.8D-M3-3	16	150	8.8 / D	190	LC	157
HB16-150-10.9E-M3-1	16	150	10.9 / E	300	LC	157
HB16-150-10.9E-M3-2	16	150	10.9 / E	300	LC	157
HB16-150-10.9E-M3-3	16	150	10.9 / E	300	LC	157
HB20-150-8.8F-M3-1	20	150	8.8 / F	300	LC	245
HB20-150-8.8F-M3-2	20	150	8.8 / F	300	LC	245

* ①-②-③-④-⑤ : ① *type of fastener (HB) & bolt shank diameter, d_b ;*
② *bolt shank length, L ;* ③ *bolt shank grade & designation of bolt batch (A, C, D, E, F, or G) ;*
④ *method used (M1/M2: strain gauged bolts: 3 at 120°/central gauge, M3: LC = load cell) ;*
⑤ *number of specimen;*
Notes: 1. All HB fasteners are of "size 2", as in Lindapter brochure datasheet; W=45mm;
2. Refer to section 4.3 for mechanical properties of relevant bolt batches.

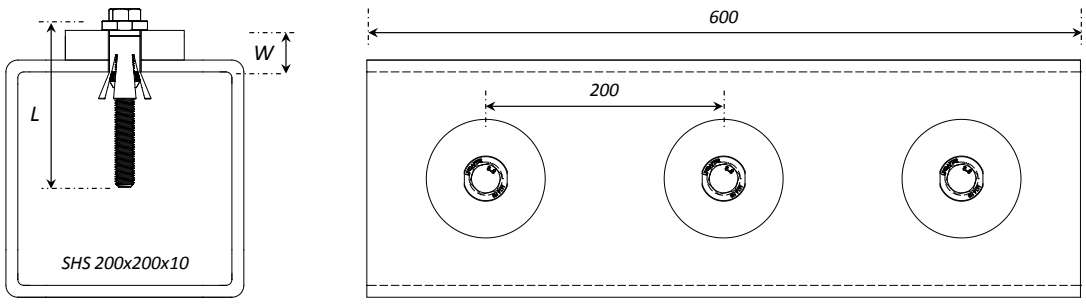

Figure 4.9 Pre-load testing setup

4.2.1 Strain gauged bolts

The indirect method to measure pre-load in the bolt was achieved with the use of bolts that were strain gauge instrumented (Figure 4.10). Pre-tension is transmitted to connected elements through the bolt head and the expanded sleeve, therefore strain below the bolt head may be used to determine the pre-load in the bolt. The purpose of the gauges is to measure the tensile strain of the bolt for translation into axial tension. The strain gauge readings represent the pre-strain in the bolt, ε_p. As the bolt still lies within its elastic region, Hooke's Law of elasticity may be applied, hence the product of the pre-strain and the bolt shank's Young's modulus of elasticity (E) results in the pre-stress in the bolt, σ_p. A net tensile stress area of the bolt, $A_{s,net}$, may then be used to express this as pre-load, F_p, as in Equation 4-2.

$$F_p = \sigma_p A_{s,net} = \varepsilon_p E A_{s,net} \qquad \text{Equation 4-2}$$

Two strain gauge configurations were tested. The force in the bolts was determined using three strain gauges mounted on flats at 120°, as shown in Figure 4.10 (a), and with the use of a specialised central gauge, depicted in Figure 4.10 (b). The three flat areas were machined directly below the head in order to accommodate the gauges. Three holes, 2mm in diameter were drilled through each head into the machined flats for the passage of instrument cable to the strain gauges. The net tensile area of this configuration is calculated based on the minor diameter of external thread ($A_{s,net} = \pi\ d_3^2/4$ *where* $d_3 = 13.546$*mm for a standard M16*). The central gauge is inserted into a pre-drilled hole in the bolt head with a bonding adhesive which advantageously, measures axial strain unaffected by flexural loading. The net tensile area of this configuration is calculated based on the nominal tensile stress area, $A_{s,nom}$, as recommended in ISO 898 (BSI 2009), minus the circular area that was drilled of diameter 2mm ($A_{s,net} = A_{s,nom} - \pi\ 2^2/4$ *where* $A_{s,nom} = 157$*mm for a standard M16*). For both strain gauged configurations, the centre point of all gauges was located at an equal depth (*X-X*) relative to the bottom of the bolt head. Six specimens were tested simultaneously, involving three of each configuration in order to reduce variability in testing under temperature conditions.

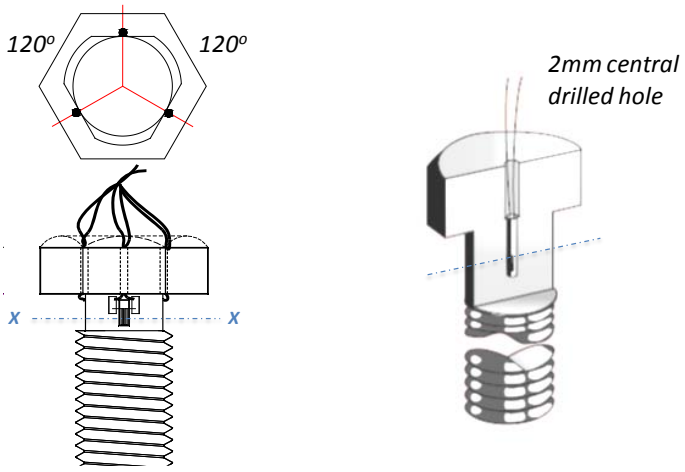

(a) three strain gauges at 120° (b) uni-axial central strain gauge

Figure 4.10 Measurement of pre-load in blind-bolt using strain gauged bolts (a) *M1*, (b) *M2*

4.2.2 Direct measurement - clamping force with load cell

Under the same testing arrangement, direct measurements of pre-load were performed on the *HB* blind-bolt with the assistance of a compression load cell (*LC*), shown in Figure 4.11. Labelled as the third method (*M3*), the countersunk size 2 Hollo-Bolts were placed through the central hole of the 130kN capacity load cell and through a clearance bolt hole in a 10mm thick 200x200 S355 *SHS*. As torque was applied, the pancake load cell measured the applied clamping load in the *HB* which was monitored thereafter over a 5 day period to allow for relaxation effects.

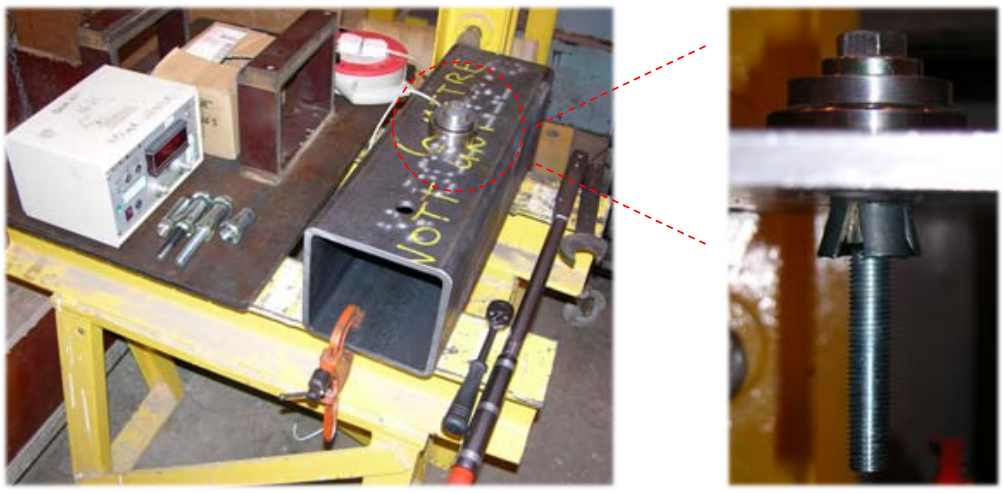

Figure 4.11 Measurement of pre-load in blind-bolt using a load cell

In comparison with the strain gauged method, the advantage of the *LC* approach is that it does not require any modifications to the geometry of the bolts for installation of gauges, hence the original bolt size is tested; allowing for $A_{s,net}$ to be taken as equal to $A_{s,nom}$. Tests were done individually due to equipment limitations and as the project evolved, this measuring technique was employed for the remainder of the pre-load testing programme as it was considered as the most efficient method; determined by sample preparation time, required resources, and simulation of actual conditions.

4.3 Material property testing

This section reports on the actual material properties of bolts, concrete and steelwork that were involved in the overall testing programme. This includes the mechanical properties of the bolt batches used in the pull-out and pre-load test specimens, and the properties of the concrete used throughout the testing. The properties of the *RHS* frame and pull-out steel box assembly are also reported.

4.3.1 Bolts

The mechanical properties of the bolt batches used throughout the testing programme are summarised in Table 4.3. Test pieces were designed and tested in accordance to ISO 898-1:2009 (BSI 2009), and the average values of the measured properties were compared with the minimum values (Table 4.4) required by the standard. The measured yield and ultimate capacities satisfy the requirements for bolts with a minimum factor of 1.08 for f_{ub} / R_m. In Figure 4.12, the bar chart demonstrates the variation in the properties of the grade 8.8 bolts that were used throughout the experimental work signifying the importance of their measurement.

Tensile tests were performed on machined and full-size bolts, where stress-strain (σ-ε) relationships were obtained in two ways; with the use of a clip-on extensometer that was attached across the test pieces, Figure 4.13 (a); and with the use of the Video Gauge (*VG*) equipment, Figure 4.13 (b). For installation reasons, the extensometer instrumentation is limited to machined test pieces, and because it is removed prior to failure to avoid any possibility of damage to it, it is also limited

to strain measurements within the yielding region. In this case, it is thus common to combine the displacements of the moveable cross-head in order to obtain the full σ-ε behaviour.

Table 4.3 Bolt properties

Bolt Batch	d_b (mm)	Bolt grade	f_{yb} (MPa)	f_{ub} (MPa)	E (GPa)	f_{yb} / $R_{p0,2}$	f_{ub} / R_m	N *	N ¥
A	16	8.8	907	1003	205	1.42	1.25	3	3
B	16	8.8	725	900	210	1.13	1.13	2	0
C	16	8.8	873	981	209	1.36	1.23	2	0
D	16	8.8	836	931	207	1.31	1.16	3	1
E	16	10.9	1086	1127	209	1.16	1.08	4	3
F	20	8.8	785	935	207	1.19	1.13	2	0
G	16	8.8	828	917	212	1.29	1.15	3	0

f_{yb} is the yield & f_{ub} is the ultimate strength; E is Young's Modulus of Elasticity;
F_{yb}=f_{yb} $A_{s,net}$ & F_{ub}=f_{ub} $A_{s,net}$;
N: number of machined bolt specimens; N¥: number of full-size bolt specimens.*

Table 4.4 Minimum required mechanical properties of bolts

	$d_b \leq 16$mm		$d_b > 16$mm	
	Grade 8.8	Grade 10.9	Grade 8.8	Grade 10.9
$R_{p0,2}$ (MPa)	640	940	660	940
R_m (MPa)	800	1040	830	1040

Extracted from Table 3 of ISO 898-1:2009 (BSI 2009);
$R_{p0,2}$ is the stress at 0.2% non-proportional elongation & R_m is the tensile strength.

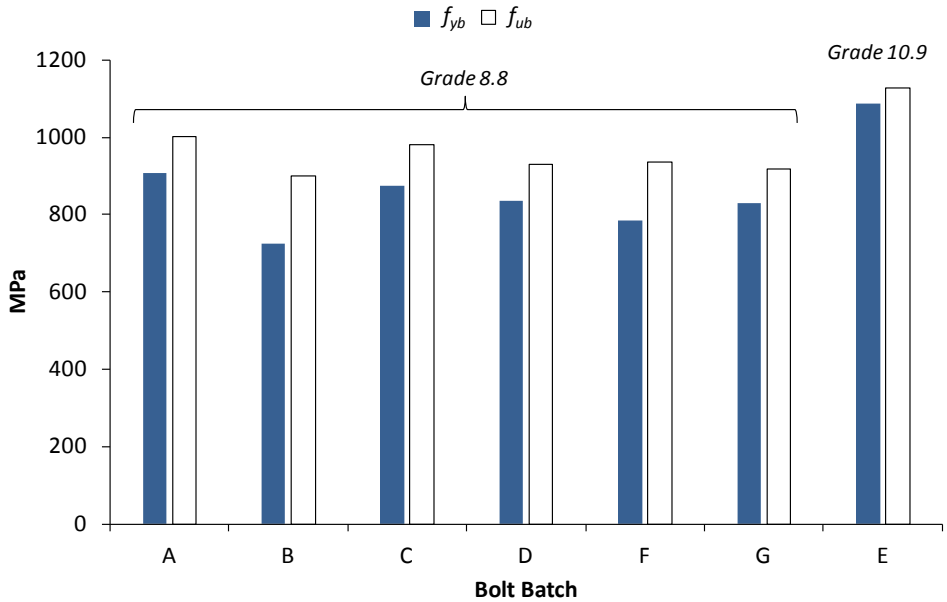

Figure 4.12 Variation in mechanical properties of bolt batches used

For these reasons, the *VG* camera was introduced for application in the tensile tests; to compare the full σ-ε data between machined and full-size test pieces. The *VG* is not physically attached to the test piece, therefore overcomes the issue of prematurely removing instrumentation, and is able to monitor the full σ-ε behaviour of test pieces. With the use of a speckle pattern applied by spray paint on the test pieces, it calculates strain by monitoring the distance between two points, thus allowing for strain measurements on machined and full-size fully threaded bolts, Figure 4.13 (c). To display the typical σ-ε relationships obtained among the *VG* and the extensometer, Figure 4.14 depicts test results of bolt batch category *D* for machined and full-size bolts. It is demonstrated that the measurements are in good agreement, particularly in the elastic region however upon ultimate strength even the *VG* data is limited due to necking of the bolt.

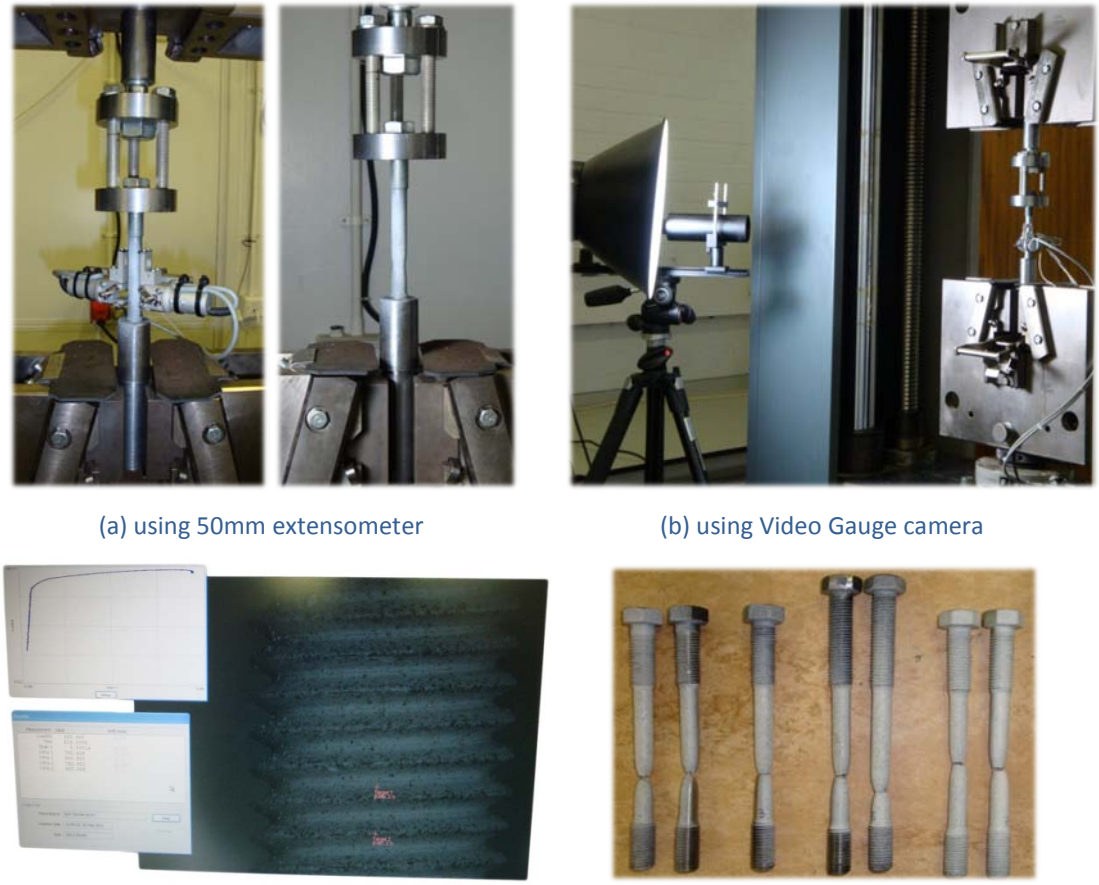

(a) using 50mm extensometer

(b) using Video Gauge camera

(c) *VG* on full-size bolts

(d) Machined test pieces (after testing)

Figure 4.13 Tensile testing for bolt properties

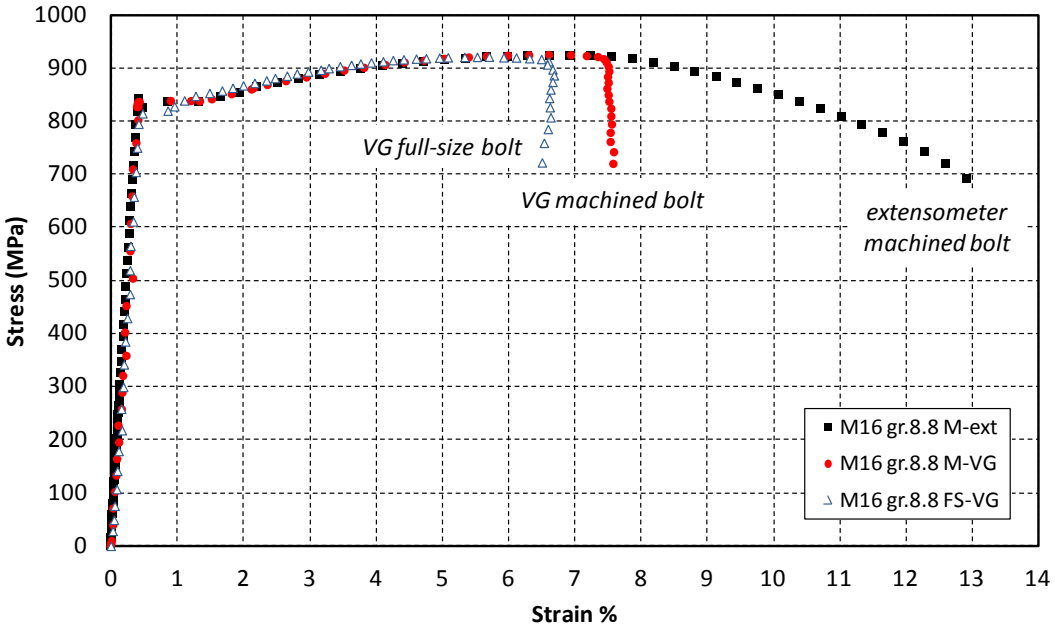

Figure 4.14 Extensometer versus *VG*: Bolt Batch *D* [machined (*M*) & full-size (*FS*) bolt]

4.3.2 Concrete

Two concrete mixes, grade *C40* and *C60* were used in pull-out specimen casting. Table 4.5 lists the concrete mix proportions. A nominal maximum aggregate size of 10mm was specified. The age and strength of the specimens on the day of testing as well as the 28-day strength of the concrete mixes are summarised in Table 4.6.

Table 4.5 Concrete mix design

Grade	*Cement type*	*Cement* (kg/m^3)	*Water* (kg/m^3)	*Fine aggregate* (kg/m^3)	*10mm coarse aggregate* (kg/m^3)
C40	CEM II / AL 32.5R	440	210	735	1020
C60*	CEM I / 52.5N	826	206	570	753

*: *Sika Viscocrete premier (High Range Water Reducer) at 20ml per 15kg CEM I / 52.5.*

Mechanical properties of the hardened concrete were determined using standard 100mm cubes. Unless otherwise stated, all cubes were air cured in order to equate with the curing conditions of the actual pull-out specimens. Pull-out specimens were allowed a minimum of 7 days for curing under room temperature conditions. Compression strength was measured just prior to testing, usually for a group of

specimens with the same concrete. The concrete infill of all specimens had gained a compressive strength of 75% of the 28-day strength, on the day of testing.

Table 4.6 Pull-out tests; compressive strength of concrete infill

Specimen index	Age * (days)	f_{cu} * (MPa)	$f_{cu,\ 28\ days}$ (MPa)	$f_{cu} / f_{cu,\ 28\ days}$
Type of fastener : HB (concrete-filled)				
HB16-100-8.8A-C40-1	7	39.0[§]	n/a	n/a
HB16-100-8.8A-C40-2	7	39.0[§]	n/a	n/a
HB16-100-8.8A-C40-3	9	39.0[§]	46.0	0.85
HB16-100-8.8A-C40-4	7	37.0	49.0	0.76
HB16-100-8.8C-C40-1	8	39.0	49.2	0.79
HB16-100-8.8C-C40-2	7	39.5	n/a	n/a
HB16-100-8.8D-C40-1	7	38.9	51.3	0.76
HB16-100-8.8D-C40-2	8	42.5	51.3	0.83
HB16-100-8.8D-C40-3	8	42.5	51.3	0.83
HB16-100-8.8D-C60-1	8	60.0	61.7	0.97
HB16-100-8.8D-C60-2	7	56.9	61.0	0.93
HB16-100-10.9E-C40-1	8	39.5	43.6	0.91
HB16-100-10.9E-C40-2	8	39.7	45.1	0.88
HB20-120-8.8F-C40-1	7	38.5	47.1	0.82
HB20-120-8.8F-C40-2	7	35.5	40.9	0.87
Type of fastener : M				
M16-150-8.8A-C40-1	7	38.0[§]	46.0	0.83
M16-150-8.8A-C40-2	8	39.0[§]	49.0	0.80
M16-150-8.8D-C40-1	7	36.0	45.0	0.80
M16-150-8.8D-C40-2	7	36.0	45.0	0.80
M16-150-8.8D-C40-3	8	36.9	45.0	0.82
M16-150-8.8D-C60-1	7	57.1	61.7	0.93
M16-150-8.8D-C60-2	7	56.9	61.0	0.93
M16-150-10.9E-C40-1	7	38.0	43.6	0.87
M16-150-10.9E-C40-2	7	39.6	45.1	0.88
M20-150-8.8F-C40-1	6	36.6	47.1	0.78
M20-150-8.8F-C40-2	6	35.4	40.9	0.87
M16-130-8.8C-C40-1	8	39.0	49.2	0.79
M16-130-8.8C-C40-2	8	41.0	n/a	n/a
M16-170-8.8B-C40-1	8	42.0[§]	n/a	n/a
M16-170-8.8B-C40-2	8	42.0[§]	n/a	n/a
Type of fastener : EHB				
EHB16-150-8.8A-C40-1	7	37.0[§]	49.0	0.76
EHB16-150-8.8C-C40-1	7	36.0	n/a	n/a
EHB16-150-8.8D-C40-1	7	41.2	50.5	0.82
EHB16-150-8.8D-C40-2	8	40.6	50.5	0.80
EHB16-150-8.8D-C40-3	8	40.6	50.5	0.80
EHB16-150-8.8D-C60-1	8	60.0	61.7	0.97
EHB16-150-8.8D-C60-2	7	56.9	61.0	0.93
EHB16-150-10.9E-C40-1	7	38.0	43.6	0.87
EHB16-150-10.9E-C40-2	7	39.6	45.1	0.88
EHB20-150-8.8F-C40-1	8	39.0	47.1	0.83

Table 4.6 *(continued)*

Specimen index	Age * (days)	f_{cu} * (MPa)	$f_{cu,\ 28\ days}$ (MPa)	$f_{cu} / f_{cu,\ 28\ days}$
EHB20-150-8.8F-C40-2	7	35.5	40.9	0.87
EHB16-130-8.8C-C40-1	7	38.0	49.2	0.77
EHB16-130-8.8C-C40-2	7	39.5	n/a	n/a
EHB16-170-8.8B-C40-1	7	40.0§	n/a	n/a
EHB16-170-8.8B-C40-2	11	46.0§	n/a	n/a
Strain gauged bolts test series				
HB16-100-8.8D-C40-4	7	32.2	41.0	0.79
M16-150-8.8D-C40-4	7	32.2	41.0	0.79
EHB16-150-8.8D-C40-4	7	32.2	41.0	0.79

**: age or average cube strength on day of testing;*
§: concrete cubes cured in water.

4.3.3 Steelwork

The average results of coupon tests relating to the mechanical properties of the *RHS* reaction frame and 20mm thick top plate employed in the pull-out testing arrangement are summarised in Table 4.7. Standard steel dog-bone test pieces were taken and a clip-on extensometer was attached across the samples for strain measurements. Test pieces were designed and tested to Annex D of BS EN 10002-1:2001 (BSI 2001b). The steelwork is of grade S355 and the test results comply with the minimum requirements of the standards (Table 4.8).

Table 4.7 Steelwork properties

Steel section	*Yield* (MPa)	*Ultimate* (MPa)	*E* (GPa)	*N* ¥
RHS frame 150x100x8	464	519	204	2
Top Plate 420x20x550	495	557	225	2

N¥: number of tests.

Table 4.8 Minimum required mechanical properties for S355 steel

	*Flat plate **	*RHS section §*
	16 < t ≤ 40mm	*t ≤ 16mm*
$R_{p0,2}$ (MPa)	345	355
R_m (MPa)	470-630	470-630

**: Extracted from Table 7 of EN 10025-2:2004;*
§: Extracted from Table A.3 of EN 10210-1:2006;
$R_{p0,2}$ is the stress at 0.2% non-proportional elongation & R_m is the tensile strength.

5 Test results, discussion and observations

In this Chapter, the raw results of the monotonic pull-out tests and the pre-load measurements are presented. The Chapter commences with a comparison of experimental data between the commercially available *HB* and the *EHB*. In addition to the recorded force-displacement and strain measurements, visual aids that were taken during and after testing are demonstrated in view of evaluating the load transfer mechanism of the *EHB* component. The parameters that affect the global force-displacement relationship of the *EHB* component are identified, and such effects are investigated in reflection with the force-slip response of its assumed individual elements. Focus is given to the experimentally determined force-bolt elongation element, and to the force-slip behaviour of the expanding sleeves and bond and anchorage elements. Moreover, the contribution of the test results towards the development of the overall component model is discussed.

5.1 Type *HB* & *EHB*

To evaluate the load transfer mechanism of the *EHB* component, it is necessary at first to identify and understand the origin of its enhanced performance in comparison with the standard commercially available Lindapter *HB* blind-bolt. The enhanced behaviour of the *EHB* component is known to be attributed to the presence of the concrete infill in combination with its mechanical anchorage; however knowledge in quantitative sources of deformability with respect to its individual elements is scarce at a single component level of sophistication. Studying the response of the standard *HB* exclusive of concrete, and that of the *HB* and *EHB* with concrete can give an insight to the magnitude of improvements provided by the concrete infill and mechanical anchorage while under identical parameter conditions. Observations of the respective failure modes can demonstrate (1) the sources of deformability that are involved in the elements of the *EHB* component, and (2) the dominant failure mechanisms that type *HB* and *EHB* exhibit.

5.1.1 Loaded & unloaded end displacements

As a first stage in developing an understanding of the load transfer mechanism of the *EHB* component, herein the tensile behaviour of type *HB* is compared with the pull-out performance of type *EHB*, in consideration of unfilled and concrete filled sections. The pull-out test results are shown in Figure 5.1 with loaded end displacements labelled as the global displacement (δ_{global}), and unloaded end displacements labelled as slip (δ_{slip}). A consistent pattern is observed among the tests, where global displacements are larger than the slip recorded at the unloaded ends. As previously mentioned, the discrepancy between them is attributed to the elongation of the internal bolt shank which is included in the global readings at the loaded end. For further conclusions, the test results are separated into loaded and unloaded end measurements in Figure 5.2 with data relating to three specimens for each configuration. It is evident that type *EHB* exhibits the highest stiffness at both ends, with minor slip recorded at its unloaded end. The next stiffest configuration is identified as that of the concrete filled type *HB*, and as expected, type *HB* exclusive of concrete exhibits the lowest stiffness of all.

The stiffness of type *HB* without concrete is seen to significantly reduce at around 40kN due to the yielding of its expanding sleeves, followed by another reduction in stiffness at around 120kN due to the yielding of its internal bolt shank. The initial stiffness of the concrete filled type *HB* is seen to reduce at around 60kN, followed by another reduction in stiffness once again at around 120kN due to the yielding of the internal bolt shank. Although the response of type *HB* is significantly improved in the presence of a concrete infill, it is found that the configuration exhibits a rather inconsistent response among the identical specimens; particularly past the 60kN force range. In contrast, the global force-displacement relationship of the *EHB* component demonstrates a consistent behaviour between the identical specimens, with an initial stiffness that is maintained up to the yield capacity of its internal bolt shank, corresponding to the 120kN force. Thereafter, once the ultimate capacity of type *EHB* is reached, a constant value of slip is observed and the resistance of the component reduces as the applied load is seen to drop.

(a) Type *HB* (specimen HB16-100-8.8D-0-1)

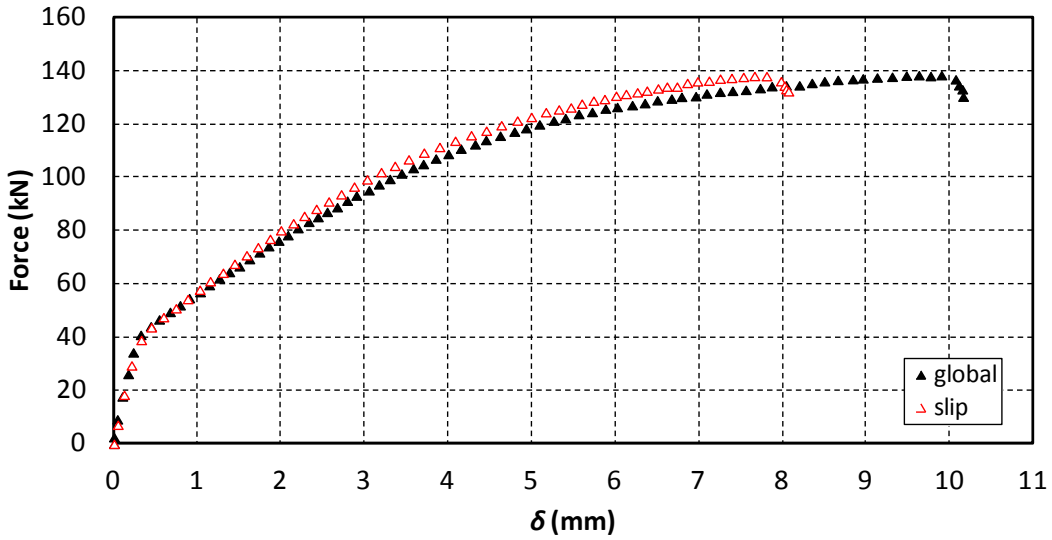

(b) Type *HB* (specimen HB16-100-8.8D-C40-1)

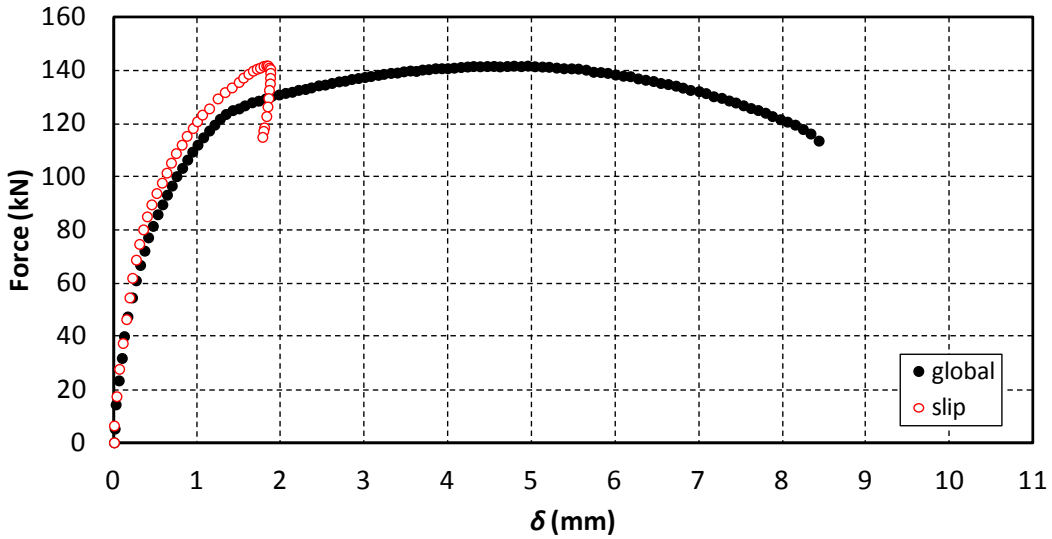

(c) Type *EHB* (specimen EHB16-150-8.8D-C40-2)

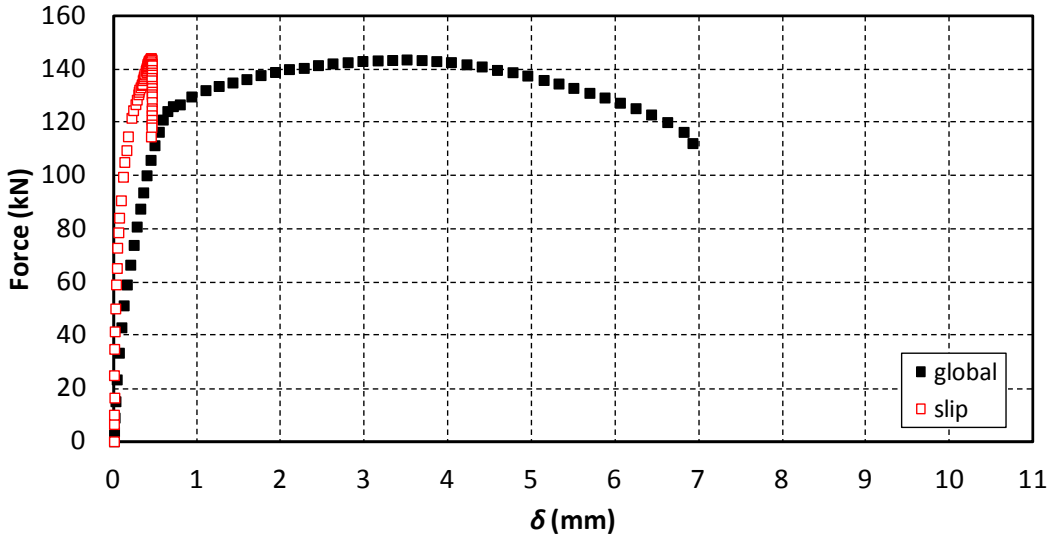

Figure 5.1 Pull-out test results for type *HB* & *EHB*

The point at which the ultimate capacity of the *EHB* component is achieved reflects with the onset of necking of its internal bolt shank, also captured and evidenced by the softening branch at the loaded end of the component. Such behaviour indicates that the applied load is fully distributed and transferred into the internal bolt shank when the ultimate strength of the internal bolt is reached.

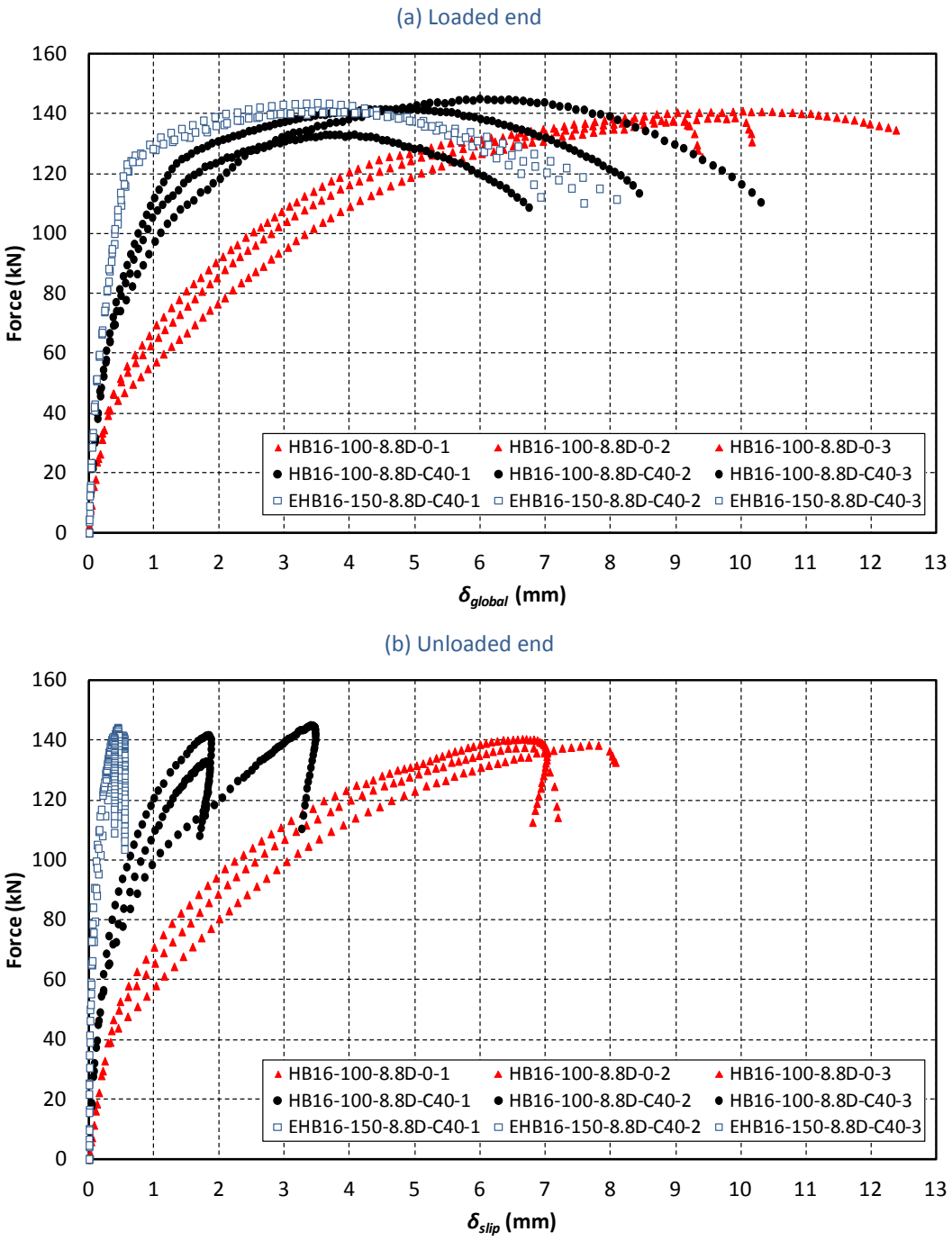

Figure 5.2 Pull-out behaviour of *EHB* in comparison with type *HB*

Therefore, preliminary analysis of the pull-out test results indicates that the enhanced performance of the *EHB* component in comparison with that of type *HB* is majorly attributed to the presence of the concrete infill. Nevertheless, the presence of the mechanical anchorage in the *EHB* component results in a more consistent and predictable force-displacement behaviour, with notably superior stiffness characteristics. The *EHB* component can provide resistance to pull-out forcing a failure in the yielding and eventual fracture of the internal bolt shank.

5.1.2 Response to pull-out and failure modes

When the *HB* blind-bolt is subject to direct tension, the load is distributed onto the connecting member through its internal bolt shank at the contact area of its threaded cone and expanding sleeves. As the load is increased, the blind-bolt tends to pull-through the clearance bolt hole. In result, a failure mode that relates to the expanding sleeves failing in shear is developed. The response of type *HB* to pull-out is depicted in Figure 5.3 where the movement of the threaded cone with respect to its original location can be clearly distinguished between the snap shot taken at its tightening stage and that prior to its ultimate state. Ultimately, the expanding sleeves of the blind-bolt shear against the connected plate in order to accommodate for the movement of the threaded cone along with the setscrew. This states that the dominant failure mechanism of type *HB* without a concrete infill is that of the mild steel expanding sleeves in shear, as identified by also in the literature. The failure mode of type *HB* does not involve thread stripping of its setscrew at the location of the threaded cone, and its response is characterised by the displacement of the system as a whole, as evidenced by visual inspections.

(a) at tightening stage (b) prior to ultimate capacity (c) Failure mode

Figure 5.3 Response of type *HB* (without concrete) with loading duration

The concrete-filled type *HB* and *EHB* both ultimately failed by bolt shank fracture. However, a closer examination of the surface of the concrete at the loaded end of the pull-out specimens revealed that the failure mode of type *HB* also involves concrete breakout, as depicted in Figure 5.4 (a). The formation of the concrete breakout occurs under the response of the tensile mechanism of the *HB*. As the fastener slips and the expanding sleeves deform and displace, a failure cone forms at the lower level of the expanding sleeves as shown in Figure 5.4 (b). Even though a concrete breakout is formed, the global force-displacement behaviour of the concrete-filled *HB* is still extensively improved in comparison with that of the unfilled *HB*. A comparison between failed test bolts of concrete-filled and unfilled type *HB* shows that this improved performance is attributed to the ability of the concrete in stiffening the expanding sleeves mechanism of the fastener. Evidently, as shown in Figure 5.4 (c), the infill reduces the deformation of the expanding sleeves to such an extent that it eliminates the dominant shear failure of the sleeves, allowing for the full tensile capacity of the internal bolt to develop.

(a) loaded end surface of pull-out specimen after testing

(b) concrete breakout

(c) effect of concrete on expanding sleeves

Figure 5.4 Failure mode of type *HB* (with concrete)

The concrete surfaces at the loaded end of type *EHB* are presented in Figure 5.5 in comparison with those of the concrete-filled type *HB*. On the contrary, it was found that the failure mode of type *EHB* did not involve a concrete breakout. This demonstrates the influence of the mechanical anchorage with respect to the distribution of the tensile force; the end anchor head of the *EHB* component has the ability to distribute the applied load within the concrete section. Consequently, the stresses that are acting on the mechanism of the expanding sleeves are relieved, and the reduction of such stresses also reduces the magnitude of the deformation and respective displacement of the sleeves. It is the distribution of force within the concrete member via mechanical anchorage that eliminates the concrete breakout which is seen in type *HB*; further justifying the enhanced stiffness characteristics of the component. To verify the observation, a closer examination of the expanding sleeves of the test specimens was performed which involved coring of the *EHB* fasteners in order to remove their expanding sleeves that were embedded in the concrete sections.

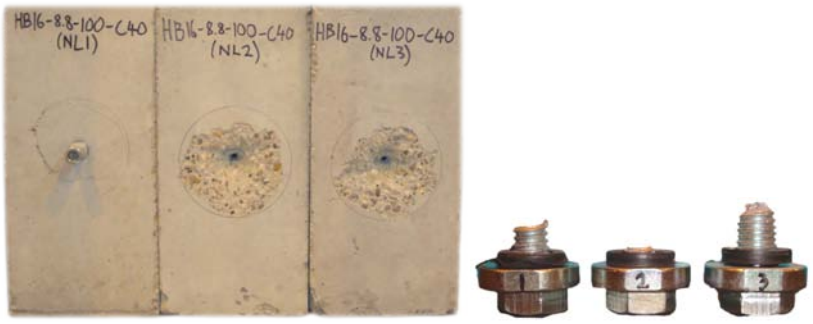

(a) specimens HB16-100-8.8D-C40-1, HB16-100-8.8D-C40-2, HB16-100-8.8D-C40-3 (left to right)

(b) specimens EHB16-150-8.8D-C40-1, EHB16-150-8.8D-C40-2, EHB16-150-8.8D-C40-3 (left to right)

Figure 5.5 Failure mode of type *EHB* in comparison with the concrete-filled type *HB*

The evolution of the failure mode from “expanding sleeves in shear” to “bolt shank fracture”, and the justification for the enhanced performance of the *EHB* component is presented in Figure 5.6. For illustration purposes, the visual aids commence with the display of the deformation that is induced in the expanding sleeves of the *HB* blind-bolt at its tightening stage due to the application of the tightening torque. Adjacent, the dominant expanding sleeves shear failure of type *HB* exclusive of concrete is presented. A demonstration of the subsequent reduction in sleeve deformation then follows by showing the tested sleeves that were involved in the concrete-filled type *HB*, and then those of the *EHB* component. It is clear that type *EHB* exhibits the minimum sleeve deformation among the varying types of fasteners, and it is concluded that the mechanical anchorage of the *EHB* component reduces extensively the deformation of the expanding sleeves element, hence the enhanced stiffness characteristics.

(a) At tightening (b) Type *HB* (c) Type *HB* (concrete) (d) Type *EHB*

Figure 5.6 Effect of mechanical anchorage on expanding sleeves

Preliminary conclusions are drawn with regard to the load transfer mechanism of the *EHB* component based on the cycle of improvements that were observed among the aforementioned testing configurations. It is apparent that the full tensile capacity of the component is achieved as tensile force is distributed into the concrete section, principally via the mechanical anchorage element, where the concrete infill plays a significant role in reducing the amount of deformation in the expanding sleeves mechanism. Minor measurements of slip in the component indicate that bolt elongation effectively occurs at the loaded outer side of the

testing configuration, in between the threaded cone and internal bolt head. Slip takes place at the contact area of the expanding sleeves and connecting member, however such slippage can only take place at the corresponding load of which local crushing of concrete in front of the end anchor head takes place. It is the purpose of the following section to identify the load at which concrete crushing occurs by investigating in more detail the response of the mechanical anchorage of the *EHB* component (signed as Type *M*) in line with appropriate data of type *EHB* and *HB*.

5.2 The individual elements of the *EHB* component

To further evaluate the load transfer mechanism of the *EHB* component, it is necessary to develop knowledge in the load transfer mechanisms of the elements of which it is comprised. To achieve this, herein the force-slip behaviour obtained from relevant pull-out tests is discussed. Focus is given to the internal bolt elongation element and to the interaction between the expanding sleeves and mechanical anchorage elements of the component.

5.2.1 Type *M* - Mechanical anchorage and bond element

With reference to the test matrix of the pull-out programme, specimens signed as type *M* were subject to pure tension in order to evaluate the response of the bond and anchorage element of the *EHB* component. The behaviour of the element is presented in Figure 5.7. Similarly, the slip of the element is smaller than its global displacement due to the elongation of the bolt shank that is included in the global readings, and three key points are identified within the plot in order to describe the behaviour of the element. The force-slip relationship of the element displays that the stiffness of the anchorage mechanism notably reduces at around 80kN and 120kN, approximately. The initial reduction in stiffness occurs due to local concrete crushing in front of the end anchor head of the mechanism, and the latter reduction is attributed to the yielding of the bolt shank. Although the initial stiffness of the mechanism is extensively reduced as concrete continues to crush, the presence of high concrete confinement and adequate embedment depth allows the anchor to resist total pull-out at the expense of a reduced stiffness.

Ultimately, type *M* failed by bolt shank fracture, and the constant slip that is observed upon the ultimate capacity of the element demonstrates the full transfer of force into the bolt shank; also evidenced by the softening branch of its global force-displacement response. The concrete surface at the loaded ends of identical specimens and the respective shank failures are depicted in Figure 5.8. The concrete section did not exhibit any evident cracking, as also observed in type *EHB*.

Type *M* (specimen M16-150-8.8D-C40-3)

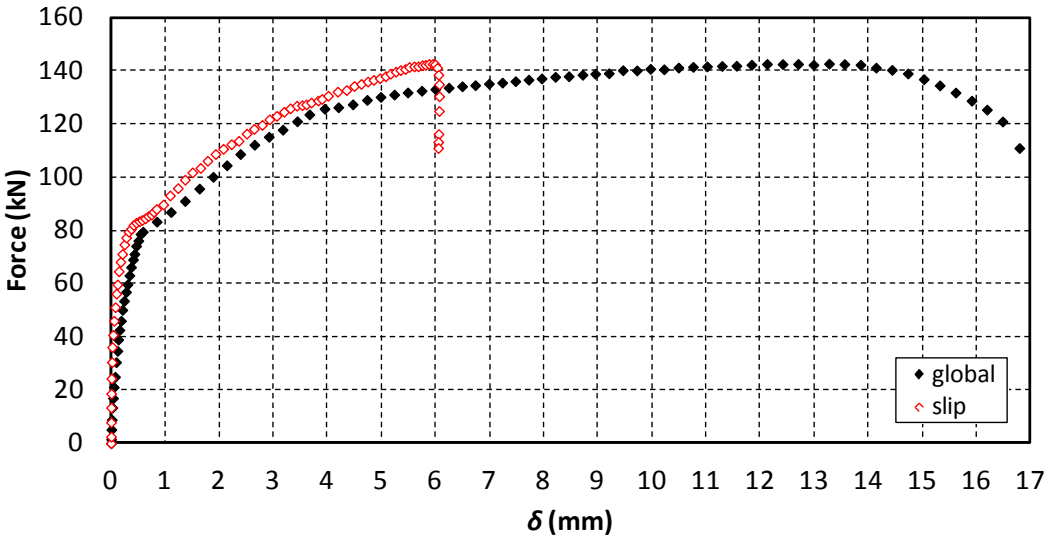

Figure 5.7 Pull-out behaviour of bond and anchorage element

Specimens M16-150-8.8D-C40-1, M16-150-8.8D-C40-2, M16-150-8.8D-C40-3 (left to right)

Figure 5.8 Failure mode of type *M*

Therefore, the load transfer mechanism of the bond and anchorage element relates to the load at which local concrete crushing occurs and to the yielding material

property of the bolt shank, exclusive of a concrete breakout formation; demonstrating an efficient development of mechanical anchorage for the provided embedment depth and concrete strength. The following section looks at the interaction of the expanding sleeves and mechanical anchorage of the *EHB*.

5.2.2 Force-slip relationship

To develop an understanding of the interaction among the expanding sleeves and mechanical anchorage elements of the *EHB* component, the force-slip relationship of the overall component is plotted along with that of the concrete filled type *HB*, and that of type *M* (Figure 5.9). The data involves pull-out specimens that carry benchmark parameters; bolts of the same batch (Batch D), of grade 8.8, with a d_b of 16mm, a concrete infill of grade *C40*, and a d_{emb} of $5.3d_b$. The force-slip behaviour is that of primary interest here because the data does not involve the elongation of the internal bolt shank. With the expanding sleeves, bond and anchorage, and bolt elongation elements being those which comprise the *EHB* component, by eliminating the source of deformability due to bolt elongation, it is thus possible to evaluate the interaction among the remaining two. The force-slip relationship of the concrete-filled type *HB* represents the expanding sleeves mechanism of the component, and that of type *M* represents its bond and anchorage mechanism.

Up to the force that corresponds to the pull-out strength of the mechanical anchorage - at which local crushing of concrete occurs in front of the end anchor head, at approximately 80kN - type *M* exhibits a stiffer response than type *HB*. This indicates that the initial stiffness of the *EHB* component is mostly attributed to the development of its mechanical anchorage. Type *HB* and *M* both allow for the full tensile capacity of the bolt shank to develop, and their force-slip relationship demonstrates resistance to pull-out from zero force to ultimate capacity. Therefore, their mechanisms do indeed interact throughout the application of a tensile force when combined together; and their interaction achieves the stiff response that is observed for the overall *EHB* component. Importantly, the increased slip of type *EHB* that is observed beyond the 80kN force can now be equated with the force at which type *M* indicates local concrete crushing in front of the end anchor head;

defined as the pull-out strength of the component with reference to the design of fastenings in concrete. This verifies the efficiency of using the force-slip relationship of type *M* to represent its mechanical anchorage. Moreover, the effect of the material property of the bolt shank is also observed, especially with regard to its yield strength (around 120kN) which forces a reduction in the post-limit stiffness of the individual elements, and the onset of bolt necking is identified by the constant slip once ultimate capacity is reached. With regard to failure modes, all relate to an eventual bolt shank fracture and a comparison of the concrete surfaces at the loaded ends of the specimens is depicted in Figure 5.10; illustrating the positive effect of the interaction of type *HB* and *M*.

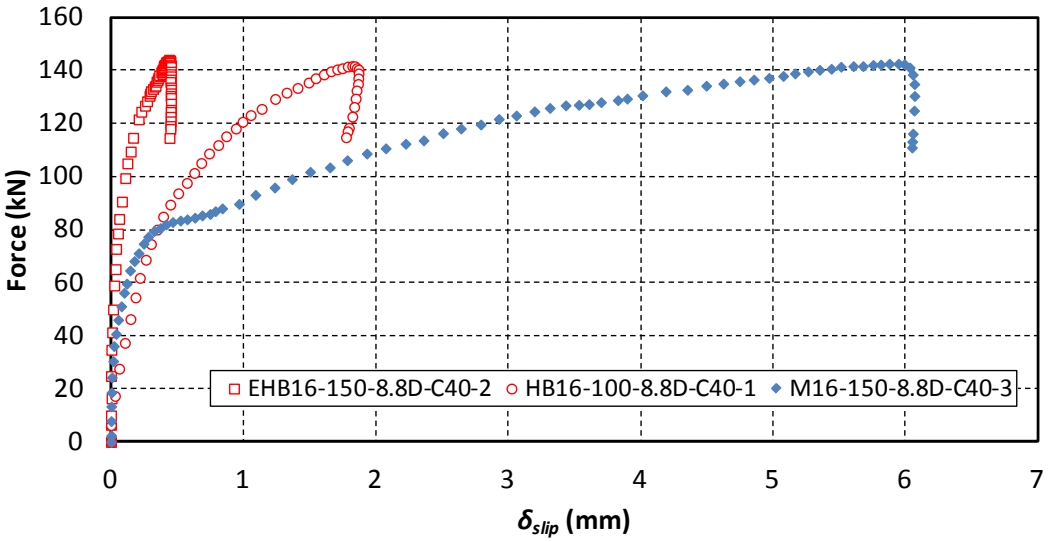

Figure 5.9 Slip response of *EHB* component and types *HB* & *M*

(a) Type *M* (b) Type *HB* (c) Type *EHB*

Figure 5.10 Concrete surface at loaded end after testing

5.2.3 Force-bolt elongation relationship (Mechanism 1)

It is the purpose of this section to discuss the source of deformability relating to the elongation of the internal bolt shank of the *EHB* component. Measurements of the response of the *EHB* to pull-out showed that bolt elongation is a source of deformability; distinguished by the difference between global and slip displacement measurements. An experimentally derived force-bolt elongation relationship for the *EHB* component is presented in Figure 5.11, determined by subtracting slip from the global displacement. As previously stated, the minor slip that was measured in the *EHB* component indicates that such bolt elongation effectively occurs at the outer side of the testing configuration. The importance of considering bolt elongation in the development of overall *EHB* component model is thus emphasized herein.

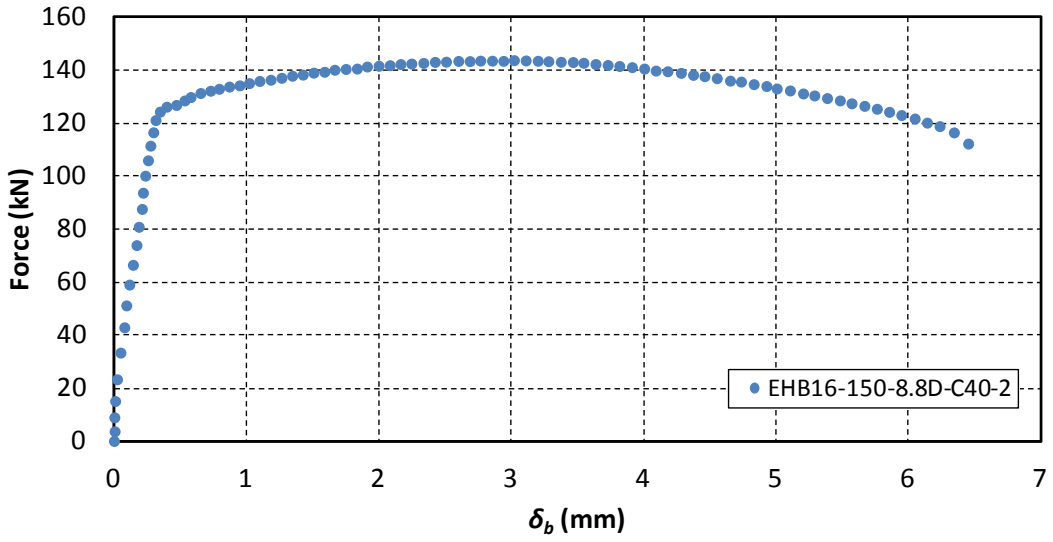

Figure 5.11 Bolt elongation element of type *EHB*

In summary, it is concluded that three individual elements contribute to the overall deformability curve of the *EHB* component, from zero force to failure; namely the expanding sleeves element, the bond and anchorage element, and the internal bolt shank elongation element. This approach where each element can be described and determined in isolation of each other provides a huge advantage in the development of the modelling part of the project.

5.3 Strain gauged bolts pull-out test series

To further investigate the load transfer mechanism of the *EHB* component, the strain gauged bolts pull-out test series was performed (see section 4.1.4). The results support the pull-out tests observations by investigating the contribution, interaction and evolution of the individual mechanisms of the component via their developing stress profiles.

The pull-out specimens involve benchmark parameters; type *M* and *EHB* have an embedment depth, d_{emb} of $5.3d_b$, and a head bearing area, A_{brg} of $2.0A_b$, where A_b is calculated based on the major bolt diameter, d_b. Strain gauges placed at $1d_b$ from the bearing face of the end anchor head of the component are used to determine the respective stress profiles. The gauges continuously monitored and recorded strain in type *M*, *HB* and *EHB*; from the tightening stage of the blind-bolts till testing. At tightening, all gauges (except those beneath the expanding sleeves for type *HB* and *EHB*) recorded negligible values of strain; close to zero compressive or tensile micro strain. Expectedly, the strain in the area of the expanding sleeves was large because the strain at that location equates with the pre-strain that is induced in the bolt due to the application of the tightening torque. Once the blind-bolts were tightened, the pull-out specimens were allowed 24hours for relaxation effects prior to casting of the concrete infill. Thereafter, the gauges monitored strain over the 7day concrete curing period to maintain an initial reading of all gauges before testing. It was found that during the curing process of the concrete infill, the strain measurements were slightly affected in the first 24hours of casting; attributed to temperature effects caused by the hydration of cement. Nevertheless, the strain readings stabilised upon the first 24hours and the residual values were recorded.

5.3.1 Stress profiles

The stress profiles of the specimens are shown in Figure 5.12 for different force levels. Stress in the bolt is determined at the locations of the strain gauges by multiplying the strain readings with Young's modulus of elasticity, *E*, and the stress profile is expressed in terms of bolt diameters from the bearing face of the *EHB* end anchor head. Because the strain recorded by the gauges is lower than the yield

strain (material property, ε_{yb}) of the bolt, Hooke's law of elasticity is applicable; where $\varepsilon_{yb} = f_{yb}/E$, and f_{yb} and E are actual properties of bolt batch *D*, as in Table 4.3.

The development of bolt stress in type *M* is shown in Figure 5.12 (a). At a force of 50kN, the maximum stress in the bolt was measured at $5d_b$ from the face of the anchor head. At a force of 70kN, the maximum stress was reached at $3d_b$. At this force level of 70kN, the maximum stress level in the bolt was nearly uniform from a point of $3d_b$ away from the head, with the slope of the stress profile leaning to zero. This indicates deterioration of bond as the strain is uniform at different embedded locations. At a force of 90kN, the maximum stress level in the bolt remains at $3d_b$, however the bolt stress close to the anchor head at $1d_b$ is seen to increase significantly, indicating the development of head bearing action. Ultimately, the sample reached 106kN with the bolt shank fracturing at $3d_b$.

The development of bolt stress in type *HB* is shown in Figure 5.12 (b). As anticipated, for all force levels the maximum stress in the bolt is measured at the location of the expanding sleeves mechanism, at the equivalent $5d_b$ from the face of the *EHB* end anchor. Even though the stress in the bolt at the equivalent $3d_b$ is extensively lower than that at the equivalent $5d_b$, the development of stress at $3d_b$ indicates development of bond resistance. The 102.8kN force level equates with the yield strength of the bolt shank in consideration of its net tensile stress area, $A_{s,net}$, and the 115kN force equates with the ultimate capacity that was reached by the specimen in the pull-out test. The bolt shank eventually fractured at $5d_b$ at the location of the strain gauge which was installed beneath the expanding sleeves; justified as it was the weakest area closest to the application of the tensile load.

The development of bolt stress in type *EHB* is shown in Figure 5.12 (c). As seen in type *HB*, for all force levels the maximum stress in the bolt is measured at the location of the expanding sleeves, at $5d_b$ from the bearing face of its anchor head. At a force of 60kN, between 3 and $4d_b$, the slope of the stress profile levels which indicates deterioration of bond resistance. At forces of 80kN and higher, the stress profile between 1 and $2d_b$ indicates development of head bearing stress as the slope leans to zero, and the lower from maximum stress level in the bolt remains at $3d_b$. Likewise with type *HB*, the bolt shank ultimately fractured at 114kN, at $5d_b$.

(a) Type *M*: specimen M16-150-8.8D-C40-4

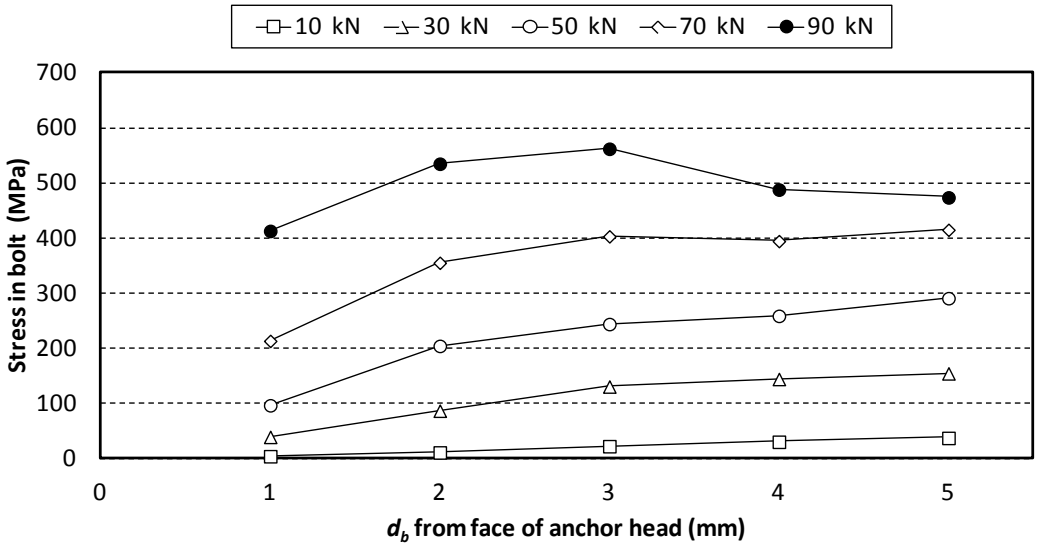

(b) Type *HB*: specimen HB16-100-8.8D-C40-4

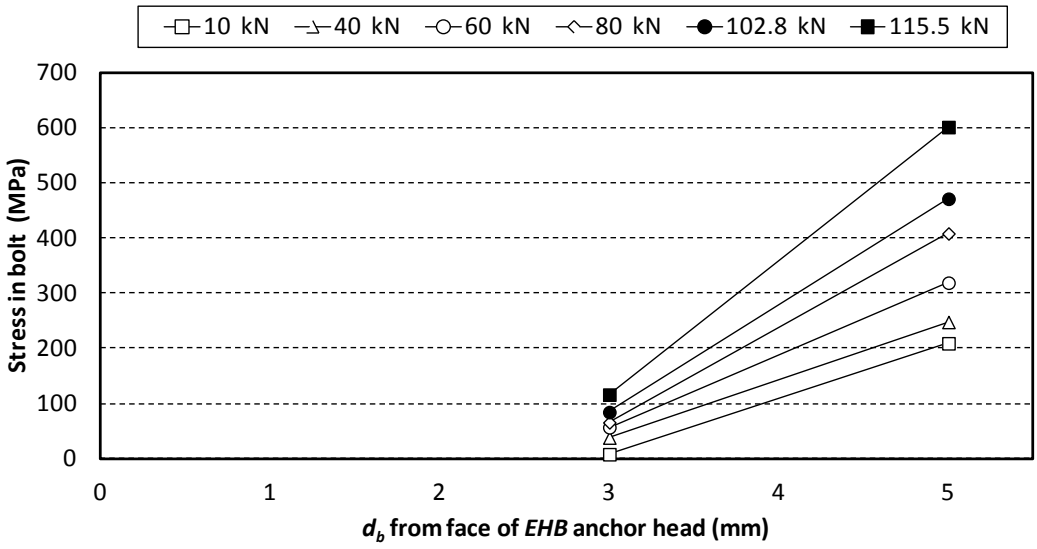

(c) Type *EHB*: specimen EHB16-150-8.8D-C40-4

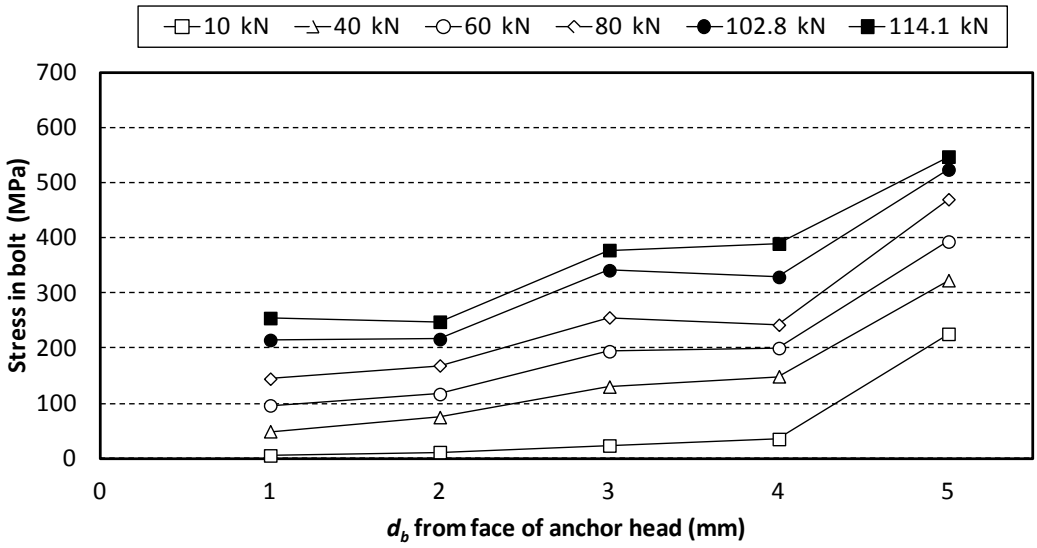

Figure 5.12 Stress profiles

In view of investigating the load transfer mechanism of the *EHB* component in accordance with the obtained stress profiles, the stress-strain distribution along the bolts can be used per Figure 5.13 in order to determine the development and contribution of the individual mechanisms that comprise the *EHB* component.

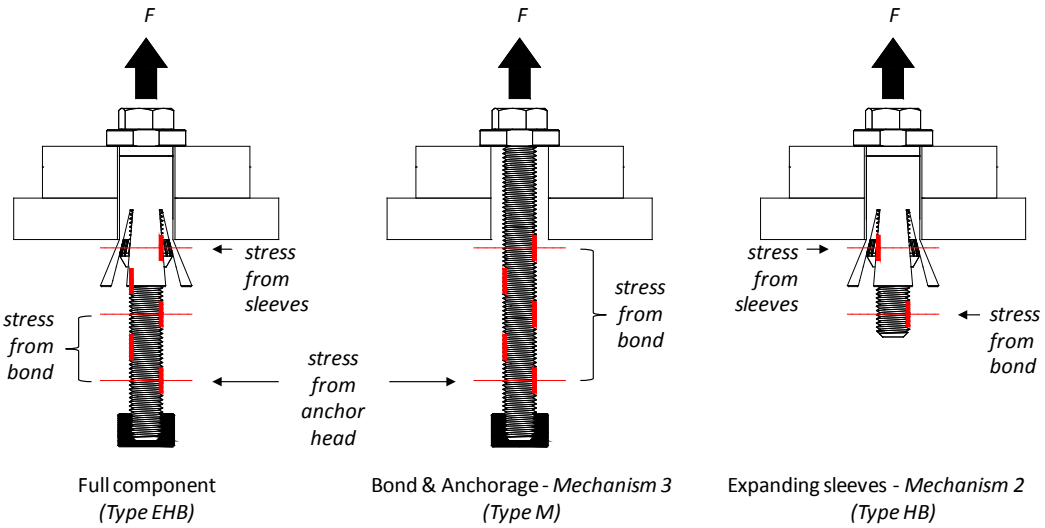

Figure 5.13 Development of stress in bolt

For type *HB*, the stress in the bolt at the equivalent $3d_b$ (at far bottom embedded location) is due to the development of bond resistance, and at $5d_b$ (below sleeves) the stress in the bolt is due to the development of the expanding sleeves mechanism, plus the development of bond resistance. To assess the development of bolt stress among type *HB* and *EHB*, the stress in the bolt of type *EHB* was measured at identical locations. Since the stress profile of type *EHB* indicated that bond and head bearing develop respectively at $3d_b$ and $1d_b$ from the face of the anchor head, the stress in the bolt at $5d_b$ is thus attributed to the development of the expanding sleeves mechanism, plus development of bond resistance, plus development of head bearing action. With regard to type *M*, the development of stress in the bolt at $1d_b$ from the face of the anchor head is attributed to the development of head bearing, whereas at $5d_b$ the stress in the bolt is due to the development of bond resistance plus development of head bearing action.

In order to determine the contribution of the developing elements with the applied loading, it is necessary to translate the applied force into total stress in the bolt. Because the nominal tensile stress area of the bolts was modified to accommodate for the installation of the strain gauges, it is required to determine their net tensile stress area, $A_{s,net}$, to account for the modifications in the transformation of force into stress. Figure 5.14 (a) depicts the effective net area of the bolts; calculated in consideration of the central and diagonal holes which accommodate the wiring of the strain gauges; and based on the assumption that the flats on which the gauges were installed are tangent to the minor diameter of the bolt, d_3, as the minimum thread was removed in the machining process. It is determined that the modifications in the geometry of the bolts result in a 22% reduction in cross sectional area with respect to the original nominal tensile stress area, $A_{s,nom}$. A visual inspection of the fractured strain gauged bolts confirms the applicability of $A_{s,net}$ for the effective tensile stress area, demonstrated in Figure 5.14 (b).

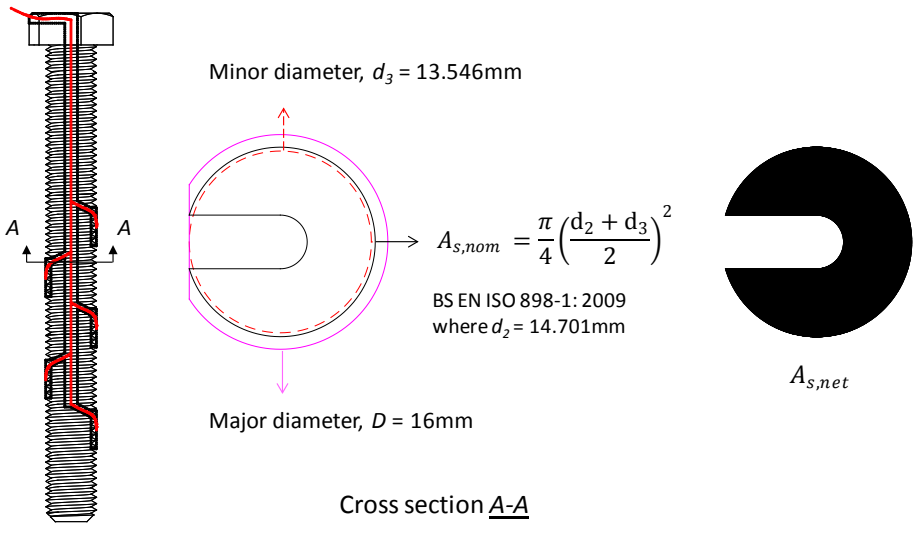

(a) Calculation of $A_{s,net}$

(i) Type *M* (ii) Type *HB* (iii) Type *EHB* (iv) $A_{s,net}$

(b) Actual fractured strain gauged bolts

Figure 5.14 Net tensile stress area

5.3.2 Type *M*: development of bond & anchorage

The stress profile data was used to determine the development of bond stress along the bolt in specimen *M16-150-8.8D-C40-4* as shown in Figure 5.15. The stress that is in the bolt at $1d_b$ from the bearing face of the head develops due to head bearing action. The remaining stress in the bolt of that closest to the concrete surface is attributed to development of bond; provided by the surface contact between the threads of bolt shank and concrete infill. Development of bond stress along the bolt is therefore calculated by deducting the stress that is developed in the bolt at $1d_b$ from the stress that is in the bolt at $5d_b$.

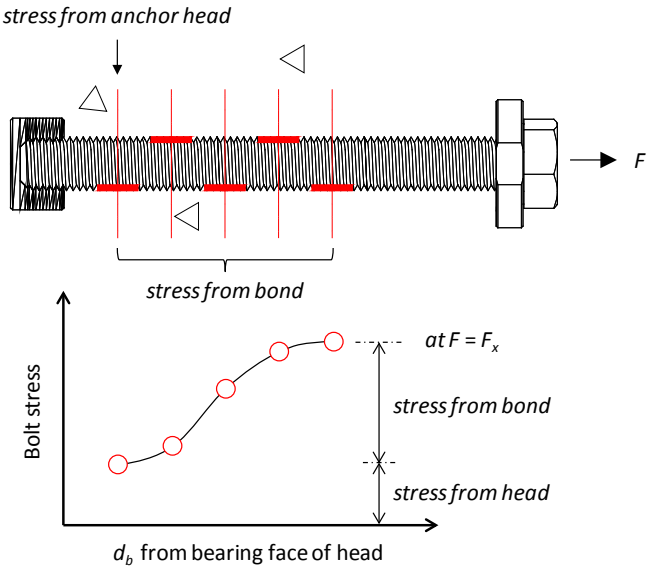

Figure 5.15 Type *M*: analysis of stress profile

Figure 5.16 shows that the development of the headed bolt was composed of a combination of bond plus a contribution from head bearing. It is found that the end anchor head provided a significant boost to the development of the bolt, and that deterioration of bond resistance initiates at a total stress of 550MPa, which equates with the 70kN force level in the stress profile whose slope leaned to zero.

Thus, anchorage of type *M* consisted of a two step process, in which bolt force was at first carried by bond, then as the bond reached its maximum level and began to deteriorate, anchorage shifted towards the anchor head. The final development of

the bolt was comprised of the peak bearing capacity of the anchor head plus a diminished bond contribution. The remaining contributor to the development of stress in the bolt is due to elongation of the bolt shank and force transfer losses.

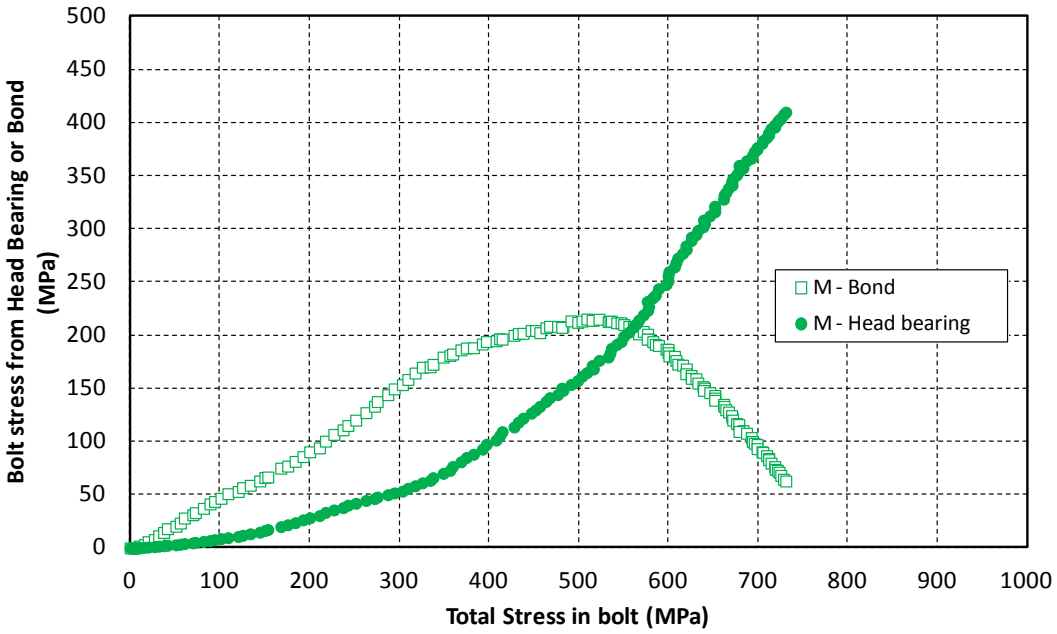

Figure 5.16 Components of bolt stress provided by bond & bearing in M16-150-8.8D-C40-4

5.3.3 Type *HB*: development of bond & expanding sleeves

The development of bond stress along the bolt and the development of the expanding sleeves mechanism in specimen *HB16-100-8.8D-C40-4* are shown in Figure 5.17. The bond contribution is represented by the stress at the far bottom of the fastener, as the stress in the bolt at this location develops due to the resistance provided by bond with the concrete. The stress in the bolt beneath the expanding sleeves includes the stress generated due to bond, thus by subtracting the bond contribution the remaining stress below the sleeves is due to the contribution of the expanding sleeves mechanism. Bond stress is shown to develop however the force in the bolt is mostly carried by the mechanism of the expanding sleeves. It is demonstrated that the expanding sleeves mechanism is engaged at a total stress of 200MPa; the equivalent stress level that was already present in the bolt when it was tightened. This indicates that the expanding sleeves mechanism of type *HB*

engages and develops when the pre-load in the bolt is overcome. At a total stress of 350MPa, the development rate of bond resistance reduces and simultaneously, there is a change in stiffness in the development of the mechanism of the expanding sleeves. The decrease in bond and sudden increasing stiffness of the sleeves mechanism indicates the transfer of additional force into the mechanism of the expanding sleeves. The consequent reduction in stiffness at a total stress of 600MPa is attributed to the yielding of the expanding sleeves mechanism, which also indicates the stress at which excessive slip initiates due to the deformation of the sleeves. Thus, tensile force in type *HB* is primarily distributed by the expanding sleeves mechanism which provides a 50% contribution, alongside with bond which provides a 10% contribution at failure. The remaining development of stress is attributed to bolt elongation and force transfer losses.

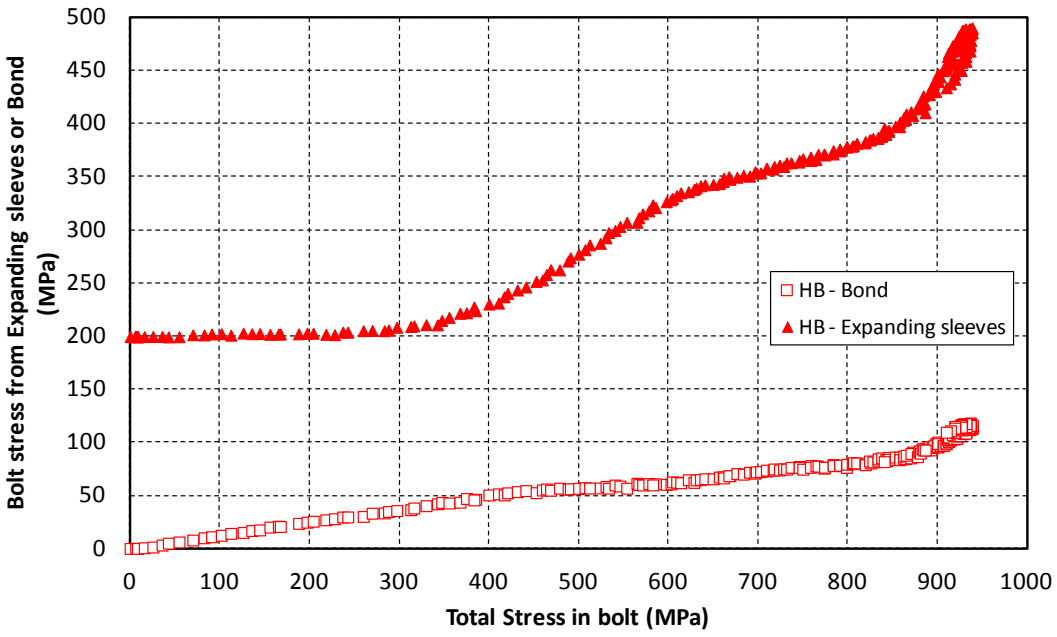

Figure 5.17 Bolt stress provided by bond & expanding sleeves in HB16-100-8.8D-C40-4

5.3.4 Type *EHB*: development of bond, anchorage & exp. sleeves

The development of the elements of type *EHB* in specimen *EHB16-150-8.8D-C40-4* are shown in Figure 5.18. Head bearing stress is represented by the stress that is in the bolt at $1d_b$ from the bearing face of the head which develops due to head

bearing action. Bond contribution along the embedded bolt is determined by deducting the head bearing stress that develops at $1d_b$ from that which develops at $3d_b$ from the face of the end anchor head. The development of the mechanism of the expanding sleeves is represented by the stress that develops in the bolt at $5d_b$ from the face of the end anchor minus the contributions of bond and head bearing; determined by deducting the stress measured at $3d_b$ from that measured at $5d_b$.

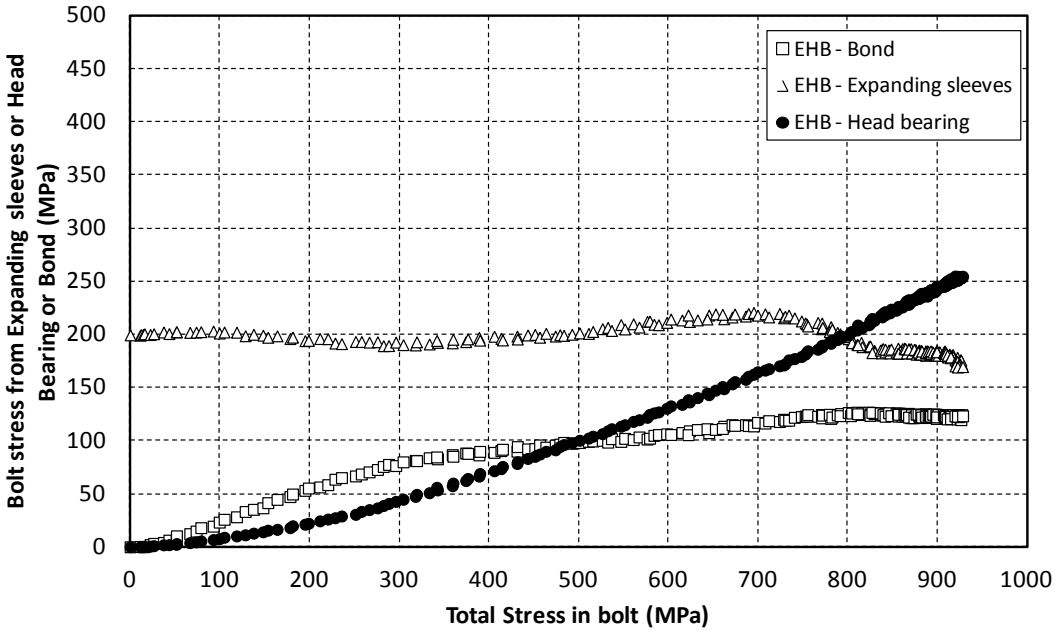

Figure 5.18 Bolt stress provided by bond, bearing, & exp. sleeves in EHB16-150-8.8D-C40-4

Likewise with type *HB*, the contribution of pre-load in the bolt is indicated by the initial level of stress in the mechanism of the expanding sleeves. Once the total stress in the bolt reaches the value of pre-stress in the bolt, the trend shows a slight decrease in the contribution of the sleeves mechanism which indicates the transfer of force into the bond and head bearing elements; evidenced by their development in the stress range. At a total stress of 300MPa, the development of the expanding sleeves mechanism starts to peak as bond contribution deteriorates, and a significant development of head bearing is observed. This indicates that as bond deteriorates, anchorage is shifted towards the end anchor head of the component, and the overall tensile force is primarily distributed among the mechanism of the expanding sleeves and that of the end anchor head element. It is also observed that

when head bearing contribution reaches that of the mechanism of the sleeves (at a total stress of 800MPa), thereafter the contribution of the expanding sleeves mechanism and that provided by bond both stabilise to a constant value, whereas head bearing continues to develop.

Thus, tensile force in type *EHB* is primarily carried by a combination of resistance provided by the expanding sleeves mechanism and that over head bearing action. At ultimate capacity, it is found that head bearing contributes around 30% to the development of stress in the bolt, the expanding sleeves mechanism provides a 20% contribution, and bond resistance which has not entirely deteriorated provides up to 10%. The remaining development of stress in the bolt is attributed to bolt shank elongation and possible losses that are involved in the transfer of the tensile force among the elements.

5.3.5 Evaluation of the load transfer mechanism of type *EHB*

The mechanics of the *EHB* component were observed and recorded to evaluate the manner in which the capacity of the component is developed. Herein, a comparison is drawn among the mechanics of the *EHB* and the commercially available *HB* in consideration of concrete-filled sections. The development of the elements in type *HB* is compared with the development of those which comprise type *EHB* in Figure 5.19. As anticipated, due to the longer threaded bolt shank in the *EHB*, the bond contribution is higher for type *EHB*. With regard to the mechanism of the expanding sleeves, in type *EHB* its contribution is a lot lower than that observed in type *HB*. This demonstrates that the bond and head bearing element of type *EHB* can distribute tensile force while relieving the stress that is acting on its sleeves mechanism; which is known to be prone to a dominant shear failure. This observation verifies and explains pull-out test inspections which report that the expanding sleeves in type *EHB* exhibit reduced deformation with comparison to those in type *HB*. The development of head bearing stress, generated on the concrete in front of the anchor head at its end, and the additional development of bond along the extended bolt shank reduces the deformation of the expanding sleeves mechanism.

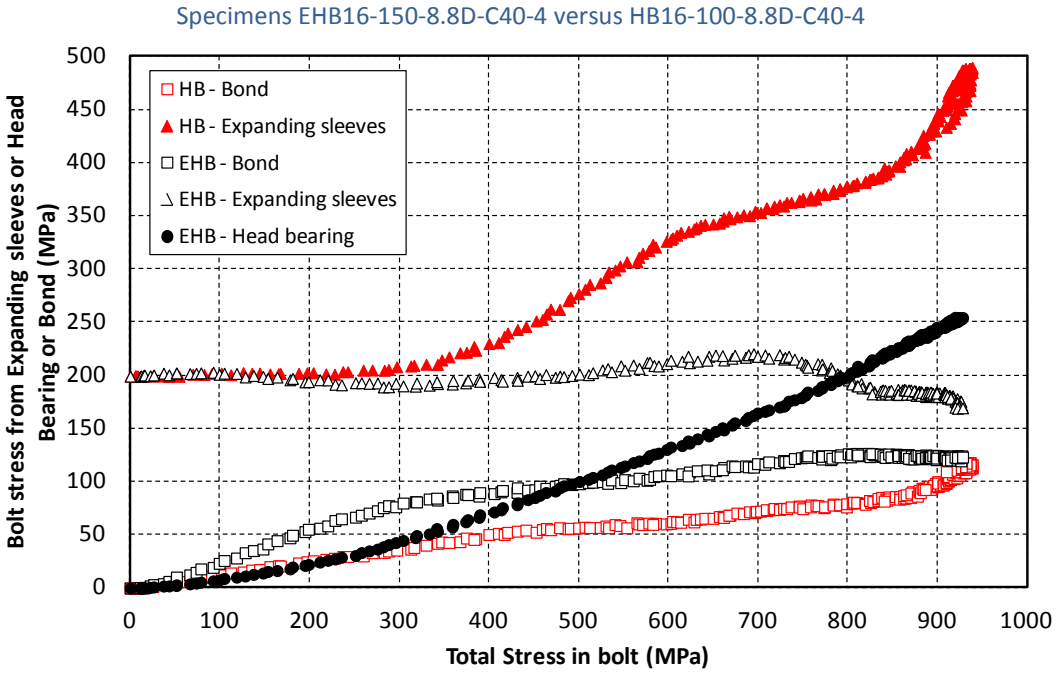

Figure 5.19 Development of bolt stress components in types *HB* & *EHB*

In summary, it is concluded that the expanding sleeves, bond and head bearing elements contribute to the deformability of the *EHB* component; from its tightening stage up to its ultimate failure.

5.4 Global force-displacement behaviour of *EHB* component

This section presents the raw pull-out test results with regard to the parameters affecting the global force-displacement relationship of the *EHB* component. A comparison of the loaded end displacement is drawn among the varying parameter specimens that were investigated in the test matrix, and the parameter which seems to affect mostly the response of the overall component is identified. The investigative parameters involve the strength of the concrete infill, the grade and diameter of the internal bolt, and the embedment depth.

5.4.1 Effect of concrete strength

The effect of increasing the strength of the concrete infill from grade *C40* to *C60* is shown in Figure 5.20. It is found that the initial stiffness of the *EHB* component is markedly enhanced in the case of the higher concrete grade, with the effect evidently seen once the pre-load in the bolt is overcome. With regard to strength,

the *EHB* component is not seen to be affected by the parameter variation. For the investigated concrete grades, the yield and ultimate strength of the component both correspond with the yield and ultimate strength of the internal bolt shank, respectively. This indicates that the yield strength and ultimate capacity of the *EHB* component are independent of the strength of the concrete infill when a variation in grade of *C40* to *C60* is considered.

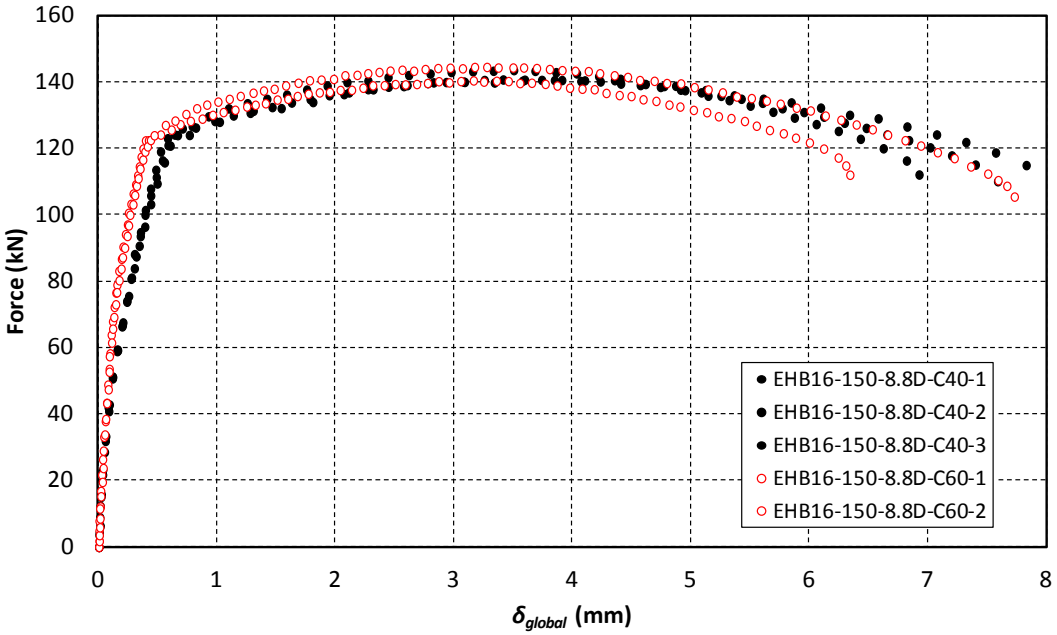

Figure 5.20 Effect of concrete strength on *EHB* force-global displacement relationship (raw)

In terms of ductility, the component is seen unaffected by the variation in concrete strength. Since the commencement of the softening branch of the component (upon ultimate strength) corresponds with the onset of internal bolt necking, it is thus concluded that the ductility of the *EHB* component is also directly related to the mechanical properties of the internal bolt shank. Moreover, the failure mode among the different concrete strength specimens was not altered; likewise with the grade *C40* specimens, the high strength concrete pull-out specimens failed by bolt shank fracture upon ultimate capacity, and the loaded end surface did not exhibit any form of concrete breakout.

5.4.2 Effect of bolt grade

The effect of using an internal bolt of higher grade, under increased tightening torque conditions in the *EHB* component is presented in Figure 5.21. It is shown that when grade 10.9 bolts are employed in the *EHB*, the initial stiffness of the component is marginally improved and maintained to a much higher force. On the other hand, the post-limit stiffness of the component (upon yielding) is notably reduced in the case of the higher bolt grade. Expectedly, the yield and ultimate strength of the component is increased in the case of the higher bolt grade. Such notable effects are attributed to the difference in mechanical properties between grade 8.8 and 10.9 bolts - which exhibit different force-deformability responses - in combination with the effects arising from the level of pre-load that is induced in the internal bolts of the assemblies.

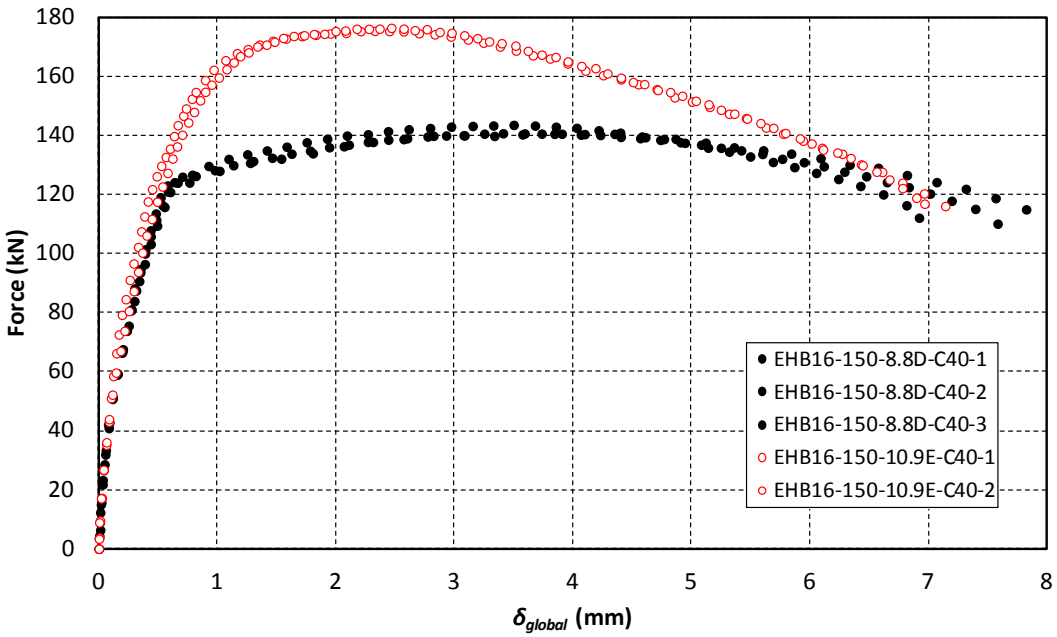

Figure 5.21 Effect of bolt grade on *EHB* force-global displacement relationship (raw)

The ductility capacity of the component is seen unaffected by the variation in bolt grade, however a sharp drop in resistance is observed upon ultimate capacity for grade 10.9 specimens. Generally, bolts of grade 10.9 are characterised as non-ductile in comparison with grade 8.8 bolts, and this general behaviour is observed in the test results herein; the linear softening branch of the grade 10.9 pull-out specimens indicates the limited ductility of high grade bolts. Nevertheless, the

failure mode among the different bolt grade specimens was not altered; likewise with the bolt grade 8.8 specimens, the grade 10.9 specimens failed by bolt shank fracture upon ultimate capacity and the loaded end surface did not exhibit any form of concrete breakout. Thus, the use of grade 10.9 bolts in comparison with 8.8 improves the stiffness and strength characteristics of the *EHB* component at the expense of a reduction in post-limit stiffness due to the mechanical properties involved in high grade bolts. The test results demonstrate the ability of type *EHB* in distributing the additional applied forces when internal bolts of grade 10.9 are employed; allowing for their full tensile capacity to develop.

5.4.3 Effect of bolt diameter

Figure 5.22 compares the force-global displacement relationship of the *EHB* component in consideration of 16 and 20mm internal bolt diameters, with the latter involving an increased tightening torque. It is found that the initial stiffness of the component is enhanced to some extent in the case of the larger bolt diameter, and as anticipated, it is also maintained to a much higher force. The yield and ultimate strength, as well as the ductility of the component increase notably with the variation in bolt diameter; nevertheless the failure mode of the specimens involved the yielding and eventual fracture of the internal bolt shank.

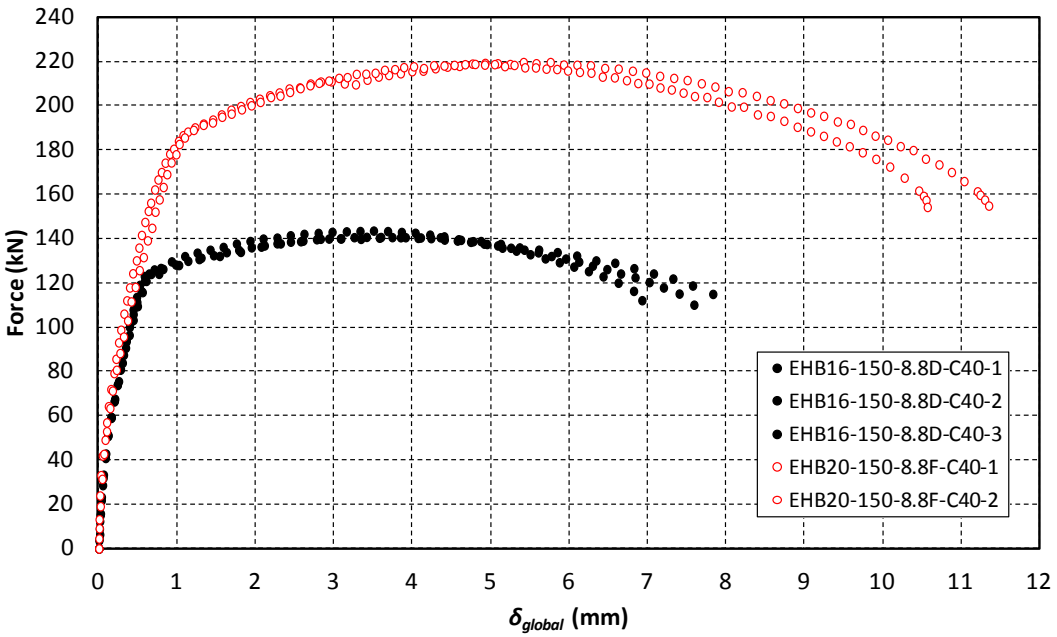

Figure 5.22 Effect of bolt diameter on *EHB* force-global displacement relationship (raw)

5.4.4 Effect of embedded depth

The response of the *EHB* component with varying embedded depth, d_{emb}, is shown in Figure 5.23. The comparison involves specimens with internal bolt shanks of 130, 150 and 170mm long which equate with embedded depths of 4.0, 5.3 and 6.5d_b, respectively. It is indicated that the initial stiffness of the component is not significantly affected with the variation in d_{emb}; however a discrepancy is seen among the strength of the pull-out specimens. As each category of d_{emb} specimens involved a different bolt batch, the discrepancy of the data in the yield and ultimate states is attributed to the variation in the mechanical properties of the internal bolts. Similarly, the effects relating to the post-limit stiffness of the component are due to the variation in the mechanical properties of the internally employed bolts.

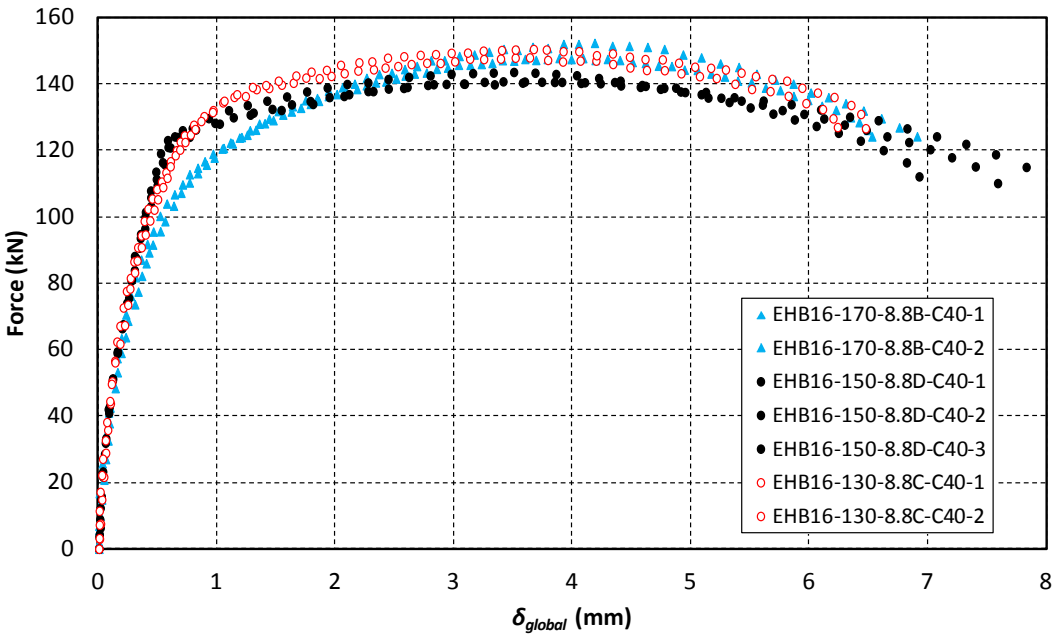

Figure 5.23 Effect of embedded depth on *EHB* force-global displacement relationship (raw)

The ductility of the component is also observed as unaffected to the variation in d_{emb}, and the failure mode of the component did not alter with respect to the benchmark specimen; all failed by internal bolt fracture upon ultimate capacity, exclusive of concrete breakout. It is thus felt that the stiffness, strength and ductility of the *EHB* component are not dependent upon d_{emb} when embedded

depths of 4.0 to 6.5d_b are considered. Moreover, it is concluded that type *EHB* allows for the full tensile capacity of the component to develop when an embedded depth, d_{emb} of 4.0d_b is provided, equating with the minimum possible shank length.

5.4.5 Effect of parameter variation on Mechanism 1 - Bolt elongation

In consideration of the investigative parameters, the experimentally derived force-bolt elongation relationships of the *EHB* component are shown in Figure 5.24. As anticipated, it is found that the stiffness and strength of the mechanism is directly related to the mechanical properties of the internal bolt of the component.

(a) *M16* grade *8.8* internal bolts

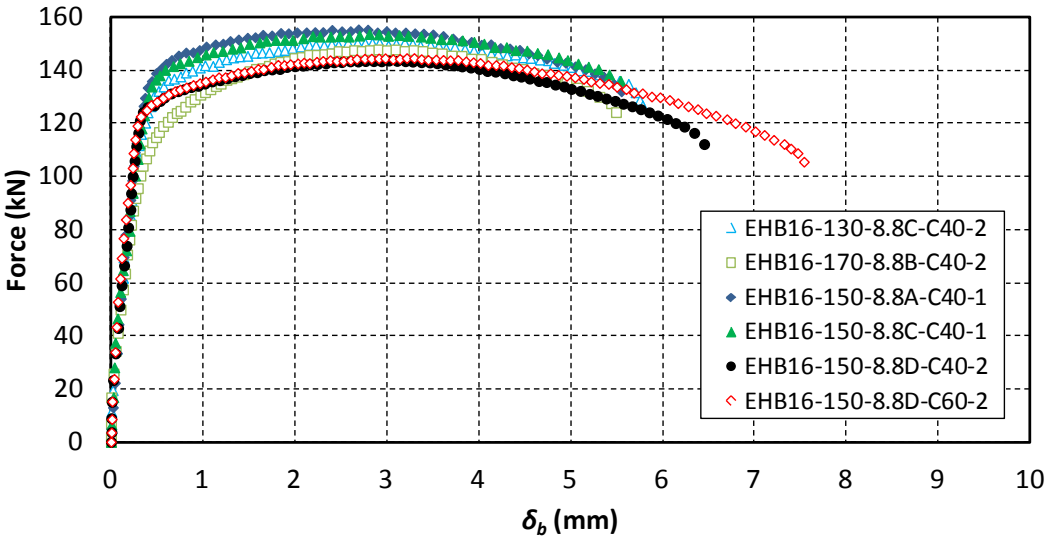

(b) Effect of bolt diameter & grade: *M16/M20* gr.*8.8*, *M16* gr.*8.8/10.9*

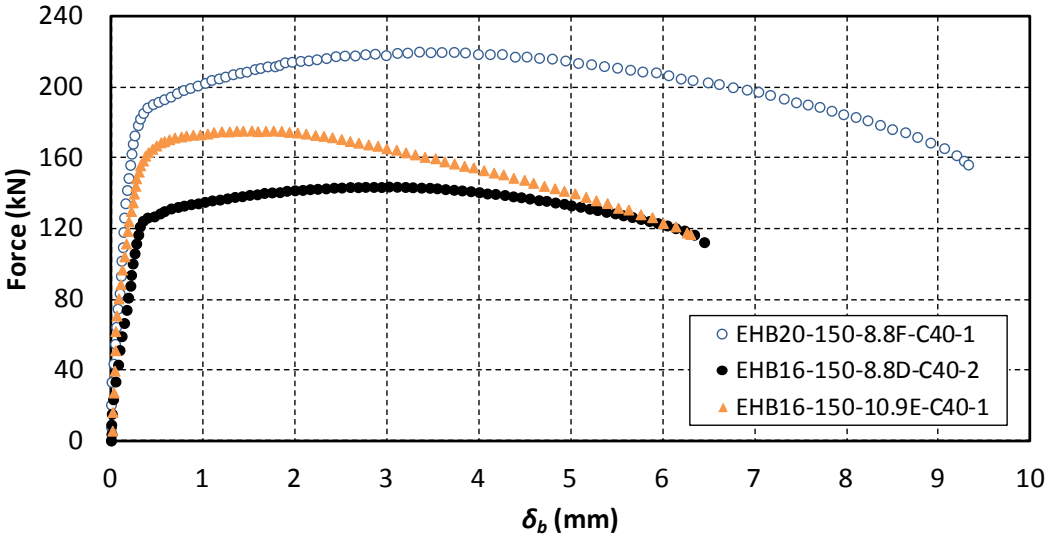

Figure 5.24 *EHB* force-bolt elongation relationship (raw)

The experimental force-δ_b relationship for *M16* grade 8.8 internal bolts is presented in Figure 5.24 (a). It is observed that the initial stiffness of the mechanism is consistent and not affected by the variation in d_{emb} but a discrepancy among the yield and ultimate strength of the data is notable; attributed to the difference in mechanical properties between the bolt batches. In contrast, the initial stiffness of the force-δ_b mechanism is seen to increase in the cases where *M20* grade 8.8 or *M16* grade 10.9 internal bolts were employed; as highlighted in Figure 5.24 (b). Due to the higher tightening torque involved in the *M20* gr.8.8 and *M16* gr.10.9 it is therefore anticipated that the level of pre-load in the internal bolt also governs the stiffness of the force-δ_b mechanism of the *EHB* component in addition to the size and mechanical properties effects. Importantly a suitable model that is to represent the response of the bolt elongation element in the overall *EHB* component model can be evaluated against the experimental data presented herein.

5.5 Mechanism 2 - Expanding sleeves

This section presents experimental data relating to the testing of the concrete-filled type *HB*. Test data and observations with regard to benchmark specimens are first presented, followed by results which demonstrate the effects on the behaviour of the element due to a variation in parameters; namely concrete strength, bolt grade, and bolt diameter. Focus is given to the stiffness, strength, ductility, and ultimate failure modes. Moreover, the relevance of the force-slip relationships with respect to the expanding sleeves mechanism of the *EHB* component is discussed.

5.5.1 Benchmark behaviour: *HB16-100-8.8-C40*

A total of nine benchmark concrete-filled type *HB* specimens were tested. The specimens involve an internal bolt of 16mm diameter of grade 8.8, embedded in a *C40* concrete mix. The force-slip relationship of the benchmark specimens is shown in Figure 5.25, with highlight given to the groups of bolt batches that were employed in the testing.

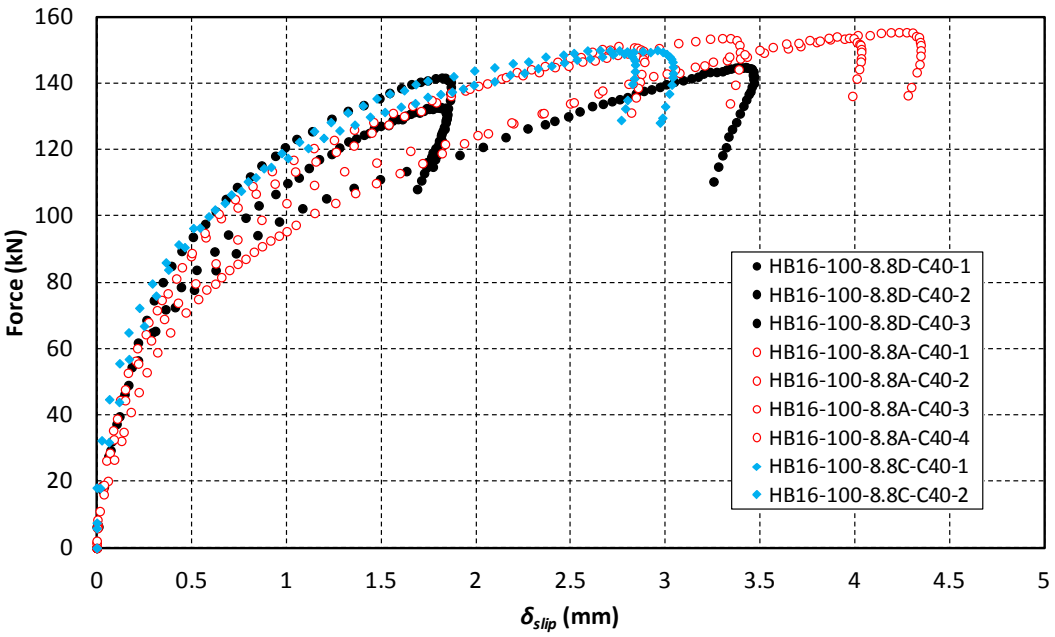

Figure 5.25 Force-slip relationship for expanding sleeves (benchmark HB16-100-8.8-C40)

An initial reduction in stiffness is commonly observed at around 60kN. Thereafter though, it is evident that three specimens exhibit a rather different response to that

observed by the remaining six; *HB16-100-8.8D-C40-3*, *HB16-100-8.8A-C40-3*, and *HB16-100-8.8A-C40-4*. The post-limit stiffness of these specimens is lower than that of the others, and this behaviour is not attributed to the properties of the various bolt batch groups. On the other hand, the discrepancy in ultimate capacity is attributed to the variation in mechanical properties among the groups. With regard to ductility, a relation is shown between bolt batch group specimens and ductility capacity; higher ductility is exhibited by group *A* and *C* specimens whose internal bolts allowed for higher ultimate forces. All nine specimens failed by the yielding and eventual fracture in the internal bolt shank, alongside with a concrete breakout forming at their loaded end surface (Figure 5.26).

(a) Fractured internal bolt shanks: 1-2 Batch C, 3-6 Batch A, 7-9 Batch D

(b) Loaded end surfaces

Figure 5.26 Benchmark specimen failure mode (HB16-100-8.8-C40)

To understand whether the scatter of the test data is related to the extent of concrete breakout, a closer examination of the failure surface of the specimens was carried out, in consideration of the concrete strength of each specimen that was measured on the day of testing. In accordance with the observations it was not possible to identify a pattern that is related to the test results, and the discrepancy among the experimental results is thus justified by the non-homogeneous behaviour of concrete as a material, and to the variation in mechanical properties of bolts. For the benchmark specimen herein, it is however concluded that the

failure mode involves a concrete cone breakout of diameter 175mm, which forms at an approximate angle of 20^{o} to the horizontal, as shown in Figure 5.27.

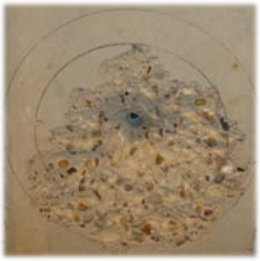
HB16-100-8.8A-C40-1

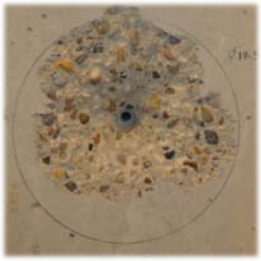
HB16-100-8.8A-C40-2

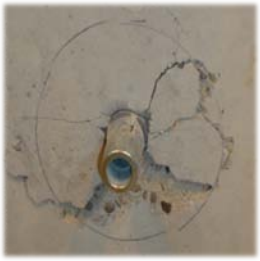
HB16-100-8.8A-C40-3

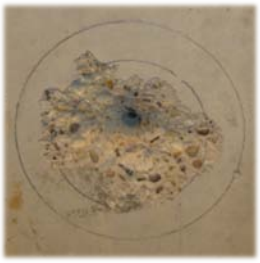
HB16-100-8.8A-C40-4

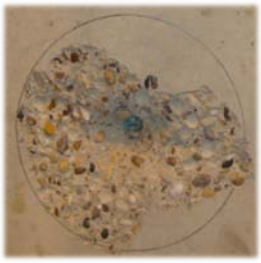
HB16-100-8.8C-C40-1

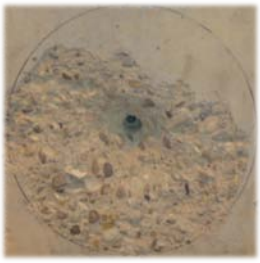
HB16-100-8.8C-C40-2


HB16-100-8.8D-C40-1

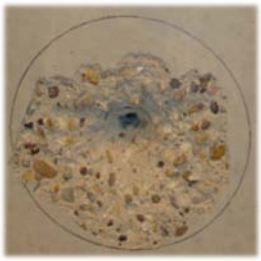
HB16-100-8.8D-C40-2

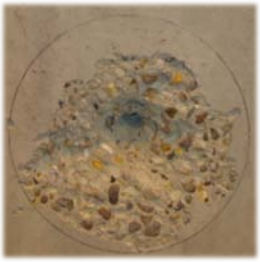
HB16-100-8.8D-C40-3

(a) Measurement of breakout diameter


(b) Failure diameter 175mm


(c) Breakout forming at approx. 20^{o}

Figure 5.27 Formation of concrete breakout in benchmark specimen (HB16-100-8.8-C40)

5.5.2 Effect of concrete strength

The effect of increasing the strength of the concrete infill from grade *C40* to *C60* is shown in Figure 5.28. It is found that the initial stiffness of type *HB* is enhanced in the case of the higher concrete grade, with the effect evidently seen once the pre-load in the bolt is overcome. With regard to strength, the *HB* blind-bolt is not seen to be affected by the parameter variation; the global yield and ultimate strength of type *HB* both correspond with the yield and ultimate strength of the internal bolt shank, respectively. This indicates that the global yield strength and ultimate capacity of type *HB* are independent of the strength of the concrete infill when a variation in grade of *C40* to *C60* is considered.

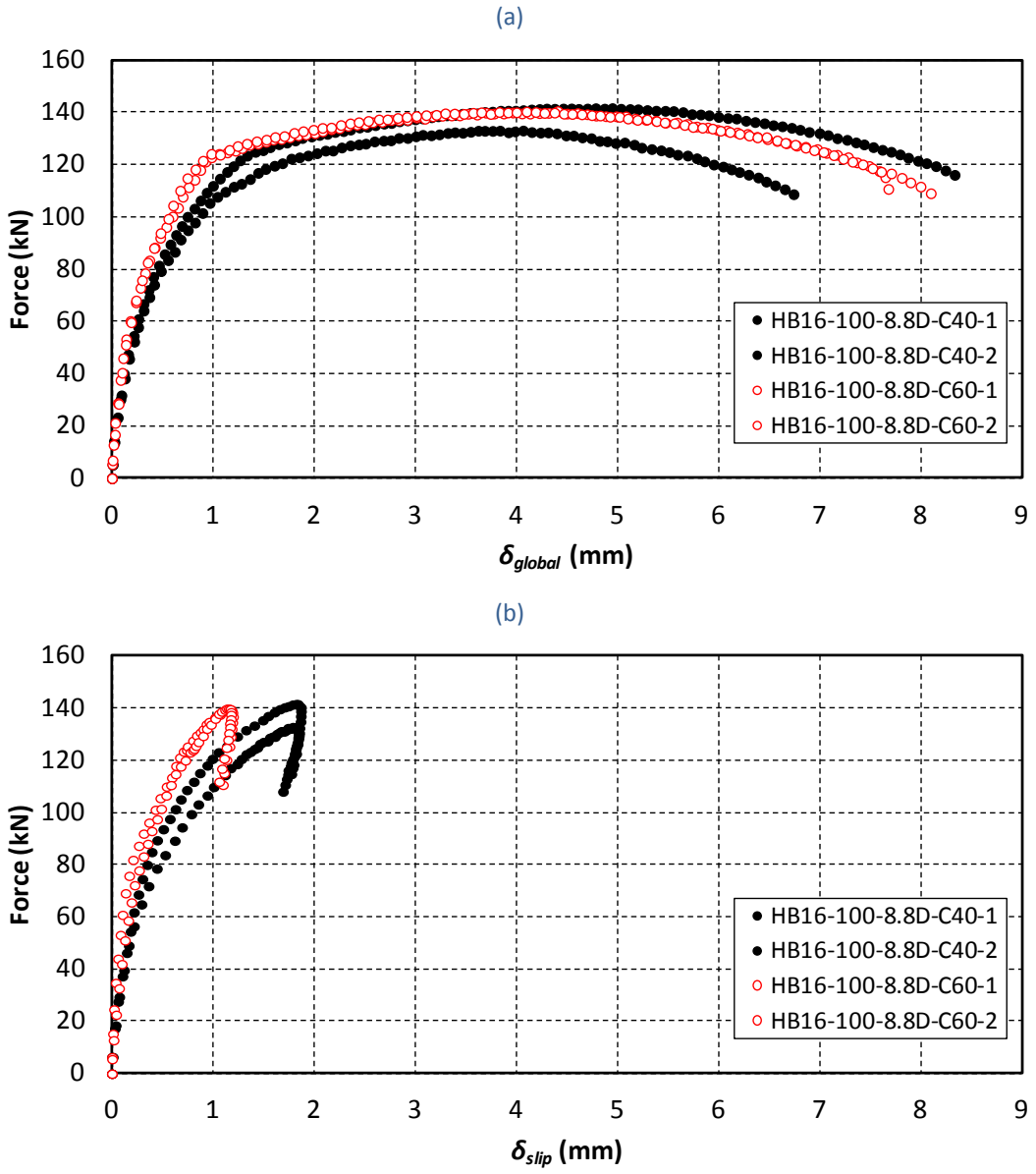

Figure 5.28 Effect of concrete strength on tensile behaviour of type *HB*

Similarly, with respect to the unloaded end slip, the improvement in the tensile behaviour of type *HB* with increasing concrete strength is shown in Figure 5.28 (b). A visual inspection of the loaded end surface of the high concrete grade *HB* specimens indicated that the enhanced characteristics of type *HB* are attributed to the ability of the high strength of the concrete infill in resisting the formation of a concrete breakout. In contrast with the grade *C40* specimens, the *C60* grade pull-out specimens failed by bolt shank fracture upon ultimate capacity, but the loaded end surface did not exhibit any form of concrete breakout (Figure 5.29).

Figure 5.29 Effect of high strength concrete on failure mode (in HB16-100-8.8D-C60-1)

The enhanced response of type *HB* with increasing concrete strength is reflected with the enhanced performance seen in the *EHB* component when a high strength concrete infill is considered. Thus, this indicates that the resulting effect on the behaviour of type *EHB* in high grade concrete is partly attributed to the improved characteristics of its expanding sleeves mechanism.

5.5.3 Effect of bolt grade

The effect of using an internal bolt of higher grade, under increased tightening torque conditions in the concrete-filled type *HB* is presented in Figure 5.30. It is shown that when grade 10.9 bolts are employed in type *HB*, the initial stiffness is not affected however it is maintained to a much higher force. Conversely, the post-limit stiffness (upon yielding) is significantly reduced, whereas the global yield and ultimate strength of type *HB* increase in the case of the higher bolt grade; attributed to the mechanical properties of grade 10.9 bolts. The ductility capacity of

type *HB* is seen unaffected by the variation in bolt grade however resistance is seen to drop immediately upon ultimate capacity in the grade 10.9 specimens.

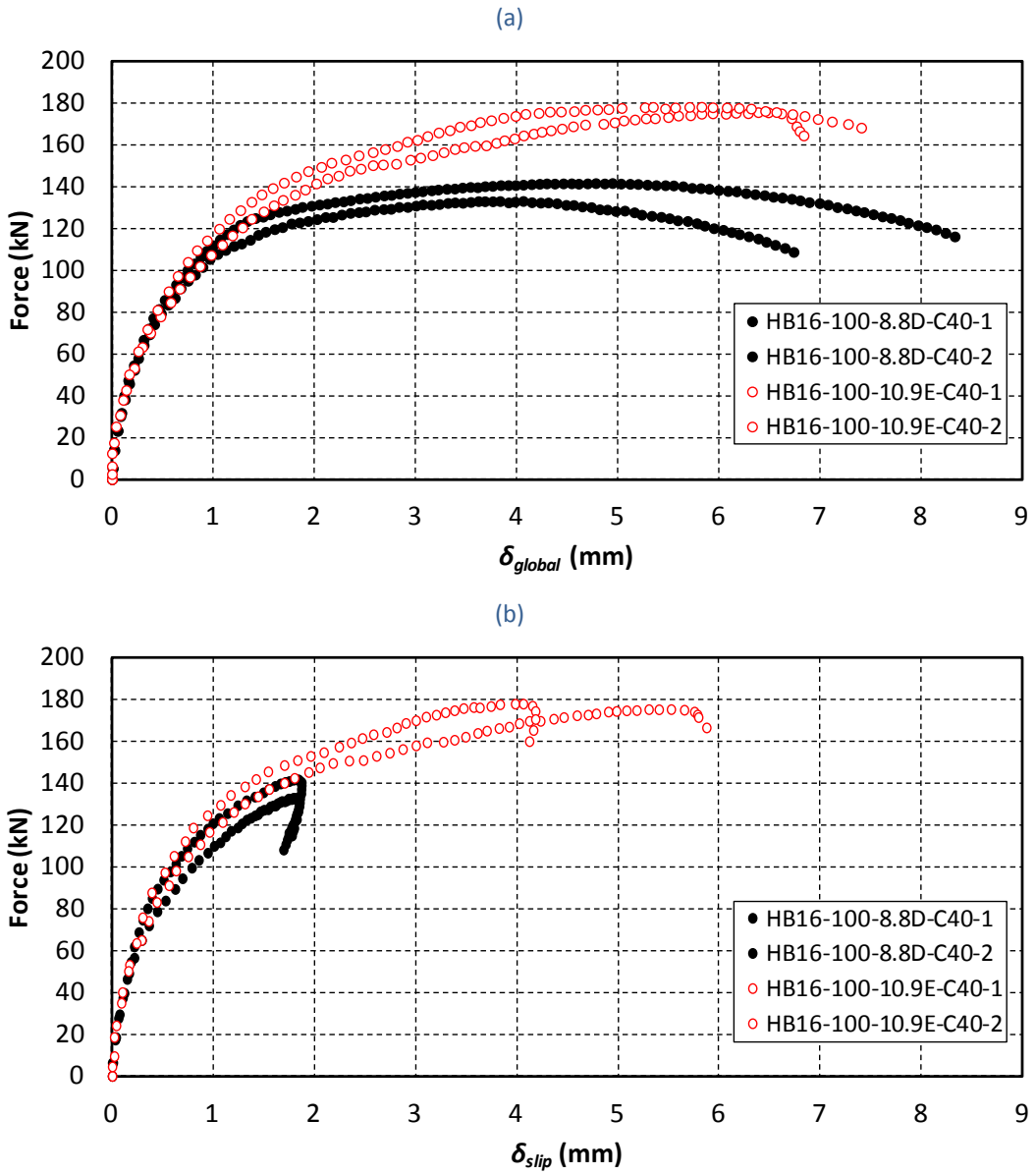

Figure 5.30 Effect of bolt grade on tensile behaviour of type *HB*

Although the employment of grade 10.9 internal bolts seems to improve the tension characteristics of type *HB*, the failure mode that the configuration exhibits hinders its application. The ultimate failure of grade 10.9 specimens was found to be due to a combination of the expanding sleeves failing in shear and a concrete breakout that formed at its loaded end surface, depicted in Figure 5.31 (a).

(a) Breakout & sleeves in shear (b) HB16-100-10.9E-C40-1 vs EHB16-150-10.9E-C40-1

Figure 5.31 Failure mode of internal bolt grade 10.9 in type *HB*

Such an alteration in failure mode demonstrates that the expanding sleeves element in type *HB* is the limiting factor when grade 10.9 bolts are considered. The configuration of type *HB* does not allow for forces higher than those anticipated in grade 8.8 to be reached without exhibiting the dominant shear failure of its expanding sleeves. In contrast, the *EHB* component allows for the tensile capacity of grade 10.9 bolts to develop; attributed to its ability in reducing the deformation of the expanding sleeves element by distributing the additional force via development of mechanical anchorage. A comparison of the loaded end surface of types *HB* and *EHB* is shown in Figure 5.31 (b) to present the ability of the *EHB* component in developing the full capacity of internal bolts of grade 10.9, exclusive of sleeves failing in shear and concrete breakout formations.

5.5.4 Effect of bolt diameter

Figure 5.32 presents the effect on the tensile behaviour of the type *HB* in consideration of 16 and 20mm internal bolt diameters, with the latter involving an increased tightening torque. It is found that the initial stiffness is enhanced to some extent in the case of the larger bolt diameter, and as anticipated, it is also maintained to a much higher force. The global yield and ultimate strength, as well as the ductility increase notably with the variation in bolt diameter; nevertheless the failure of the specimens involved the yielding and eventual fracture of the internal bolt shank, in combination with a concrete breakout at the loaded surface. The force-slip relationship of type *HB* with varying d_b is shown in Figure 5.32 (b).

(a)

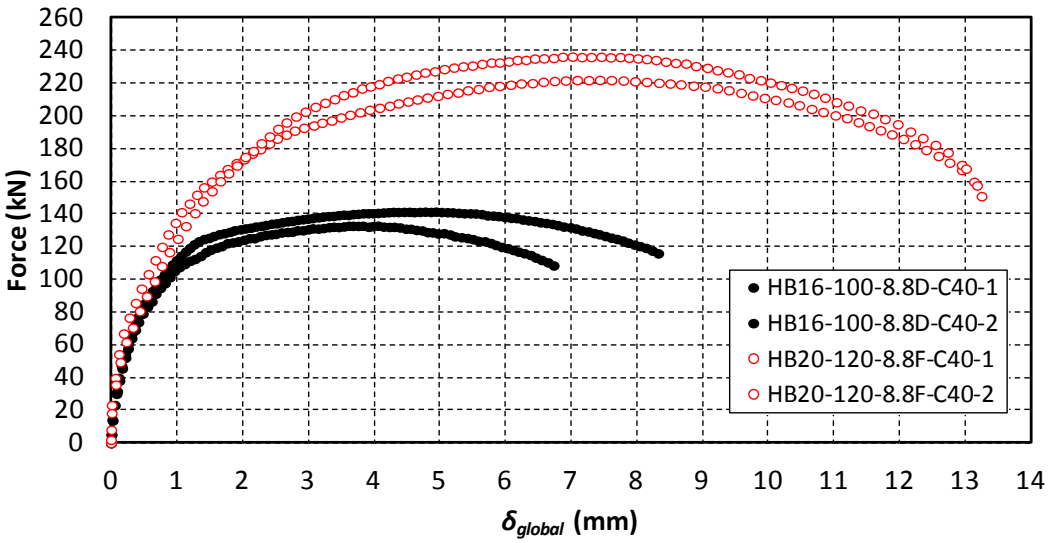

(b)

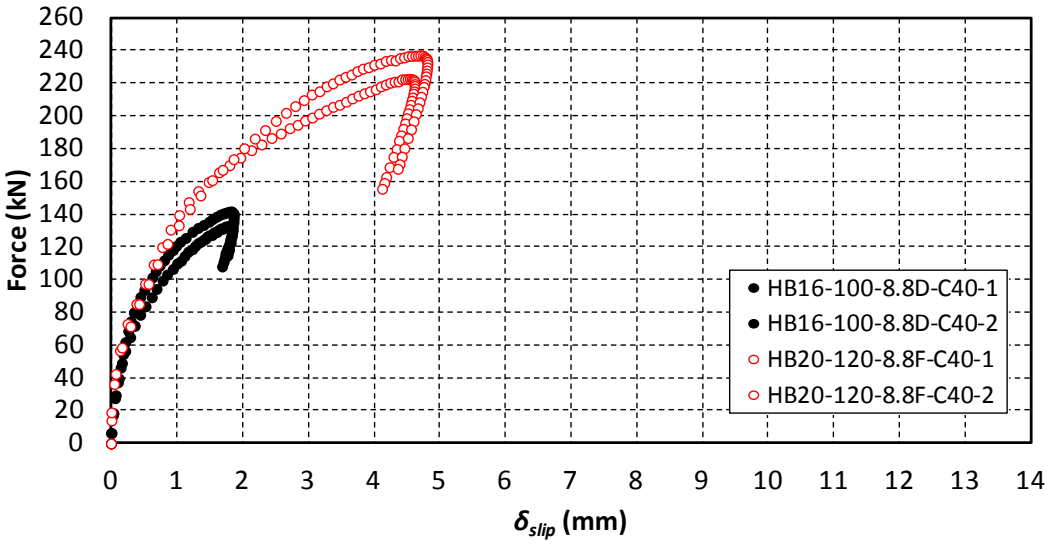

Figure 5.32 Effect of bolt diameter on tensile behaviour of type *HB*

The size effect with respect to the failure of type *HB* is shown in Figure 5.33 (a), where the extent of concrete breakout is compared with that of the benchmark specimen when d_b is 16mm. It is found that the diameter of the concrete cone breakout increases from 175mm to 215mm when an internal bolt of 20mm diameter is considered; attributed to the larger size of the expanding sleeves element in type *HB20*. On the contrary, type *EHB20* was able to develop the full tensile capacity of the 20mm internal bolt, exclusive of any formation of concrete breakout, as depicted in Figure 5.33 (b).

(a) Effect of bolt diameter size (HB16-100-8.8-C40 vs HB20-120-8.8F-C40-1)

(b) Type *HB* & *EHB* (HB20-120-8.8F-C40-1 vs EHB20-150-8.8F-C40-1)

Figure 5.33 Failure mode of 20mm internal bolt diameter in type *HB*

5.6 Mechanism 3 - Mechanical anchorage & bond

This section presents experimental data relating to the testing of the mechanical anchorage and bond element of the *EHB* component, with the element specimens signed as type *M*. Test data and observations with regard to benchmark specimens are first presented, followed by results which demonstrate the effects on the behaviour of the element due to a variation in parameters; namely concrete strength, bolt grade, bolt diameter, and embedded depth. Focus is given to the stiffness, pull-out strength, ductility, and ultimate failure modes. In representation of the anchorage element of the *EHB* component, herein only the force-slip relationship of type *M* specimens is presented as such data is considered to characterise the behaviour of the element in elimination of bolt elongation.

5.6.1 Benchmark behaviour: *M16-150-8.8-C40*

A total of five benchmark type *M* specimens were tested. The specimens involve a 16mm diameter bolt, of grade 8.8, embedded at $5.3d_b$ in a *C40* concrete mix, with a head bearing area, A_{brg} of $2.0A_b$. The force-slip relationship of the benchmark specimens is shown in Figure 5.34, with highlight given to the groups of bolt batches that were employed in the testing. The initial stiffness of the specimens is found to be in good agreement, but a variation in pull-out strength is observed among the test data; where pull-out strength is defined as the force at which local

concrete crushing occurs in front of the end anchor head. The pull-out strength is evidenced by the earliest notable reduction in stiffness of the force-slip relationship, and the observed variation is primarily attributed to the difference in the properties of the concrete infill of the specimens. Although there is a discrepancy in pull-out strength, upon forces higher than the pull-out strength, it is observed that the trend of the post-limit stiffness of the benchmark specimens is comparable, with slippage increasing at an equivalent slope, in parallel. The final reduction in stiffness which is seen in the 120-140kN force range corresponds with the yield strength of the test bolts; indicating an obvious relation between the element and the yield strength of the bolt shank.

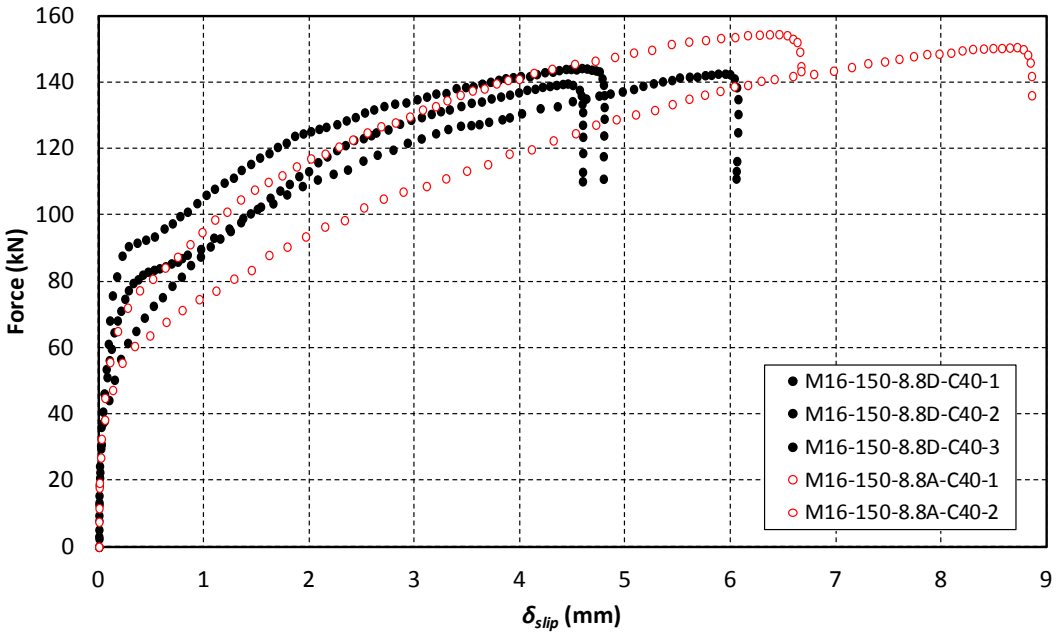

Figure 5.34 Force-slip relationship for anchorage element (benchmark M16-150-8.8-C40)

Ultimate strength was reached by forcing the yielding and eventual fracture in the bolt shank. All benchmark specimens failed by bolt shank fracture, exclusive of any formation of a concrete breakout. With reference to the design of fastenings in concrete, such behaviour is characterised as ductile, demonstrating adequate development of mechanical anchorage and bond by the headed bolt.

5.6.2 Effect of concrete strength

The effect of increasing the strength of the concrete infill from grade *C40* to *C60* is shown in Figure 5.35. It is found that the initial stiffness of the element is markedly enhanced in the case of the higher concrete grade, reaching a pull-out strength that is equivalent with the yield strength of the bolt shank. On the other hand, the ultimate strength of the element is not seen to be affected by the parameter variation. Likewise with the grade *C40* specimens, the *C60* specimens failed by bolt shank fracture, with no involvement of a concrete breakout failure.

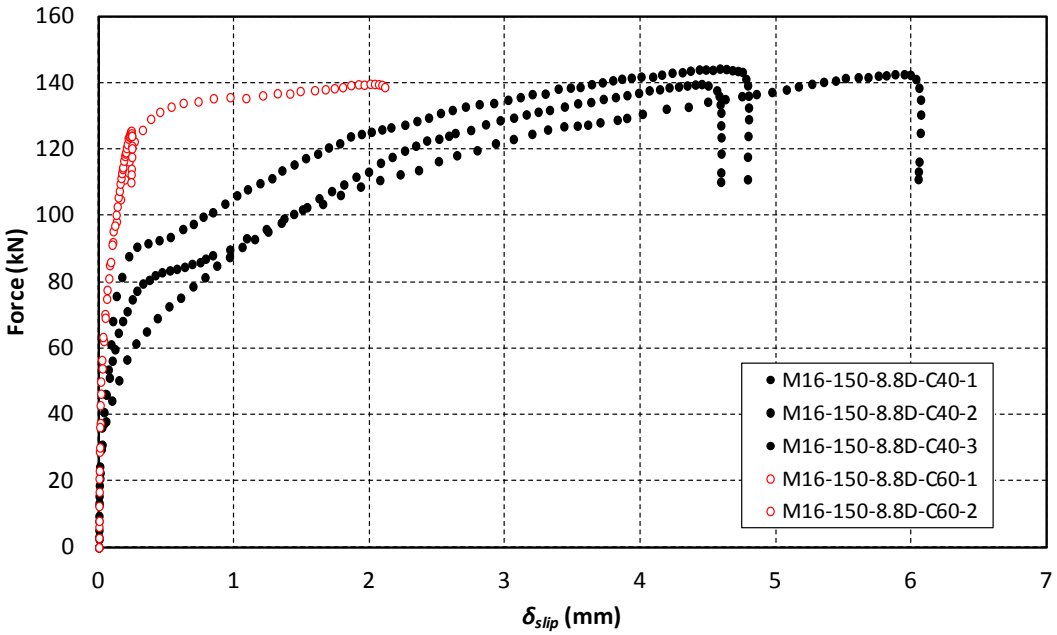

Figure 5.35 Effect of concrete strength on force-slip relationship of type *M*

It is thus indicated that the pull-out strength of type *M* is directly related to the strength of the concrete infill when a variation in grade of *C40* to *C60* is considered; an effect that is reflected in the force-global displacement relationship of the *EHB* component. This observation also agrees with the literature which states that pull-out strength of mechanical anchorage is dependent upon concrete strength.

5.6.3 Effect of bolt grade

The effect of using a bolt of higher grade is presented in Figure 5.36. It is shown that when grade 10.9 bolts are employed in type *M*, the initial stiffness of the

element is not affected however it is maintained to a higher force. The pull-out strength of grade 10.9 bolts is larger however the post-limit stiffness of the element (upon pull-out strength) is found to be comparable with that of grade 8.8 specimens; up to the yield strengths of the bolt shanks, an equivalent slope is seen. Likewise with the behaviour exhibited by the benchmark grade 8.8 specimens, the subsequent and final reduction in stiffness which is seen in the 160-180kN force range corresponds with the yield strength of the test bolts; indicating the relation between the element and the mechanical properties of the bolt shank.

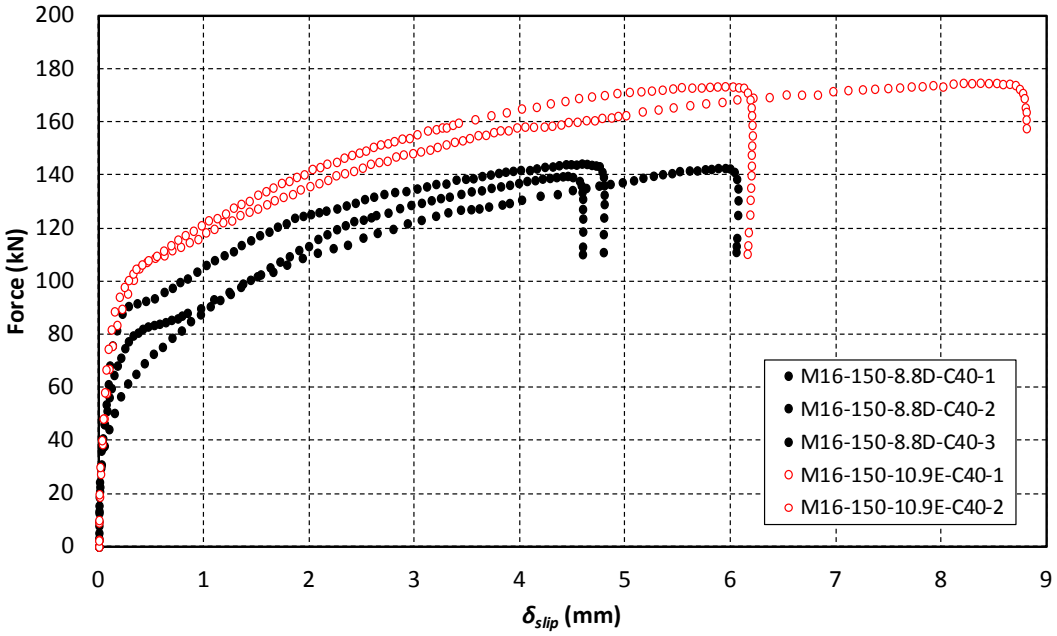

Figure 5.36 Effect of bolt grade on force-slip relationship of type *M*

Expectedly, the ultimate strength of the component is increased in the case of the higher bolt grade; attributed to the difference in mechanical properties between grade 8.8 and 10.9 bolts. Nevertheless, type *M* is able to develop the full capacity of grade 10.9 bolts, with a failure mode that is exclusive of concrete breakout. With regard to ductility capacity, the element of grade 10.9 is also comparable to that of grade 8.8, reflecting the effect that was seen in the force-global displacement relationship of the *EHB* component when grade 10.9 bolts are considered.

5.6.4 Effect of bolt diameter

The force-slip relationship of type *M* with varying d_b is shown in Figure 5.37, in consideration of 16 and 20mm bolt diameters, with the latter involving an identical head bearing area, A_{brg} of $2.0A_b$. It is found that the initial stiffness of the element is not influenced by the parameter variation, but is maintained to a much higher force. The pull-out strength is higher in the case of the larger bolt diameter, and as anticipated, the ultimate strength as well as the ductility of the element both increase notably with the variation in bolt diameter. The higher pull-out strength is attributed to the larger head bearing area, A_{brg} that is provided by the end anchor head of the 20mm bolt diameter specimens. This observation is in agreement with the literature which states that pull-out strength of mechanical anchorage is dependent upon head bearing area. Nevertheless the failure mode of the specimens involved the yielding and eventual fracture of the bolt shank, exclusive of concrete breakout; demonstrating that type *M* is able to develop the full tensile capacity of 20mm diameter, grade 8.8 bolts.

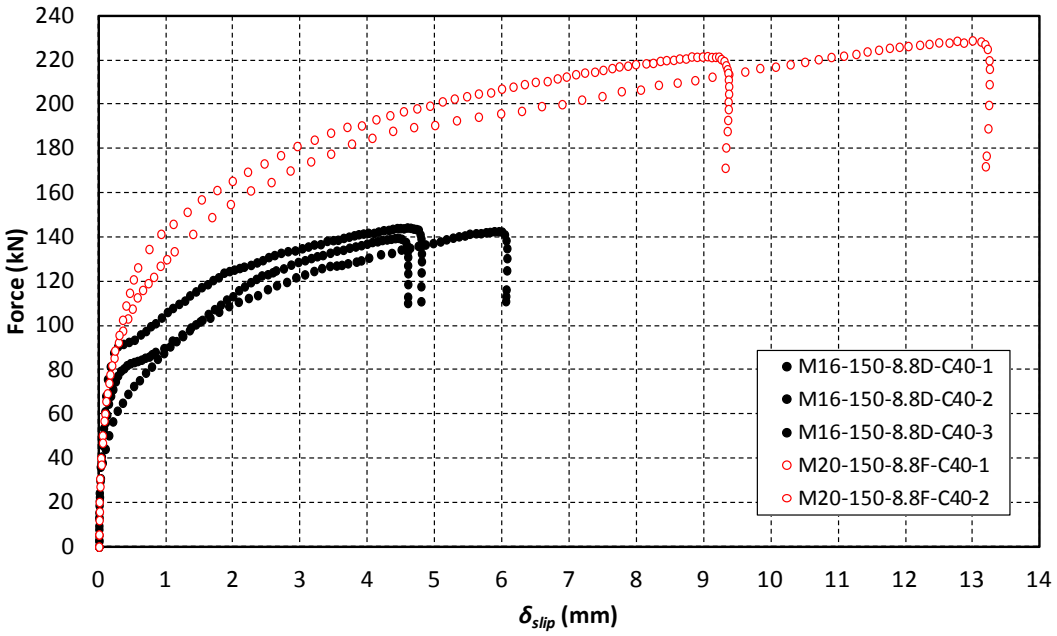

Figure 5.37 Effect of bolt diameter on force-slip relationship of type *M*

5.6.5 Effect of embedded depth

The response of type *M* with varying embedded depth, d_{emb}, is presented in Figure 5.38. The comparison involves specimens with bolt shanks of 130, 150 and 170mm long which equate with embedded depths of 4.0, 5.3 and 6.5d_b, respectively. It is indicated that the initial stiffness and pull-out strength of the element is not significantly affected with the variation in d_{emb}; however some discrepancy is seen in the post-limit response. As each category of d_{emb} specimens involved a different bolt batch group and varying concrete properties, the discrepancy of the data in the post-limit and ultimate states is attributed to the variation in the mechanical properties of the bolts and concrete infill.

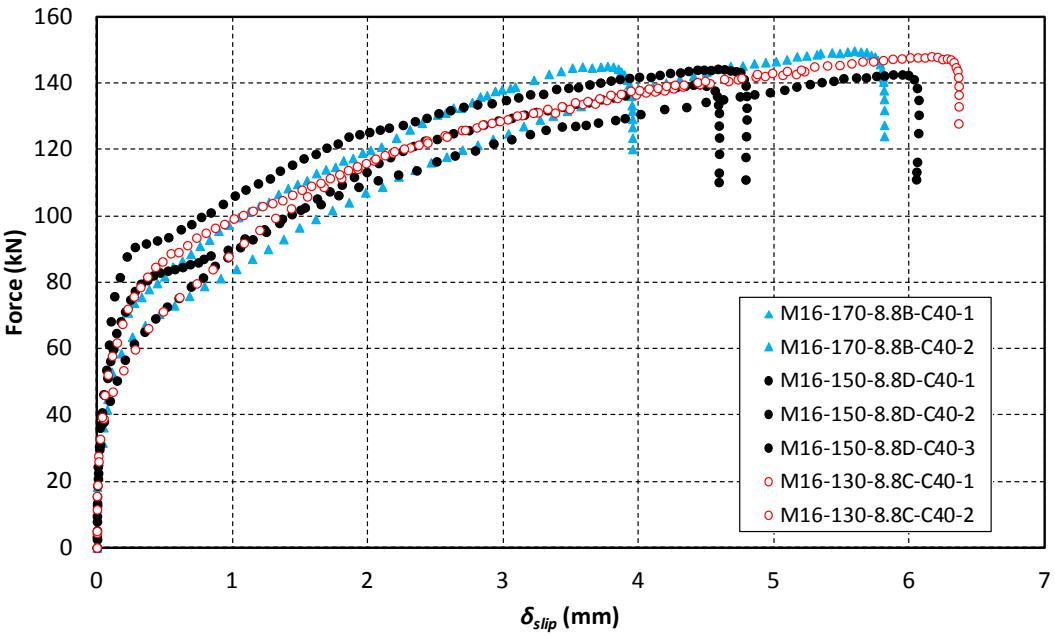

Figure 5.38 Effect of embedded depth on force-slip relationship of type *M*

The ductility capacity of the element is observed as unaffected to the variation in d_{emb}, and moreover the failure mode of the element did not alter with respect to the benchmark specimen; all failed by bolt shank fracture upon ultimate capacity, without the formation of a concrete breakout. This reflects the effect seen in the force-global displacement relationship of the *EHB* component which concluded that the stiffness, strength and ductility of the component are not dependent upon d_{emb} when embedded depths of 4.0 to 6.5d_b are considered.

5.7 Reliability of pull-out test results

The purpose of this section is to present the reliability of the pull-out test results. Repeating testing was carried out throughout the testing programme, with a minimum of two tests being performed for each configuration, and two independent displacement measurement techniques being adopted. To begin with, the experimental results are evaluated against visual inspections. Then, reliability is determined via confidence levels in test data that was obtained between the independent displacement measurement techniques.

5.7.1 Visual inspections

To verify the magnitude of the displacements that were involved in the pull-out specimens, basic visual inspections were performed with loading duration and after failure. During the testing, the separation between the loading frame and plate at the loaded end of the test set-up was confirmed by continuously monitoring, and cross checking the readings that were being recorded with the use of steel strips of known thickness; typically checked in increments of 0.5mm. The cross check points were found to be in very good agreement with the recording data, demonstrating the efficiency of the test setup and involved instrumentation.

Upon failure, test bolts were cored out of the specimens to establish whether the residual readings were sensible, as well as to observe what had actually occurred internally in the samples. Figure 5.39 depicts the typical observation of cored test pieces that relate to type *EHB* and *M*. The difference in residual slip at the unloaded end is clearly distinguished between the two types, with type *M* displaying much larger residual slip; a difference which is confirmed in the force-slip readings. Importantly, it is also revealed and confirmed by coring observations that the failure mode of type *M* involves excessive concrete crushing that takes place in front of the end anchor head. This indicates that the pull-out strength of type *M* specimens was indeed reached and surpassed, however the element was able to resist entire pull-out via the development of head bearing with the above remainder, undamaged concrete layer. In contrast, for the *EHB* component, local concrete crushing in front of the end anchor head was not visible to the naked eye.

EHB16-170-8.8B-C40-1 EHB16-170-8.8B-C40-2 Slip at unloaded end

(a) Type *EHB*

M16-170-8.8B-C40-1 M16-170-8.8B-C40-2 Slip & concrete crushing

(b) Type *M*

Figure 5.39 Typical coring observations

5.7.2 Video Gauge versus linear potentiometers

Two independent displacement measurement techniques were adopted in the pull-out testing programme; standard linear potentiometers, and the Video Gauge (*VG*) camera instrumentation. Table 5.1 outlines the actual measurement techniques that were implemented in the reporting of test results in this Chapter. Primarily, the *VG* was employed in the representation of global displacement, δ_{global}, to ensure the capture of full tensile behaviour.

To determine the confidence level in the pull-out testing results, a comparison was drawn among the measurements which were obtained by the separate methods.

The *VG* data was compared with that obtained by the linear potentiometers and it was found that the results were in very good agreement throughout the testing programme; within 95% confidence intervals. A selection of test data with respect to benchmark specimens is shown in Figure 5.40 to demonstrate a comparison between the independent instrumentation results within 95% confidence intervals. Figure 5.40 (a) and (b) present the F-δ_{global} and F-δ_b relationship obtained by testing of the *EHB* component, respectively. In Figure 5.40 (c), the F-δ_{slip} relationship of the commercially available *HB* (without concrete) is shown. Subsequently, the F-δ_{global} and F-δ_{slip} behaviour of the concrete filled type *HB* are presented in Figure 5.40 (d) and (e), respectively. And lastly, in Figure 5.40 (f), the F-δ_{slip} response of type *M* is shown. Evidently, the results obtained by the independent displacement measurement techniques fall within 95% confidence, indicating a high level of reliability of testing results; which is further enhanced by repeated testing of identical specimens.

Table 5.1 Displacement measurement technique used in reporting of test results

Specimen index	δ_{slip}	δ_{global}	Specimen index	δ_{slip}	δ_{global}
HB16-100-8.8D-0-1	VG*	LP*	M16-150-8.8D-C60-2	VG	VG
HB16-100-8.8D-0-2	VG	LP	M16-150-10.9E-C40-1	VG	VG
HB16-100-8.8D-0-3	VG	LP	M16-150-10.9E-C40-2	VG	VG
HB16-100-8.8A-C40-1	LP	VG	M20-150-8.8F-C40-1	VG	VG
HB16-100-8.8A-C40-2	LP	LP	M20-150-8.8F-C40-2	VG	VG
HB16-100-8.8A-C40-3	LP	VG	M16-130-8.8C-C40-1	LP	VG
HB16-100-8.8A-C40-4	LP	VG	M16-130-8.8C-C40-2	LP	VG
HB16-100-8.8C-C40-1	LP	VG	M16-170-8.8B-C40-1	LP	LP
HB16-100-8.8C-C40-2	VG	VG	M16-170-8.8B-C40-2	LP	LP
HB16-100-8.8D-C40-1	VG	VG	EHB16-150-8.8A-C40-1	LP	VG
HB16-100-8.8D-C40-2	VG	VG	EHB16-150-8.8C-C40-1	VG	VG
HB16-100-8.8D-C40-3	VG	VG	EHB16-150-8.8D-C40-1	LP	VG
HB16-100-8.8D-C60-1	VG	VG	EHB16-150-8.8D-C40-2	LP	VG
HB16-100-8.8D-C60-2	VG	VG	EHB16-150-8.8D-C40-3	LP	VG
HB16-100-10.9E-C40-1	LP	LP	EHB16-150-8.8D-C60-1	VG	VG
HB16-100-10.9E-C40-2	LP	LP	EHB16-150-8.8D-C60-2	VG	VG
HB20-120-8.8F-C40-1	LP	VG	EHB16-150-10.9E-C40-1	VG	VG
HB20-120-8.8F-C40-2	LP	VG	EHB16-150-10.9E-C40-2	VG	VG
M16-150-8.8A-C40-1	LP	VG	EHB20-150-8.8F-C40-1	LP	VG
M16-150-8.8A-C40-2	LP	LP	EHB20-150-8.8F-C40-2	LP	VG
M16-150-8.8D-C40-1	VG	VG	EHB16-130-8.8C-C40-1	LP	VG
M16-150-8.8D-C40-2	LP	VG	EHB16-130-8.8C-C40-2	LP	VG
M16-150-8.8D-C40-3	VG	VG	EHB16-170-8.8B-C40-1	LP	LP
M16-150-8.8D-C60-1	VG	VG	EHB16-170-8.8B-C40-2	LP	LP

** VG: Video Gauge; LP: Linear Potentiometers.*

(a) EHB16-150-8.8D-C40-2

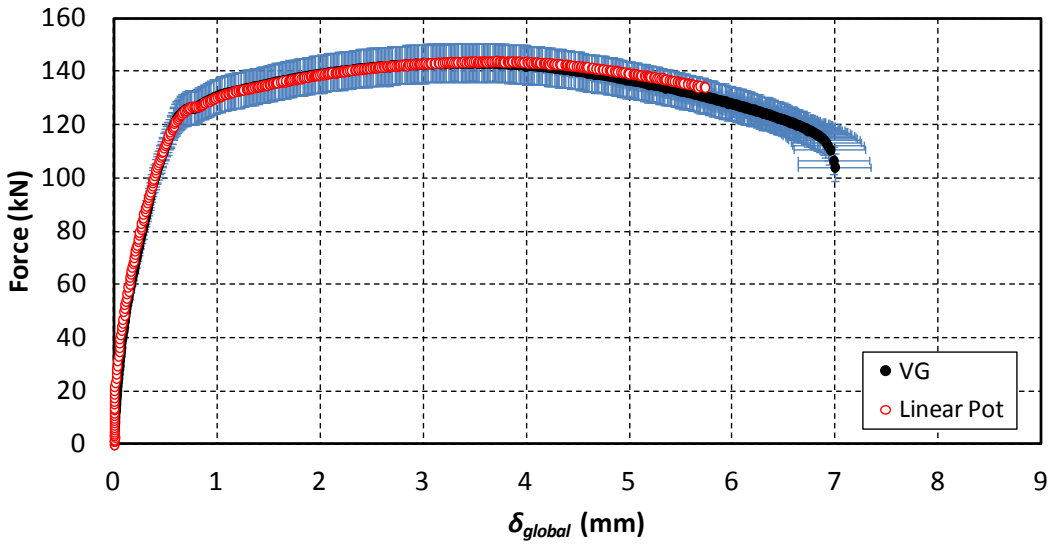

(b) EHB16-150-8.8D-C40-2

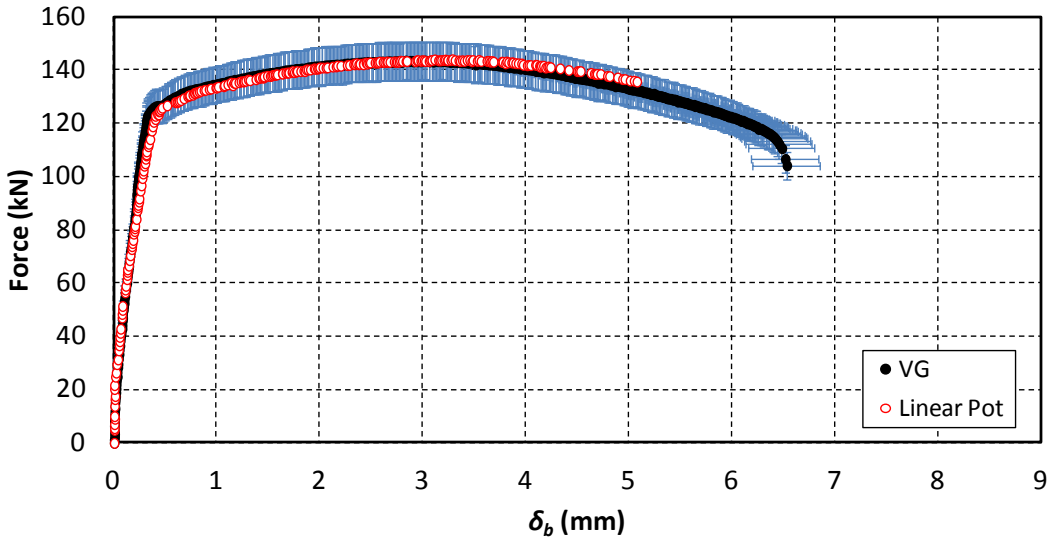

(c) HB16-100-8.8D-0-1

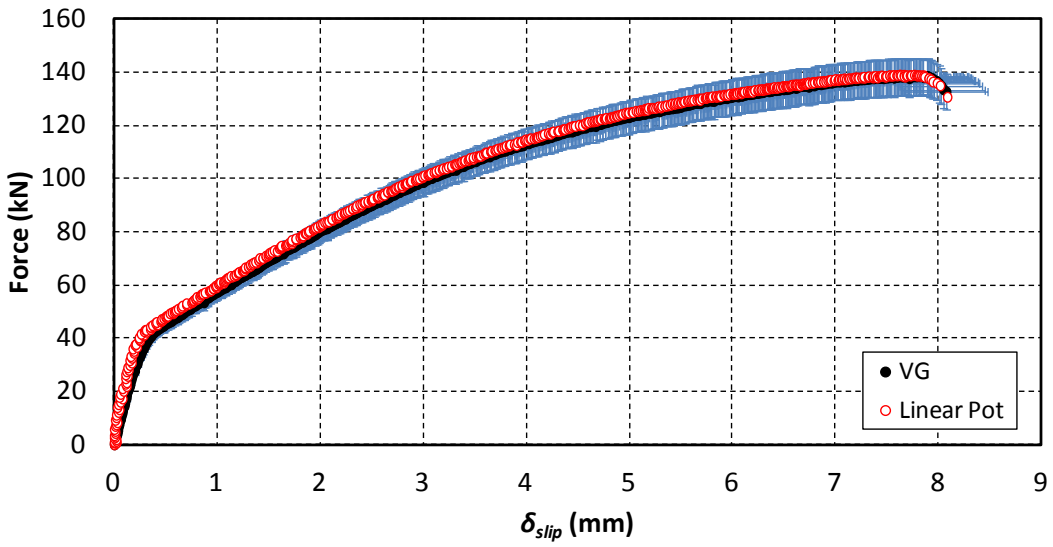

(d) HB16-100-8.8D-C40-1

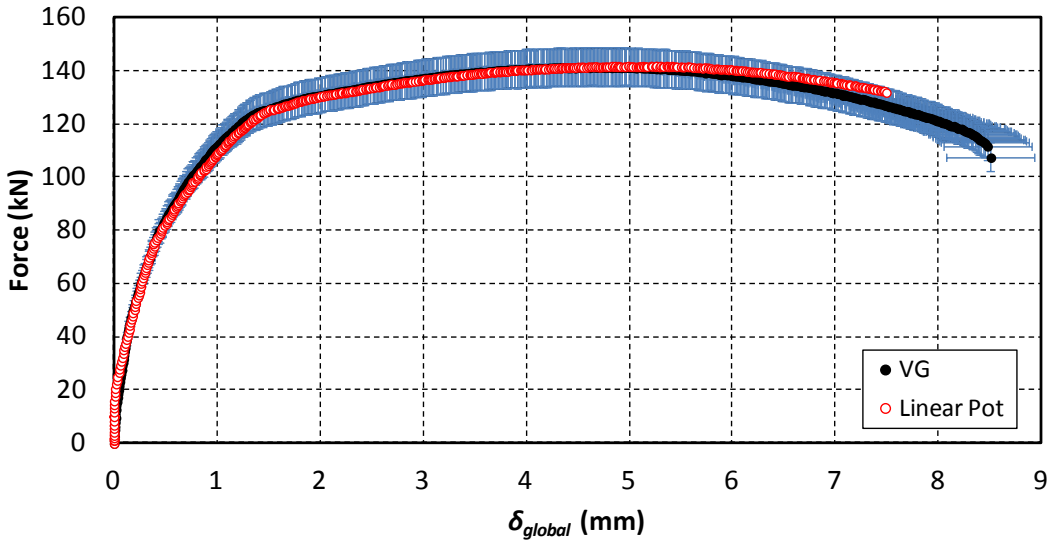

(e) HB16-100-8.8D-C40-1

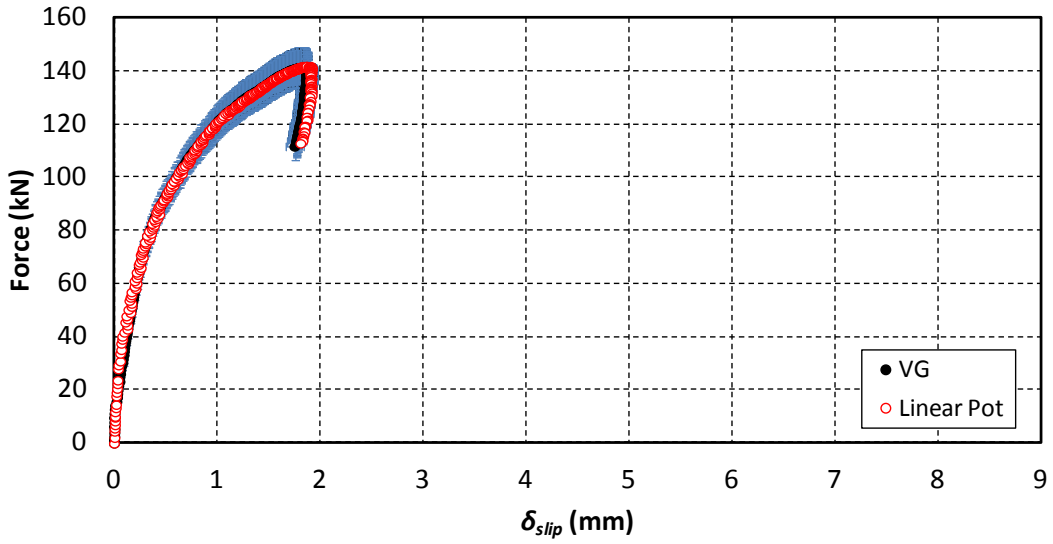

(f) M16-150-8.8D-C40-3

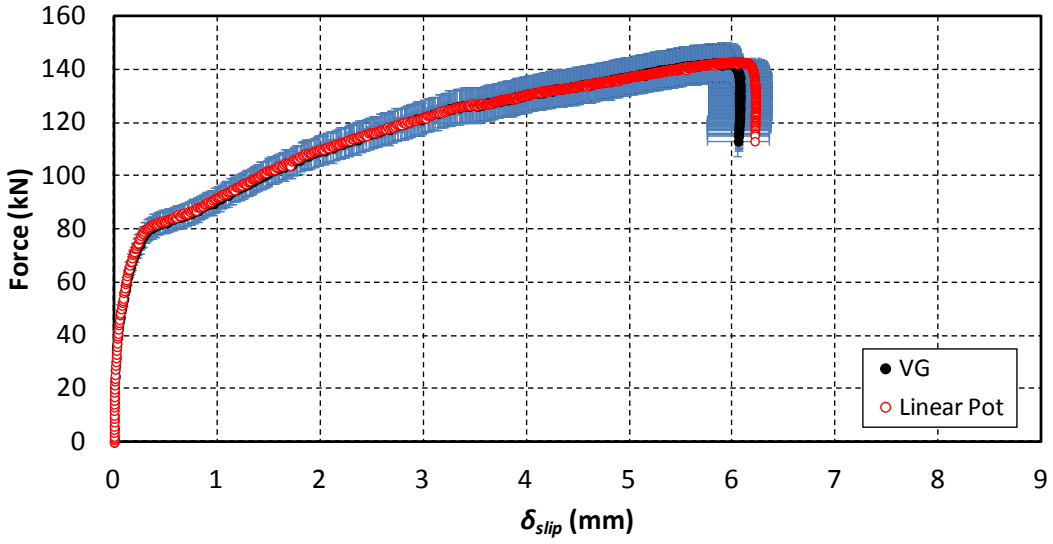

Figure 5.40 Displacement measurement techniques within 95% confidence intervals

5.8 Experimental results of pre-load in *EHB* component

Herein the raw pre-load testing results are presented, and observations with respect to the initial and residual pre-load values are discussed. Test parameters involve different bolt batch groups, relating to a variation in the grade and size of the internal bolt within the blind-bolt system. Focus is given to the relaxation rate and to the experimental results obtained by different testing methodologies.

A summary of the test results is outlined in Table 5.2, where $F_{p,\,ini}$ and $F_{p,\,res}$ are the initial and residual pre-load measurements, respectively. The initial value is taken as that which was recorded once the applied tightening torque was reached, and the residual value is represented by that upon 120 hours of reaching the initial pre-load. Correspondingly, $F_{p,\,2h}$ is defined as the pre-load value that was measured after two hours in tightening. To begin with, pre-load relaxation was monitored over the five day period via three separate methods. A comparison of the pre-load relaxation behaviour between the methods is shown in Figure 5.41, with that of (a) and (b) relating to indirect measurements and that of (c) to direct measurements.

Table 5.2 Summary of pre-load testing results

Specimen index	$F_{p,\,ini}$ (kN)	$F_{p,\,res}$ (kN)	$F_{p,\,res}/F_{p,\,ini}$	$F_{p,\,res}/F_{p,\,2h}$
HB16-100-8.8G-M1-1	45.1	40.2	0.89	0.96
HB16-100-8.8G-M1-2	45.1	38.5	0.85	0.94
HB16-100-8.8G-M1-3	47.7	38.6	0.81	0.91
HB16-100-8.8G-M2-1	32.0	10.6	0.33	0.78
HB16-100-8.8G-M2-2	38.8	31.7	0.82	0.95
HB16-100-8.8G-M2-3	30.6	23.9	0.78	0.92
HB16-150-8.8A-M3-1	25.1	21.8	0.87	0.96
HB16-150-8.8A-M3-2	22.7	20.9	0.92	0.98
HB16-150-8.8A-M3-3	21.0	20.0	0.95	1.00
HB16-150-8.8C-M3-1	22.7	20.8	0.92	0.97
HB16-150-8.8C-M3-2	29.3	26.0	0.89	0.97
HB16-150-8.8C-M3-3	21.1	16.6	0.79	0.93
HB16-150-8.8D-M3-1	32.9	30.1	0.92	0.99
HB16-150-8.8D-M3-2	28.8	25.5	0.89	0.99
HB16-150-8.8D-M3-3	21.9	20.7	0.94	0.98
HB16-150-10.9E-M3-1	51.7	46.0	0.89	0.97
HB16-150-10.9E-M3-2	59.0	53.1	0.90	0.98
HB16-150-10.9E-M3-3	41.5	35.7	0.86	0.93
HB20-150-8.8F-M3-1	39.8	32.6	0.82	0.96
HB20-150-8.8F-M3-2	32.9	28.8	0.88	0.95

Refer to section 4.2 for detailed description of testing methodology.

(a) Method 1, strain gauged bolts (3 at 120°)

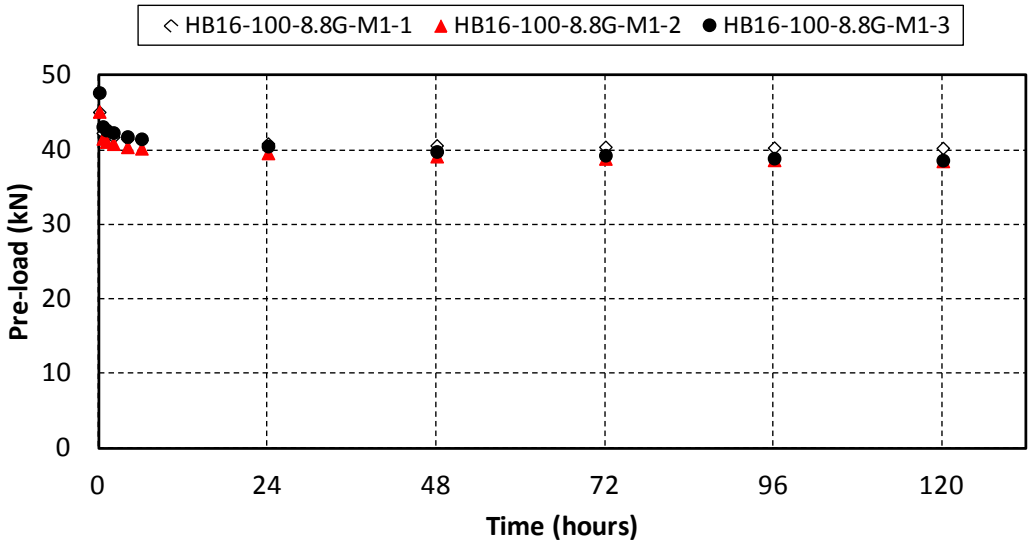

(b) Method 2, strain gauged bolts (central gauge)

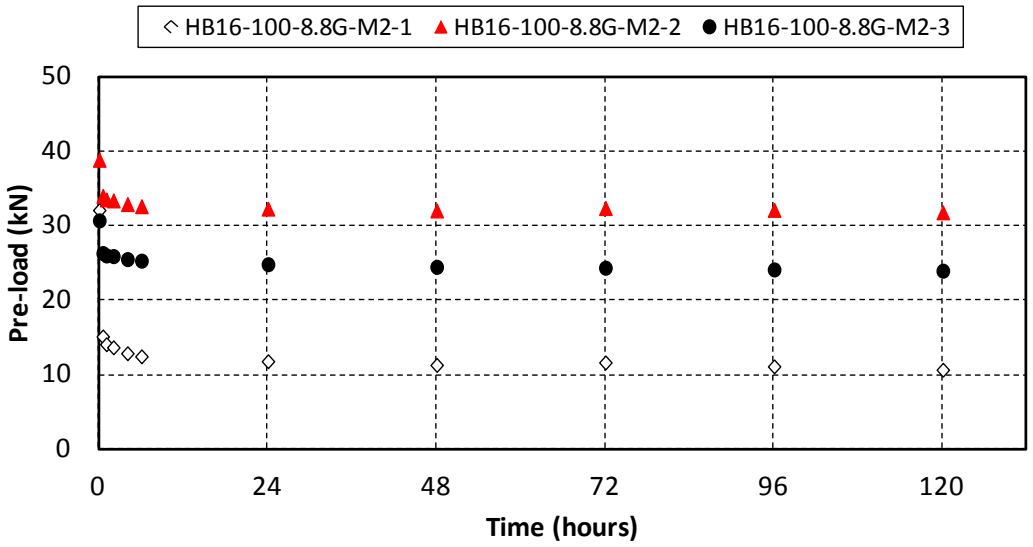

(c) Method 3, direct clamping force using load cell

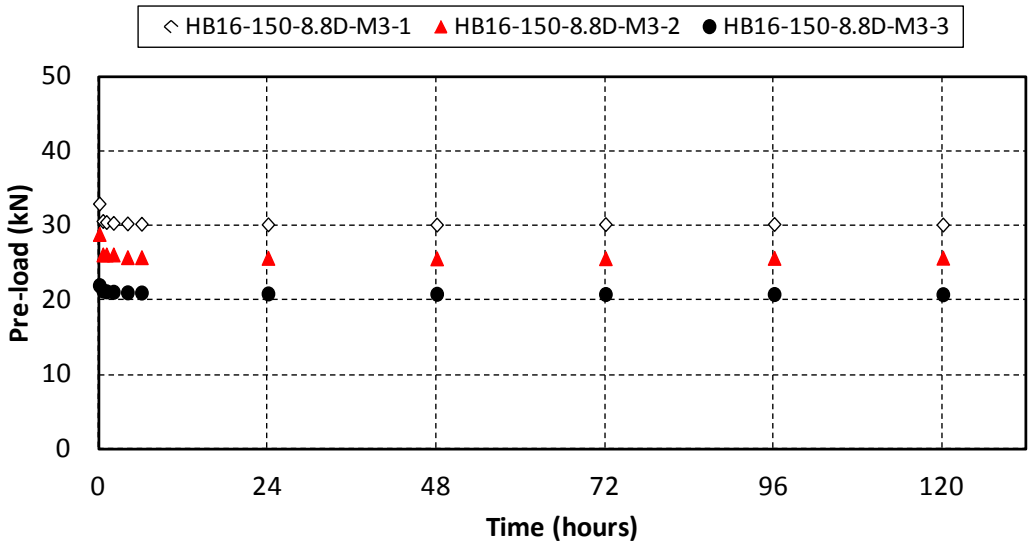

Figure 5.41 Pre-load relaxation under different testing methods

It is found that the indirect method which involved the mounting of three strain gauges below the bolt head (signed as method 1) exhibits the least scatter among three identical tests, but a much higher value in pre-load is measured with respect to that achieved by the other testing methodologies. The other indirect method which involved a central strain gauge (signed as method 2) exhibits a large scatter among three identical tests, with an evident outlier behaviour being recorded in specimen *HB16-100-8.8G-M2-1*; which is neglected in latter analysis. Nevertheless, the pre-load measurements that were obtained by the remaining specimens in method 2 are within the measuring range of that which was recorded by the direct clamping force method (signed as method 3). Overall, the general pattern of pre-load relaxation with time is in agreement between the results of the separate test methods. Most of the pre-load relaxation occurs within two hours of tightening, and the rate of relaxation significantly reduces thereafter, furthermore stabilising upon a period of 24 hours. This indicates the adequacy of the separate methods however some discrepancy in the test results still remains to be justified. It is felt that the level of pre-load measurements in the bolt differs due to inconsistencies in torque which was applied with the use of a handheld torque wrench; as also identified by in the literature which states that a common torque wrench is said to produce pre-load with an accuracy of ±30% (Bickford 2008).

Since the preparation of the strain gauged bolts required a large amount of labour, and considering that the test bolts involve a reduction in tensile stress area to accommodate for the installation of the gauges, the efficiency of the indirect method is in question. Taking also into account the accuracy level involved in standard torque wrenches, it is thus considered that the ease test setup of the direct clamping force method is sufficient for the purposes of the measurements in this programme. Hence method 3 was adopted for the remaining programme.

In Figure 5.42, dimensionless ratios are plotted to display the amount of pre-load relaxation upon 2 hours of tightening with respect to overall pre-load relaxation. From the ratios of $F_{p,\,res}$ / $F_{p,\,ini}$ it is identified that a range of 5-22% of relaxation in pre-load occurred among the test specimens over a period of 5 days. From the ratios of $F_{p,\,res}$ / $F_{p,\,2h}$ it is found that at least 90% of pre-load relaxation was reached

in all specimens within two hours of tightening. For demonstration purposes and to emphasize on the relaxation rate in the two hour period, the typical pre-load relaxation rate over the initial 24 hours in tightening is shown in Figure 5.43. With regard to the effect on the level of pre-load in the bolt due to the variation in the investigative parameters, it is found that the relaxation rate of the pre-load is unaffected by the variation, as evidenced by the dimensionless ratios. However, a higher pre-load is measured in the case of the grade 10.9 specimens, in contrast with that measured in the 20mm bolt specimens which seems to be unaffected by the increasing tightening torque due to the larger bolt diameter size.

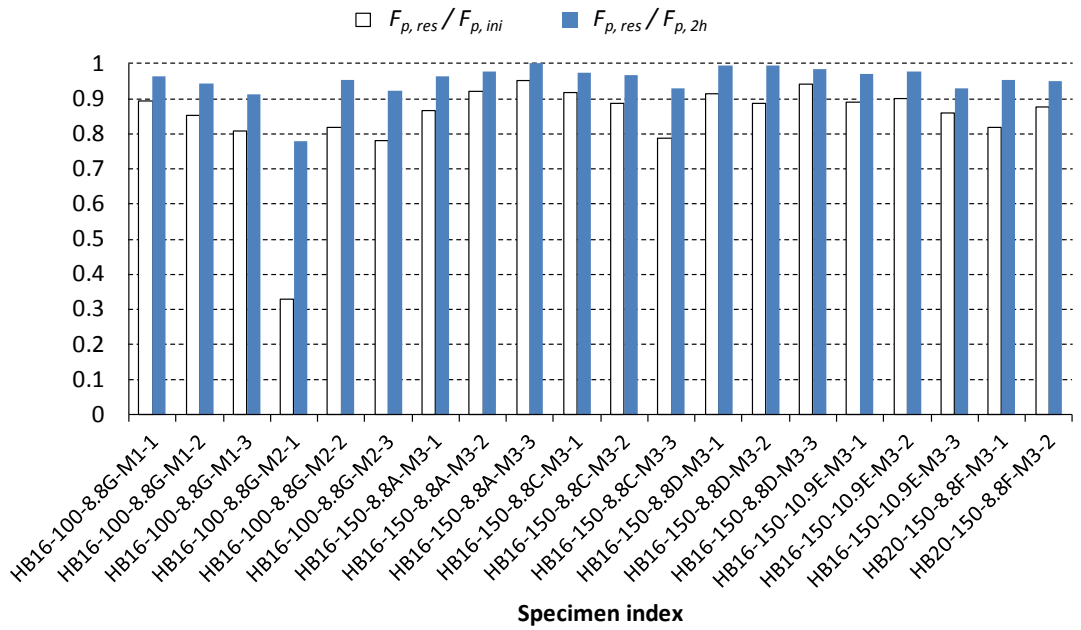

Figure 5.42 Initial & residual pre-load ratios

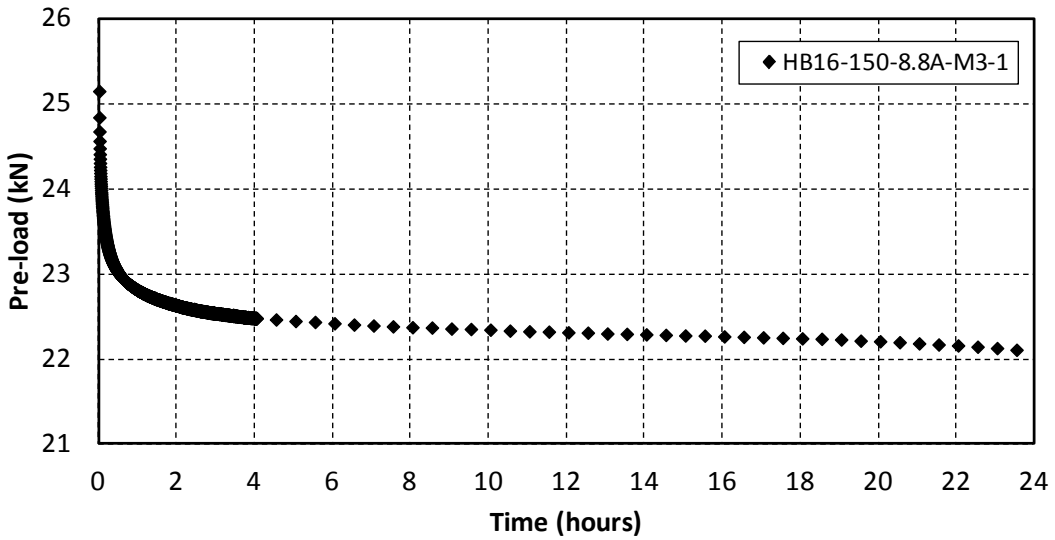

Figure 5.43 Typical pre-load relaxation over first 24 hours in tightening

5.9 Concluding remarks

This Chapter has presented the raw experimental results with regard to the pull-out and pre-load testing programme. In the course of the presented data, it was demonstrated that the aim of the testing plan was satisfied and the equivalent research objectives were established. The Chapter has satisfied research objectives relating to the evaluation of the load transfer mechanism of the *EHB* component, and quantification of its full non-linear global force-displacement relationship, in consideration of the main parameters affecting its response. Moreover, the effects on the tensile behaviour due to a variation in parameters were determined in reflection with the performance of its assumed individual elements. The findings of the experimental work are summarised as below:

Evaluation of the load transfer mechanism of the *EHB* component

- Pull-out testing demonstrated that the superior stiffness characteristics of the *EHB* component in comparison with those of the commercially available Lindapter *HB* blind-bolt (in consideration of unfilled and concrete-filled sections) are attributed to the ability of its mechanical anchorage in distributing tensile force within the concrete member. As this additional ability of force distribution is provided, the deformation relating to the expanding sleeves mechanism of the component is significantly reduced, and the formation of a concrete breakout failure is eliminated; further justifying the improved performance of the component with respect to that exhibited by the concrete-filled type *HB*.
- Pull-out testing of the bond and anchorage element of the *EHB* component (signed as type *M*) has determined the force levels which relate to the local crushing of concrete in front of the end anchor head of the component, defined as the pull-out strength. The testing also identified that the post-limit stiffness of the element is dependent upon the mechanical properties of the internal bolt shank.
- Pull-out testing has verified that three elements contribute to the deformability curve of the *EHB* component up to failure. Namely, the sources of deformability originate from the elongation of the internal bolt shank, the deformation of the expanding sleeves mechanism, and from the slip of the mechanical anchorage element. The initial stiffness of the component is primarily

attributed to that of its mechanical anchorage element, and the force-slip relationships of the individual elements of the component indicate that the anchorage and expanding sleeves mechanisms interact from the initial loading stage, up to the onset of necking of the components internal bolt shank. The difference between global displacement and slip measurements shows that bolt elongation is also a constant source of deformability, ahead of zero force to failure. In addition, the minor slip that was measured in the *EHB* component indicates that bolt elongation effectively occurs at the outer side of the testing configuration in between the threaded cone of the blind-bolt and hexagon bolt head.

- The mechanics of the *EHB* component were observed and recorded with the assistance of strain gauged bolts to evaluate the manner in which the capacity of the component is developed. At ultimate state, it was found that the capacity was comprised of 30% head bearing and 10% bond due to anchorage development, and 20% contribution was provided by the mechanism of the expanding sleeves. The remainder was due to bolt elongation and load transfer losses. This further validates that the individual elements contribute to the deformability of the *EHB* component, from its tightening stage up to its ultimate limit state.

The global force-displacement relationship of the *EHB* component

- The initial stiffness of the *EHB* component is affected by the variation in concrete strength, with high concrete grade specimens exhibiting higher stiffness, whereas strength and ductility are independent of the variation when *C40* and *C60* grade mixes are considered. The yield and ultimate strength, and the ductility of the component are directly related to the material property of the internal bolt shank.
- A comparison among the use of grade 8.8 and 10.9 bolts in the *EHB* component indicates that the higher bolt grade improves the stiffness and strength characteristics of the component at the expense of post-limit stiffness and ductility; attributed to the mechanical properties involved in higher grade bolts. Type *EHB* allows for the development of the full tensile capacity of grade 10.9 internal bolts.
- A comparison among the use of 16 and 20mm internal bolts in the *EHB* component indicates that the larger bolt diameter improves the stiffness and

strength characteristics of the component. Type *EHB* allows for the development of the full tensile capacity of 20mm diameter internal bolts.

- The stiffness, strength, ductility and failure of the *EHB* component are not dependent upon d_{emb} when embedded depths of 4.0 to 6.5d_b are considered. The minimum possible shank length for type *EHB* (size 2 clamping thickness) is 130mm to accommodate for the end anchor head. This minimum shank length provides an embedded depth of 4.0d_b for the component, and an investigation of varying embedded depths has shown that the minimum d_{emb} is satisfactory in developing the full tensile capacity of the component. This allows for the employment of shorter shank lengths in the *EHB* component without affecting the characteristics of the component, which furthermore provides more flexibility in the design of joints in consideration of double sided and perpendicular joint configurations as less embedment is found internally of the tubular columns.

Mechanism 2 - Expanding sleeves (type *HB*)

- The global yield and ultimate strength of type *HB* are independent of the strength of the concrete infill, but the stiffness is dependent upon concrete strength when a variation in grade of *C40* to *C60* is considered. This reflects the improvement in type *EHB*, indicating that the enhanced performance of type *EHB* in a *C60* mix is partly attributed to the improved performance of its expanding sleeves acting in a higher grade concrete.
- The use of grade 10.9 bolts in comparison with 8.8 improves the stiffness and strength characteristics of type *HB* at the expense of a sudden ultimate failure. The failure mode involves a dominant shear failure of the expanding sleeves element which does not allow for the full tensile capacity of the internal bolt to develop. In contrast, when grade 10.9 internal bolts are employed in type *EHB*, the component allows for their full tensile capacity to develop.
- The size effect with respect to the failure of type *HB* shows that the extent of concrete breakout in comparison with that of the benchmark specimen when d_b is 16mm increases from 175mm to 215mm when an internal bolt of 20mm diameter is considered; attributed to the larger size of the expanding sleeves element in type *HB20*. On the contrary, type *EHB20* was able to develop the full

tensile capacity of the 20mm internal bolt, exclusive of any formation of concrete breakout.

Mechanism 3 - Mechanical anchorage & bond (type *M*)

- The pull-out strength of type *M* is found to primarily be dependent upon the head bearing area A_{brg}, and the strength of the concrete infill.
- A variation in the investigative parameters did not alter the failure mode of type *M*; all configurations allowed for the full tensile strength of the bolts to develop, and failure occurred by fracture in the bolt shank, exclusive of concrete breakout. Such effects are reflected with those seen in the global force-displacement relationship of the *EHB* component, indicating the efficiency of the measured force-slip relationship of type *M* towards the representation of the anchorage element in the *EHB* component.

Reliability

- The reliability of the test results was addressed by repeated testing, visual inspections, and independent displacement measurement techniques.
- Linear Potentiometer and Video Gauge data is found to be within 95% confidence intervals, demonstrating a high level of reliability in displacement measurements throughout the pull-out testing programme.

Pre-load testing

- A range of 5-22% of relaxation in pre-load occurred among the test specimens over a period of 5 days, with at least 90% of the relaxation taking place within two hours of tightening.
- A higher pre-load is induced in the blind-bolt system when grade 10.9 internal bolts are employed, however for the same increased tightening torque this effect was not observed in the case of 20mm internal bolt diameter specimens.
- The relaxation rate of the pre-load was found to be unaffected by the variation in the investigative parameters.

6 Data analysis

The following Chapter reports on the detailed analysis of the key experimental data that was collected throughout the testing programme of this research. The analysis involves normalisation, idealisation, curve fitting, regression, and statistical analysis for the presented data. It commences with a focus on the prediction of the relationship between torque and pre-load induced within the blind-bolt system, including relaxation effects. Normalisation of data that relates residual pre-load with the ultimate strength of the internal bolts follows. Then elastic limit ratios are obtained for the internal bolts from measurements taken during material property testing. Moreover, with the aid of the experimental knowledge that was developed with respect to failure modes, it is the purpose of the Chapter to propose: (a) a model related to the force-bolt elongation (F-δ_b) response of the internal bolt of the *EHB* component (*Mechanism 1*), and (b) models related to the force-slip (F-δ_{slip}) response of the expanding sleeves (*Mechanism 2*), and mechanical anchorage and bond (*Mechanism 3*) elements of the *EHB* component.

6.1 Pre-load in blind-bolt system

The further analysis of the measurements of pre-load induced in the *HB* blind-bolt system involves statistical and probability analysis of the experimental nut factor, *K* and normalisation of data relating the pre-load with the mechanical properties of the internal bolts. The objectives of the analysis involve the proposal of an appropriate nut factor for application in the short-form equation that is to predict the residual pre-load in the blind-bolt assembly. Also a focus of the analysis is the development of data for incorporation into the overall *EHB* component model.

6.1.1 Nut factor, *K*

It has been stated in section 3.2.1 that it is common to express the pre-load in a bolting system as a function of tightening torque, bolt diameter and a so-called nut factor, *K*. On the basis of this short-form equation, the experimentally derived *K* factor is calculated here as in Equation 6-1, where $F_{p,\ res}$ is the experimentally

measured residual pre-load (see Table 5.2), *T* is the tightening torque and d_b is the bolt diameter (see Table 4.2). The nut factor *K* is determined for the pre-load test specimens and sample statistics are carried out as below to draw conclusions about postulated models of the underlying data-generating mechanism.

$$K = \frac{T}{F_{p,res}\, d_b} \qquad \text{Equation 6-1}$$

At first, a normality test is performed to assess the likelihood that the nut factor data set (K_1, …, K_n) comes from a normal distribution. The normality test would determine whether the normal (Gaussian) distribution may be adopted to model the experimental results obtained for the nut factor *K*; where the term distribution refers to the possible values of the variable *K* along with some measure of how frequently they occur. In statistics, the Shapiro-Wilk test tests the null hypothesis that a sample came from a normally distributed population (Shapiro et al. 1965). For the nut factor data set herein, it is found that the Shapiro-Wilk normality test suggests that the data is approximately normal, with a statistical significance testing (p value) of 0.616. This result is interpreted as follows: a significance level of 0.05 would deem as extraordinary any result that is within the most extreme 5% of all possible results under the null hypothesis. In this case a p-value less than 0.05 would result in the rejection of the null hypothesis at the 5% (significance) level. When the null hypothesis is rejected, the result is said to be statistically significant. In other words, if the significance value is greater than 0.05, the data is said to be normal, whereas if it is less than 0.05, it is determined that the data has a significant deviation from a normal distribution.

Experimental data, in the form of a representative sample of observations, enable to draw inferences about a population of interest. Because populations are often too large to be adequately studied in a specified time period or within designated budgetary constraints, in this scenario the testing of say multiple pre-load specimens, it is thus sometimes necessary to use sample statistics to represent the population; with the standard deviation being a measure of the variability of the

sample observations. However, when estimating the standard deviation of a population from a sample of it, an error is introduced by assuming the sample mean to be the population mean, the latter being not known in this case. It can be proven though that the error so introduced may be corrected by replacing *N* in the denominator of the standard deviation equation by *N*-1 (Neville et al. 1986); where *N* is the sample size. As the resulting measurements of *K* are a sample of a population, *N*-1 is used towards the calculation of the standard deviation herein to account for such an error and the data is treated as a continuous random variable.

The histograms in Figure 6.1 illustrate the frequency distribution of the experimental data related to the nut factor, *K*; constructed by dividing the range of the data into several intervals (of equal length), counting the number of observations in each interval, known as the frequency in the interval. A by-product of the frequency histogram is the relative frequency histogram which graphs the proportions (counts/sample size *N*) or percentages (proportions x 100) of observations in each interval rather than the frequencies (counts) themselves. The use of relative frequencies (or percentages) in histograms ensures that the total area under the bars is equal to one (or 100%). This facilitates the comparison of the resultant distribution with that of a theoretical probability distribution, where the total area of the distribution also equals one. Relative frequency histograms that are symmetric and bell-shaped are said to have the shape of a normal curve. For the experimental nut factor *K* it is observed that the height of the bars suggests a shape similar to the form of the normal bell-shaped curve.

The probability density function (pdf) of a random variable describes the relative frequencies of different values for that random variable and can be used to compute probabilities of continuous random variables. The normal curve is typically used as a probability model to characterise measurements where the density or height of the curve above the axis of measurement values represents the likelihood of obtaining a value. Probabilities for any range of measurement values can thus be calculated from the probability model once the model parameters are specified. In the normal distribution, only the mean (μ) and the standard deviation (σ) are needed to completely specify the probability model (Mason et al. 2003). The area

under the distribution curve between any two points (i.e. the integral of the probability density function between them) represents the probability that the value of *K* (within a sample) will lie between these two values. The superimposed curve of the theoretical normal model in Figure 6.1 (b) provides a good approximation to the actual distribution of the sample of measurements represented by the vertical bars. This demonstrates that the sample data is approximately normal. However, it is the accuracy of the estimate of the population value which is of primary interest.

(a) Frequency

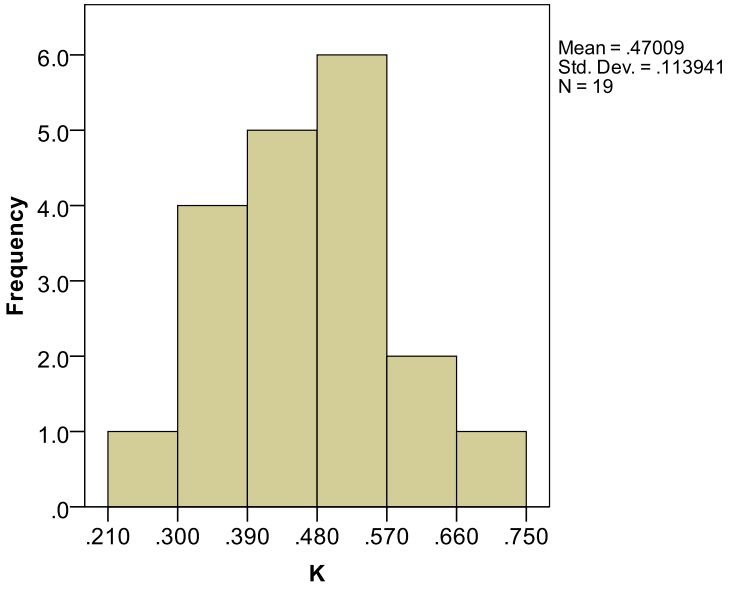

(b) Relative frequency & confidence intervals

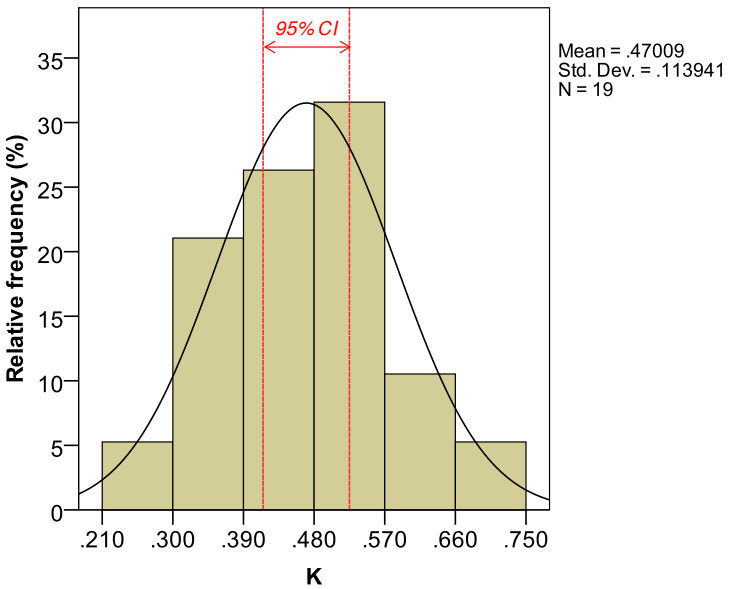

Figure 6.1 Histograms for nut factor *K*

Statistical inference is concerned with using probability concepts to quantitatively deal with uncertainty in obtaining representative values. To assess the estimate of the mean of the population (using the sample mean), confidence intervals are commonly constructed around the sample mean with the use of the standard error. The standard error reflects the variability of the mean values, as if the study were repeated a large number of times; calculated by dividing the sample standard deviation (σ) with the square root of the size of the sample, N. In consideration of the size of the sample (N=19) and the Central Limit Theorem, the t-distribution with N-1 degrees of freedom is used in the determination of the confidence limits for K. Because the size of the sample is relatively small, it is recognised by the Central Limit Theorem that the use of the normal distribution for the confidence interval of the population mean can give rise to substantial inaccuracies; hence the use of the t-distribution in the calculation. The data suggests that the 95% confidence interval for the mean lies between 0.470 ± 0.055; taking us from a lower bound K of 0.415 to an upper bound K of 0.525 with a 95% probability. Obviously, if the procedure is repeated over a number of samples, different intervals will be obtained. However the 95% probability level tells us that in 95 cases out of 100, the population mean will lie in the calculated interval; referred to as the 95% confidence interval. In other words this means that with probability 0.95 the sample comes from a data generating process with population mean μ in the range of 0.415 to 0.525.

6.1.2 Torque versus residual pre-load

The illustrative scatter plot in Figure 6.2 graphs the mean residual measurements of pre-load against the ratio of the tightening torque to bolt diameter (T/d_b); prepared in consideration of *HB* blind-bolts of grade 8.8 for bolt diameters of 16 and 20mm, and of grade 10.9 for 16mm bolt diameters. Since the experimental measurements were conducted under torque control, the ratio of T/d_b is taken as the independent variable and plotted accordingly on the x axis. Linear regression using least squares displays the best fit line for the data while being set to the origin (0, 0). It is the inverse of the slope of the line that relates to the nut factor K and it is found that the equation of the trend-line suggests a value of 0.443 for K with respect to the range of the investigative parameters.

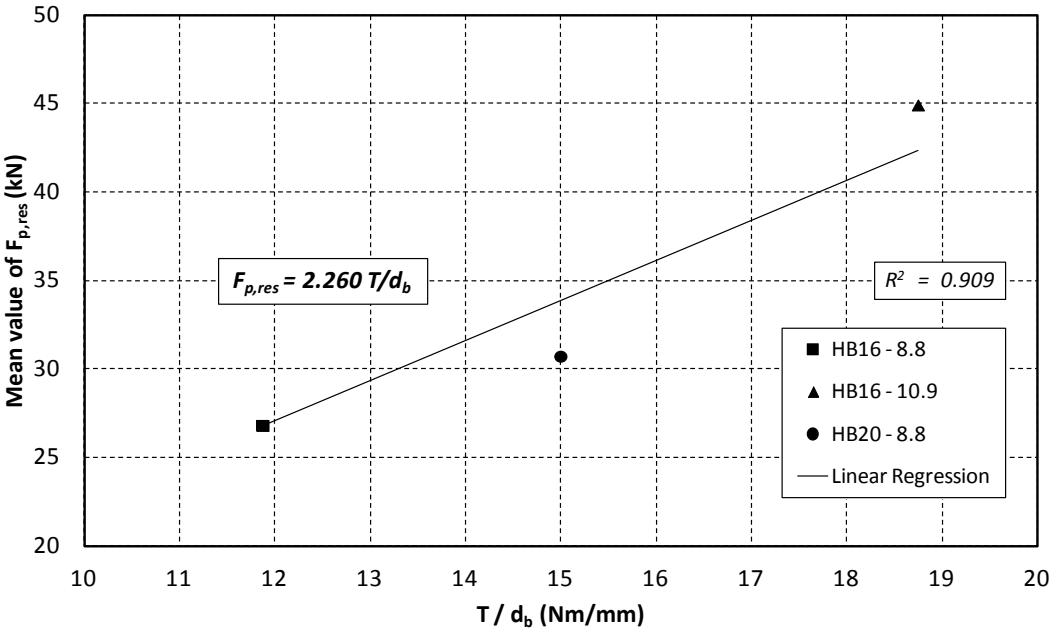

Figure 6.2 Linear regression of mean residual pre-load versus T/d_b

In comparison with *K* values that are recommended for standard steel fasteners - which typically lie within the range of 0.15 to 0.25 - it is established that the resulting nut factor *K* for representation in the *HB* blind-bolt is larger than that typically applied in standard bolting. With reference to the text that is reported in section 3.2.1, because it is anticipated that the magnitude of pre-load developed in a *HB* assembly is lower than that of a standard bolt, at an equivalent tightening torque, it would thus be expected to encounter a larger nut factor. On the basis of the short-form equation, a larger value of *K* would result in less pre-load.

Some additional comments regarding the nut factor are as follows. The *K*, or nut factor, can be thought of as anything that increases or decreases the friction within the blind-bolt assembly. This is a combination of three sub-factors in the case of the *HB* blind-bolting system: (1) geometrical factor - size of threads, (2) a thread friction related factor - the friction between the threads of the bolt and the threads of the threaded cone, (3) an under head and expanding sleeves friction related factor - the friction of the head and sleeves against the surface they rotate on. There are numerous real-world complications which ensure that no two bolts respond exactly the same to a given torque; damaged threads, hole misalignment, the type and amount of lubricant, temperature and many other factors can absorb a large

amount of the input torque and thereby decrease the amount of energy that actually becomes pre-load. Complete control is impossible. The *K* value can thus be thought of as anything and everything that affects the relationship between torque and pre-load.

6.1.3 Normalisation of residual pre-load

It is the purpose of this section to normalise the pre-load measurements with the relevant mechanical properties of the internal bolts that were employed in the testing. The bar chart shown in Figure 6.3 presents the results of the normalisation process, with the reporting values corresponding to the mean value of each *HB* blind-bolt category. The normalised ratios of residual pre-load to actual yield and ultimate strength (see Table 4.3) depict the effect of the variation in bolt diameter and bolt grade within the *HB* system. In consideration of the varying range, it is established that the relative level of pre-load induced in the *HB16* and *HB20* of grade 8.8 is not affected by the size factor even though a higher input torque was applied in the case of the *HB20*. In contrast, the relative level of pre-load in the *HB16-10.9* - which involves an internal bolt of higher grade that is tightened at an equal torque with that applied in the *HB20* - is higher than that in the *HB16-8.8*. An increase of around 65% is observed in the level of pre-load relative to the ultimate strength of the internal bolt; determined by the difference in the ratio of $F_{p,res}/F_{ub}$.

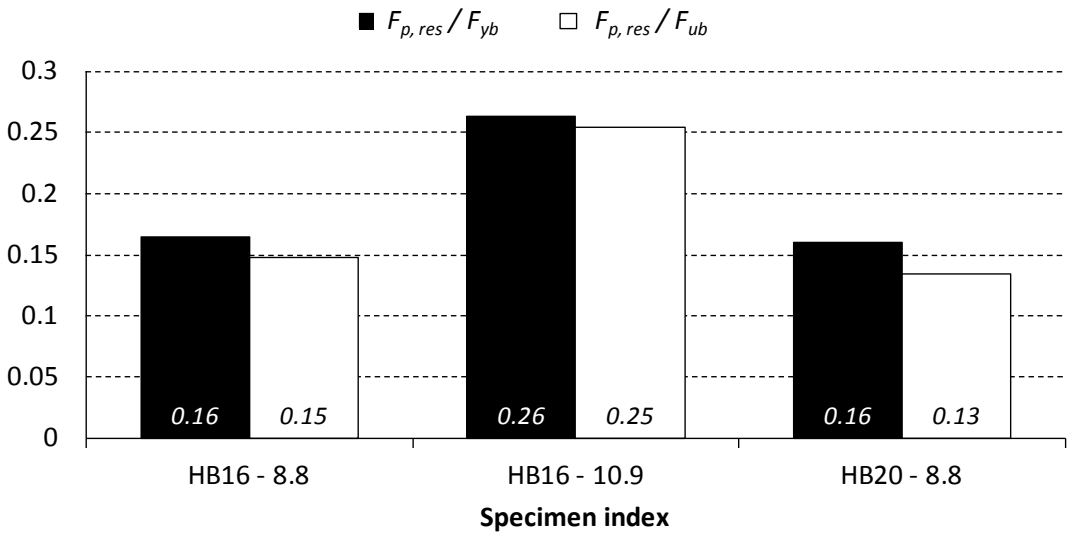

Figure 6.3 Ratios of residual pre-load to yield and ultimate strength

With respect to the development of the overall *EHB* component model, it is the normalised ratios such as the above which are proposed to represent the level of pre-load that is induced in the internal bolt of the blind-bolt system. A value of $0.15F_{ub}$ is recommended for bolts of grade 8.8 and a value of $0.25F_{ub}$ is suggested for bolts of grade 10.9. At this stage it is considered essential to incorporate this level of pre-load into the overall component model. The influence of excluding pre-load effects is investigated and detailed in latter parts of the thesis.

6.2 Mechanism 1 - Bolt elongation

Herein, a semi-empirical model with linear characteristics is proposed to represent the force-bolt elongation (F-δ_b) behaviour for the internal bolt that is involved in the *EHB* component. The model is calculated with respect to a piecewise four segment linear response and is presented in the form of F-δ_b notation charts. The proposed models distinguish between bolts of grade 8.8 and 10.9, incorporating pre-load on the basis of normalised residual values. The development of the model also involved the derivation of elastic and inelastic limits, and its predictions are compared with relevant experimental data, detailed below.

6.2.1 Elastic limit ratios

When considering the non-linear behaviour of bolts or bolted joints, it is necessary to know when the elastic limit of the bolt has been reached. Manufacturer test certificates and relevant design codes do specify an elastic limit in accordance with the mechanical properties of bolts. However they simply report or specify a nominal yield and ultimate strength which leads to an elastic-perfectly plastic material model. Depending on the level of sophistication required this may or may not suffice. Since the non-linear behaviour of the *EHB* component is being considered, it is required to capture its post-limit and ultimate behaviour with considerable accuracy.

In this thesis, the elastic limit of the internal bolt that is used in the *EHB* component is defined as the stress at 0.2% offset strain and is labelled as f_{yb}. By dividing the measured elastic limit by the bolt's ultimate strength, a ratio can be defined and

used to predict the onset of inelastic behaviour. The resulting ratios of f_{yb} to f_{ub} are summarised in Table 6.1, alongside descriptive statistics. The average ratio obtained from the tension tests is 0.883 with a standard deviation of 0.030 for grade 8.8 bolts, and the average ratio for grade 10.9 bolts is determined at 0.952 with a standard deviation of 0.005. Eurocode 3 (CEN 2005) recommends ratios of 0.80 for grade 8.8 bolts and 0.90 for grade 10.9 bolts for f_{yb} / f_{ub}. For the sake of simplicity, ratios of 0.85 and 0.90 are recommended for the onset of inelastic behaviour for bolts of grade 8.8 and 10.9, respectively.

Table 6.1 Internal bolts elastic limit ratios

Grade	Batch	*f_{yb} (MPa)	*f_{ub} (MPa)	f_{yb} / f_{ub}	*st.dev*	*mean*
8.8	A	921	1023	0.900		
	A	915	1020	0.897		
	A	917	1026	0.894		
	A	876	983	0.891		
	B	725	900	0.806		
	C	874	981	0.891		
	C	872	981	0.889		
	D	864	950	0.910		
	D	832	926	0.898		
	D	832	924	0.900		
	D	814	922	0.883		
	F	785	935	0.840	0.030	0.883
10.9	E	1067	1116	0.956		
	E	1094	1146	0.954		
	E	1091	1154	0.946		
	E	1092	1147	0.952	0.005	0.952

** Mechanical properties obtained by material property testing (see section 4.3.1)*

To sum up, so far the level of pre-load that is induced in the internal bolt of the *EHB* component has been related to the ultimate strength of the internal bolt, and elastic limit ratios for the internal bolt have been suggested; also relative to the ultimate strength of the internal bolt. For the full refinement of an appropriate tension bolt model for application in the *EHB* component model, it remains to define an expression for the elastic stiffness of the element, as well as suitable values for the post-limit and ultimate stiffness coefficients.

6.2.2 Tetra-linear tension bolt models

Based on the current literature and observations of *EHB* component and individual tension bolt tests, the bolt stiffness models presented in Figure 6.4 were developed; with that relating to bolts of grade 8.8 and grade 10.9 shown in (a) and (b), respectively. The bolt stiffness model is comprised of four linear segments. The first segment models the bolt before its pre-load is overcome, the second segment models the bolt during the linear-elastic portion of its response, the third segment models the bolt after initial yielding has started, and the fourth segment represents the bolt after it has reached a plastic state.

The force levels used to distinguish between the different states are based on the analysis of experimental results that were obtained as part of this research investigation. The initial force levels that are used to distinguish the pre-load region are based on the findings of normalisation of pre-load data. The force levels used to distinguish between elastic and inelastic behaviour were determined from material property tests. A limit of 85% of the tensile capacity is used to identify the onset of yielding for bolts of grade 8.8 whereas a limit of 90% is used for bolts of grade 10.9. With regard to the ultimate force level, for notation purposes the resistance of the model is intentionally represented by F^u, the ultimate capacity of the *EHB* component; in reflection of the ultimate strength of its internal bolt. Experimental evidence indicated that the ultimate capacity of the component was restricted to the ultimate strength of its internal bolt, hence the relation between the two. Another characteristic of the model is that it employs stiffness coefficients for the post-limit and ultimate region that are directly related to its linear-elastic response.

With respect to stiffness, until the pre-load in the bolts is overcome (segment 1), they are assumed to be infinitely rigid (where the value of $1000k_x^e$ was deemed a sufficiently high stiffness). Thereafter, the linear-elastic bolt stiffness k_x^e governs the response; from the pre-load force until first yield (segment 2), at which point the elastic stiffness is reduced by 95% for grade 8.8 and by 90% for grade 10.9 bolts (segment 3). Finally, the plastic portion of the bolt's response (segment 4) is modelled by assuming a stiffness of 1% (for grade 8.8) and of 1.5% (for grade 10.9) of the elastic stiffness. The post-limit stiffness coefficient used to calculate $\mathrm{k_x^p}$ in

segment 3, and the ultimate stiffness coefficient used to calculate k_x^u in the plastic portion were determined by trial and error curve fits of the experimental data.

(a) Grade 8.8 bolts

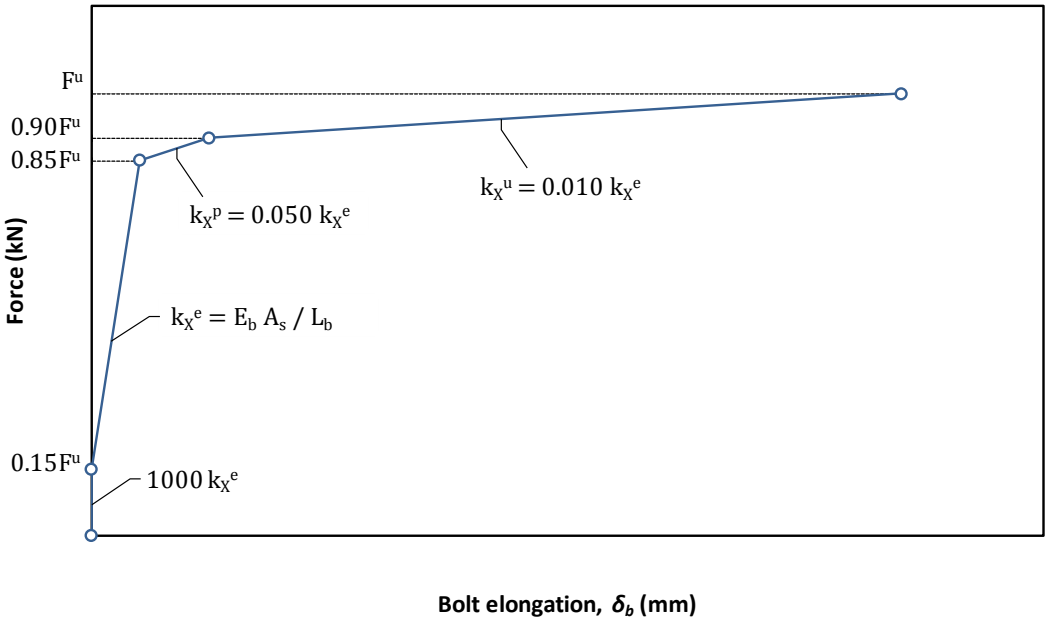

(b) Grade 10.9 bolts

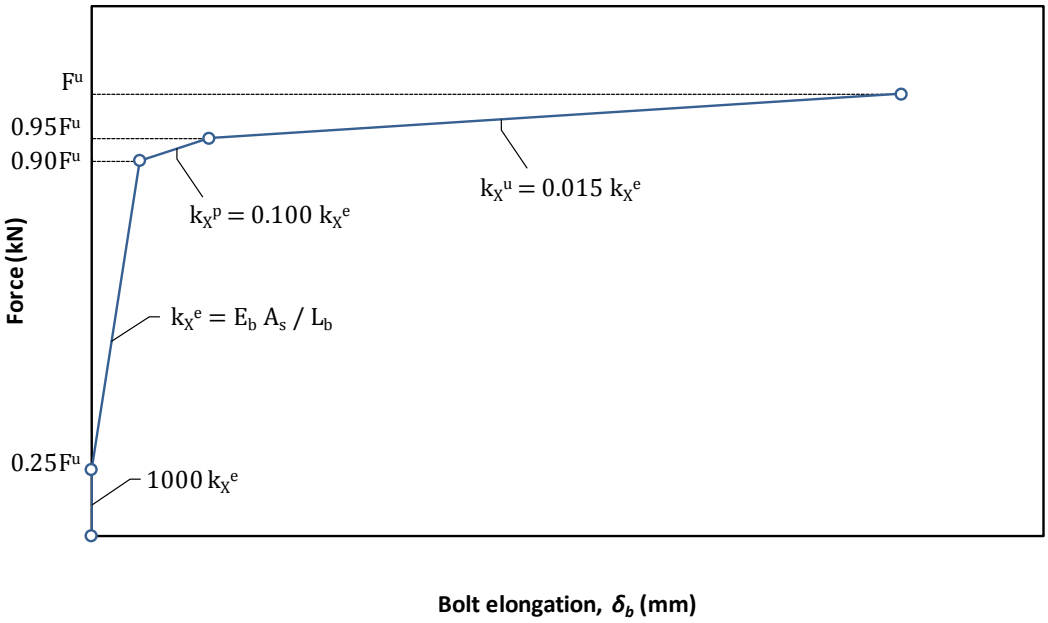

Figure 6.4 Mechanism 1 stiffness models (k_b)

The elastic stiffness of the bolt, k_x^e is calculated as recommended in Barron (1998) on the basis of the familiar form $k=EA/L$ for the stiffness of an axially loaded

member with uniform cross section. This approach is justified by the involvement of a fully threaded internal bolt within the *EHB* blind-bolt which allows for the definition of a uniform stress area. However the expression requires an assumption concerning the stress levels which will allow us to estimate an effective length for the bolt that is somewhere between the true length and the grip length. Assuming that the average stress level in the head of the bolt is one-half the body stress, the effective length for the *EHB* internal bolt can be determined as schematically shown in Figure 6.5 and mathematically expressed in the form of Equation 6-2. Taken as equal to the grip length (total thickness of material and collars), plus half the sum of the height of the bolt head and the height of the *HB* (or *EHB*) cone, the proposal of L_b herein is suggested on the basis of the stiffness expression of a standard bolt–nut–washer system (Bickford 2008; CEN 2005). In summary therefore, in the overall calculation for k_x^e, L_b is the effective length (or bolt elongation length), E_b is the bolt's Young's Modulus of elasticity, and A_s is denoted for the bolt's tensile stress area. Moreover, t_{bh} is the thickness of the hexagon bolt head (as extracted from Table 5 of BS 3692:2001), H is the thickness of the collar of the *HB* (or *EHB*) blind-bolt, t_{HBc} is the depth of the *HB* (or *EHB*) cone, and W is the clamping thickness; where notation for H and W is as per Lindapter type *HB* product brochure.

$$L_b = H + W + \frac{(t_{bh} + t_{HBc})}{2} \qquad \text{Equation 6-2}$$

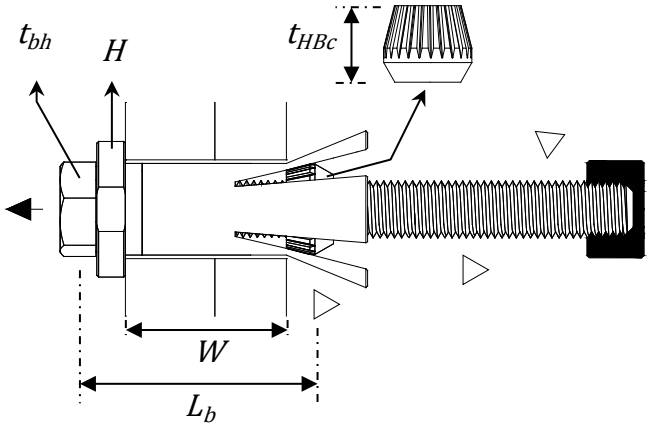

Figure 6.5 Effective length, L_b for internal bolt of *EHB* component

It should be noted that in the case that a partly non-threaded shank was involved within the effective length of the internal bolt of the *EHB* component, the proposed expression for k_x^e would not be valid (by not satisfying the assumption of a constant stress area) and modifications would be required for the common stiffness expression of an axially loaded member using varying cross sectional properties. For reference, a standard bolt stiffness model for application in T-stub modelling was suggested by Swanson et al. (2001); employing an elastic limit ratio of 0.85 and stiffness coefficients of 0.100 and 0.020 for the post-limit and ultimate regions, for grade 8.8 bolts, in account of standard bolting pre-load effects. Corresponding values recommended in this study are found to be in good agreement with the model suggested by Swanson for bolts of grade 8.8. Unfortunately bolts of grade 10.9 were not included as part of the study and thus a comparison is not viable.

6.2.3 Evaluation of models

Bolt model predictions are compared graphically with relevant experimental data in Figure 6.6, and regression analysis is performed to quantify the goodness of fit for the model; reported by R^2 values, the coefficient of determination. Since the bolt models are proposed for representation of the deformability element of the internal bolt of the *EHB*, their evaluation should relate to experimental data obtained via *EHB* component pull-out testing. With reference to section 5.2.3, the experimental type *EHB* $F\text{-}\delta_b$ curve is used towards the evaluation of the bolt model predictions. Benchmark behaviour is shown in Figure 6.6 (a) representing an *M16* grade *8.8* internal bolt, whereas the grade *10.9* model is shown in (b), and that of a larger d_b is presented in (c) for an *M20* of grade *8.8*. The correspondent properties that are used in the model for the calculation of k_x^e are actual material properties; a Young's Modulus, E_b is employed according to bolt batch (see Table 4.3). The tensile stress area of the bolt is determined as per ISO 898 (BSI 2009), and *W* is taken as 45mm - as in test setup - for the calculation of the effective length, L_b. Finally, the input value for F^u adopts the maximum force that was obtained in the type *EHB* test. It is found that the model represents with sufficient accuracy the elongation of the bolt over the assumed effective length, L_b, capturing the key characteristics of the element, with R^2 values close to 1 indicating the good fit for the model.

(a) M16 grade 8.8

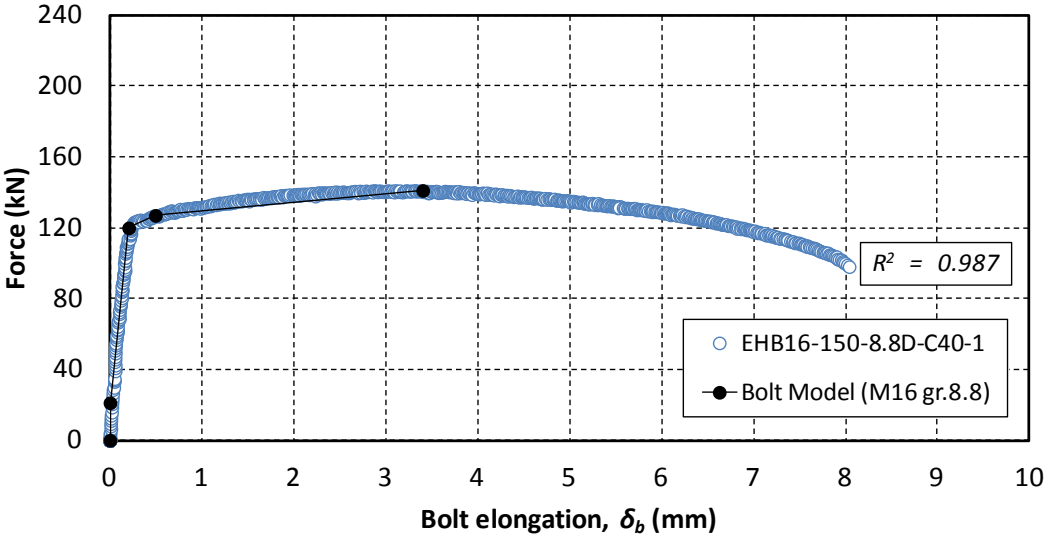

(b) M16 grade 10.9

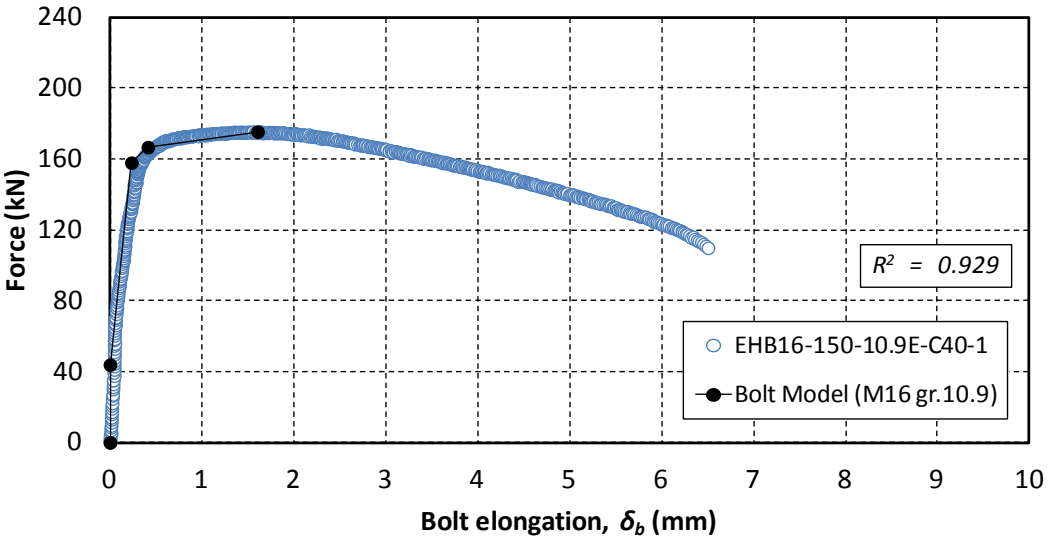

(c) M20 grade 8.8

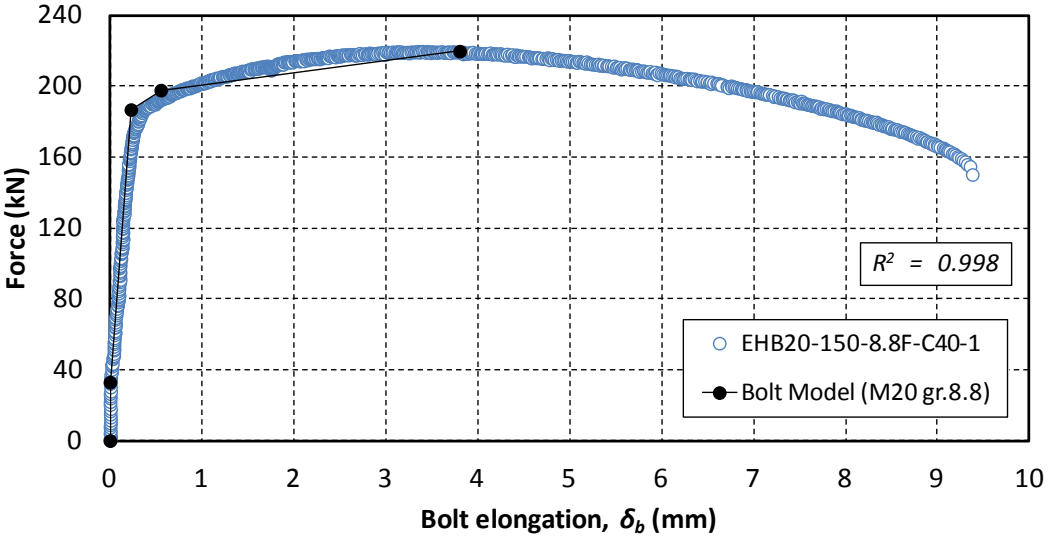

Figure 6.6 Model, experimental & regression analysis (F-δ_b with parameter variation)

A closer examination of the effects on the F-δ_b behaviour of the element when a larger d_b and higher bolt grade is considered is illustrated in Figure 6.7. It is demonstrated that the model predictions certainly follow the trend of the experimental data and moreover, the significance of the level of pre-load is identified with respect to the initial and elastic stiffness region of the element.

(a) Experimental data

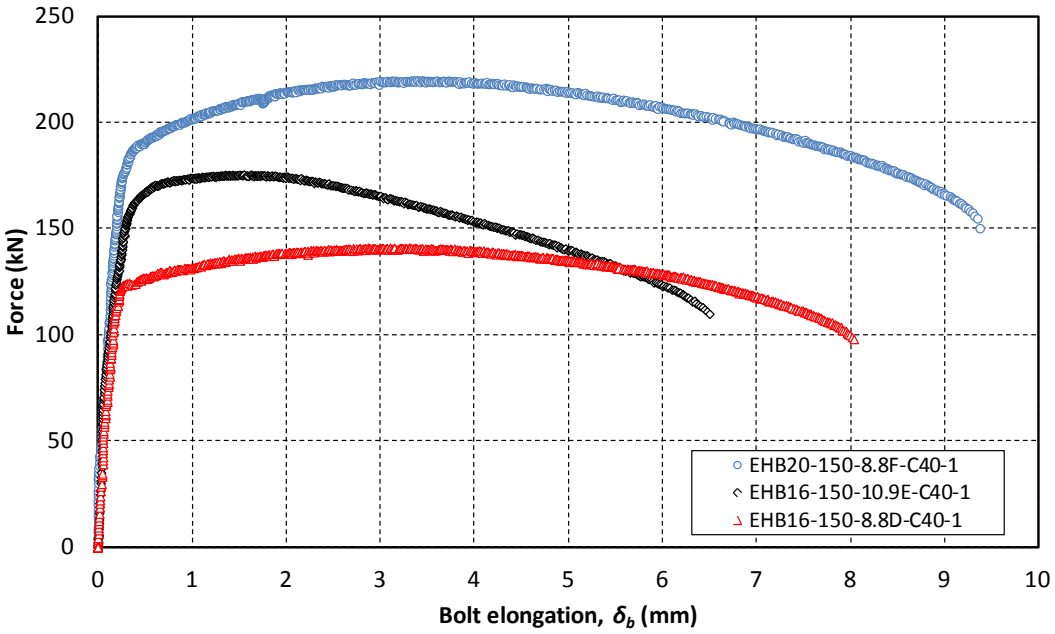

(b) Equivalent tension bolt models

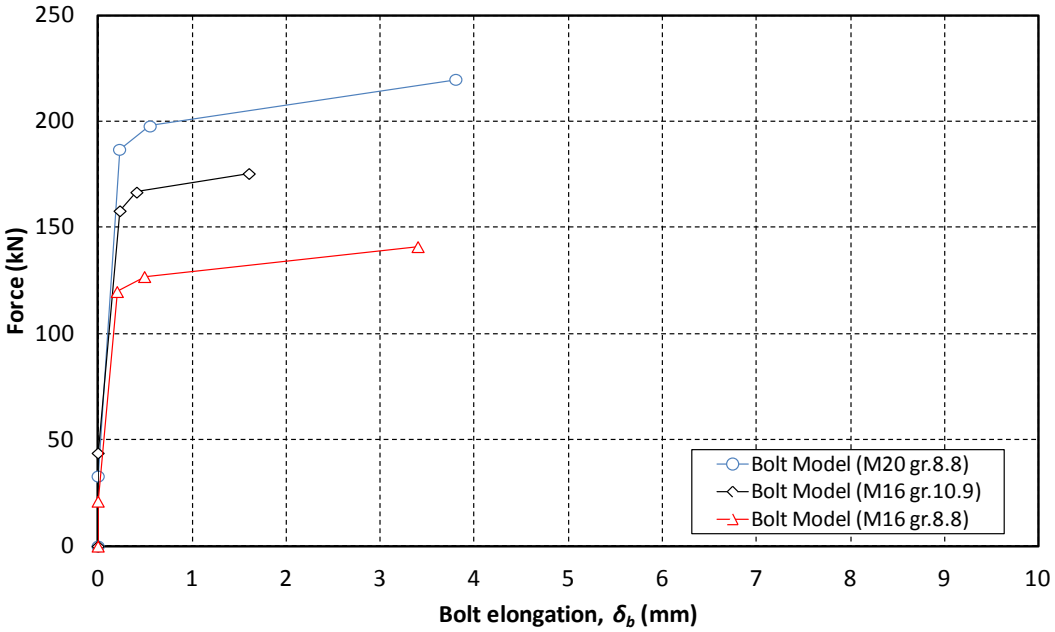

Figure 6.7 Effects of parameter variations on the F-δ_b behaviour

6.3 Mechanism 2 - Type *HB* (expanding sleeves)

In this section the experimental data related to the $F\text{-}\delta_{slip}$ relationship of type *HB* is normalised and regression analysis is performed with respect to a piecewise three segment linear curve fit of the data. On the basis of the normalised models and the respective failure mode of the element, tri-linear idealised force-slip models are proposed for representation of the expanding sleeves element that is involved in the *EHB* component, in consideration of the investigative parameter effects. The models are summarised in a table formation, accompanied with a notation chart.

6.3.1 Normalised $F\text{-}\delta_{slip}$ response and regression analysis

Due to the variation in ultimate strength that was observed among pull-out specimens - even among those within the same parameter category - it is first necessary to normalise the test results prior to the execution of any regression analysis for the data. Herein the force is normalised with the actual maximum force, $F_{test,\ max}$ that was reached in the corresponding type *HB* pull-out test; noting that by dividing all *Y* axis values by a constant does not change the best fit curve.

Regression is most often used by scientists and engineers to visualize and plot the curve that best describes the shape and behaviour of their data. Regression procedures find an association between independent and dependent variables that, when graphed on a Cartesian coordinate system, produces a straight line, plane or curve; commonly known as curve fitting. For the purposes of this study, to simplify non-linear behaviour, a tri-linear curve fit is used in the idealisation of the force-slip relationship for type *HB* and type *M*. This is deemed as satisfactory in capturing the primary features in the response of these elements. The normalised force is treated as the dependent variable and the slip is treated as the independent variable whose selection is justified by the manner in which the experimental pull-out tests were performed. As the testing was conducted under displacement control, the measuring restoring force increases only with increasing displacement; hence the dependence of force on displacement.

Figure 6.8 presents the normalised global curve fits for each parameter category, with the idealised benchmark behaviour of the element being displayed in Figure

6.8 (a), followed by the cases of using a higher concrete strength, bolt grade and bolt size shown in Figure 6.8 (b), (c) and (d), respectively. In regression, R^2 is the coefficient of determination, the most common statistical measure of how well the regression model describes the data. R^2 values have no units and typically range from 0 to 1, with values close to 1 indicating a good fit and a value of 1 indicating that the regression model perfectly fits the data. The corresponding R^2 values are thus also reported within the plots to quantify goodness of fit of the models.

(a)

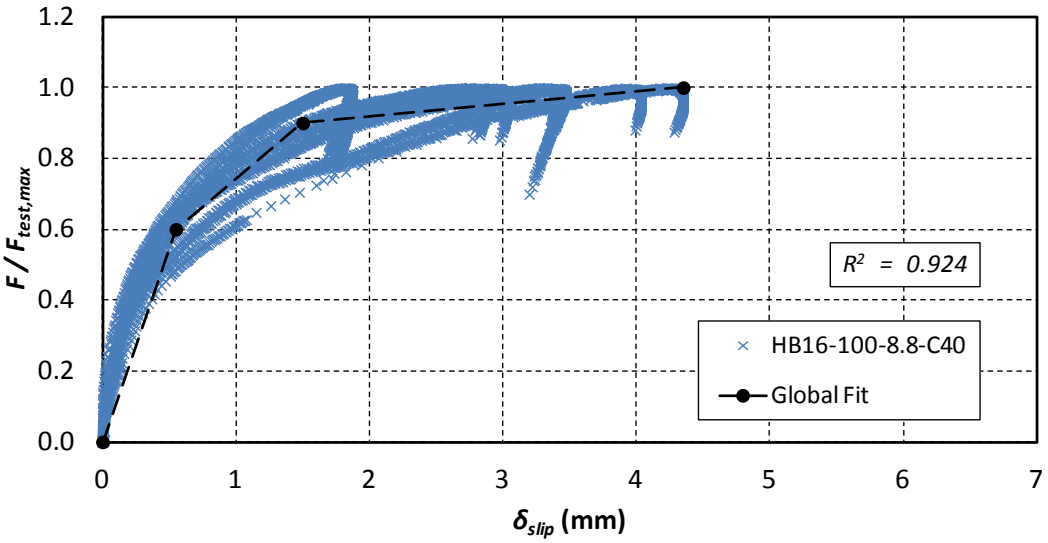

(b)

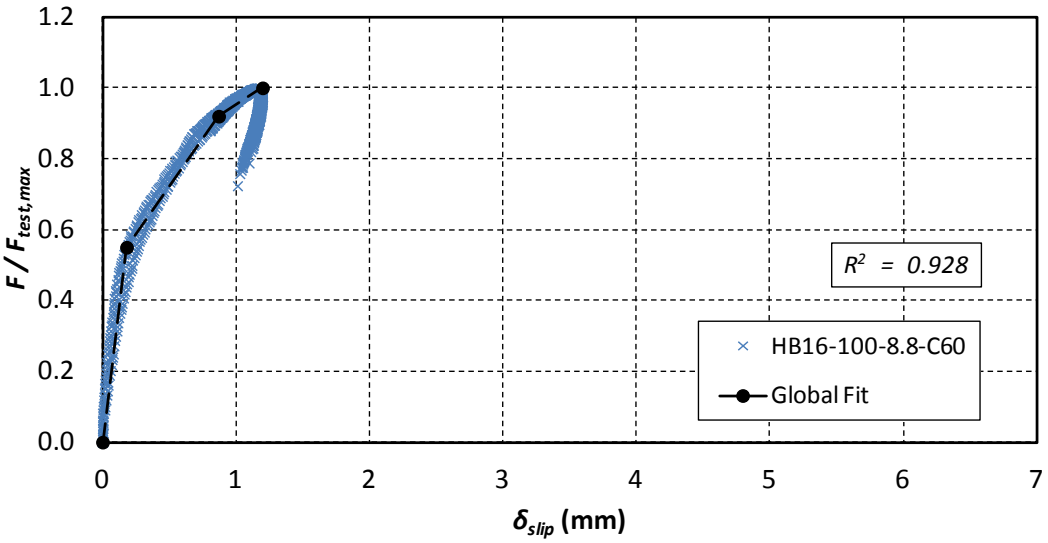

(c)

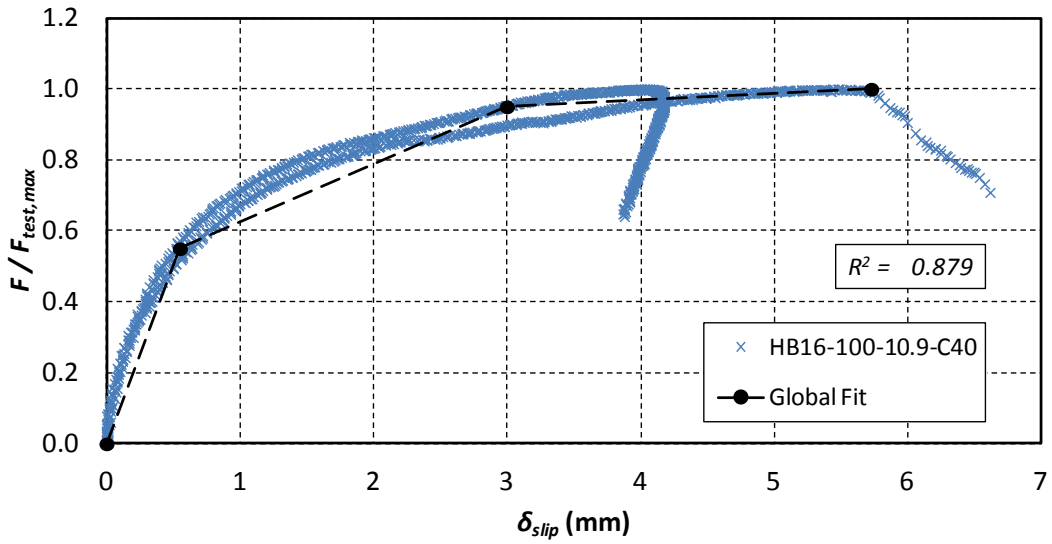

(d)

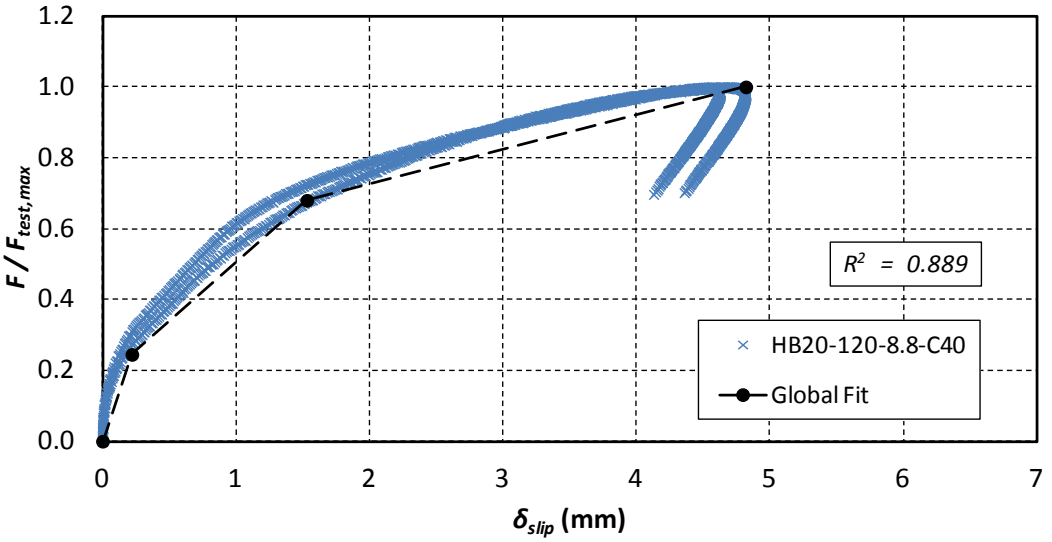

Figure 6.8 Normalisation & idealisation of type *HB* data (*F*-δ_{slip} with parameter variation)

6.3.2 Tri-linear idealised models

On the basis of the normalisation and global curve fitting results, the force-slip models for type *HB* - which have tri-linear characteristics - are calculated as shown in the notation chart of Figure 6.9; where k_x^e denotes the initial stiffness of the element, k_{norm}^e denotes the normalised initial stiffness of the element, μ^p and μ^u are the strain hardening coefficients, respectively, for the post-limit (k_x^p) and ultimate (k_x^u) stiffness, and F^u is the ultimate capacity of the component. The complete data

input for the proposed models is summarised in Table 6.2, where the quantitative values for k_{norm}^{e}, μ_p, μ_u and the correspondent force ranges have been determined from the normalised-idealised force-slip relationships (which were previously shown graphically in Figure 6.8). In brief, the model solutions simply require an input for F^u for their calculations. The model indexes display the geometrical, mechanical and material properties for appropriate selection in their use.

Experimental evidence concluded that the concrete-filled type *HB* is able to develop the full tensile capacity of its internal bolt. Likewise, the *EHB* component was also able to develop the full capacity of its internal bolt when subject to direct tension. And because the ultimate failure modes of the aforementioned types were both due to bolt shank fracture, it is thus considered valid to relate the ultimate capacity of element type *HB* with that of the ultimate capacity of the *EHB* component, F^u; in other words to use F^u in the representation of the ultimate strength of the concrete-filled type *HB* which evidently equates with the ultimate strength of the internal bolt that is used within the blind-bolt assembly. The above text justifies the presence of F^u in the idealised models for type *HB* which represent the expanding sleeves mechanism of the *EHB* component. From the index of Table 6.2 it should also be recognised that the models have been classified according to a concrete compressive strength class. With the aid of the compressive cube strengths that were recorded for the pull-out specimens type *HB*, it is found that all of the corresponding models are determined as normal strength concrete (because compressive strength class ≤ *C50*/*60*), with the benchmark strength being classified as *C30*/*37* and the higher strength specimens being classified as *C50*/*60*; noting that the first number adjacent to *C* is the minimum characteristic cylinder strength whereas the other numerical figure is the minimum characteristic cube strength, at 28 days (BSI 2000a).

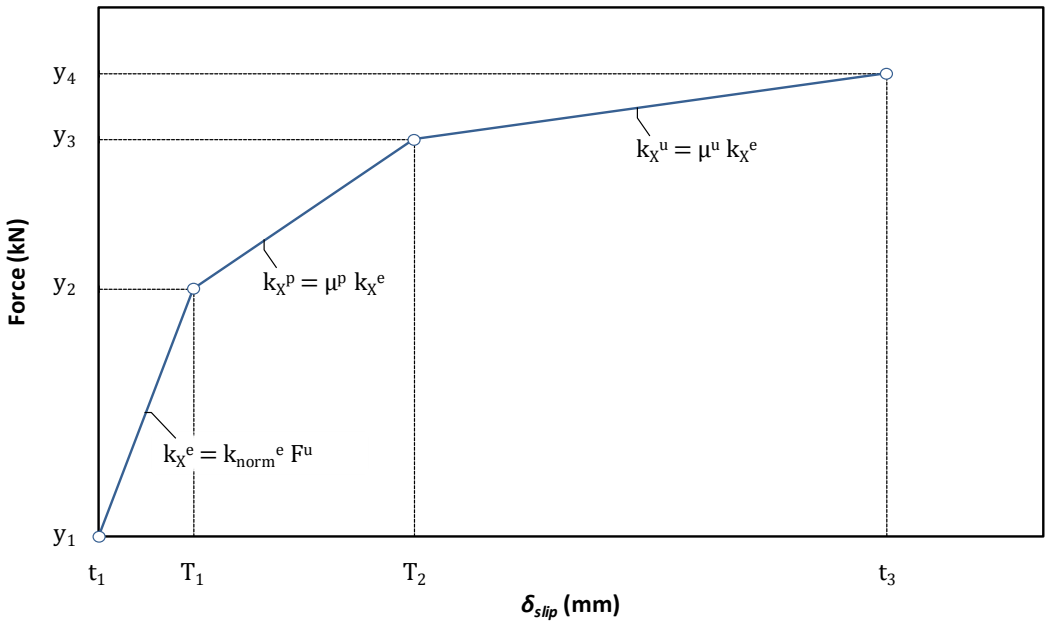

Figure 6.9 Tri-linear idealisation: notation chart for individual mechanism models

Table 6.2 Mechanism 2 stiffness models (k_{HB})

*Index	$y_1 < F \le y_2$	k_{norm}^e (mm^{-1})	$y_2 < F \le y_3$	μ_p	$y_3 < F \le y_4$	μ_u
HB16-8.8-C37	$0 < F \le 0.60\ F^u$	1.091	$0.60\ F^u < F \le 0.90\ F^u$	0.289	$0.90\ F^u < F \le F^u$	0.032
HB16-8.8-C60	$0 < F \le 0.55\ F^u$	3.056	$0.55\ F^u < F \le 0.92\ F^u$	0.175	$0.92\ F^u < F \le F^u$	0.080
HB16-10.9-C37	$0 < F \le 0.55\ F^u$	1.000	$0.55\ F^u < F \le 0.95\ F^u$	0.163	$0.95\ F^u < F \le F^u$	0.018
HB20-8.8-C37	$0 < F \le 0.25\ F^u$	1.114	$0.25\ F^u < F \le 0.68\ F^u$	0.298	$0.68\ F^u < F \le F^u$	0.087

** C37 & C60 are the minimum characteristic cube strengths for normal strength/weight concrete at 28 days; compressive strength classification to BS EN 206-1:2000.*

6.3.3 Stiffness charts at primary force levels

To explore the effects that the investigative parameters have on the stiffness, *k* of the expanding sleeves element, the type *HB* force-slip models which were presented in the previous section are calculated (by input of F^u) and stiffness charts are plotted at selective force steps (Figure 6.10). The important feature of these stiffness charts is that they capture key characteristics in the behaviour of the parametric models with increasing force levels.

As an input for F^u, the analysis here has employed the maximum forces which were obtained in the *EHB* component pull-out tests - of equivalent parameters - and the resulting mean values of *k* are graphed. The format of the stiffness charts involve k

on the *y*-axis (which represents either k_x^e, k_x^p, or k_x^u; determined according to correspondent force level) and on the *x*-axis of the charts, it is the appropriate variable that represents the variation in parameter that is graphed (e.g. f_{cu} for variation in compressive strength). The values along the *x*-axis are determined based on actual material properties that were involved in the testing of type *HB*.

As demonstrated in Figure 6.10 (a), the increase in concrete compressive strength has a significant effect on the stiffness of mechanism 2, particularly within the initial stiffness region (*0-0.55F*^{u}). Within the post-limit stiffness region (*0.60-0.90F*^{u}) however, the quantitative magnitude of improved stiffness reduces in comparison with that seen in the initial region. Although a reduction is observed, the overall stiffness within the element involving a higher strength concrete is still greater. The plotted values of f_{cu} were determined by mean cube strengths on day of testing.

The effect on the stiffness of mechanism 2 due to a variation in bolt grade is illustrated in Figure 6.10 (b). The lower bound values for f_{ub} represent benchmark behaviour (of grade 8.8 involving the mean of bolt batches A, C & D) whereas the upper bound values for f_{ub} equate with type *HB* of grade 10.9 (involving batch E). It is noticeable that within the very first stiffness region (*0-0.55F*^{u}), the stiffness of the element is higher in the case of the higher bolt grade; attributed to the level of pre-load that is induced in the element at its tightening stage. And with increasing force levels, it is observed that the stiffness characteristics of the element are marginally influenced with increasing f_{ub}. This primarily indicates that there is an improvement within the initial stiffness region of the element when higher bolt grades are employed within the system. The plotted values of f_{ub} were determined by mean results obtained via material property testing (of relevant bolt batches).

With regard to the effects on the stiffness of mechanism 2 when a larger bolt size is considered, these are presented in Figure 6.10 (c), with an increasing d_b plotted on the *x*-axis. From the stiffness chart it is clearly identified that the stiffness of the element is appreciably increased within the equivalent force levels; attributed primarily to the size effect of the expanding sleeves system itself. The plotted values of d_b are nominal sizes for the internal bolt that is used in the blind-bolt assembly.

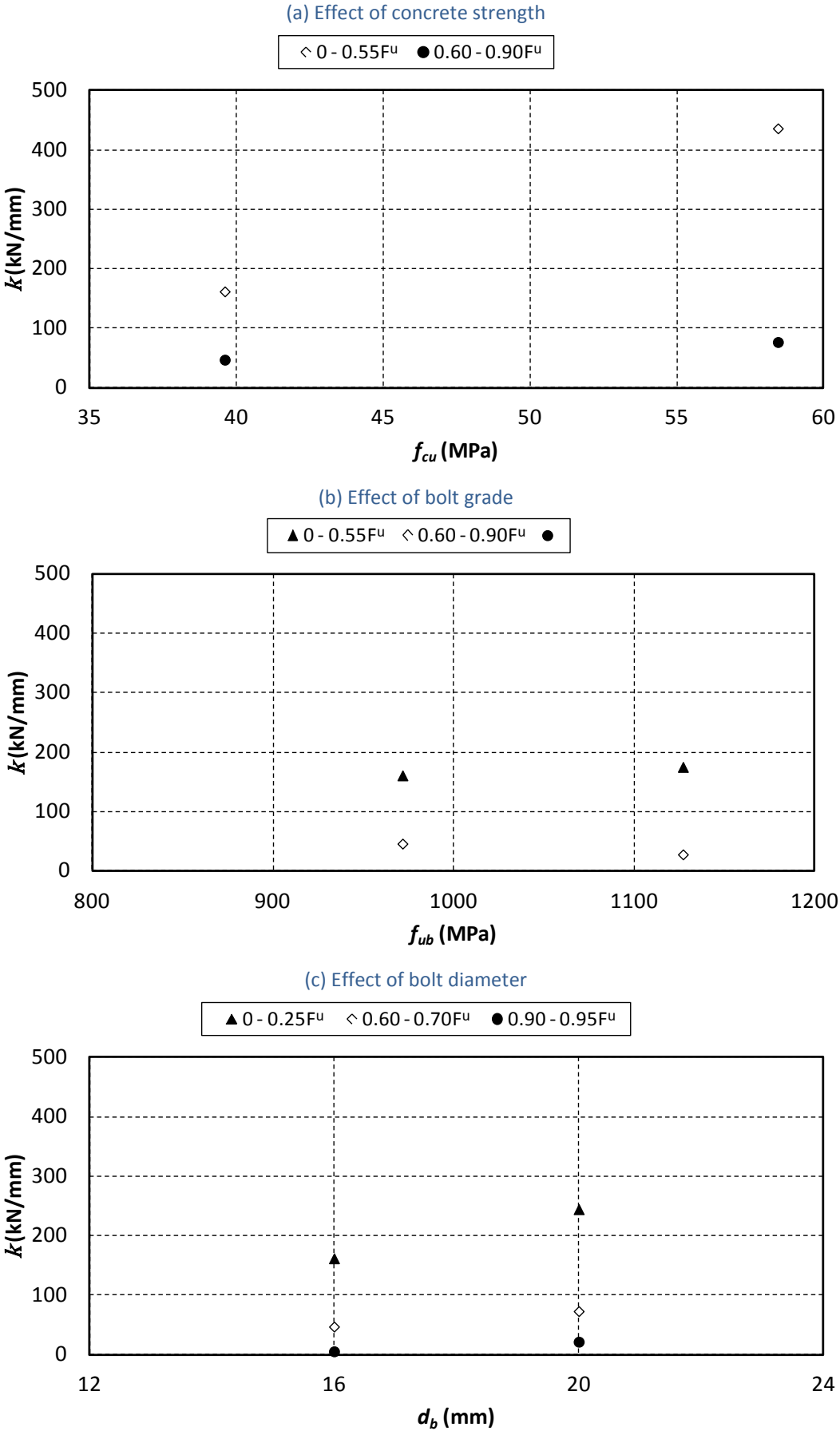

Figure 6.10 Effect of parameter variation on stiffness of mechanism 2

6.4 Mechanism 3 - Type *M* (mechanical anchorage & bond)

Following the sequence of analysis carried out for type *HB* in section 6.3, it is the purpose of this section to present the normalised-idealised experimental data related to the F-δ_{slip} behaviour of type *M*. Similarly, regression analysis is performed with respect to a tri-linear fit of the data and the proposed force-slip models are summarised in a table format. Such models are to be employed for representation of the mechanical anchorage and bond element that is involved in the *EHB* component; in consideration of the investigative parameter effects.

6.4.1 Normalised F-δ_{slip} response and regression analysis

Figure 6.11 presents the normalised global curve fits for each investigative parameter category involved in type *M*, with the idealised benchmark behaviour of the element being displayed in Figure 6.11 (a). Tri-linear fits in the cases of using a higher concrete strength, bolt grade and bolt size follow in Figure 6.11 (b), (c), and (d), respectively. Moreover, curve fitting related to varying embedded depths for type *M* are shown in Figure 6.11 (e) and (f) which involve embedded depths of $4.0d_b$ and $6.5d_b$, respectively, whereas the benchmark d_{emb} is at $5.3d_b$. R^2 values are correspondingly reported within the plots to quantify goodness of fit of the models.

(a)

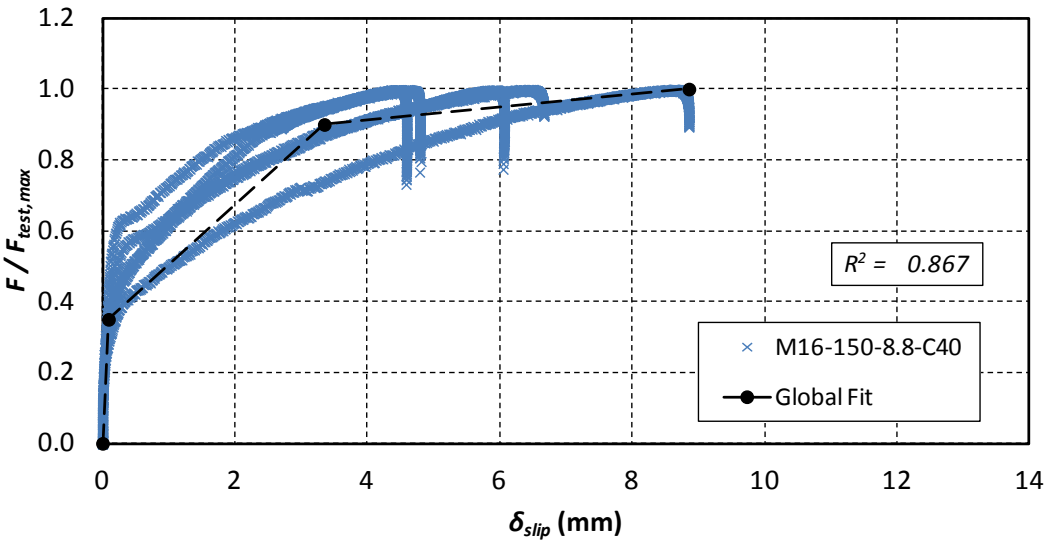
1.2
1.0
0.8
0.6
0.4
0.2
0.0
F / F test,max
0
2
4
6
8
10
12
14
δslip (mm)
R² = 0.867
M16-150-8.8-C40
Global Fit

(b)

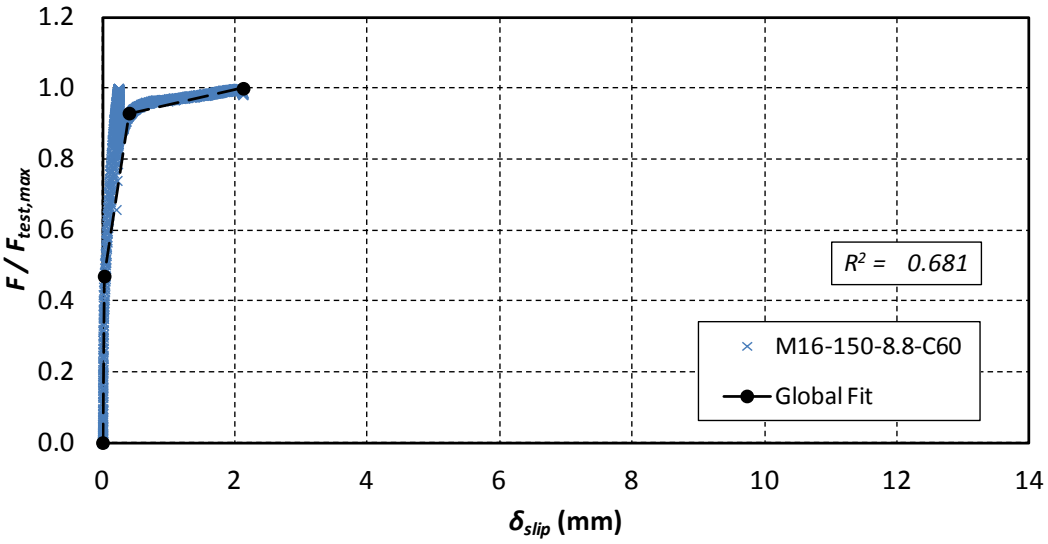
1.2
1.0
0.8
0.6
0.4
0.2
0.0
F / F test,max
0
2
4
6
8
10
12
14
δslip (mm)
R² = 0.681
M16-150-8.8-C60
Global Fit

(c)

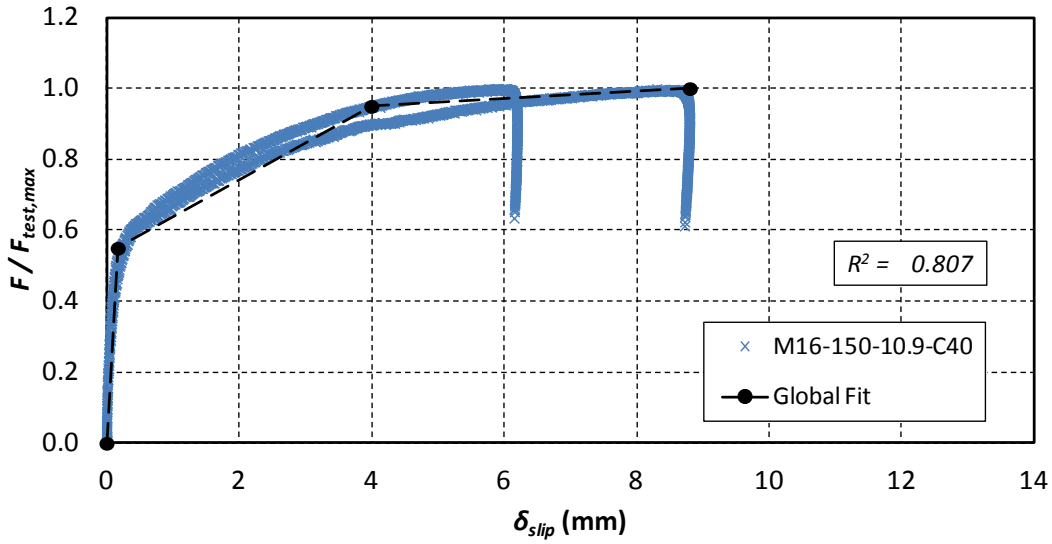
1.2
1.0
0.8
0.6
0.4
0.2
0.0
F / F test,max
0
2
4
6
8
10
12
14
δslip (mm)
R² = 0.807
M16-150-10.9-C40
Global Fit

(d)

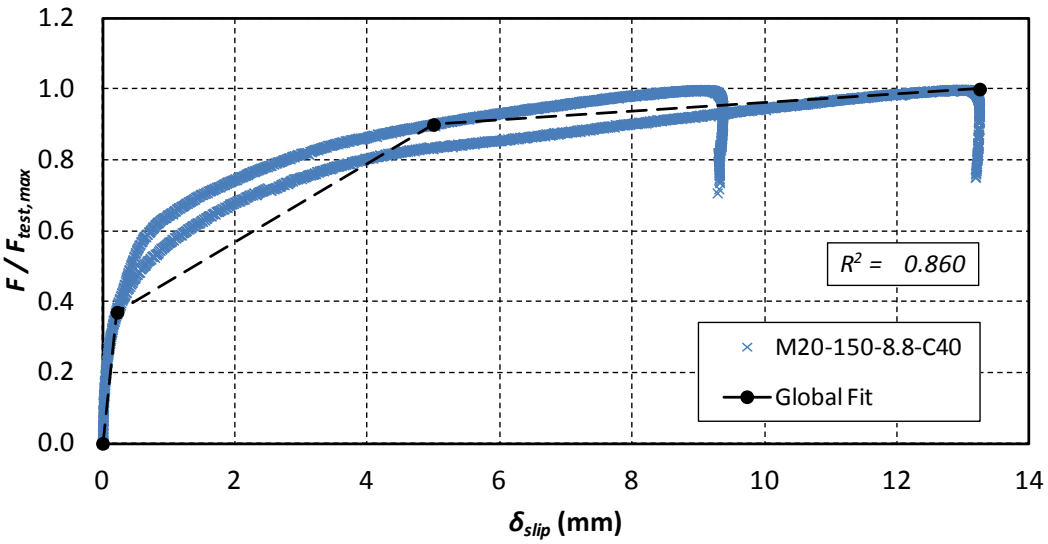

(e)

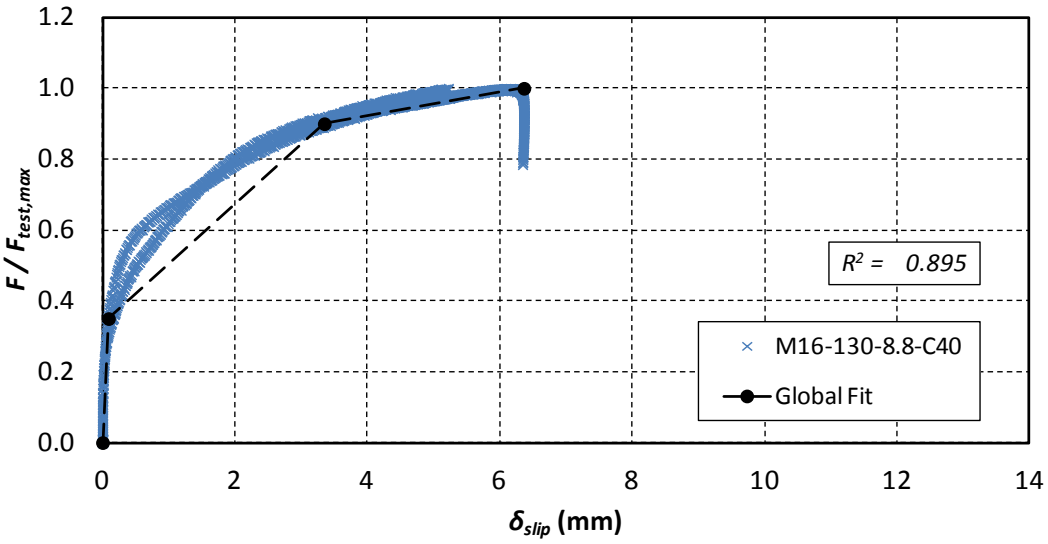

(f)

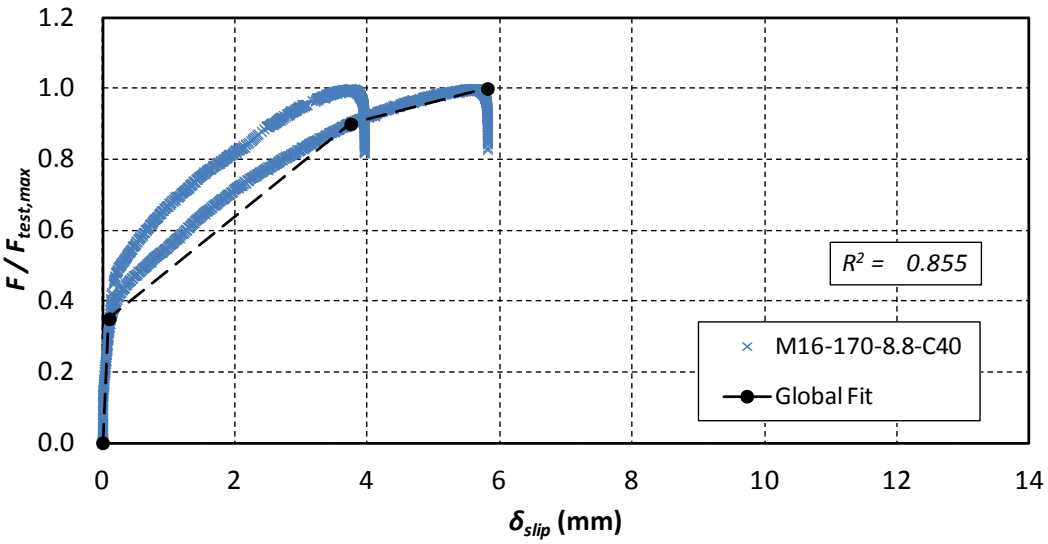

Figure 6.11 Normalisation & idealisation of type *M* data (*F*-δ_{slip} with parameter variation)

6.4.2 Tri-linear idealised models

The data input for the proposed force-slip models for type *M* - which have tri-linear characteristics - is summarised in Table 6.3; the models are calculated as previously detailed in section 6.3.2 with the use of the notation chart of Figure 6.9. The quantitative values for k_{norm}^{e}, μ_p, μ_u and the correspondent force ranges have been determined from the normalised-idealised force-slip relationships (which were illustrated graphically in Figure 6.11). Likewise with the force-slip type *HB* models, the type *M* model solutions simply require an input for F^u for their calculations, with the model indexes displaying the geometrical, mechanical and material properties for appropriate selection in their use. The presence of F^u in the idealised models for type *M* - which represent the mechanical anchorage and bond mechanism of the *EHB* component - is once again justified by the experimental evidence which demonstrated a common ultimate failure mode among type *M* and the *EHB* component under pull-out testing (which was due to bolt shank fracture).

From the index of Table 6.3 it is also recognised that the models have been classified according to a compressive strength class and an embedded depth that is defined in terms of d_b. With the aid of the cube strengths that were recorded for the pull-out specimens of type *M*, it is found that all of the corresponding models are determined as normal strength concrete, with the benchmark strength being classified as *C30/37* and the higher strength specimens as *C50/60* (BSI 2000a).

Table 6.3 Mechanism 3 stiffness models (k_M)

*Index	$y_1 < F \le y_2$	k_{norm}^{e} (mm^{-1})	$y_2 < F \le y_3$	μ_p	$y_3 < F \le y_4$	μ_u
M16-8.8-C37-5.3d_b	$0 < F \le 0.35\ F^u$	3.889	$0.35\ F^u < F \le 0.90\ F^u$	0.043	$0.90\ F^u < F \le F^u$	0.005
M16-8.8-C60-5.3d_b	$0 < F \le 0.47\ F^u$	18.800	$0.47\ F^u < F \le 0.93\ F^u$	0.065	$0.93\ F^u < F \le F^u$	0.002
M16-10.9-C37-5.3d_b	$0 < F \le 0.55\ F^u$	3.235	$0.55\ F^u < F \le 0.95\ F^u$	0.032	$0.95\ F^u < F \le F^u$	0.003
M20-8.8-C37-4.0d_b	$0 < F \le 0.37\ F^u$	1.682	$0.37\ F^u < F \le 0.90\ F^u$	0.066	$0.90\ F^u < F \le F^u$	0.007
M16-8.8-C37-4.0d_b	$0 < F \le 0.35\ F^u$	3.889	$0.35\ F^u < F \le 0.90\ F^u$	0.043	$0.90\ F^u < F \le F^u$	0.009
M16-8.8-C37-6.5d_b	$0 < F \le 0.35\ F^u$	3.500	$0.35\ F^u < F \le 0.90\ F^u$	0.043	$0.90\ F^u < F \le F^u$	0.014

** C37 & C60 are the minimum characteristic cube strengths for normal strength/weight concrete at 28 days; compressive strength classification to BS EN 206-1:2000.*

6.4.3 Stiffness charts at primary force levels

To explore the effects that the investigative parameters have on the stiffness, *k* of the mechanical anchorage element, the type *M* force-slip models which were presented in the previous section are calculated by input of F^u. The stiffness charts are plotted at selective force steps in Figure 6.12; capturing the key characteristics in the behaviour of the parametric models with increasing force levels. For the input value of F^u, the analysis employs the maximum forces which were obtained in the *EHB* component pull-out tests - of equivalent parameters - and the resulting mean values of *k* are graphed. The format of the stiffness charts involve k on the *y*-axis (which represents either k_x^e, k_x^p, or k_x^u; determined according to the correspondent force level) and on the *x*-axis of the charts, it is the appropriate variable that represents the variation in parameter that is graphed. The values along the *x*-axis are determined based on actual material properties that were involved in the pull-out testing of type *M*.

As demonstrated in Figure 6.12 (a), the increase in concrete compressive strength has a major effect on the stiffness of mechanism 3, particularly within the initial stiffness region ($0\text{-}0.35F^u$). Within the post-limit stiffness region ($0.50\text{-}0.90F^u$) however, the quantitative magnitude of enhanced stiffness reduces in comparison with that seen in the initial region. Although a reduction is observed, the overall stiffness within the element involving a higher strength concrete is still greater. The plotted values of f_{cu} were determined by mean cube strengths on day of testing.

The effect on the stiffness of mechanism 3 due to a variation in bolt grade is illustrated in Figure 6.12 (b). The lower bound values for f_{ub} represent benchmark behaviour (of grade 8.8 involving the mean of bolt batches A & D) whereas the upper bound values for f_{ub} equate with type *M* of grade 10.9 (involving batch E). For the selected force ranges, it is shown that the overall stiffness of the element is not significantly affected by the variation in bolt grade. This stiffness behaviour is observed because the response of the element is dictated by the development of its mechanical anchorage. The plotted values of f_{ub} were determined by mean results obtained via material property testing (of relevant bolt batches).

When a larger bolt size is considered in type *M*, the effect on its stiffness is shown in Figure 6.12 (c), with increasing d_b plotted on the *x*-axis. From the stiffness chart it is identified that within the equivalent force levels, the stiffness of the element reduces with increasing d_b; attributed primarily to the size effect of the end anchor head itself. The plotted values of d_b are nominal sizes for the anchored bolt.

In consideration of a variation in embedded depth, d_{emb} in type *M*, the effect on its stiffness is shown in Figure 6.12 (d). It is demonstrated that for the investigative range of d_{emb}, the variation does not have any major effect on its initial or post-limit stiffness regions. Such an effect is anticipated due to the minor changes in magnitude of embedded depths among the models.

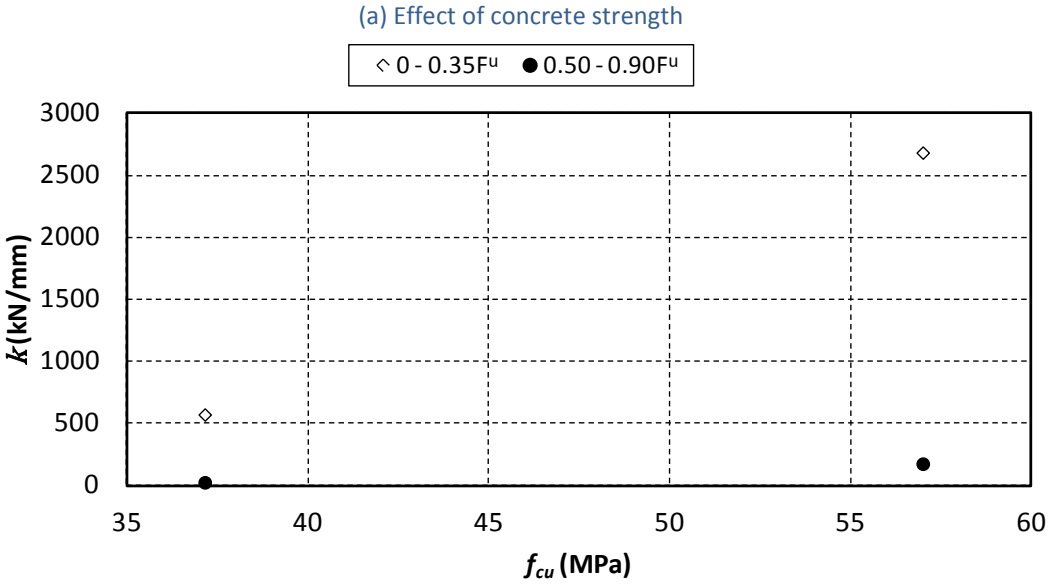

(b) Effect of bolt grade

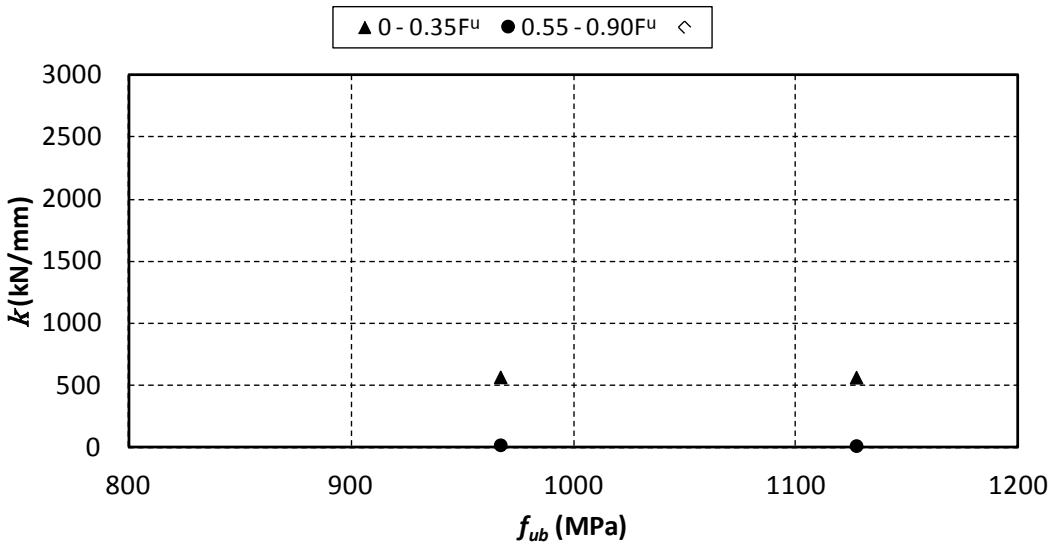

(c) Effect of bolt diameter

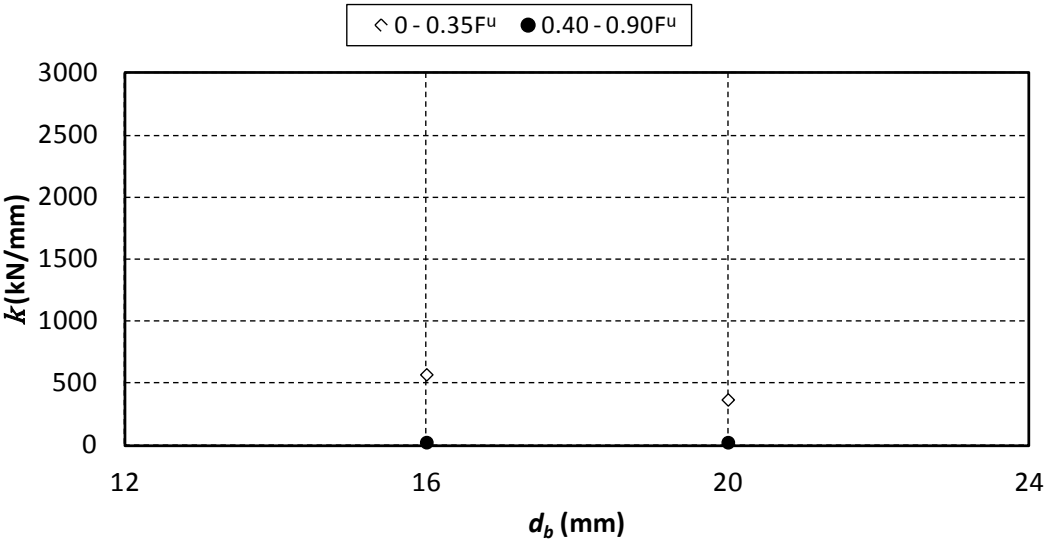

(d) Effect of embedded depth

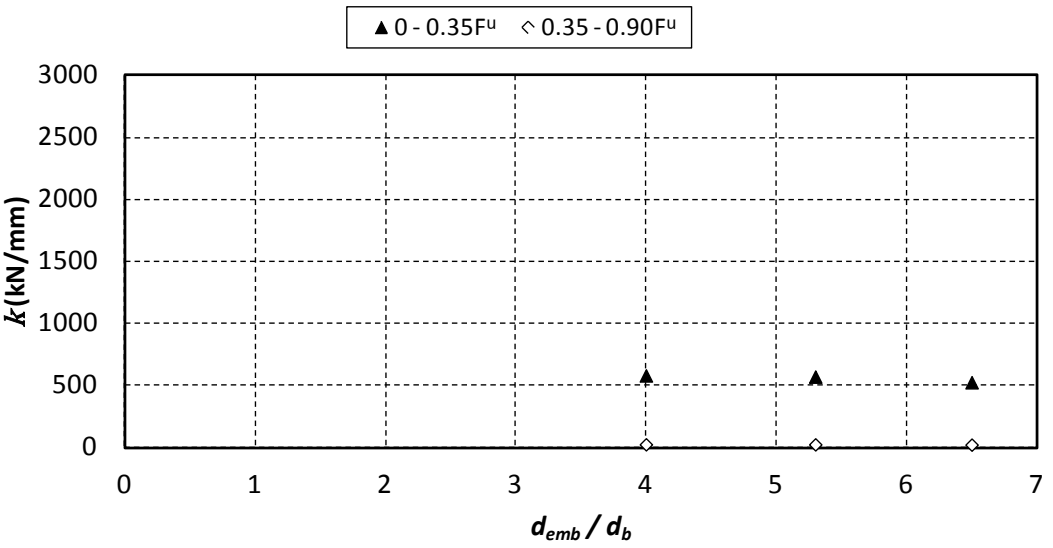

Figure 6.12 Effect of parameter variation on stiffness of mechanism 3

6.4.4 Pull-out strength equation

With reference to the published procedures involved in the calculation of pull-out strength within the design field of fastenings to concrete (see section 3.4.1), it is the purpose of this section to determine an appropriate experimental factor that can be used in the prediction of the pull-out strength of type *M*. Hereafter, pull-out strength is denoted as *P*; noting that notation used in reference codes does differ.

Current equations that predict the pull-out strength of headed fasteners involve the compressive strength of the concrete in which the anchor is embedded, the net bearing area of the anchor, and an experimental factor which varies accordingly with the test method in which the compressive strength of the concrete is determined; by cube or cylinder testing. For instance, in the American code of ACI 318 (ACI 2008b), pull-out strength is determined with the use of cylinder strength, and a factor of 8 is employed; as expressed in Equation 6-3. While European codes which use cube strength, such as the UK implementation of CEN/TS 1992-4-2:2009 adopt a factor of 6; as outlined in Equation 6-4. These formulae suggest a constant conversion factor of 0.75 for cube to cylinder strength (i.e. f_c'=0.75f_{cu}). Because only cube strengths were measured throughout this programme, for the calculations of $P_{(ACI)}$ in the following analysis, the actual measured cube strength f_{cu} is converted to cylinder strength using appropriate conversion tables which are provided in BS EN 206-1:2000 (BSI 2000a); using interpolation where necessary. It is felt that the conversion tables would result in more accuracy for the conversion rather than the constant factor of 0.75. On the basis of the below equations, values are determined for $P_{(ACI)}$ and $P_{(CEN)}$ with respect to the properties involved in type *M* pull-out tests.

when using compressive cylinder strength:

$$P_{(\mathrm{ACI})} = 8\, A_{brg}\, f_c' \qquad \textbf{Equation 6-3}$$

when using compressive cube strength:

$$P_{(\mathrm{CEN})} = 6\, A_{brg}\, f_{cu} \qquad \textbf{Equation 6-4}$$

In order to assess the predictions of $P_{(ACI)}$ and $P_{(CEN)}$ however, it is first necessary to define the experimental (actual measured) pull-out strength of type *M*. This would then allow for a direct comparison of the calculated data. For the purposes of this study, the experimental pull-out strength is denoted as P_{test} and it is determined as the force level which corresponds to a slip of 0.3mm; extracted from the raw F-δ_{slip} behaviour of type *M* (Figure 6.13). Having defined P_{test}, a comparison is performed in Figure 6.14 between the experimental and code values for *P*. It is observed that the code formulae tend to overestimate the experimental pull-out strength in most of the cases, where descriptive statistics result in mean ratios of $P_{test}/P_{(ACI)}$ and $P_{test}/P_{(CEN)}$ at 0.77 and 0.83, with standard deviations of 0.15 and 0.16, respectively.

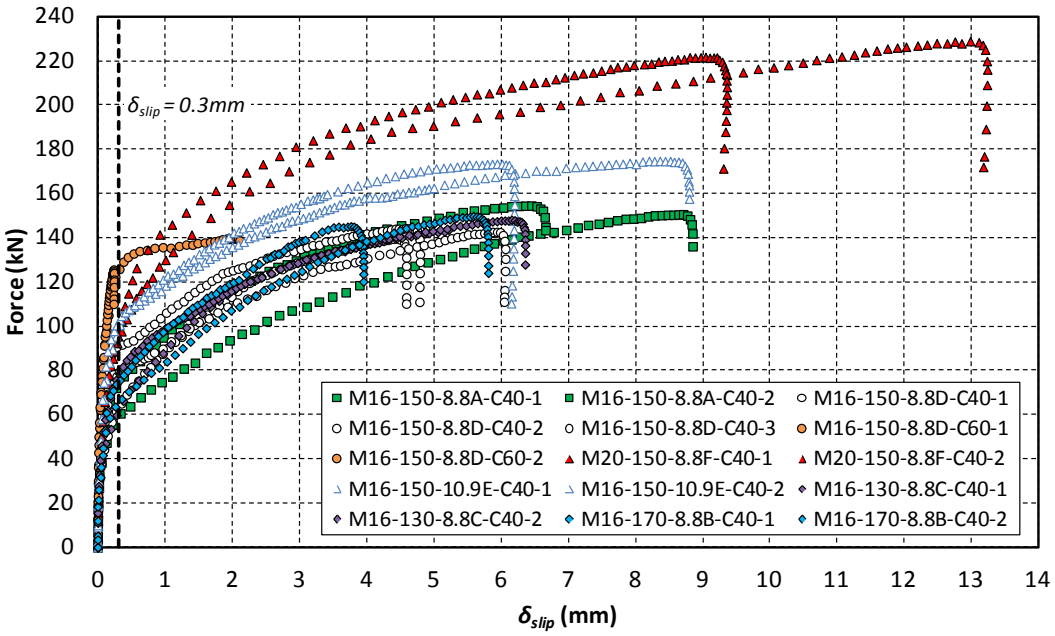

Figure 6.13 Experimental pull-out strength (P_{test}) at 0.3mm slip

It is believed that the higher code values are attributed to: (1) the requirement of a development length which is not considered in the functions of pull-out strength, and (2) the requirement of a head bearing area which is also not considered in the expressions. In other words, d_{emb} is not included in the calculation of *P*, but it is

indirectly taken into account in the design of fastenings by requiring a minimum development length - which would equate with the magnitude of d_{emb} in the case of type *M*. Similarly, the codes set a limit on the ratio of A_{brg}/A_b to be greater than 4, which is larger than that of type *M*. This would imply that different embedded depths (longer) and different anchor head sizes (larger) would be involved in the equivalent headed fasteners to which the ACI and CEN codes are applicable to, hence the discrepancy in Figure 6.14. It is worthwhile highlighting here that the embedded depth involved in the *EHB* component is restricted to the size of the connecting hollow section, and the size of its end anchor head is restricted to the size of the clearance bolt hole. Nevertheless, on the basis of the same principles involved in the pull-out equations which were detailed above, it is possible to derive an experimental factor for representation in a pull-out equation for type *M*; with this experimental factor being calculated as the ratio of P_{test} / A_{brg} f_{cu}, for each type *M* test performed, using actual measured f_{cu}.

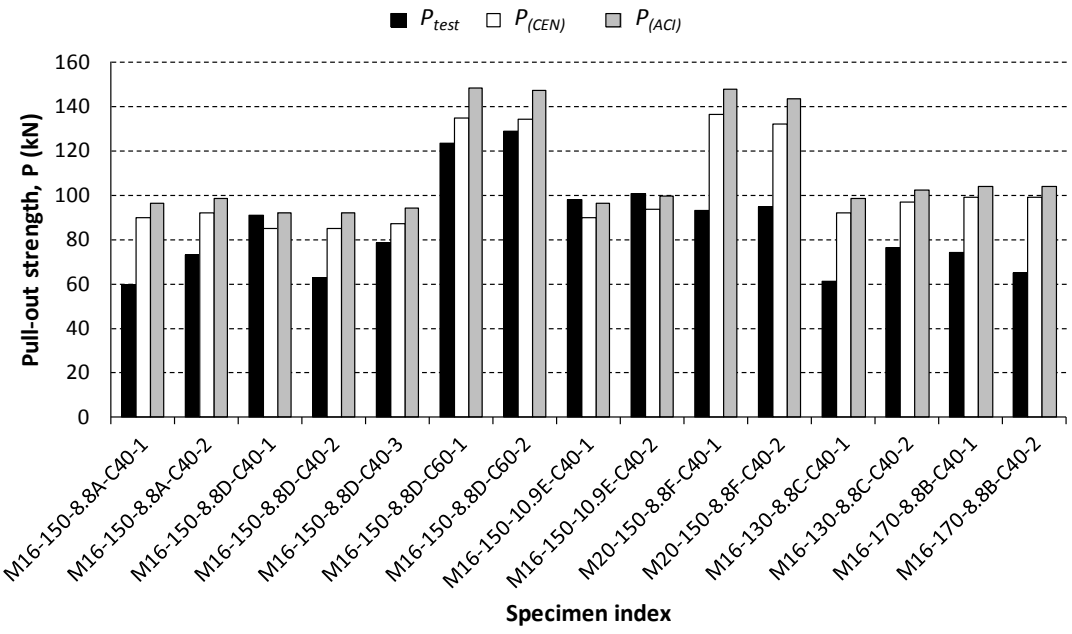

Figure 6.14 Comparison of experimental pull-out strength with design code predictions

Table 6.4 summarises the P_{test} values with correspondent concrete strength, bearing area, and ratio of P_{test} / A_{brg} f_{cu} (the experimental factor); indexed in type *M* specimen order. From the calculated ratios of P_{test} / A_{brg} f_{cu}, it is suggested that a mean value of 5.0 could be adopted as a factor in the pull-out equation, hereafter labelled as the modified pull-out equation for element type *M*. This mean value has a standard deviation of 0.95, and the 95% confidence interval for the mean has a lower bound of 4.47, and an upper bound of 5.52. The results of the modified pull-out equation are reported under $P_{predicted}$ in Table 6.4, where $P_{predicted}$ is the predicted pull-out strength of type *M*. To evaluate the application of the experimental factor 5.0 within the pull-out equation for type *M*, the ratios of $P_{test}/P_{predicted}$ are plotted in Figure 6.15. The bar chart demonstrates that the predicted pull-out strength is consistently higher than 80% of the experimental pull-out strength. The ratios of $P_{test}/P_{predicted}$ have a mean value of 1.0, with a 95% confidence interval of 0.89 to 1.10, and a standard deviation of 0.19.

Table 6.4 Predicted pull-out strength in type *M (using modified factor)*

Specimen index	A_{brg} (mm^2)	$^{*} f_{cu}$ (MPa)	$^{\S} f_c'$ (MPa)	P_{test} (kN)	P_{test} / A_{brg} f_{cu}	$P_{predicted}$ (kN)
M16-150-8.8A-C40-1	393	38.0	30.6	59.4	4.0	74.6
M16-150-8.8A-C40-2	393	39.0	31.3	73.2	4.8	76.5
M16-150-8.8D-C40-1	393	36.0	29.3	91.2	6.4	70.7
M16-150-8.8D-C40-2	393	36.0	29.3	63.0	4.5	70.7
M16-150-8.8D-C40-3	393	36.9	29.9	78.6	5.4	72.4
M16-150-8.8D-C60-1	393	57.1	47.1	123.4	5.5	112.1
M16-150-8.8D-C60-2	393	56.9	46.9	128.8	5.8	111.7
M16-150-10.9E-C40-1	393	38.0	30.6	97.7	6.5	74.6
M16-150-10.9E-C40-2	393	39.6	31.6	100.5	6.5	77.7
M20-150-8.8F-C40-1	621	36.6	29.7	93.3	4.1	113.5
M20-150-8.8F-C40-2	621	35.4	28.9	94.5	4.3	109.7
M16-130-8.8C-C40-1	393	39.0	31.3	61.2	4.0	76.5
M16-130-8.8C-C40-2	393	41.0	32.5	76.5	4.8	80.5
M16-170-8.8B-C40-1	393	42.0	33.1	74.4	4.5	82.4
M16-170-8.8B-C40-2	393	42.0	33.1	64.8	3.9	82.4

** compressive cube strength on day of testing;*

§ equivalent compressive cylinder strength on day of testing to BS EN 206-1:2000.

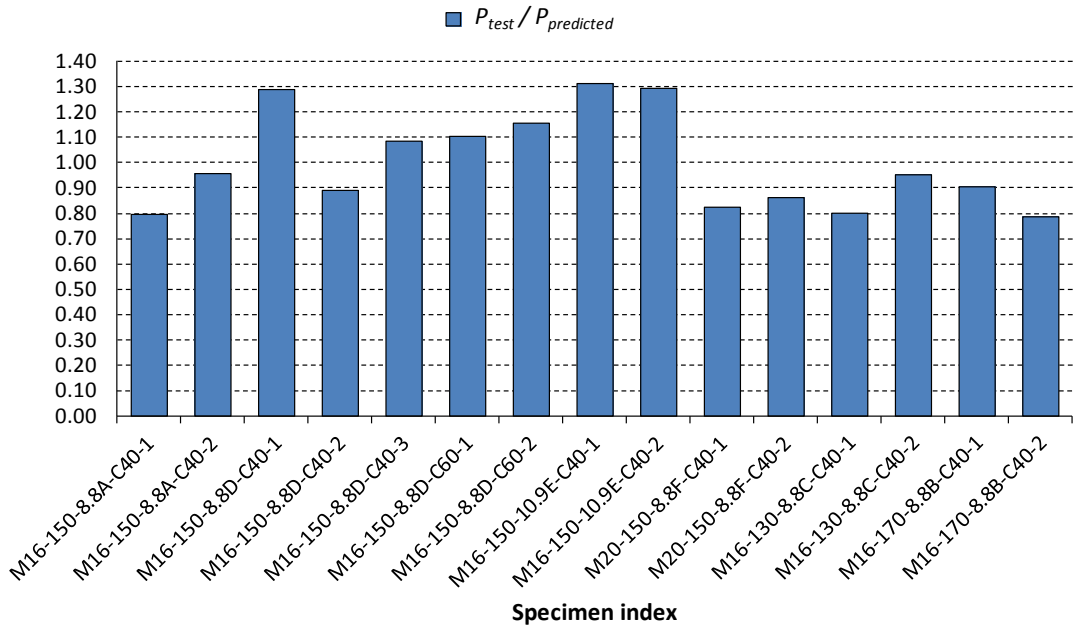

Figure 6.15 Ratios of experimental to predicted pull-out strength *(using modified factor)*

In consideration of the investigative parameters involved in the testing of type *M*, pull-out strength charts are presented in Figure 6.16 to quantify the effects that the variation in parameters have on the pull-out strength of the element. For comparison, the charts involve average results for the experimental and the predicted pull-out strengths, where $P_{predicted}$ is determined by the modified pull-out equation as below.

$$P_{predicted} = 5.0\, A_{brg}\, f_{cu} \qquad \textbf{Equation 6-5}$$

The effect of concrete strength is shown in (a), the effect of bolt grade is shown in (b), the effect of bolt diameter size (which involves a larger A_{brg}) is illustrated in (c), and lastly, the effect of d_{emb} in terms of d_b is demonstrated in (d). Overall, it is found that the predicted pull-out strengths follow the trend of the experimental data. Noticeably, and as anticipated, an increase in concrete strength and size of bolt diameter seem to have the largest effect on the pull-out strength of type *M*. With increasing f_{cu} and d_b, the pull-out strength of type *M* also increases, considerably.

This is attributed to the enhanced bearing strength that is provided by higher strength concrete, and to the larger bearing area that is provided by larger end anchor heads (which are involved in the case of employing a larger d_b). With respect to a variation in bolt grade, it is concluded that there is no major effect on the pull-out strength of type *M* when the investigative bolt grades are considered. Similarly, for the investigative embedded depths, it is observed that the predicted and experimental values for *P* fall within a 10kN region, indicating that for the investigative range of d_{emb}, the variation in d_{emb} does not radically affect the pull-out strength of the element.

(a) Effect of concrete strength

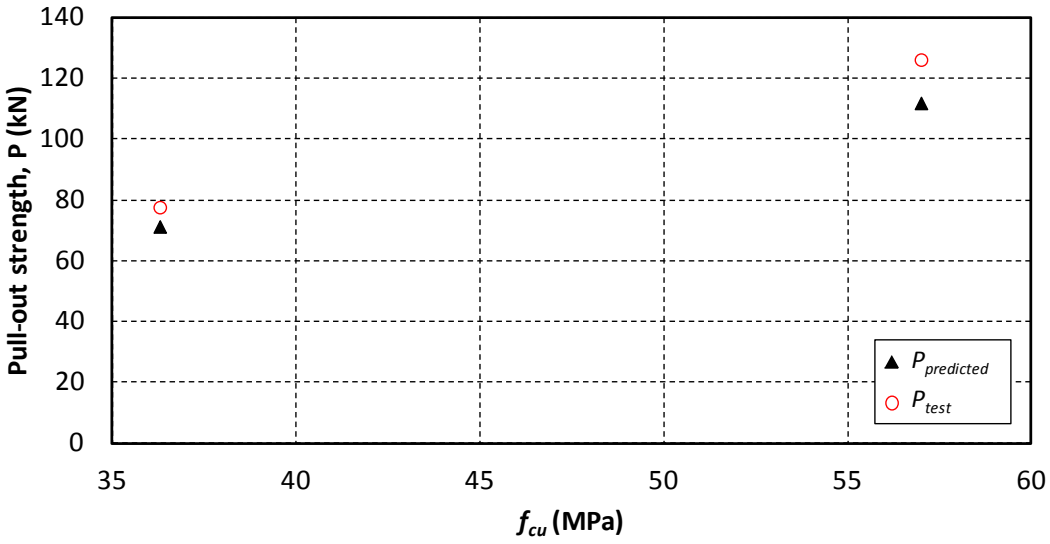

(b) Effect of bolt grade

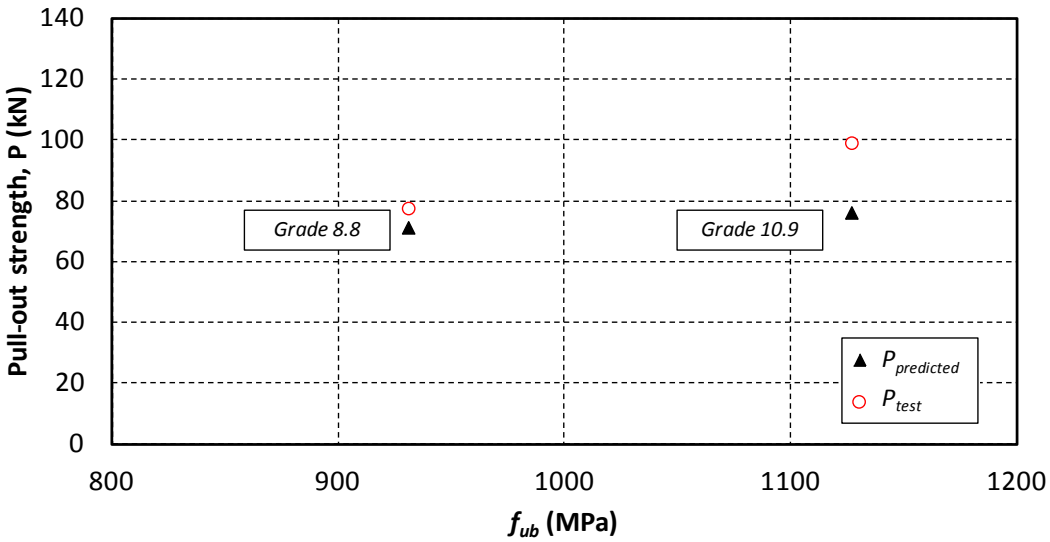

(c) Effect of bolt diameter

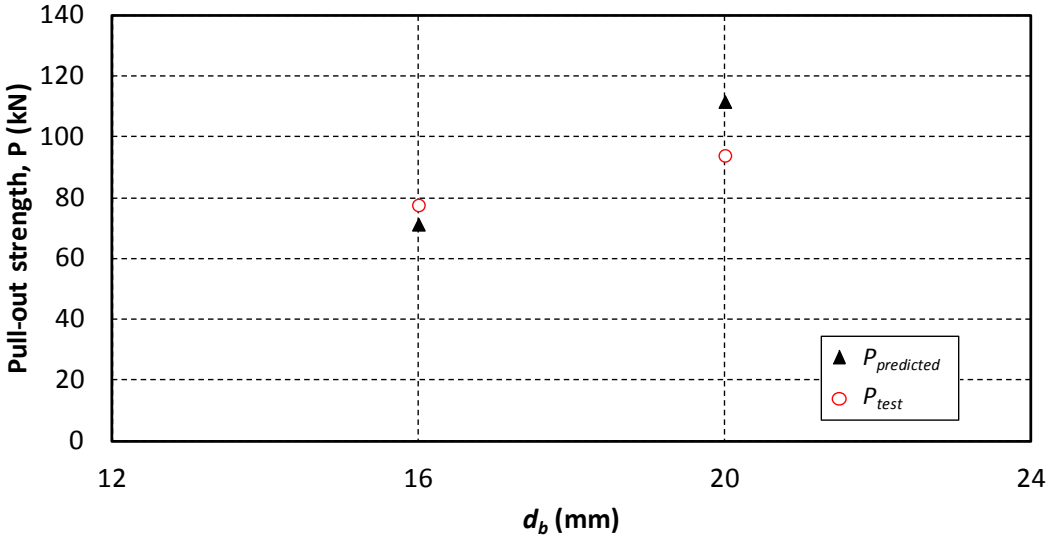

(d) Effect of embedded depth

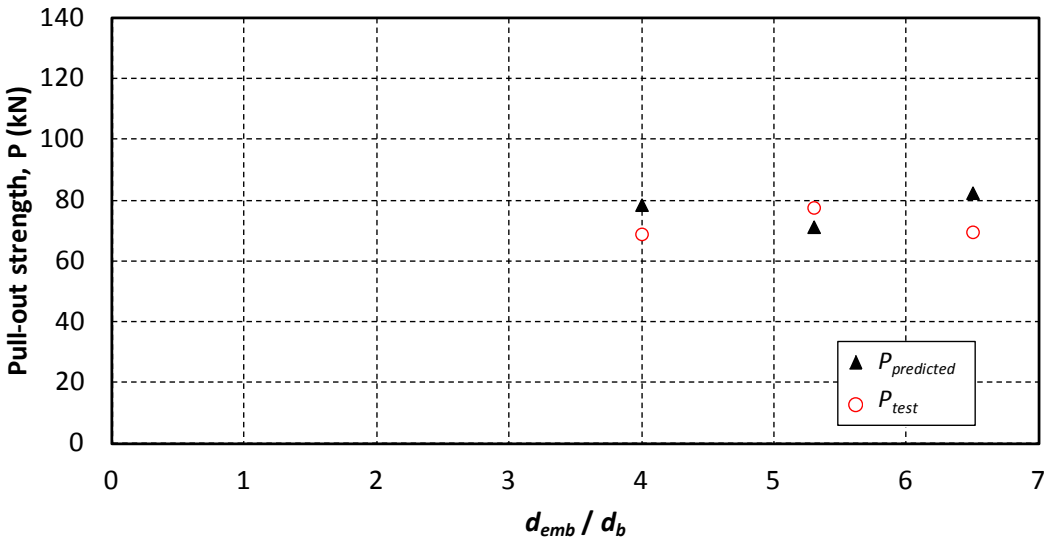

Figure 6.16 Effects on the pull-out strength of type *M* due to a variation in parameters

Some additional comments regarding the above analysis are as follows. The strengths that are estimated by $P_{predicted}$ for type *M* do not directly equate with the force levels at which the initial stiffness of type *M* reduces (i.e. $P_{predicted}$ does not reflect the initiation of post-limit stiffness for the element). Rather, the modified pull-out equation should be considered as an expression that estimates the force at which local concrete crushing occurs in front of the end anchor head of type *M* due to bearing action; as also defined by in the relevant design codes. Such local

concrete crushing does reduce the stiffness of the overall *EHB* component, however due to the interaction of the mechanical anchorage and expanding sleeves mechanisms, and due to the presence of highly confined concrete, it is implied that with respect to the behaviour of the *EHB* component, such force levels generally will not be the beginning of a total pullout failure. Moreover, the above formulations assume cracked concrete at service load levels, and the respective code limits that are imposed on the compressive strength of concrete (for application of the pull-out strength equations) have been checked for in comparison with the compressive cube testing measurements.

6.5 Concluding remarks

This Chapter has presented the detailed analysis of the data related to the principal pull-out and pre-load test results, where regression analysis and statistical tools have been used to quantify the integrity of the analysis. In the course of the presented analysis, idealised models are proposed for the response of the individual elements of the *EHB* component. A semi-empirical, tetra-linear force-bolt elongation model that incorporates pre-load and inelastic effects is proposed for the stiffness of the internal bolt of the *EHB* component. Empirical tri-linear force-slip models are proposed for the stiffness related to the expanding sleeves and mechanical anchorage elements of the *EHB* component. The models were prepared in consideration of the investigative parameters involved in this study, and the effects on the stiffness of the elements due to a variation in the parameters were explored. It was demonstrated that the compressive strength of the concrete infill has the most significant effect on the stiffness of the concrete embedded elements.

The Chapter satisfies research objectives associated with the evaluation and development of suitable models for the individual mechanisms (or elements) that contribute to the overall deformability curve of the *EHB* component; in consideration of the main parameters affecting their response. Importantly, the analysis performed in this Chapter forms the foundation for the development of the overall *EHB* component model that is presented in the next Chapter of the thesis.

7 Modelling

The force-displacement behaviour of the component "Bolts (*EHB*) in tension" and that of its individual elements was investigated experimentally by means of tensile pull-out tests. Based on the findings of the experimental programme, stiffness models were proposed for the individual elements of the component; denoted as *Mechanisms 1-3.* This chapter summarises the individual element models and proposes an appropriate procedure for their assembly; in view of predicting the global force-displacement (F-δ_{global}) response of the *EHB* component. An equivalent spring model is proposed for the tension response of the component, whose predictions are graphed with experimental data for comparison, and evaluated using regression analysis and 95% prediction bands. Excluding internal bolt pre-load effects when estimating the component's F-δ_{global} relationship are also investigated, and the significance of including pre-load effects within the calculations is highlighted. In consideration of the investigative parameters, the component model predictions are used to quantify the effects on the stiffness of the component when a variation in f_{cu}, f_{ub}, d_b, and d_{emb} is considered; achieved via the development of component stiffness charts. Additionally, the *EHB* component is classified in terms of ductility according to a classification system that is currently suggested in the literature. And lastly, the proposed component model is employed in an equivalent T-stub (non-prying) model whose predictions are compared with experiments that were obtained in companion studies.

7.1 Equivalent spring model

When fasteners are used to assemble a joint, they are usually pre-loaded so that there is a residual compressive force placed on the joint members. The fastener supplies this force by being stretched from its free-state length during the tightening process. This is comparable to stretching a helical spring. Although the typical fastener may not stretch as much as a spring, it does behave like a spring. Therefore, a helical spring may be used to characterise the tension behaviour of the *EHB* component, however it is necessary to define the most important property of

the spring; its stiffness. It has been demonstrated that three mechanisms (or elements) contribute to the overall deformability curve of the component; namely, bolt elongation, expanding sleeves, and mechanical anchorage. In this section an equivalent spring model is presented to characterise an assembly procedure for these individual mechanisms.

It is proposed to estimate the overall tensile behaviour of the *EHB* component with the use of an equivalent massless spring model, formed as shown in Figure 7.1. Each spring is characterised by a multi-linear force-displacement relationship (see section 7.1.1) and the arrangement of the springs was developed based on observations of the pull-out test results. The model approximates the behaviour of the component by placing the expanding sleeves (k_{HB}) and mechanical anchorage (k_M) mechanisms in a parallel arrangement, while in series with the bolt elongation (k_b) mechanism. The equivalent stiffness of the spring model, k_{EHB} is determined on the foundation of basic spring theory (see section 7.1.2).

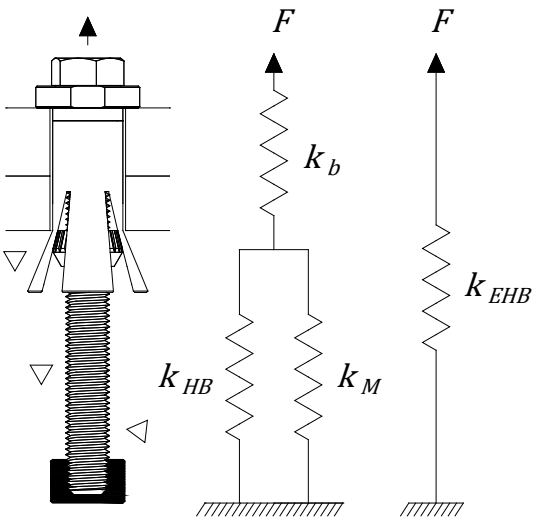

Figure 7.1 Equivalent spring model for component "Bolt (*EHB*) in tension"

7.1.1 Spring characteristics

The pull-out test results have signified that the response of the individual mechanisms that comprise the component "Bolts (*EHB*) in tension" is non-linear. For simplicity, tri and tetra-linear curves are used to approximate the non-linear behaviour of these mechanisms. A semi-empirical, four segment linear tension bolt model is used to model the bolt elongation mechanism, whereas an idealised experimental three segment linear force versus slip is used to model both, the expanding sleeves and mechanical anchorage mechanisms at the unloaded end. The idealised force-bolt elongation model that is proposed to represent the flexibility of the internal bolt of the *EHB* component, k_b is shown in Figure 7.2. The idealised force-slip models for mechanisms k_{HB} and k_M are summarised in Table 7.1 (a) and (b), respectively; determined as illustrated on the notation chart of Figure 7.3. More details relating the development and calculation procedures of these idealised models can be found in Chapter 6. For validation purposes, actual material properties are used in the assembly process, and F^u represents the ultimate capacity of the component which in essence equates with the ultimate experimental pull-out force and strength of the internal bolt.

(a) Grade 8.8

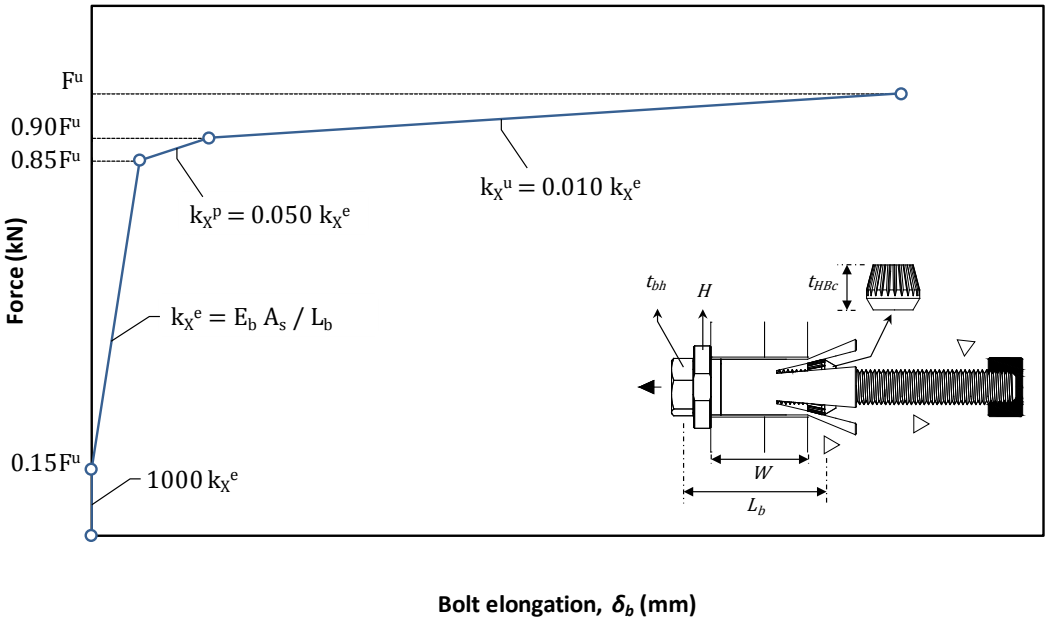

(b) Grade 10.9

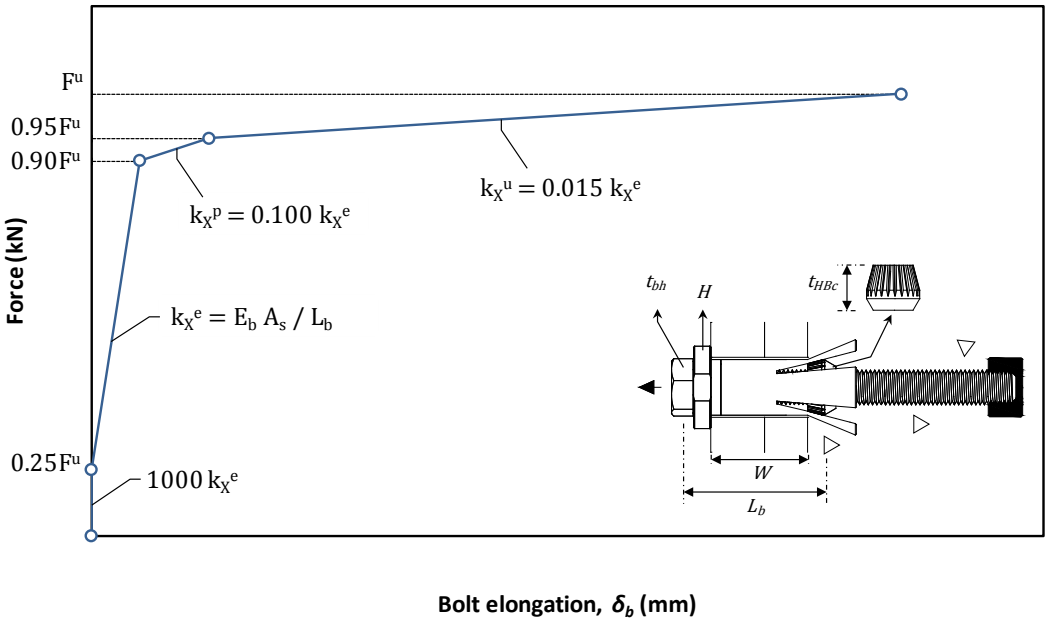

Figure 7.2 Spring characteristics for k_b

Table 7.1 Spring characteristics for k_{HB} & k_M

(a) k_{HB} (stiffness related to expanding sleeves element of *EHB* component)

*Index	$y_1 < F \le y_2$	k_{norm}^{e} (mm^{-1})	$y_2 < F \le y_3$	μ_p	$y_3 < F \le y_4$	μ_u
HB16-8.8-C37	$0 < F \le 0.60\ F^u$	1.091	$0.60\ F^u < F \le 0.90\ F^u$	0.289	$0.90\ F^u < F \le F^u$	0.032
HB16-8.8-C60	$0 < F \le 0.55\ F^u$	3.056	$0.55\ F^u < F \le 0.92\ F^u$	0.175	$0.92\ F^u < F \le F^u$	0.080
HB16-10.9-C37	$0 < F \le 0.55\ F^u$	1.000	$0.55\ F^u < F \le 0.95\ F^u$	0.163	$0.95\ F^u < F \le F^u$	0.018
HB20-8.8-C37	$0 < F \le 0.25\ F^u$	1.114	$0.25\ F^u < F \le 0.68\ F^u$	0.298	$0.68\ F^u < F \le F^u$	0.087

(b) k_M (stiffness related to mechanical anchorage & bond element of *EHB* component)

*Index	$y_1 < F \le y_2$	k_{norm}^{e} (mm^{-1})	$y_2 < F \le y_3$	μ_p	$y_3 < F \le y_4$	μ_u
M16-8.8-C37-5.3d_b	$0 < F \le 0.35\ F^u$	3.889	$0.35\ F^u < F \le 0.90\ F^u$	0.043	$0.90\ F^u < F \le F^u$	0.005
M16-8.8-C60-5.3d_b	$0 < F \le 0.47\ F^u$	18.800	$0.47\ F^u < F \le 0.93\ F^u$	0.065	$0.93\ F^u < F \le F^u$	0.002
M16-10.9-C37-5.3d_b	$0 < F \le 0.55\ F^u$	3.235	$0.55\ F^u < F \le 0.95\ F^u$	0.032	$0.95\ F^u < F \le F^u$	0.003
M20-8.8-C37-4.0d_b	$0 < F \le 0.37\ F^u$	1.682	$0.37\ F^u < F \le 0.90\ F^u$	0.066	$0.90\ F^u < F \le F^u$	0.007
M16-8.8-C37-4.0d_b	$0 < F \le 0.35\ F^u$	3.889	$0.35\ F^u < F \le 0.90\ F^u$	0.043	$0.90\ F^u < F \le F^u$	0.009
M16-8.8-C37-6.5d_b	$0 < F \le 0.35\ F^u$	3.500	$0.35\ F^u < F \le 0.90\ F^u$	0.043	$0.90\ F^u < F \le F^u$	0.014

** C37 & C60 are the minimum characteristic cube strengths for normal strength/weight concrete at 28 days; compressive strength classification to BS EN 206-1:2000.*

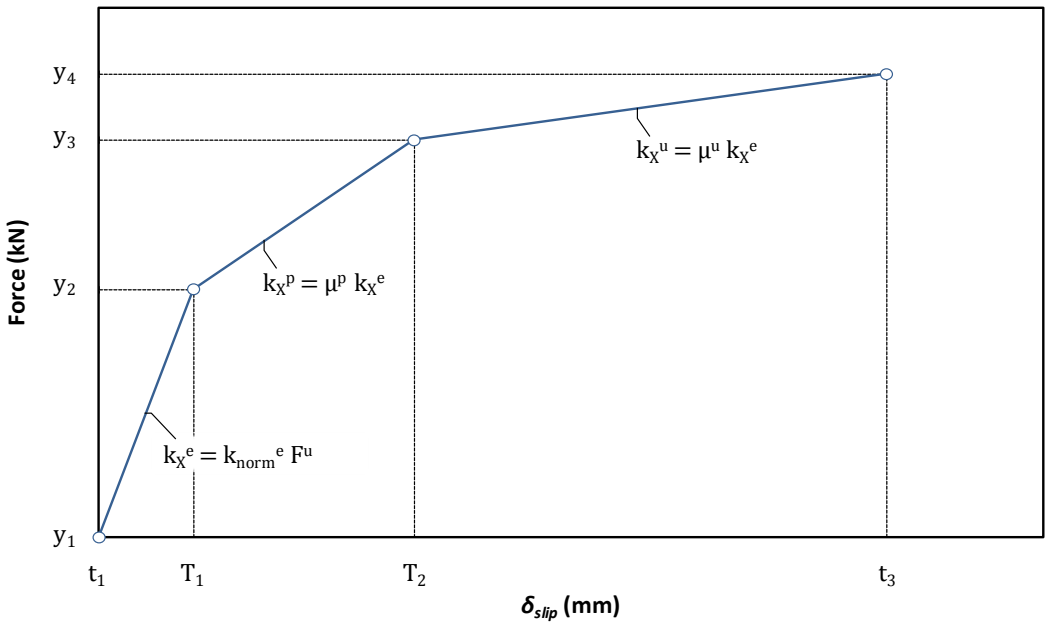

Figure 7.3 Notation chart for k_{HB} & k_M

7.1.2 Assembly

The equivalent *EHB* component spring model involves elements that are connected in parallel and in series. Using basic spring theory, it is possible to determine an effective spring constant, k_{EHB} that represents the assembly process of the individual elements. This process is described as having first to express an effective spring for those in parallel (for k_{HB} and k_M) and then to assemble the combination of the effective parallel spring with that of k_b in series. To illustrate the basic spring formulations, equivalent spring models for parallel and serial configurations are schematically shown in Figure 7.4. When the elements are arranged in parallel configuration, the resulting properties of the assembly can be obtained from the following equations.

$$F_{\mathrm{Rd}} = F_{Rd\,1} + F_{Rd\,2} \qquad \text{Equation 7-1}$$

$$k = k_1 + k_2 \qquad \text{Equation 7-2}$$

$$\delta_{Cd} = \min(\delta_1; \delta_2) \qquad \text{Equation 7-3}$$

For elements in serial configuration, the following formulas apply,

$$F_{\mathrm{Rd}} = \min(F_{Rd\,3}; F_{Rd\,4}) \qquad \text{Equation 7-4}$$

$$k = \left(\frac{1}{k_3} + \frac{1}{k_4}\right)^{-1} \qquad \text{Equation 7-5}$$

$$\delta_{Cd} = \delta_3 + \delta_4 \qquad \text{Equation 7-6}$$

where k is the stiffness and δ_{Cd} is the deformation capacity.

(a) Parallel configuration

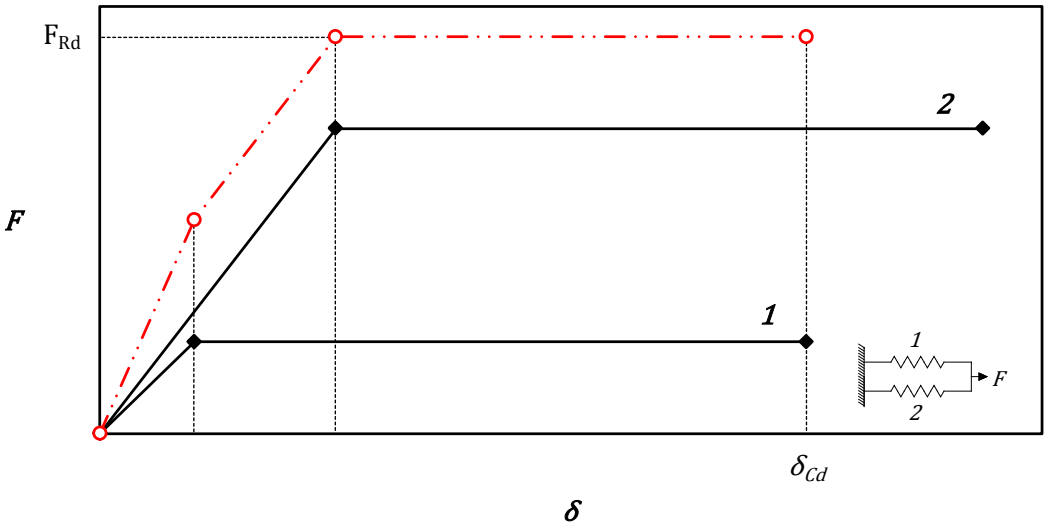

(b) Serial configuration

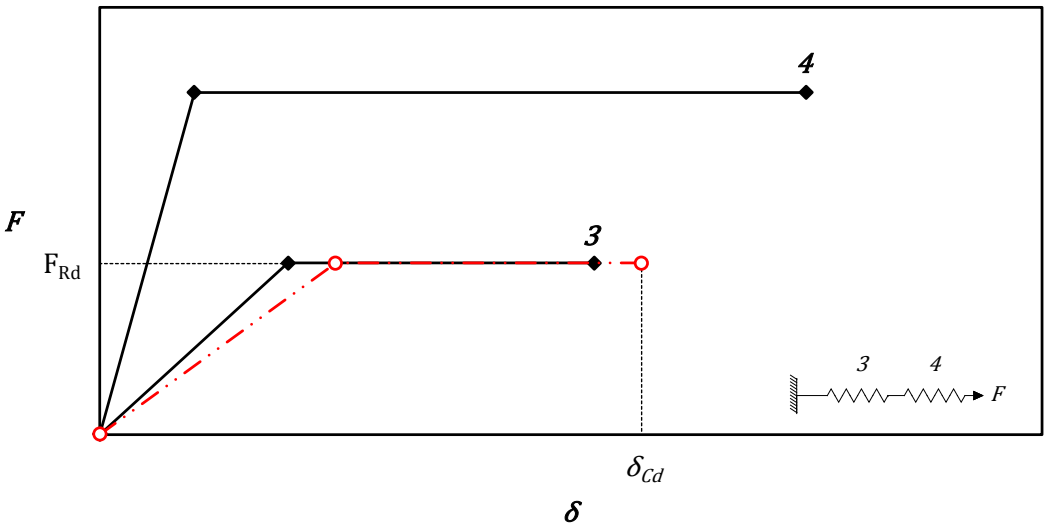

Figure 7.4 Assembly of springs

On the basis of the same principles, by extending the above formulation for springs with tri and tetra-linear characteristics, the equivalent *EHB* component model is calculated accordingly. Regarding the ultimate strength of the component model, F^u, experimental evidence indicated that the ultimate failure mode of the *EHB* component was due to bolt shank fracture. Therefore, F^u should be equal with the ultimate strength of the internal bolt model, and by no means should the component model allow for such force levels to be exceeded. This is achieved by imposing the spring arrangement that is proposed in section 7.1 which involves k_b in a serial configuration. With k_b being positioned in series, it is ensured that the

ultimate (and yield) capacity of the internal bolt is captured in the prediction of the component's *F-δ*$_{global}$ behaviour. This further justifies the arrangement of the equivalent spring model. A theoretical expression that can be used to estimate the ultimate strength of the *EHB* component is outlined in Equation 7-7; with the resistance function representing a steel failure.

$$F^u = f_{ub}\, A_s \qquad \text{Equation 7-7}$$

For demonstration purposes, an assembly of an equivalent *EHB* component spring model is graphed with the characteristics of its individual elements in Figure 7.5; utilising the proposed models on the basis of estimating the *F-δ*$_{global}$ behaviour of the pull-out test specimen with index *EHB16-150-8.8D-C40-2*. This would imply: the use of bolt batch D properties for the bolt model; the selection of suitable models for k_{HB} and k_M in consideration of the parameters stated in the *EHB* specimen index; and the input of the respective ultimate experimental force for F^u.

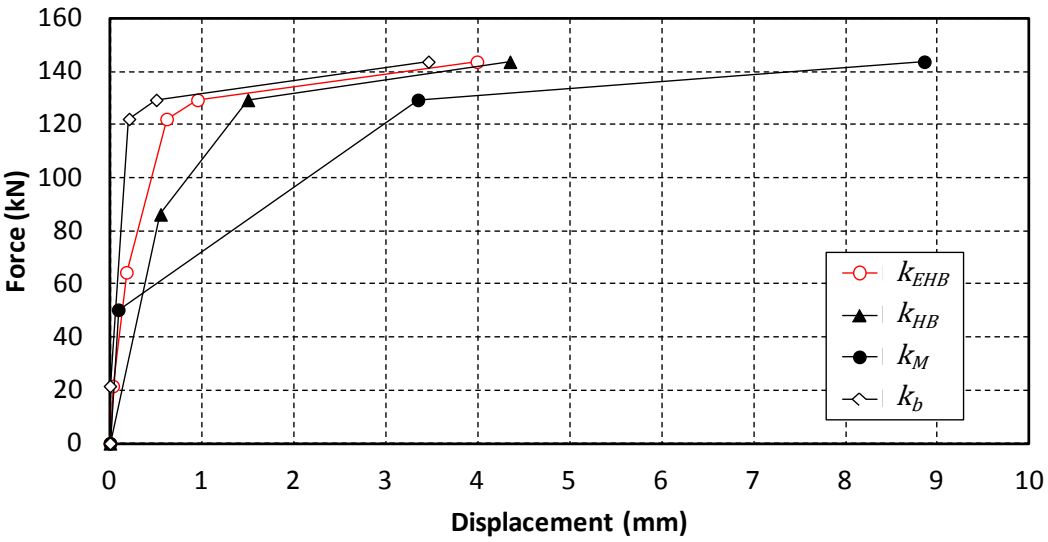

Figure 7.5 Spring characteristics & assembly of *EHB* component spring model

For example, in line with the type *EHB* specimen index, element models for k_{HB} and k_M should involve an internal bolt diameter of 16mm, of grade 8.8, with an embedded depth, d_{emb} of $5.3d_b$ (due to the employment of an internal bolt of total length, *L* of 150mm and a clamping thickness, *W* of 45mm that was used in the test set-up). Moreover, conforming with the concrete strength of the pull-out specimen on its day of testing (see Table 4.6 for type *EHB*), it is identified that a minimum compressive strength class of *C37* is applicable in the selection of k_{HB} and k_M. Therefore, by re-arranging the specimen index in the form of *EHB16-5.3d_b-8.8-C37*, it is clearly recognised that for k_b the suitable model would be that of grade 8.8 while using batch D properties, for k_{HB} the index of the model would equate with *HB16-8.8-C37*, and for k_M the required model index would be *M16-8.8-C37-5.3d_b*. The model behaviour presented in Figure 7.5 was determined on the basis of these indexes and it is shown that the equivalent spring model results in a multi-linear (five piece segment) $F\text{-}\delta_{global}$ relationship by an assembly of its individual elements.

7.2 Comparison of component model with experimental data

Equivalent spring model predictions are compared graphically to experimental force-displacement curves in Figure 7.6 for comparison and validation purposes. The experimental results were taken from tensile pull-out tests that were conducted as part of this work (type *EHB* pull-out testing). The graphs in Figure 7.6 involve predictions with respect to all of the investigative parameters that were involved in this study, as reported by the specimen index on each chart legend.

It is concluded that the estimates of the equivalent spring model compare well with the experimental data. A penta-linear $F\text{-}\delta_{global}$ behaviour is predicted for the component within the range covered by the investigative parameters; capturing with good agreement the initial, post-limit and ultimate stiffness response. The suggested levels of pre-load are found to represent with fair accuracy the initial behaviour of the component for bolts of grade 8.8 and of 10.9. Overall, the model predictions follow the yielding trend of the experimental data with sufficient accuracy.

(a)

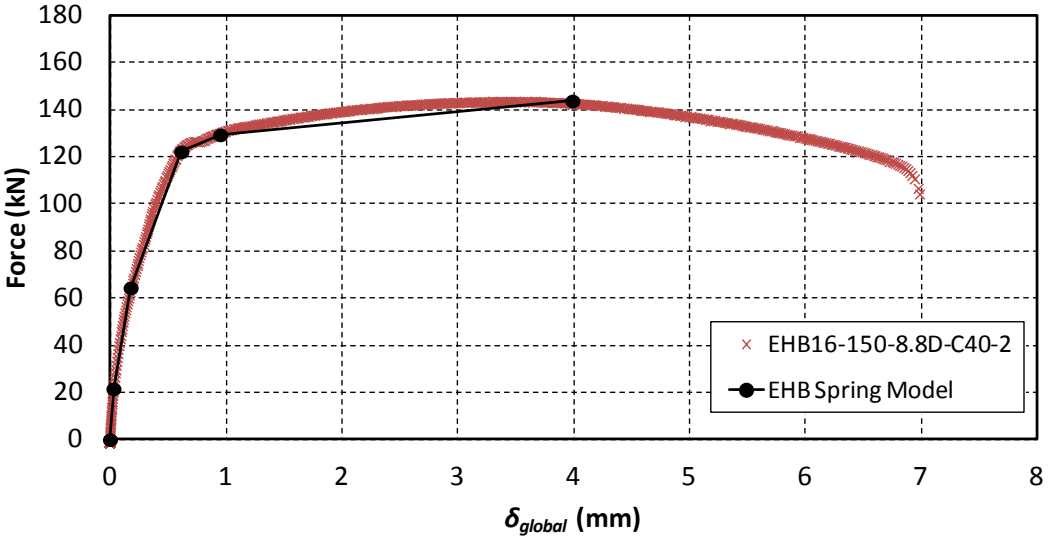
Force (kN)
δ_{global} (mm)
EHB16-150-8.8D-C40-2
EHB Spring Model

(b)

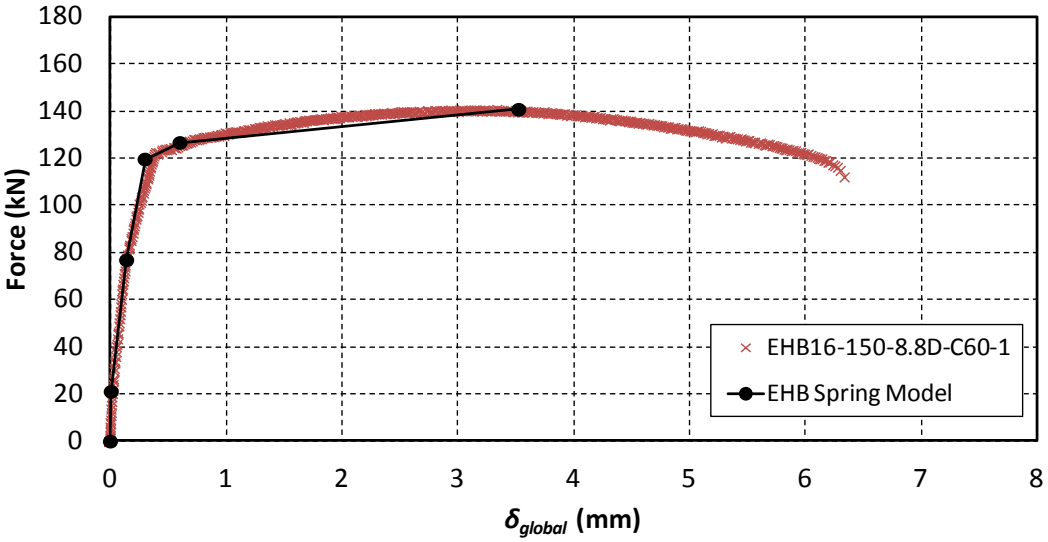
Force (kN)
δ_{global} (mm)
EHB16-150-8.8D-C60-1
EHB Spring Model

(c)

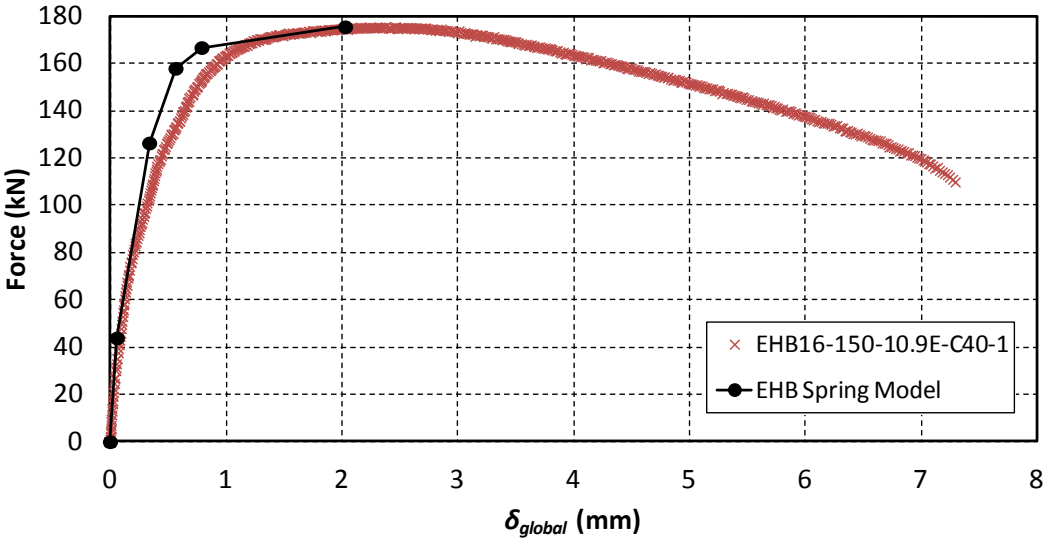
Force (kN)
δ_{global} (mm)
EHB16-150-10.9E-C40-1
EHB Spring Model

(d)

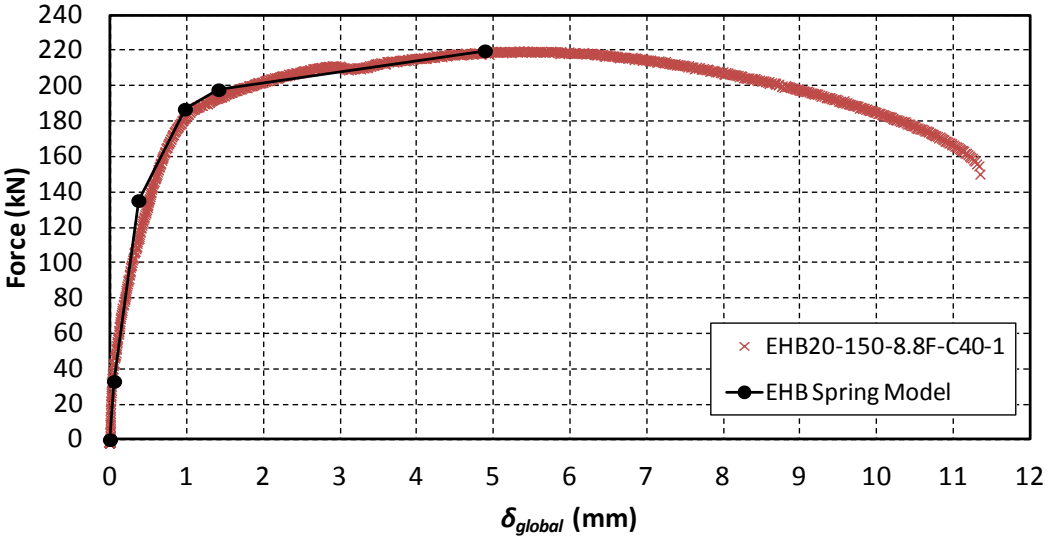

(e)

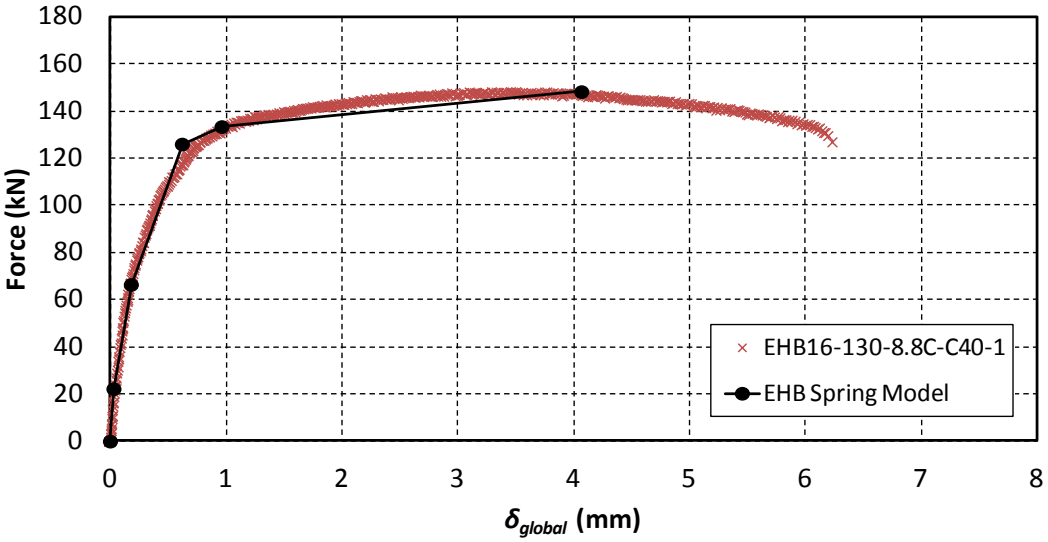

(f)

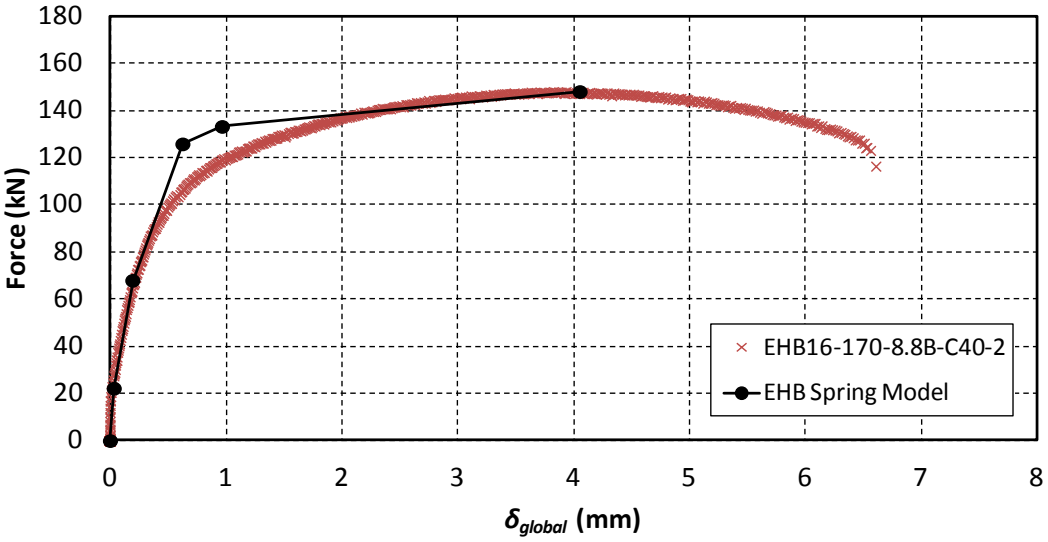

Figure 7.6 Spring model predictions compared with experimental data

Notably, the softening branch of the $F\text{-}\delta_{global}$ relationship is not captured by the component model. This is because such behaviour was intentionally neglected in the modelling process for the component; achieved by excluding the softening material behaviour of the internal bolt within the tension bolt model, k_b. When bolts are subject to direct tension, softening initiates with the onset of bolt necking at ultimate levels. Such behaviour is not required to be captured in the component model because structurally, such behaviour represents catastrophic failure which anyhow should be avoided in the design of bolted joints.

7.2.1 Regression analysis and 95% prediction band

For validation purposes, and to quantify the goodness of fit for the equivalent *EHB* component spring models, regression analysis including the 95% prediction band is performed in Figure 7.7. The analysis runs up to the deformation capacity of the models, with the charts of Figure 7.7 graphing the analysis related to the use of: various bolt batches at benchmark behaviour in charts (a) to (d), a *C60* concrete mix in (e), grade 10.9 bolts in (f), a larger bolt diameter in (g), and the use of varying embedded depths in (h) and (i). Using least squares, R^2 values are reported among the aforementioned charts, with values close to 1 being found; demonstrating a good fit for the component models. But to further the evaluation of the *EHB* spring models, a 95% prediction band is used; also graphed within the same charts, using curve fitting software. The term prediction band refers to the region of uncertainties in predicting the response for a single additional observation at each point within a range of independent variable values. It is computed with respect to a desired confidence level p, whose value is typically chosen to be 95%, and is represented by two curves lying on opposite sides of the fit. In other words, the prediction band shows the scatter of the data. If many more data points were collected, it is expected that 95% will fall within the prediction band (Motulsky et al. 2004). Regarding the $F\text{-}\delta_{global}$ behaviour herein, the prediction band is the interval of force values, for a given global displacement value, within which 95% of all experimental points in a series of repeated measurements are expected to fall. This suggests, the narrower the interval, the better the predictive nature of the model.

(a)

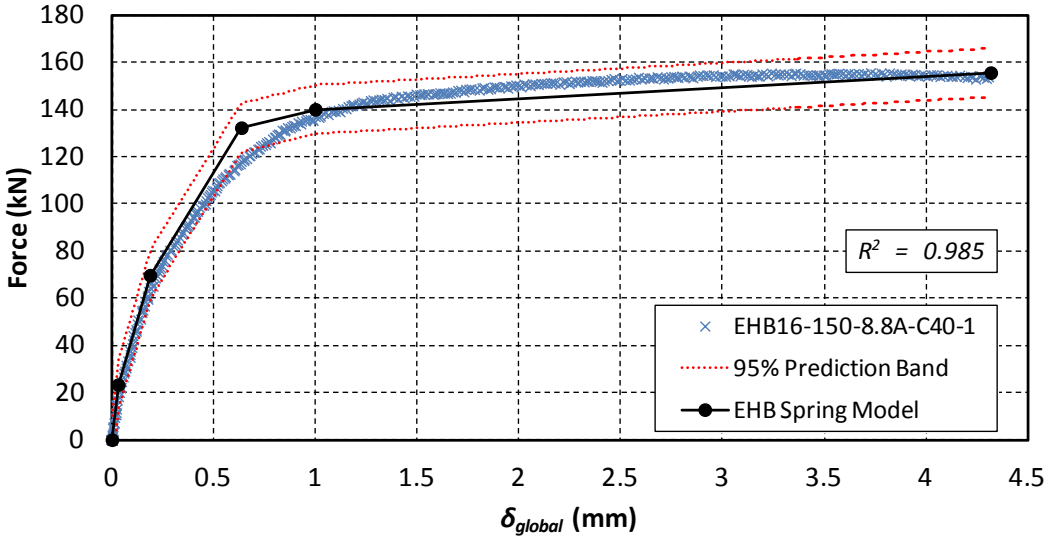
Force (kN)
δ_{global} (mm)
R^2 = 0.985
EHB16-150-8.8A-C40-1
95% Prediction Band
EHB Spring Model

(b)

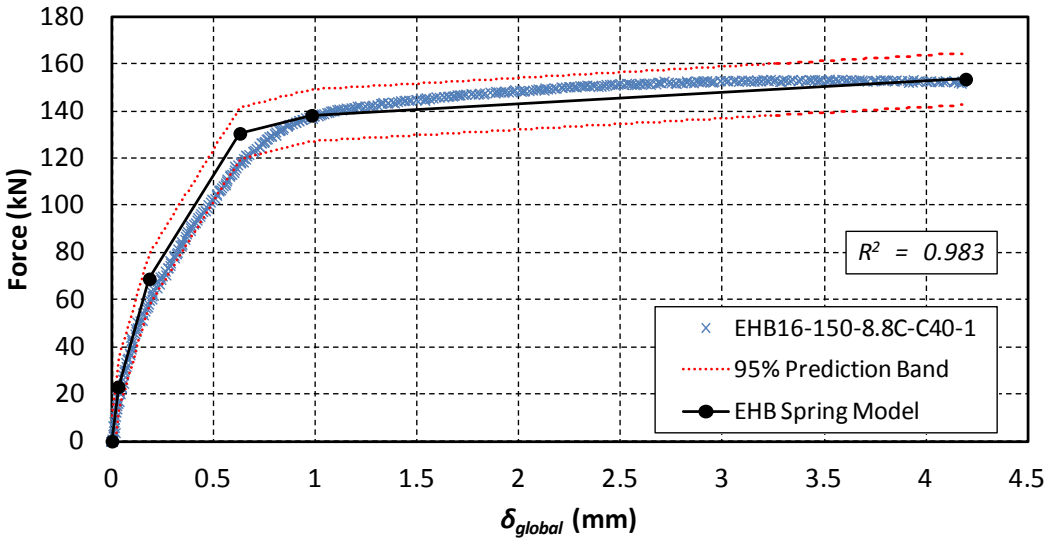
Force (kN)
δ_{global} (mm)
R^2 = 0.983
EHB16-150-8.8C-C40-1
95% Prediction Band
EHB Spring Model

(c)

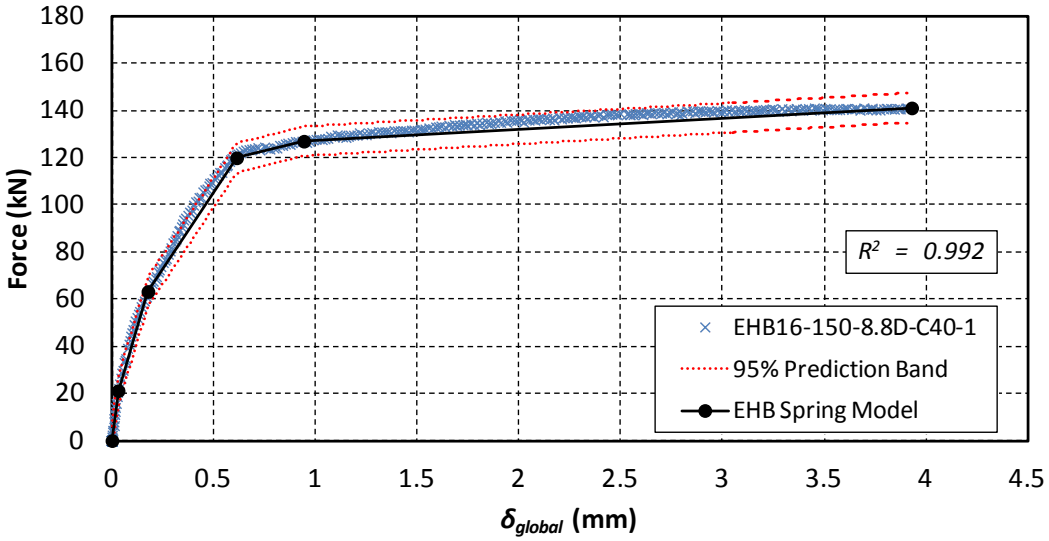
Force (kN)
δ_{global} (mm)
R^2 = 0.992
EHB16-150-8.8D-C40-1
95% Prediction Band
EHB Spring Model

(d)

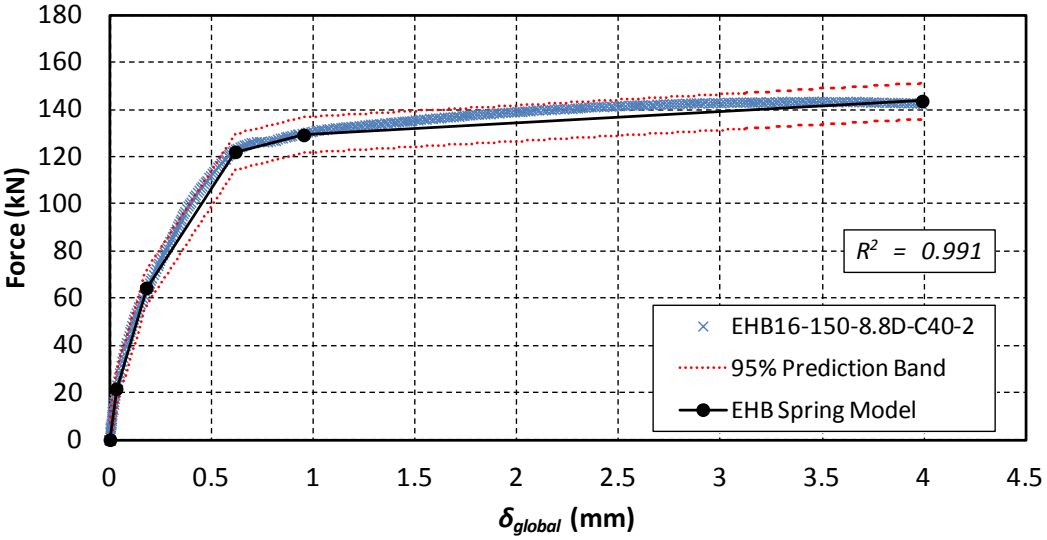
Force (kN)
δ_{global} (mm)
R^2 = 0.991
EHB16-150-8.8D-C40-2
95% Prediction Band
EHB Spring Model

(e)

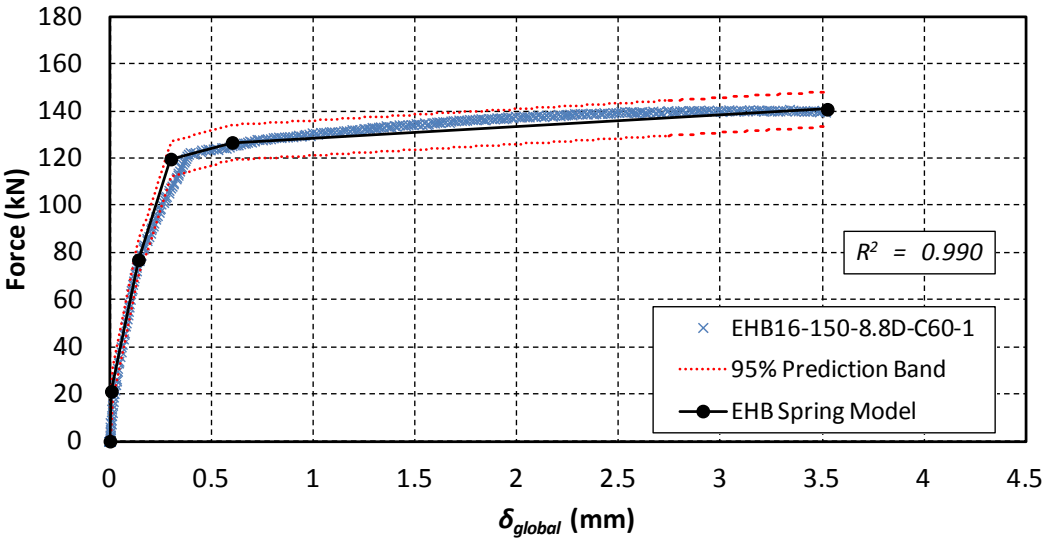
Force (kN)
δ_{global} (mm)
R^2 = 0.990
EHB16-150-8.8D-C60-1
95% Prediction Band
EHB Spring Model

(f)

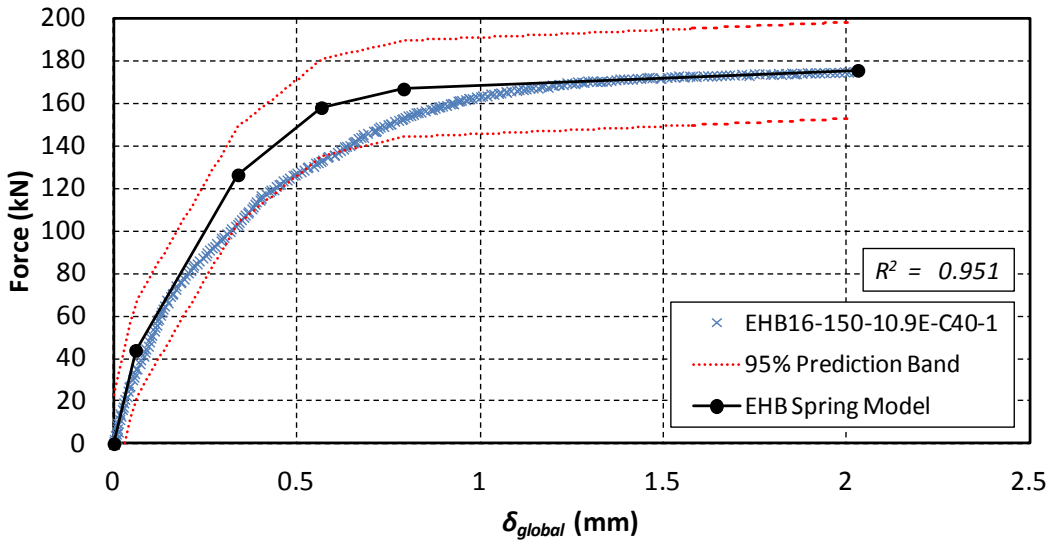
Force (kN)
δ_{global} (mm)
R^2 = 0.951
EHB16-150-10.9E-C40-1
95% Prediction Band
EHB Spring Model

(g)

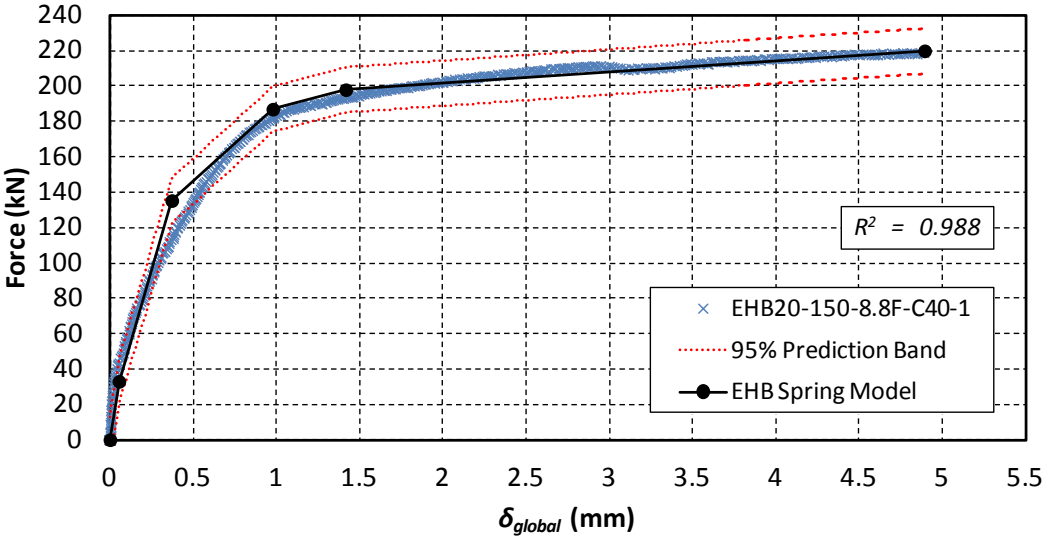

(h)

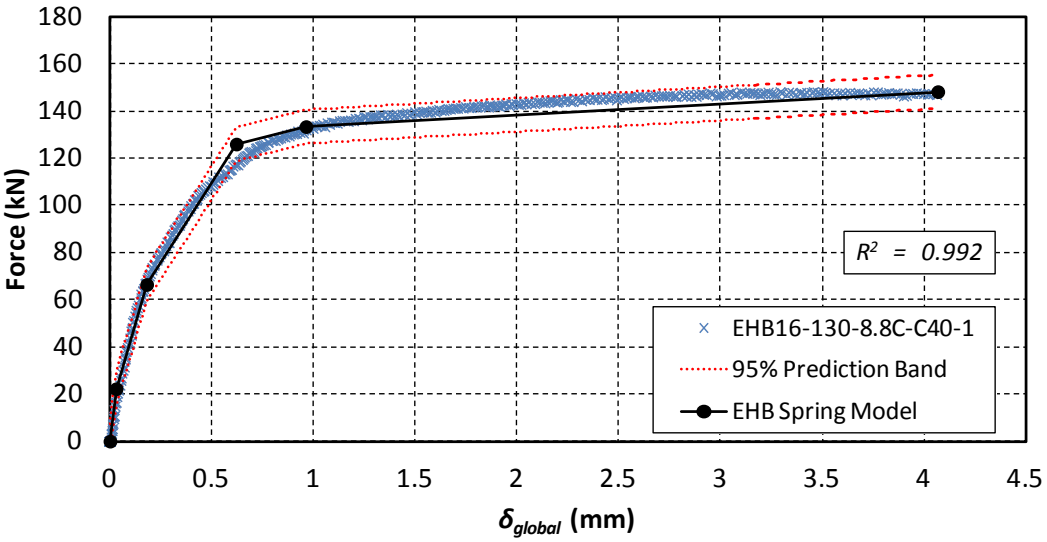

(i)

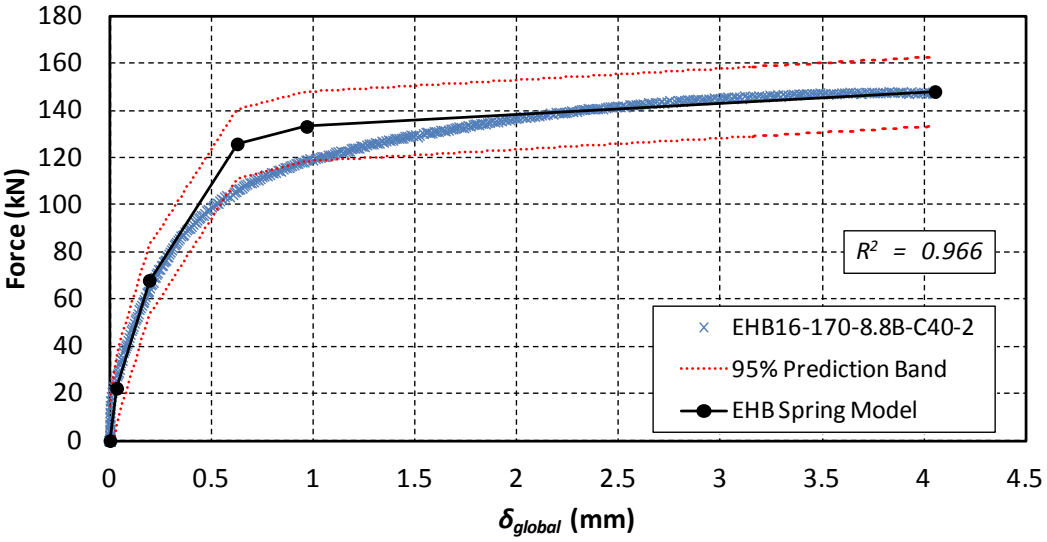

Figure 7.7 Regression analysis & 95% prediction band

It is concluded that at the 95% prediction band level, the *EHB* component model predicts with sufficient accuracy the experimental data in consideration of different bolt batches and varying parameters such as concrete strength, bolt grade, bolt diameter, and embedded depth. The narrowest prediction band is found to be that of which involves benchmark behaviour (chart c), whereas that possessing the widest band is found to be that of which involves bolts of grade 10.9 (chart f).

7.2.2 Effect of excluding pre-load from model calculations

To investigate the effect of excluding pre-load, the equivalent stiffness of the proposed *EHB* spring model (previously shown in Figure 7.1) is determined by modifying the tension bolt model, k_b. The internal bolt model k_b is modified by transforming the tetra-linear model into a tri-linear model, simply exclusive of its first pre-loading segment (Figure 7.8).

(a) Grade 8.8

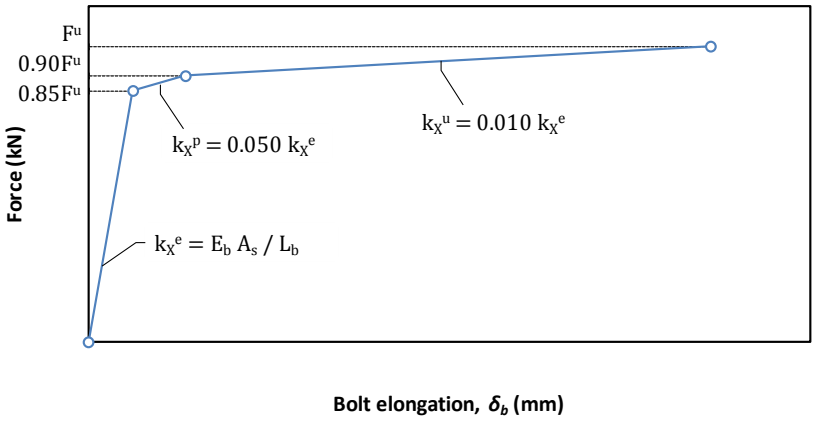

(b) Grade 10.9

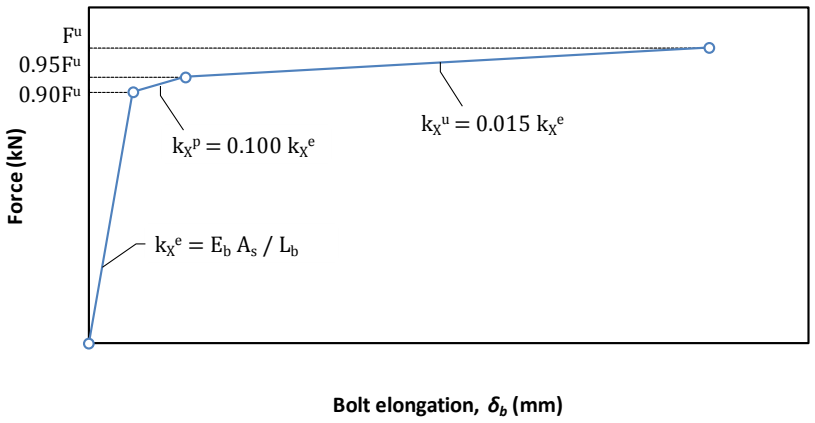

Figure 7.8 Modified internal bolt model (k_b) to investigate effect of excluding pre-load

In Figure 7.9, the predictions of the *EHB* component model, inclusive and exclusive of pre-load effects are graphed with relevant experimental data to emphasize the importance of considering its effect. For both bolt grades, the significance of including pre-load in the assembly of the component model is highlighted in the plots. When pre-load effects are excluded, the initial and post-limit stiffness region of the component is highly underestimated. It is therefore recommended that pre-load is incorporated into the assembly of the proposed component model.

(a) Grade 8.8

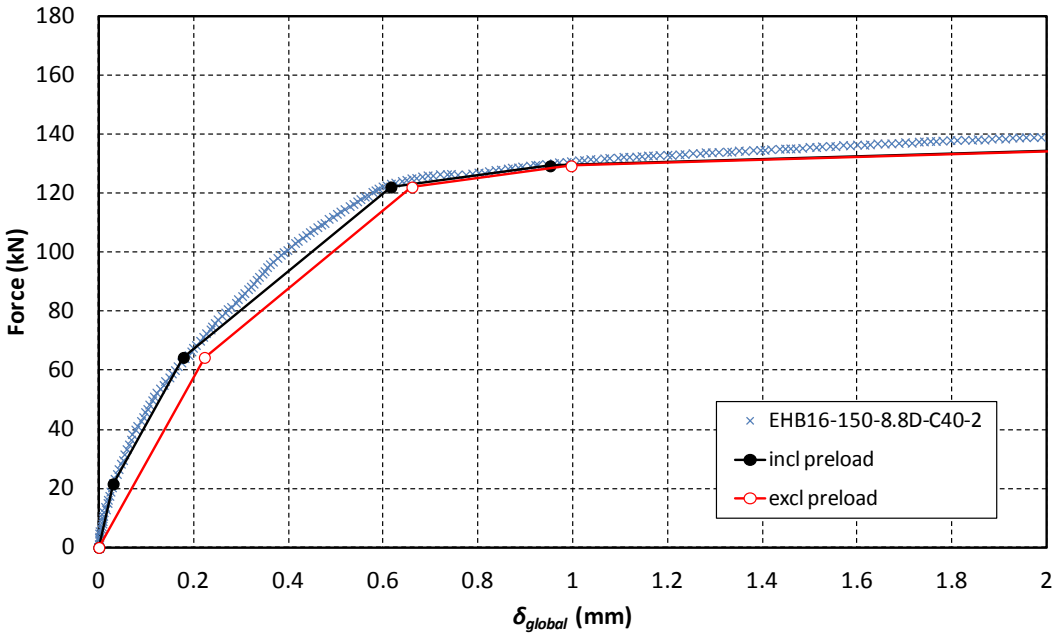

(b) Grade 10.9

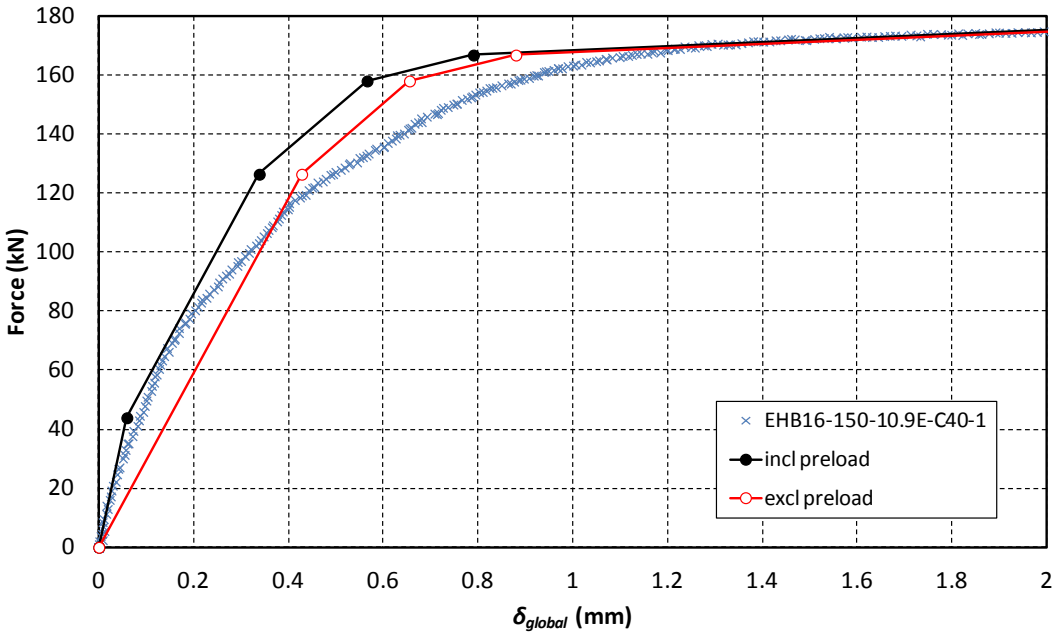

Figure 7.9 Model predictions including/excluding pre-load effects

7.3 Component model stiffness charts

To explore the effects that the investigative parameters have on the stiffness, *k* of the *EHB* component, the predictions of the equivalent *EHB* spring models - which were presented in the previous section - are used and stiffness charts are plotted at selective force steps. The format of the stiffness charts involve stiffness, k on the *y*-axis, and on the *x*-axis of the charts, it is the appropriate variable that represents the variation in parameter that is graphed (e.g. f_{cu} for variation in concrete compressive strength). The stiffness on the *y*-axis, k represents the component stiffness, k_{EHB} which varies along its multi-linear F-δ_{global} response; determined according to correspondent force level. The values along the *x*-axis are calculated based on actual material properties that were involved in the testing of type *EHB*. Mean values are reported with respect to both axis, with the benchmark behaviour in all cases being determined on the basis of the average response of component models for benchmark specimens *EHB16-150-8.8D-C40-1*, *EHB16-150-8.8D-C40-2* and *EHB16-150-8.8D-C40-3*. The feature of the stiffness charts is that they capture the key characteristics in the behaviour of the parametric models with increasing force levels.

7.3.1 Concrete strength, f_{cu}

The effect on the stiffness of the component due to a variation in concrete strength is illustrated in Figure 7.10. The lower bound values for f_{cu} represent benchmark behaviour; for an internal bolt of grade 8.8, with a d_b of 16mm, whose respective stiffness is determined on the basis of average behaviour of component models for benchmark specimens *EHB16-150-8.8D-C40-1*, *EHB16-150-8.8D-C40-2* and *EHB16-150-8.8D-C40-3*. The value of f_{cu} for benchmark behaviour corresponds with the mean cube strength, f_{cu} on the day of testing for the benchmark specimens, whereas the upper bound values for f_{cu} equate with the mean cube strength of the specimens *EHB16-150-8.8D-C60-1* and *EHB16-150-8.8D-C60-2*, also on their day of testing to cover the higher strength range. In Figure 7.10, it is shown that the increase in compressive strength has a significant effect on the stiffness of the component. Enhanced stiffness characteristics are particularly evident within the

initial (*0.15-0.45F^u*) and post-limit (*0.55-0.85F^u*) stiffness region. This suggests that higher concrete infill strength has the ability to increase the component's stiffness from the point at which pre-load force is overcome (at *0.15F^u*).

The stiffness of the component model at benchmark level is consistently lower than that of its higher concrete strength assembly, however, upon yielding of the internal bolt (*0.85-0.90F^u*), it is observed that the overall stiffness within the component is not affected by the variation in concrete strength. At *0.9F^u*, where the internal bolt (of grade 8.8) is now assumed to be plastic, the stiffness of the component is seen to not be affected. It is therefore concluded that, up to the yielding of the component's internal bolt, the strength of the concrete infill is found to significantly affect the stiffness of the component, but upon internal bolt yielding, no further contribution is identified with respect to stiffness. This is explained as the behaviour of the component is entirely dominated by its limiting strength factor; the strength of its internal bolt once it has gone plastic.

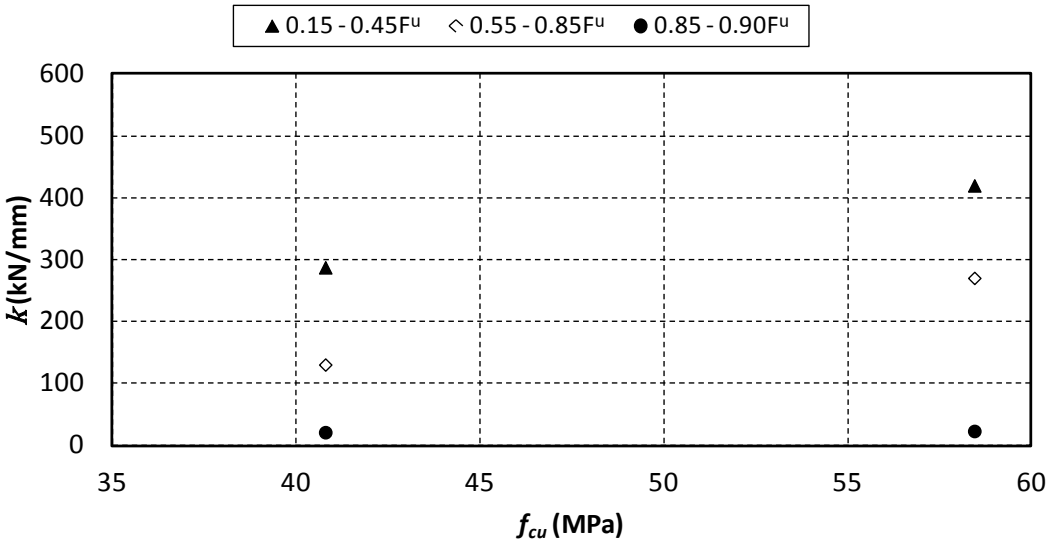

Figure 7.10 Effect of concrete strength on stiffness of *EHB* component

7.3.2 Bolt grade, f_{ub}

The effect on the stiffness of the component due to a variation in bolt grade is illustrated in Figure 7.11. The variation in bolt grade is represented by the change in ultimate bolt strength, f_{ub}, which is higher in the case of grade 10.9 bolts. Thus, the lower bound values for f_{ub} represent benchmark behaviour (of grade 8.8 involving bolt batch D) whereas the upper bound values for f_{ub} equate with type *EHB* of grade 10.9 (involving batch E). The plotted values of f_{ub} were determined by mean results obtained via material property testing (of relevant bolt batches). Mean stiffness values for the upper bound were determined on the basis of model predictions relating to specimens *EHB16-150-10.9E-C40-1* and *EHB16-150-10.9E-C40-2*. The force levels of the stiffness chart in Figure 7.11 were selected in view of capturing stiffness effects when: (a) the benchmark pre-load level is overcome but that of the higher bolt grade component still falls within its pre-loading region ($0.15\text{-}0.25F^u$); (b) approximately 50-75% of relative, ultimate component capacity is reached ($0.45\text{-}0.72F^u$); and (c) when the internal benchmark bolt has gone plastic but that of the higher bolt grade component has just reached its elastic limit ($0.85\text{-}0.90F^u$).

It is noticeable that within the selected force levels, the stiffness of the grade 10.9 *EHB* component is consistently higher with respect to that of the benchmark behaviour. The higher stiffness within the first force level ($0.15\text{-}0.25F^u$) is clearly attributed to the additional pre-load that is induced in grade 10.9 bolts due to a higher tightening input torque. As pre-load is overcome in the benchmark behaviour (at $0.15F^u$), its stiffness thereafter reduces, whereas on the contrary, the grade 10.9 component maintains its initial stiffness up to $0.25F^u$. This certainly results in a knock on stiffness effect regarding the next stiffness regions. Hence the improved initial stiffness characteristics when bolts of higher grade are employed within the *EHB* component. Moreover, with increasing force levels, it is observed that the stiffness characteristics of the component are still improved with increasing f_{ub}; at 50, 75 and 90% of relative ultimate component capacity, F^u. Unsurprisingly, within $0.85\text{-}0.90F^u$, the benchmark stiffness approaches very low values, whereas that of the grade 10.9 exhibits a fairly much higher stiffness;

attributed to the fact that the internal bolt of grade 8.8 is within its elastic-plastic transition stage whereas the grade 10.9 bolts are yet to reach their elastic limit.

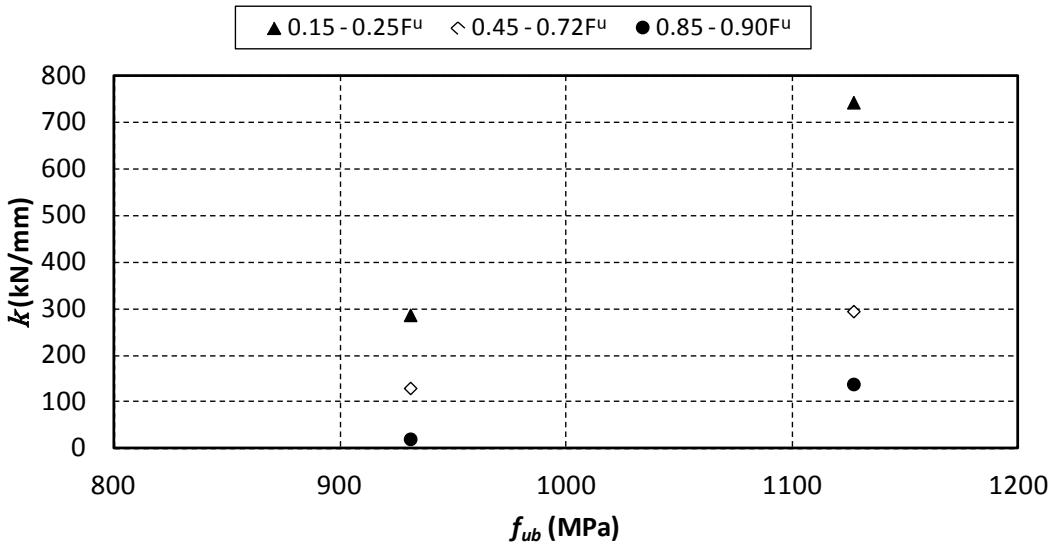

Figure 7.11 Effect of bolt grade on stiffness of *EHB* component

It is therefore concluded that the stiffness characteristics of the *EHB* component improve with increasing f_{ub}; assuming that the upper bound involves a higher tightening input torque. Improvements are seen within the initial, post-limit and ultimate stiffness region of the component when a higher bolt grade is employed within the system.

7.3.3 Bolt diameter, d_b

When a larger bolt diameter size is considered in the *EHB* component, the effect on its stiffness at selective force steps is shown in Figure 7.12; with increasing d_b plotted on the *x*-axis, where the values of d_b are nominal sizes for the internal bolt that is used in the blind-bolt assembly. Mean stiffness values for the upper bound of the chart (at d_b=20mm) were determined on the basis of component model predictions related to specimens *EHB20-150-8.8F-C40-1* and *EHB20-150-8.8F-C40-2*. Because the stiffness chart relates to *EHB* components that are comprised of

internal bolts of grade 8.8 for both diameter sizes, the equivalent force levels relating to the pre-load and elastic limit of their internal bolt are common. Such regions would thus be of primary interest with respect to exploring the effects on the stiffness of the component due to the variation in d_b. Therefore, the stiffness chart involves two force levels regarding the assembly of the component models: (a) *0.15-0.45F*^{u} which equates with the region from which pre-load is overcome up to approximately 45% of the ultimate component capacity; and (b) *0.85-0.90F*^{u} which represents the region in which the internal bolts exceed their elastic limit, but prior to reaching their plastic state. From the stiffness chart it is identified that within the selected equivalent force levels, the stiffness of the component is insignificantly affected by the variation in bolt diameter size. In fact, very similar stiffness characteristics are observed between the two.

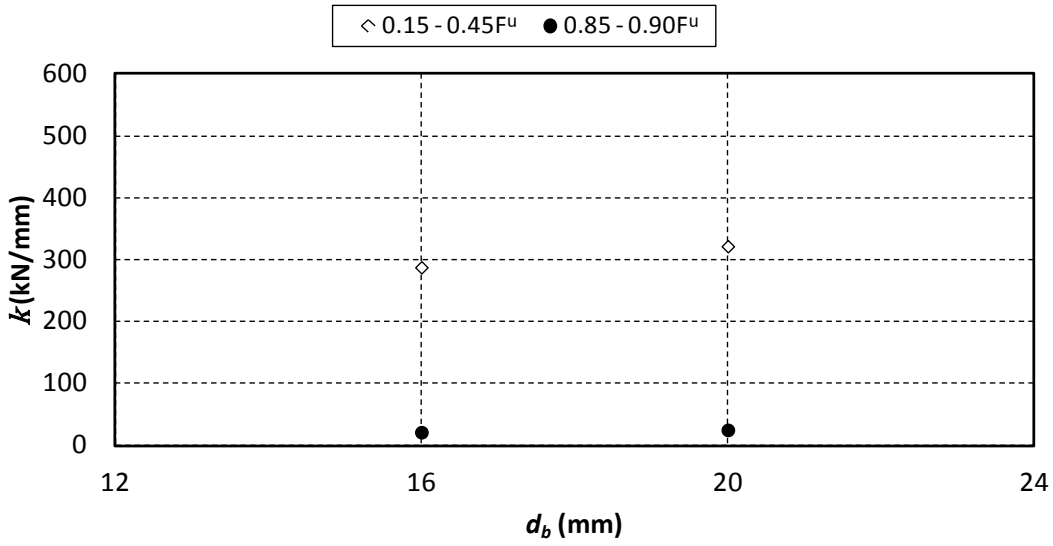

Figure 7.12 Effect of bolt diameter size on stiffness of *EHB* component

7.3.4 Embedded depth, d_{emb}

In consideration of a variation in embedded depth, d_{emb} within the *EHB* component, the effect on its stiffness is shown in Figure 7.13. Mean stiffness values were determined on the basis of model predictions relating to specimens *EHB16-130-8.8C-C40-1* and *EHB16-130-8.8C-C40-2* for the lower bound (at $4.0d_b$), and to specimens *EHB16-170-8.8B-C40-1* and *EHB16-170-8.8B-C40-2* for the upper bound (at $6.5d_b$). The stiffness chart considers force levels from the point at which pre-load is overcome (at $0.15F^u$), up to the point at which the internal bolt has reached its plastic state (at $0.90F^u$). It is concluded that for the investigative range of d_{emb}, the variation does not have any major effect on the initial, or post-limit, or ultimate stiffness region of the component. Such an effect is anticipated due to the minor changes in magnitude of embedded depths among the models.

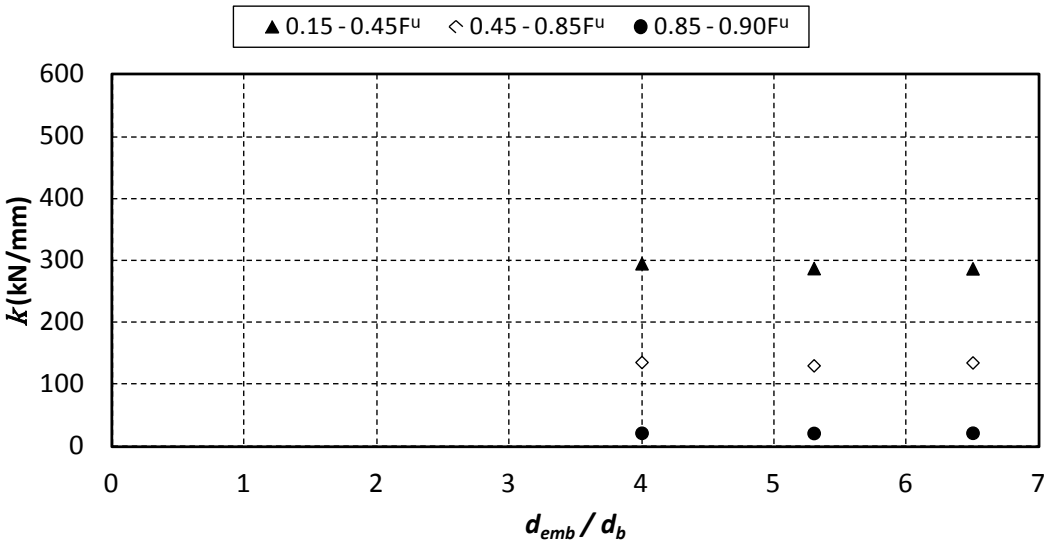

Figure 7.13 Effect of embedded depth on stiffness of *EHB* component

7.4 Component ductility index, λ

It has been stated that the overall behaviour of a structural joint is dictated by the behaviour of it single components. Consequently the rotation capacity of a joint is bound by the deformation capacity of its single components. Therefore, before considering the available rotation capacity of a joint, the available deformation capacity of its components has to be determined. It is the purpose of this section to define and classify the deformation capacity of the *EHB* component with respect to actual (experimental), and equivalent spring model results.

In accordance with Kuhlmann et al. (1998), joint components may be classified into three main groups in terms of their force-displacement behaviour:

- Components with high ductility, Figure 7.14 (a),
- Components with limited ductility, Figure 7.14 (b),
- Components with brittle failure, Figure 7.14 (c).

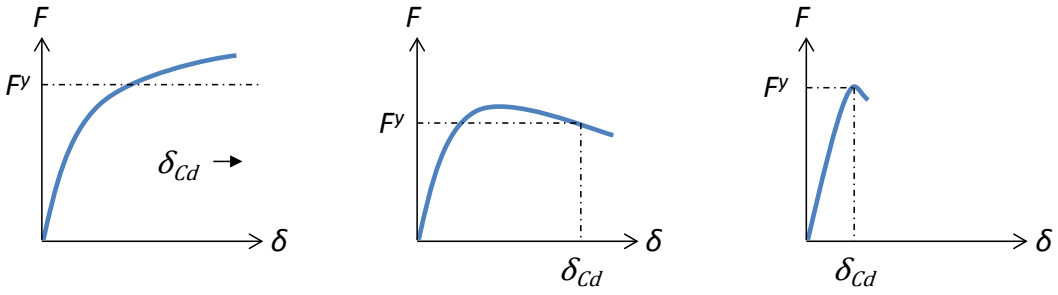

(a) High ductility (b) Limited ductility (c) Brittle failure

Figure 7.14 Ductility classes for joint components

Components with high ductility present a force-deformation curve that changes from an initial carrying mode into a second carrying mode, which allows increasing deformation with increasing force. The deformation capacity of the component is very high or nearly unlimited, not imposing any bounds on the overall rotation ability of the joint. Components with limited ductility are characterised by a force-

deformation curve that exhibits a limit point and a subsequent softening response. In this ductility class, the characteristic available deformation capacity of the component is defined as the deformation (δ_{Cd}) belonging to the point at which the force-deformation curves reach the level of the characteristic force (F^y) again. Brittle failure components behave linearly until failure, allowing very little deformation before their sudden collapse.

Based on the work by Kuhlmann et al. (1998), Da Silva at al. (2002) proposed a component ductility classification system for endplate joint components. The proposed classification system involves: (a) a component ductility index, denoted as λ in this thesis; and (b) ductility limits for each component ductility class that was proposed by Kuhlmann et al. (1998). The component ductility index, λ is determined by the ratio of component collapse to yield displacement; Equation 7-8.

$$\lambda = \frac{\Delta^u}{\Delta^y} \qquad \textbf{Equation 7-8}$$

And the ductility limits suggested by Da Silva et al. (2002) for the three component ductility classes are:

- Class 1: $\lambda \geq 20$, for components with high ductility,
- Class 2: $3 \leq \lambda < 20$, for components with limited ductility,
- Class 3: $\lambda < 3$, for components with brittle failure.

In a qualitative way, the experimental, non-linear, global force-displacement curves of the *EHB* component indicate that the component exhibits limited ductility behaviour; justified by the observation of a limit point and subsequent softening with increasing deformation. But to quantitatively classify the *EHB* component in terms of ductility, in order to calculate its ductility index, λ, it is first necessary to define the component yield (Δ^y) and collapse (Δ^u) displacement.

Regarding Δ^y, it is suggested that it is determined at the force level which equates with the elastic limit of the internal bolt of the component; denoted as F^y and taken

as $0.85F^u$ for grade 8.8, and $0.90F^u$ for grade 10.9 bolts. On the other hand, Δ^u is determined at the point at which the force-displacement softening curve reaches the level of the force F^y again. To schematically demonstrate the aforesaid, typical yield and collapse displacements - that are used in the calculation for the *EHB* ductility index λ - are presented in Figure 7.15 (a) for benchmark behaviour and in Figure 7.15 (b) for *EHB* components with internal bolts of grade 10.9.

(a) Grade 8.8

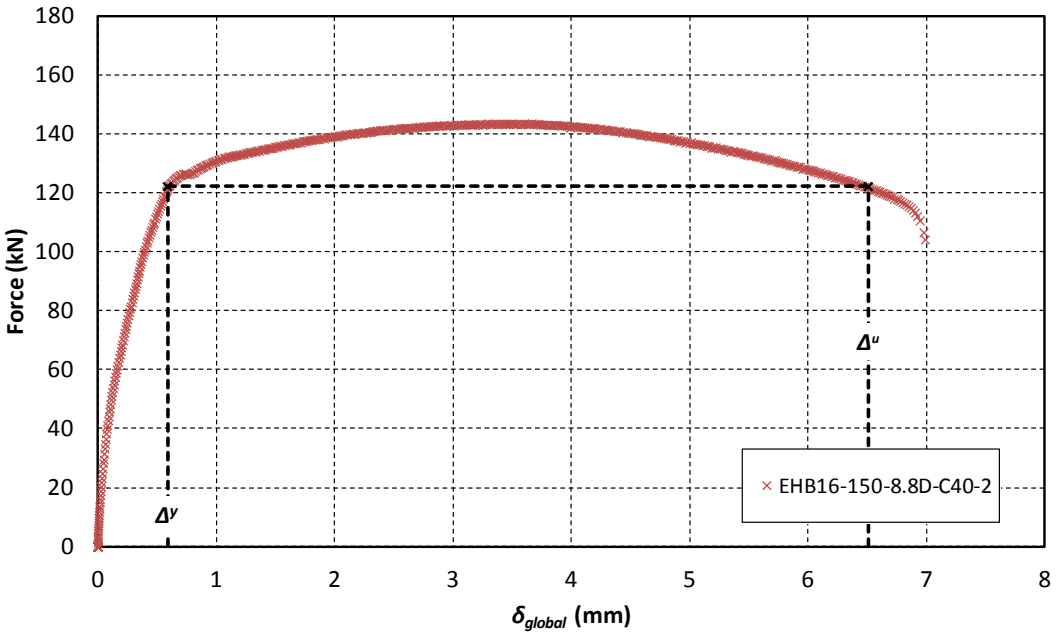

(b) Grade 10.9

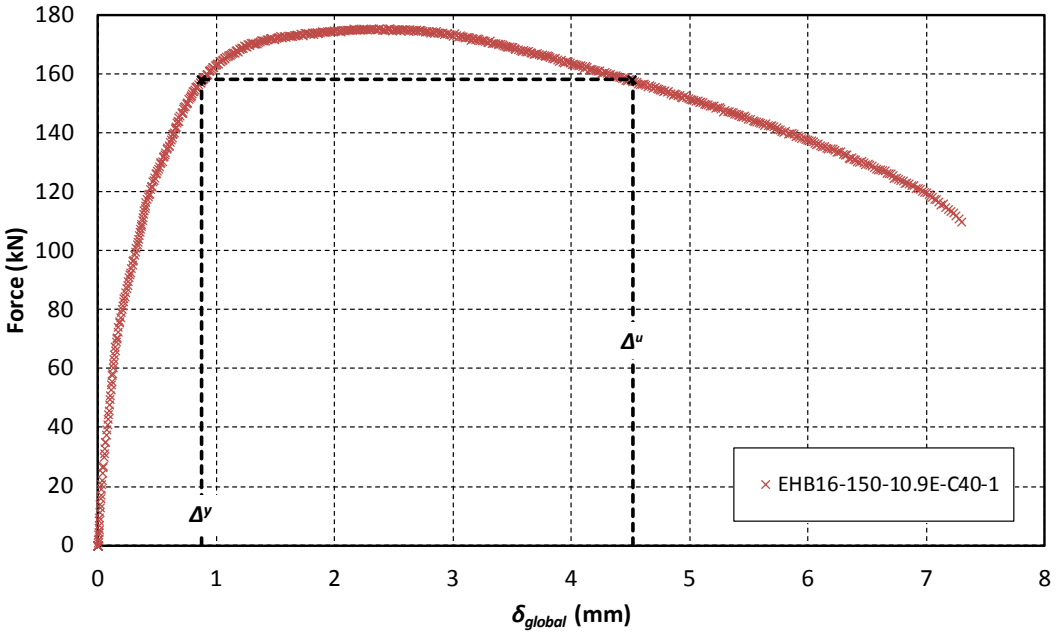

Figure 7.15 Ductility index for *EHB* component (using experimental curve)

7.4.1 Classification using experimental curve

Using the full non-linear experimental F-δ_{global} curve, an evaluation of the ductility indexes for type *EHB* yields the results of Figure 7.16. Based on the ductility classification system suggested by Da Silva at al. (2002) for endplate joint components (detailed in section 7.4), it is found that the *EHB* component can be classified as Class 2: with limited ductility.

The evaluation involves a variation in parameters related to: concrete strength, f_{cu}; internal bolt grade, f_{ub}; internal bolt diameter size, d_b; and varying embedded depths, d_{emb}. The largest index is exhibited by the component which involved a grade *C60* concrete infill, and the lowest ductility index is seen in the case of using grade 10.9 bolts. In consideration of over/under strength effects, the component's benchmark behaviour is investigated by means of using different bolt batches; shown by the first five specimens that are placed on the x-axis. The ductility classification of the component is found to be unaffected among these, demonstrating consistency in the results.

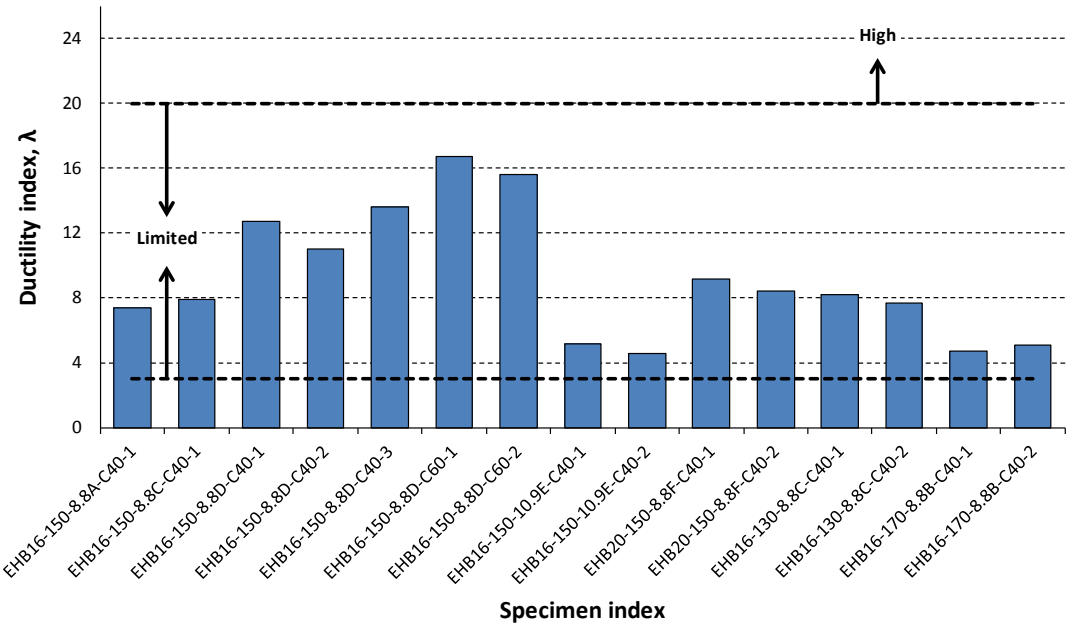

Figure 7.16 Type *EHB*: component ductility classification (using experimental curve)

Overall, for the tested range, the achieved ductility indexes show that the *EHB* component is mostly related to the lower bound of the limited ductility class. Noting, however, that although grade 10.9 bolts have satisfied the limited ductility classification, their ductility index lies very close to the boundary between limited and brittle, indicating brittle behaviour.

7.4.2 Ductility of component model

To compare the ductility index that is predicted by the component model with that which is obtained from the actual experimental curve, herein, two ductility indexes are determined for each type *EHB* pull-out test; denoted as λ_{Model} and λ_{Actual} (see Figure 7.17 for benchmark behaviour). The model index is calculated on the basis of the $F\text{-}\delta_{global}$ assembly of the equivalent *EHB* spring model, and the actual index is determined directly from the experimental $F\text{-}\delta_{global}$ curve. In both cases, regarding the yield displacement (Δ^y), the same definition applies with that outlined in section 7.4, whereas the collapse displacement (Δ^u) is taken as that which corresponds with the ultimate capacity of the component. Because the component model curve does not meet the yield force beyond ultimate strength (as a result of not including material softening behaviour), the ultimate state behaviour has been adopted in order to allow for a reasonable comparison of ductility. Although the model and actual data should not be treated in the same way, nevertheless, the λ_{Model} and λ_{Actual} indexes are determined to investigate the accuracy in the prediction of the component ductility capacity at ultimate state.

Ductility index ratios of λ_{Actual} / λ_{Model} are plotted in the bar chart of Figure 7.18. These dimensionless ratios show that the λ_{Actual} index is consistently lower than the λ_{Model} index. On average, λ_{Actual} is at 75% of the predicted λ_{Model}. It is therefore concluded that, at the ultimate state, the *EHB* component model overestimates the ductility of the component. This is because the component model does not capture precisely the component collapse displacement Δ^u. Additionally, in order to capture the global ductility capacity of the *EHB* component, the component model should include material softening behaviour, essentially within the internal bolt element.

(a) λ_{Model} (using spring model assembly)

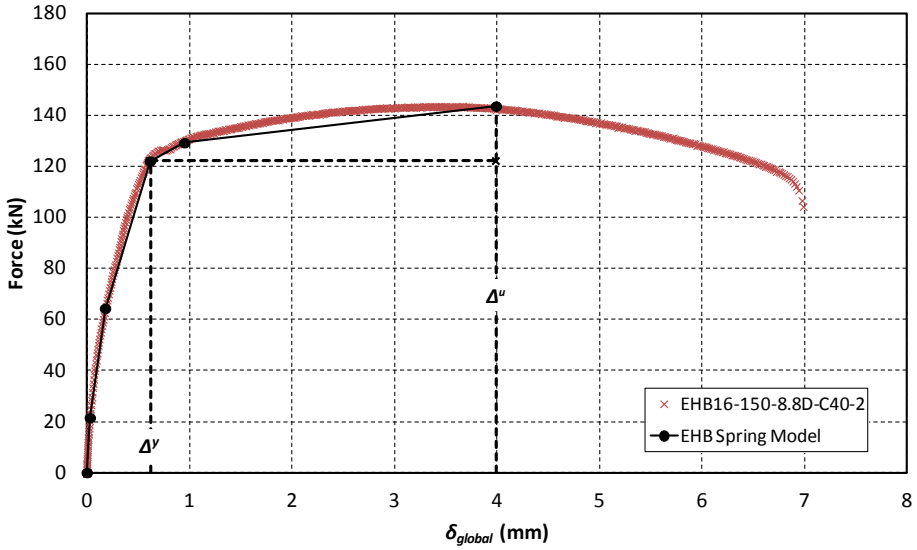

(b) λ_{Actual} (using experimental curve)

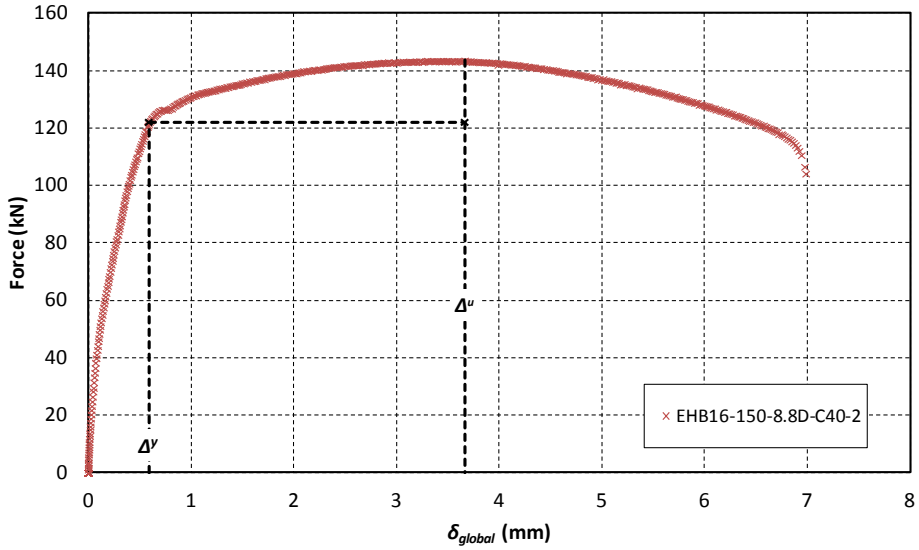

Figure 7.17 Comparison of model & actual index (at ultimate state)

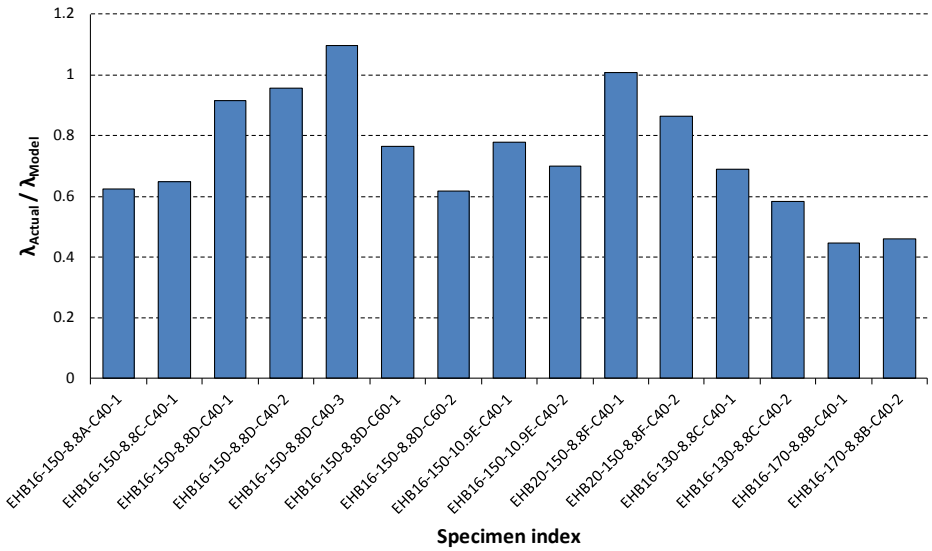

Figure 7.18 Ductility index ratios (λ_{Actual} / λ_{Model})

7.4.3 Ductility index charts

To further evaluate the *EHB* component's actual and model ductility indexes at ultimate state, the previously determined indexes (see section 7.4.2) are presented in the form of ductility index charts here with respect to parameter variations. The format of the ductility index charts involve λ on the *y*-axis (which represents either λ_{Model}, or λ_{Actual}, according to correspondent parameter), and on the *x*-axis of the charts, it is the appropriate variable that represents the variation in parameter that is graphed (e.g. f_{cu} for variation in compressive strength). The values along the *x*-axis are determined based on actual material properties that were involved in the testing of type *EHB*. The charts involve mean values for repeating type *EHB* specimens with respect to both axis, with the benchmark behaviour in all cases being determined on the basis of the average response of benchmark specimens *EHB16-150-8.8D-C40-1*, *EHB16-150-8.8D-C40-2* and *EHB16-150-8.8D-C40-3*. In consideration of the parameters that were investigated in this study, the respective ductility indexes of actual and model predictions are shown in Figure 7.19. Importantly, an overall examination of Figure 7.19 clearly shows that the model indexes follow the trend of the actual, experimental indexes. And for the *EHB* component it is identified that:

(a) an increase in concrete compressive strength results in a higher ductility index, but still falling within the boundary of the limited ductility class, see Figure 7.19 (a);

(b) when a variation in bolt grade of 8.8 to 10.9 is considered, the ductility index of the component reduces with respect to the latter grade, involving a transition from limited ductility towards brittle behaviour, see Figure 7.19 (b);

(c) an increase in bolt diameter size results in a lower ductility index, but still falling within the boundary of the limited ductility class, see Figure 7.19 (c); and

(d) for the investigative range of embedded depths, the ductility index of the component is unaffected by the variation in d_{emb} (according to the model results). Although some discrepancy is seen between model and actual indexes, the ductility of the component still falls within the limited class, see Figure 7.19 (d);

(a)

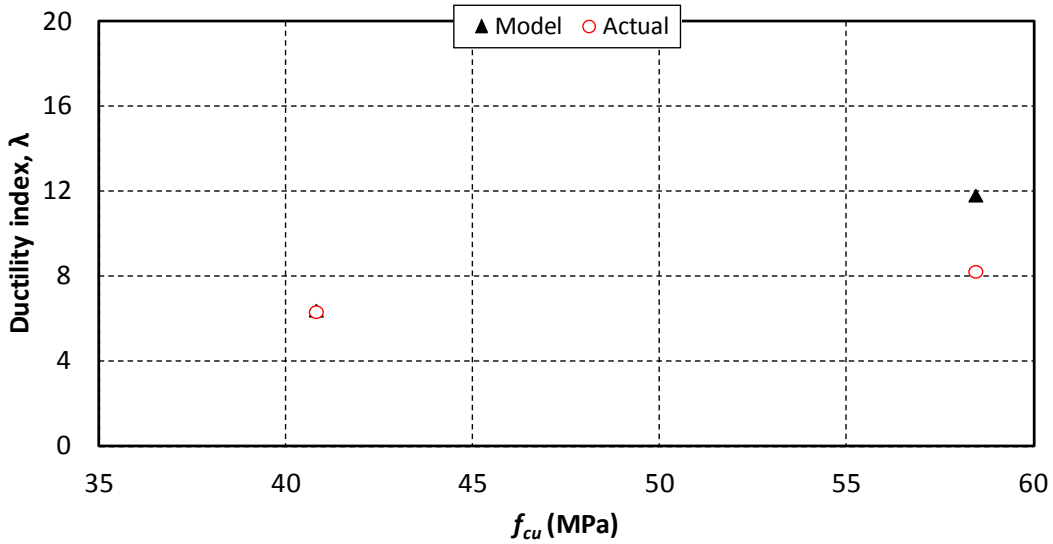
Model
Actual
Ductility index, λ
20
16
12
8
4
0
35
40
45
50
55
60
f_{cu} (MPa)

(b)

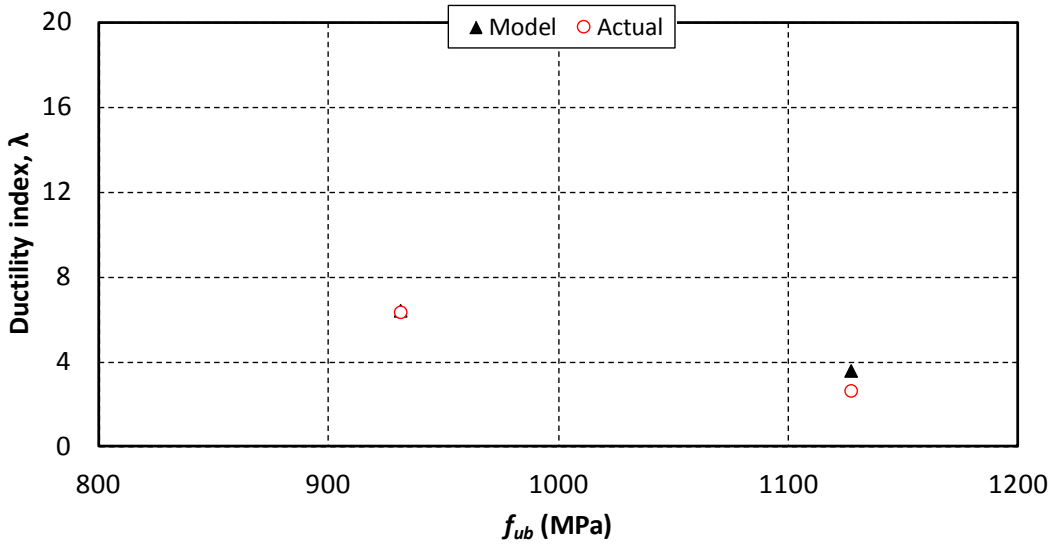
Model
Actual
Ductility index, λ
20
16
12
8
4
0
800
900
1000
1100
1200
f_{ub} (MPa)

(c)

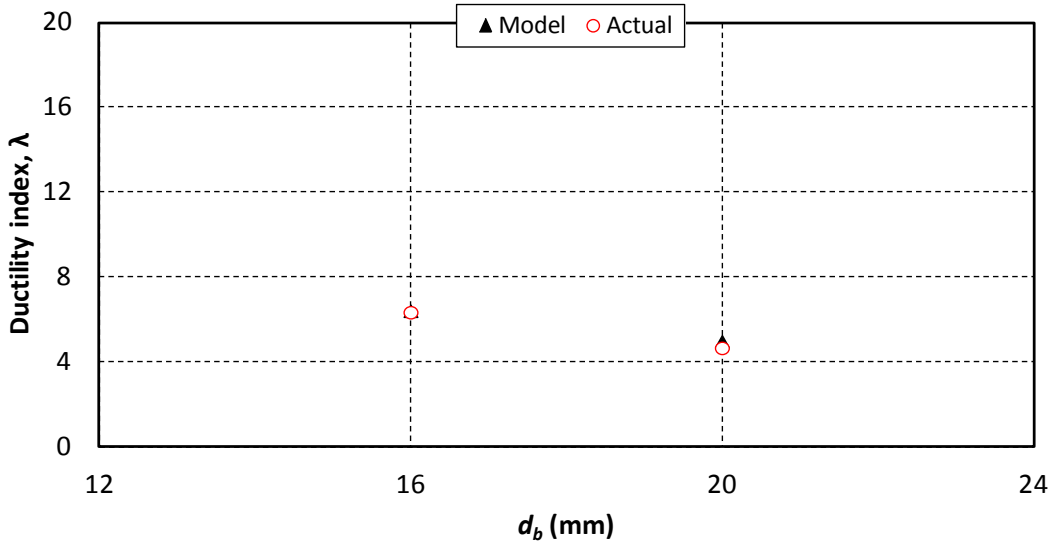
Model
Actual
Ductility index, λ
20
16
12
8
4
0
12
16
20
24
d_b (mm)

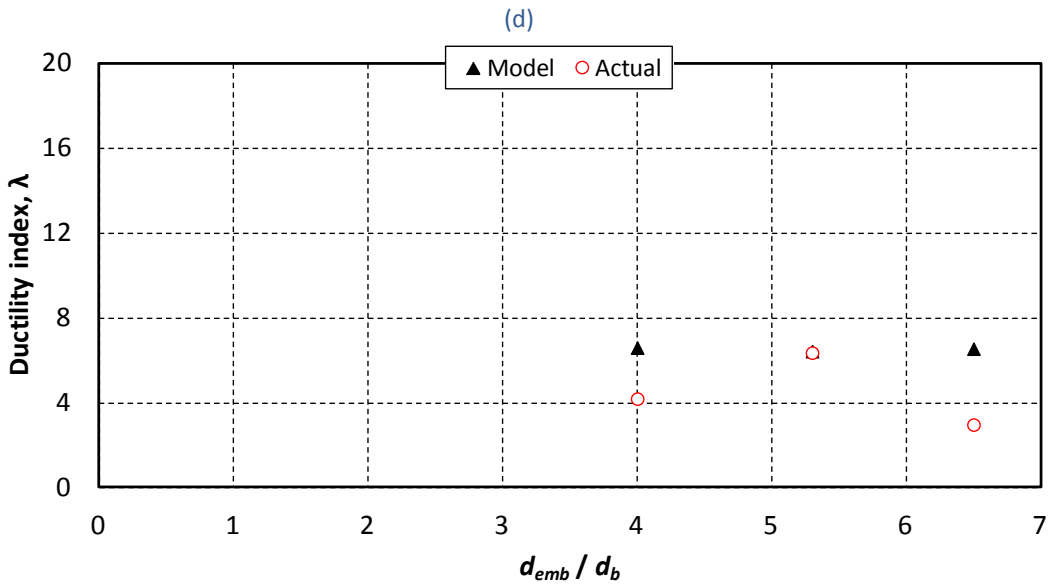

Figure 7.19 Ductility index of *EHB* component at ultimate state (with varying parameters)

7.5 Equivalent T-stub model in tension

To assess the proposed multi-linear *EHB* component model (that has effective stiffness k_{EHB}), its application is considered with reference to the T-stub model. On the basis of an assembly of its individual elements, an assembly procedure is suggested for the evaluation of a T-stub model using *EHB* fasteners. Experimental data from companion studies are used to evaluate and assess the predictions.

7.5.1 Companion experimental programme

The experimental data that relates to the following sections of this thesis have been obtained from companion studies that are reported in Ellison et al. (2004) and Pitrakkos (2008). The test setup that was adopted in the studies is first introduced, and relevant geometry and material properties are outlined. The aim is to demonstrate the manner in which the experimental data was obtained by the authors and to illustrate the suitability of the data with respect to the evaluation of the proposed *EHB* component model.

The setup that was used in the experimental programme is shown in Figure 7.20; replicating the tension region of a moment-resisting joint. It involved 50mm thick T-stubs that were connected, on opposite faces of a concrete-filled SHS 200x200x10,

by an overall of eight *EHB* blind-bolts, under a tightening torque of 190Nm. The tensile tests were performed in displacement control and the average separation of the T-stub from the face of the SHS was measured by linear potentiometers; which were fixed on the T-stubs, in line with the blind-bolts, measuring displacement relative to a target that was located mid depth of the SHS. The selected tests and corresponding specimen details are summarised in Table 7.2 and Table 7.3. These tests relate to the benchmark behaviour of the *EHB* component model; employing internal bolts of 16mm, grade 8.8, satisfying a minimum f_{cu} of 37MPa on test day.

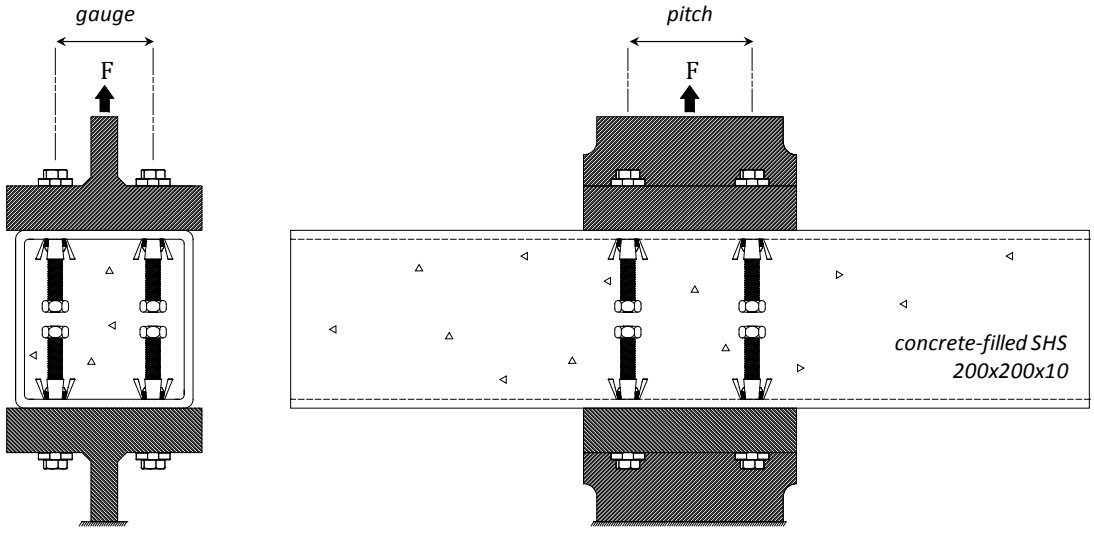

(a) cross section (b) side elevation

Figure 7.20 Opposite T-stub to SHS testing using *EHB* blind-bolts

Table 7.2 T-stub test specimens

Specimen index *	d_b (mm)	Shank length, L (mm)	Bolt grade / Batch	f_{cu} (MPa)	$F_{test,\,max}$ (kN)
EHB16-150-8.8H-C37-G120P100	16	150	8.8 / H	53.0	624.5
EHB16-150-8.8I-C37-G120P140	16	150	8.8 / I	46.5	555.8
EHB16-150-8.8I-C37-G120P100	16	150	8.8 / I	43.5	543.4

* ①-②-③-④-⑤ : ① *type of fastener (EHB) & bolt shank diameter,* d_b *;*
② *bolt shank length, L ;* ③ *bolt shank grade & designation of bolt batch (H or I) ;*
④ *grade of concrete infill (min classification based on cube strength,* f_{cu} *on day of testing) ;*
⑤ *G: bolt gauge, P: bolt pitch (determined as shown in Figure 7.20) ;*
Notes: 1. All EHB fasteners are of "size 3", as in Lindapter brochure datasheet; W=60mm;
2. Refer to Table 7.3 for mechanical properties of relevant bolt batches.

Table 7.3 T-stub test *EHB* internal bolt properties

Bolt Batch	d_b (mm)	*Bolt grade*	f_{ub} (MPa)	*E* (GPa)
H	16	8.8	955	205*
I	16	8.8	909	194

f_{ub} is the ultimate strength; E is Young's Modulus of Elasticity;
** Value was not available thus reporting assumed value.*

7.5.2 Spring model using k_{EHB} & assembly procedure

The arrangement of the equivalent spring model that is proposed to estimate the tension force-displacement behaviour of the opposite T-stub to SHS setup is presented in Figure 7.21 (a). The spring model is comprised of four springs that are positioned in a parallel configuration, where each spring is characterised by a multi-linear force-displacement response, denoted with a stiffness of k_{EHB} that is based on an assembly of their common, individual elements (i.e. k_b, k_{HB}, k_M).

The assumptions that assisted towards the development of the simplified T-stub model are outlined as follows. First of all, due to the very thick T-stub (50mm flange) that was employed in the testing that was described in section 7.5.1, it is valid to assume that prying effects can be neglected. In addition, due to the thickness of 10mm for the SHS that was used in the testing, it is sufficient to assume that the yielding of the face of the hollow section can be neglected. This latter assumption is further supported by the ultimate failure mode that was observed experimentally with respect to the selected tests, which involved bolt fracture and negligible deformations with respect to the connected and lateral faces of the hollow sections. Consequently, on the basis of these assumptions, it is implied that the modelling procedure relating to the tension T-stub configuration can be determined in accordance with the classic Mode 3, equivalent T-stub in tension model that is detailed in Eurocode 3, Part 1-8 (CEN 2005). The primary feature of Mode 3 is that the ultimate resistance of the T-stub model, F_{Rd}, is purely dependent upon the strength of its connecting fasteners; meaning that F_{Rd} is determined by the summation of the ultimate capacity of the connecting bolts, with infinite stiffness contributions from the T-stub flange element. To determine the strength (or ultimate resistance) of the T-stub model, it is also therefore necessary to

assume that force is evenly distributed among connecting bolts. With respect to the modelling process here, this means that: applied tension force should be assumed to distribute evenly among the four blind-bolts that are located on the top face of the section, as an equal and opposite reaction is resisted by the blind-bolts at the bottom face. For notation purposes, if $F_{test,max}$ is the ultimate force that was reached in the opposite T-stub to SHS testing, and F^u is the ultimate capacity of the *EHB* blind-bolt component in tension, by assuming an even distribution of force, then $F^u=F_{test,max}/4$. This leads to the notation charts of Figure 7.21 (b) and (c) which qualitatively show the characteristics of the *EHB* component spring, k_{EHB} and the resulting equivalent T-stub characteristic upon an assembly of four k_{EHB} springs in parallel. With the springs arranged in a parallel configuration, the assembly of the equivalent T-stub spring model is determined from the following equations.

$$F_{\mathrm{Rd}} = F_{Rd\,1} + F_{Rd\,2} + F_{Rd\,3} + F_{Rd\,4} = 4F^u \qquad \text{Equation 7-9}$$

$$k = k_1 + k_2 + k_3 + k_4 = 4k_{EHB} \qquad \text{Equation 7-10}$$

$$\delta_{Cd} = \Delta^u \qquad \text{Equation 7-11}$$

In brief, the solution of the T-stub model herein involves:

- A back calculation for F^u (determined by $F_{test,max}/4$),
- The selection of suitable models for k_b, k_{HB}, and k_M in line with the geometry and material properties of the connection; employing F^u to derive k_{EHB}, and
- The assembly of the equivalent T-stub model that is represented by the arrangement of springs in a parallel configuration (with k_{EHB} characteristics).

(a) Equivalent spring model

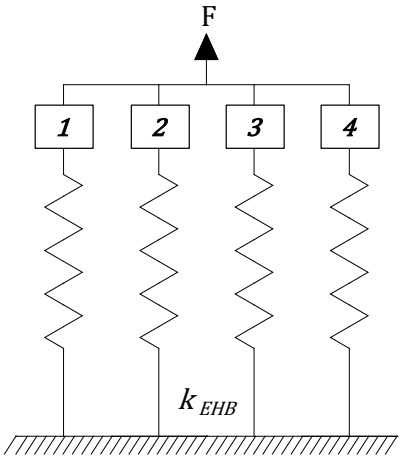

(b) Spring characteristics (k_{EHB})

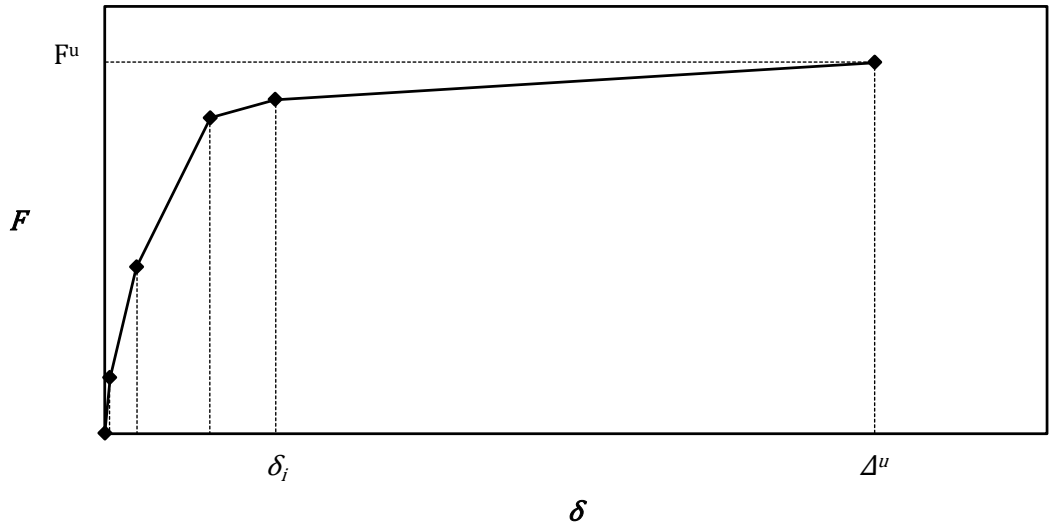

(c) Assembly

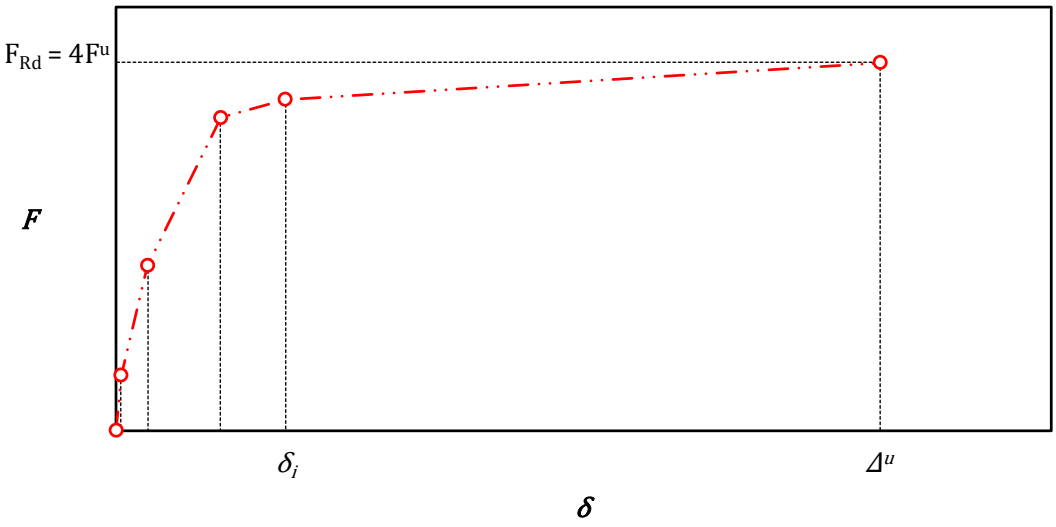

Figure 7.21 Equivalent T-stub model in tension using k_{EHB}

Regarding the assembly of k_{EHB} in line with the geometry and properties involved in the companion T-stub testing, supplementary commentary is included as follows. It was mentioned that the selected T-stub tests relate to benchmark behaviour of the *EHB* component. Therefore, with reference to section 7.1.1, the element model for k_b is selected for internal bolts of grade 8.8, and element models for k_{HB} and k_M are chosen with the index of *HB16-8.8-C37* and *M16-8.8-C37-5.3*d_b for the expanding sleeves, and mechanical anchorage elements, respectively. The input of F^u for these elements is determined on the foundation of $F_{test,max}$ achieved in the T-stub tests. The bolt elongation element model (k_b) is modified accordingly with regard to the calculations for its elastic stiffness, k_x^e by; (a) incorporating actual material values for E in accordance with those reported by the companion studies (as summarised in Table 7.3), and (b) by calculating the effective length, L_b according to the actual clamping thickness that was involved in the T-stub testing (where W = 60mm). Moreover, with respect to the embedded depth, d_{emb} of the T-stub specimens, its value is determined at 4.3d_b. For the sake of the analysis here, benchmark models which involve 5.3d_b are employed for k_M; noting that data analysis of type *M* demonstrated insignificant effects for the d_{emb} range of 4.0-6.5d_b.

7.5.3 Comparison of model with experimental data

The equivalent T-stub spring model predictions are compared with experimental data in Figure 7.22, including the reporting of corresponding R^2 values to quantify the goodness of fit. The experimental curves relate to the average separation of the T-stub from the face of SHS, with that in chart (a) obtained from Ellison et al. (2004) and those in charts (b) and (c) from Pitrakkos (2008).

With respect to this data comparison, it is identified that the tension T-stub model (using k_{EHB}) is able to predict, with sufficient accuracy, the pre-load (initial) and secant stiffness region, including the deformation capacity of the connection. The model also captures the respective force levels at which overall stiffness reductions occur, however, it tends to overestimate the yield displacement. This can be attributed to a number of reasons.

Firstly, it is mostly anticipated that the flexibility of the hollow section face - which is not included in the equivalent T-sub model here - can justify the discrepancy beyond the early stages of loading. Although the connecting faces of the tested tubes did not show significant deformation after failure, neglecting the elastic bending of this element can influence the predicted behaviour of the model.

Secondly, it is widely recognised that it is far from rare that an applied tensile force is evenly distributed among connecting test bolts due to the lack of any straightness, verticality, or consistent clamping action between connecting members for instance. This can bring into question the accuracy of the assumption related to the ultimate resistance of the T-stub connection; with that being equal to the total resistance of its connecting bolts, on which basis the *EHB* component capacity (F^u) was derived. Invalidity of this assumption can result in diverse global stiffness characteristics for the connection. By experimental means, one could justify that average T-stub separation measurements compensate for such inconsistencies, however, the effects cannot be quantified easily with respect to individual bolts. Thirdly, as a consequence of non equal force distributions among the bolts, as the bolts are loaded by the T-stub flange, some can actually be subjected to bending in addition to tension. This bending can act to reduce the overall strength of the bolts by a small amount; and further alter their stiffness response.

Lastly, regarding the manner in which the separation of the T-stub was measured in the companion studies, it is suspected that the reported separation could possibly include additional readings due to slippage. Because the linear potentiometers were fixed on the flange of the T-stub, if slippage occurred between the T-stub's stem and the jaws of the testing equipment (which are clamped together via hydraulic pressure), then this would result in higher measurements of displacement; explaining the poor agreement in yield displacement between the model and the experimental data. It is therefore suggested that the comparison of data presented in Figure 7.22 be treated in a qualitative way, with a focus on the early and final stages of the connection behaviour.

(a) Specimen EHB16-150-8.8H-C37-G120P100

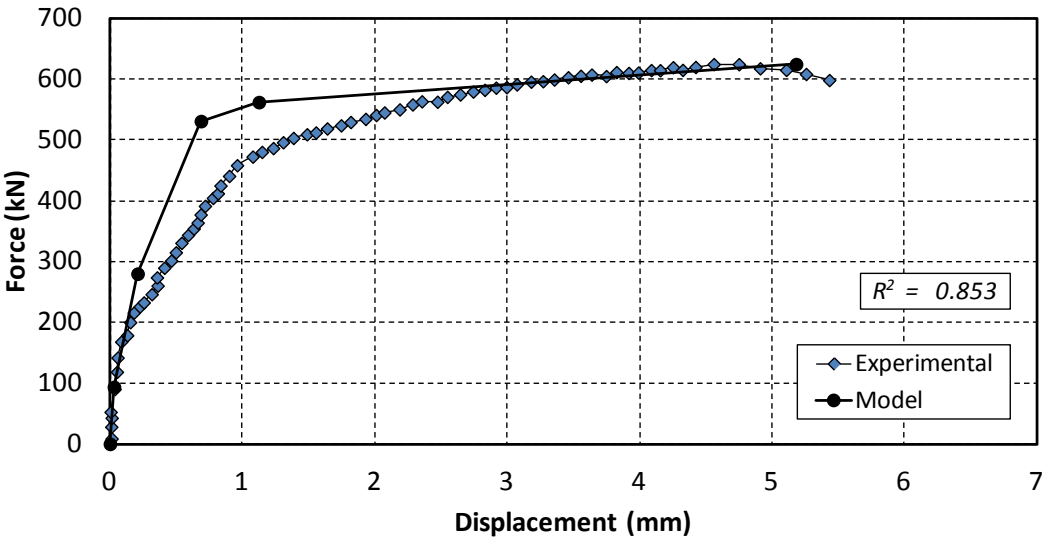

(b) Specimen EHB16-150-8.8I-C37-G120P140

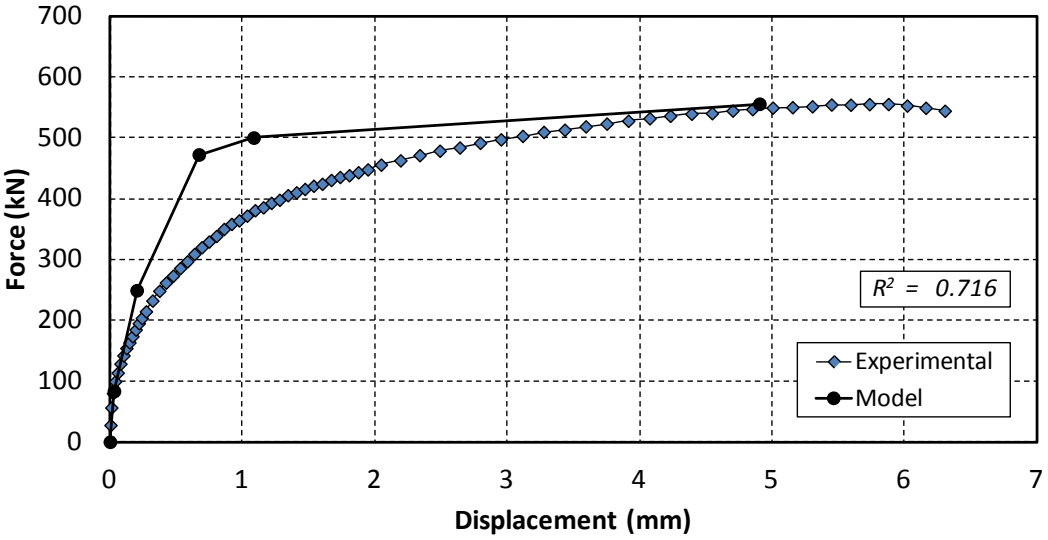

(c) Specimen EHB16-150-8.8I-C37-G120P100

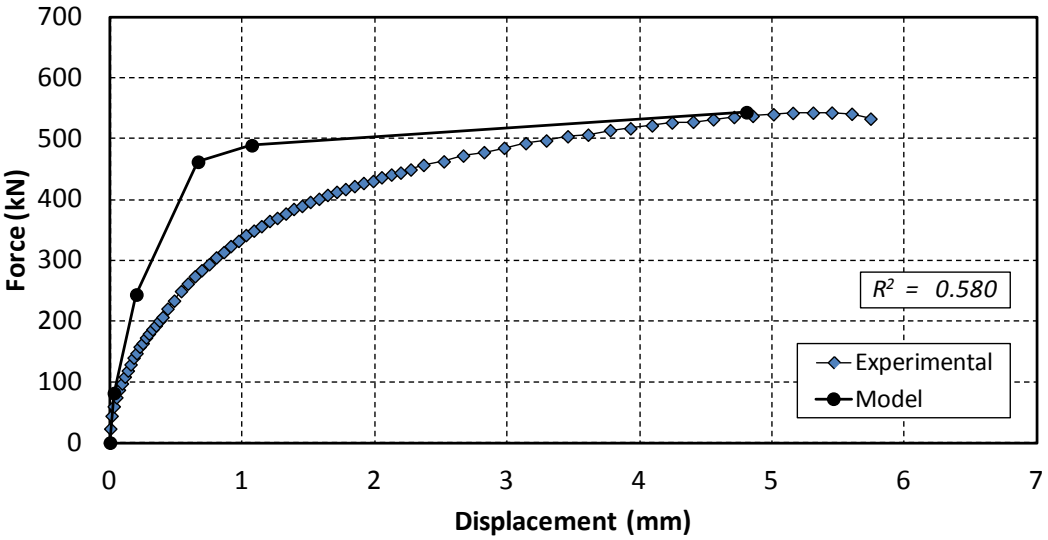

Figure 7.22 Comparison of T-stub spring model with experimental data

7.6 Chapter summary

This Chapter has presented a mechanical model to represent the tensile behaviour of the investigative joint component "Bolts (*EHB*) in tension". It is proposed to use an equivalent spring model which involves the expanding sleeves and mechanical anchorage elements being positioned in a parallel configuration, while acting in series with the bolt elongation element of the component. The assembly of the equivalent spring model results in a multi-linear F-δ_{global} tension response for the investigative component. At the 95% prediction band level, it is found that the component model predicts with sufficient accuracy the experimental data in terms of strength and stiffness; in consideration of different bolt batches, and varying parameters such as the strength of the concrete infill, the grade of the internal bolt, the diameter size of the internal bolt, and the embedded depth of the mechanical anchorage. Regarding ductility, because the mechanical model does not consider material softening behaviour, it is found that the model cannot estimate the global component collapse displacement. Yet, it is concluded that the ductility of the component, at ultimate state, can be sufficiently approximated. According to current ductility classification systems for endplate joint components that are suggested in the literature, it is identified that the *EHB* component is classified as a component with limited ductility (Class 2), within the tested range of parameters.

The Chapter satisfies research objectives associated with the proposal, and evaluation, of a suitable model that is able to predict the strength, stiffness, and ductility of the investigative joint component, in consideration of the main parameters affecting its response. It was demonstrated that the assembly of a mechanical model, which employs springs with linear characteristics, can be used to model the tension behaviour of the component on the foundation of the response of its individual elements.

8 Conclusions and recommendations

This thesis has reviewed and investigated a blind-bolted connection that has been the subject of on-going research at the University of Nottingham. The research work is associated with moment-resisting endplate joints between open and concrete-filled rectangular hollow sections, and the focus of this programme was the tensile behaviour of the connector. The novel blind-bolt that is involved in the proposed connection technology is labelled as the Extended Hollo-bolt (*EHB*). The aim of this research was to investigate whether the tension response of the *EHB* component can be modelled in such a way, to allow the component to be used in the characterisation of such structural joints within the context of the component method. On the basis of the component method, extensive experimental work has been performed to develop sufficient data that can be used to model the behaviour of the connector. A summary of the key findings of the thesis are presented in this Chapter. At the end, recommendations are included for future work.

8.1 Experimental results and data analysis

The following conclusions relate to experimental observations and detailed analysis of test data:

Global force-displacement behaviour of the *EHB* component

- Direct tension pull-out testing has demonstrated that the *EHB* component has superior stiffness characteristics than the commercially available Lindapter Hollo-bolt (*HB*) blind-bolt; in consideration of unfilled and concrete-filled sections. The enhanced response of the investigated joint component is attributed to the ability of the component's mechanical anchorage in reducing the deformation and relative slip of the system's expanding sleeves element; achieved by distributing tensile force within the concrete member, exclusive of a concrete breakout failure.
- Tensile pull-out testing has signified that three elements contribute to the overall deformability curve of the *EHB* component. Namely, the sources of deformability originate from: the elongation of the component's internal bolt, the

deformation of its expanding sleeves, and from the slip of its mechanical anchorage and bond element.

- Tensile pull-out testing has shown that the stiffness of the *EHB* component is primarily affected by a variation in the compressive strength of the concrete infill; with high concrete grade components exhibiting higher stiffness and larger ductility capacity when *C40* and *C60* grade mixes are considered. Independent of the variation in concrete strength, the yield and ultimate strength of the component are directly related to the material property of the component's internal bolt.
- A comparison between the use of grade 8.8 and 10.9 internal bolts in the *EHB* component indicates that the higher bolt grade improves the stiffness and strength of the component, with the system allowing for the full tensile capacity of grade 10.9 internal bolts to develop, but at the expense of post-limit stiffness and ductility; attributed to the brittle properties involved in higher grade bolts.
- A comparison between the use of 16 and 20mm internal bolts in the *EHB* component indicates that the larger bolt diameter size improves the stiffness and strength characteristics of the component, with the component allowing for the development of the full tensile capacity of 20mm diameter internal bolts.
- The stiffness, strength, ductility and ultimate failure of the *EHB* component are not dependent upon the embedded depth of its mechanical anchorage element within the tested range of 4.0 to 6.5d_b. This suggests that a minimum embedded depth of 4.0d_b is satisfactory in developing the tensile capacity of the internal bolt of the component, which furthermore provides more flexibility in the design of such joints in consideration of double sided and perpendicular joint configurations, as less embedment is found internally of the tubular columns.
- On the foundation of experimental evidence, within the tested range the resistance function of the *EHB* component is determined as for standard bolts; with that being taken as equal to the ultimate strength of its fully threaded internal bolt.
- According to current ductility classification systems for endplate joint components that are suggested in the literature, the *EHB* component is classified as a component with limited ductility (Class 2). In comparison with standard bolts which are classified as brittle components (Class 3), the *EHB* anchored blind-bolt is considered to have a larger ductility capacity.

Pre-load in *HB*/*EHB* blind-bolt system

- A sample of 20 pre-load test pieces were tested under torque control using a manual ratchet wrench; factory lubricated as supplied by the manufacturer. A range of 5-22% of relaxation in pre-load occurred among the test specimens over a period of 5 days, with at least 90% of the relaxation taking place within two hours of tightening. The relaxation rate of the pre-load was found to be unaffected by the variation in bolt grade and bolt diameter size.
- Using the short-form equation, an experimental nut factor *K* is proposed to estimate the relationship between tightening torque and residual pre-load. Descriptive statistics suggest a population mean for the experimentally derived nut factor *K* to lie between 0.415 and 0.525; determined by 95% confidence intervals around the sample mean. Even though it is recognised that a different interval could be obtained in the case that the testing was repeated, anyhow it is evident from this testing that general text-book nut factors cannot be assumed to be appropriate for the *HB*/*EHB* blind-bolt. The above measured interval shows that a suitable nut factor for the blind-bolt involves a higher value than that typically used for standard bolts.
- Normalised ratios of residual pre-load to actual yield and ultimate strength of the internal bolts that were employed in the testing indicate that the same proportion of pre-load is induced in the *EHB16* and *EHB20* of grade 8.8, whereas an additional 10% in relative pre-load is found in the case of the *EHB16* of grade 10.9. For representation of the residual pre-load in the blind-bolt assembly, proportions relative to the ultimate strength of the internal bolt are suggested. Proportions of $0.15f_{ub}$ for *EHB16-8.8* and *EHB20-8.8* fasteners, and proportions of $0.25f_{ub}$ are suggested for the *EHB16-10.9*.

8.2 Component model

The following conclusions relate to the development, assembly and evaluation of the proposed *EHB* component model:

- For application in the characterisation of moment-resisting blind-bolted joints - within the context of the component method - a multi-linear equivalent

spring model is proposed to represent the tensile behaviour of the *EHB* anchored blind-bolt component; with a denoted stiffness of k_{EHB}. The proposed component model has demonstrated that the behaviour of the *EHB* component can be modelled by the component method approach; employing idealised models for the behaviour of its contributing elements.

- On the foundation of semi-empirical, multi-linear idealised, element models for the elongation of the component's internal bolt, the deformation of its expanding sleeves, and the macroscopic slip of its mechanical anchorage and bond element, the component model has been shown to be capable of describing the *EHB* component response (F-δ_{global}) with reasonable accuracy. By comparing the predictions of the component model with relevant experimental data, the model illustrated its ability in capturing the stiffness and yielding trend of the component. Although the proposed component model cannot estimate the component collapse displacement, it has demonstrated that it can sufficiently estimate the component ductility at ultimate state.
- The model has highlighted the importance of involving the level of pre-load that is induced within the *EHB* component at its tightening stage; by showing that the resulting force-displacement behaviour of the *EHB* component is significantly underestimated when pre-load effects are excluded.
- Computation of the component model (in consideration of a variation in parameters) can be done with simple spreadsheets to assemble the proposed component's individual element models; making the component model a possible advantageous design tool which gives the assessor a physical feel.

Limitations

- The EC3 equivalent T-stub in tension model relates to three failure modes; Mode 1: complete yielding of the flange, Mode 2: bolt failure with yielding of the flange, Mode 3: bolt failure. The component model which was developed in this project is limited to Mode 3.
- The proposed component model does not account for material softening behaviour and its predictions are thus limited to ultimate conditions.
- The range of validity of the proposed model is limited to the tested range.

Application

The extension of the component method for the proposed connection technology was found to be limited due to insufficient knowledge in the behaviour of two basic components (signed X and Y in Figure 8.1). This research work aimed at modelling the tensile behaviour of the anchored blind-bolt (component X). The component model that was developed in this thesis is proposed to represent the response of component X, for application in a global mechanical model that is to predict the moment-rotation characteristics of the novel connection. To achieve, however, the global joint model, there is still a need to develop appropriate application rules for the bending behaviour of the column face, including its interaction with the response of the connector. It is the subject of current active research at The University of Nottingham to devise and validate such rules.

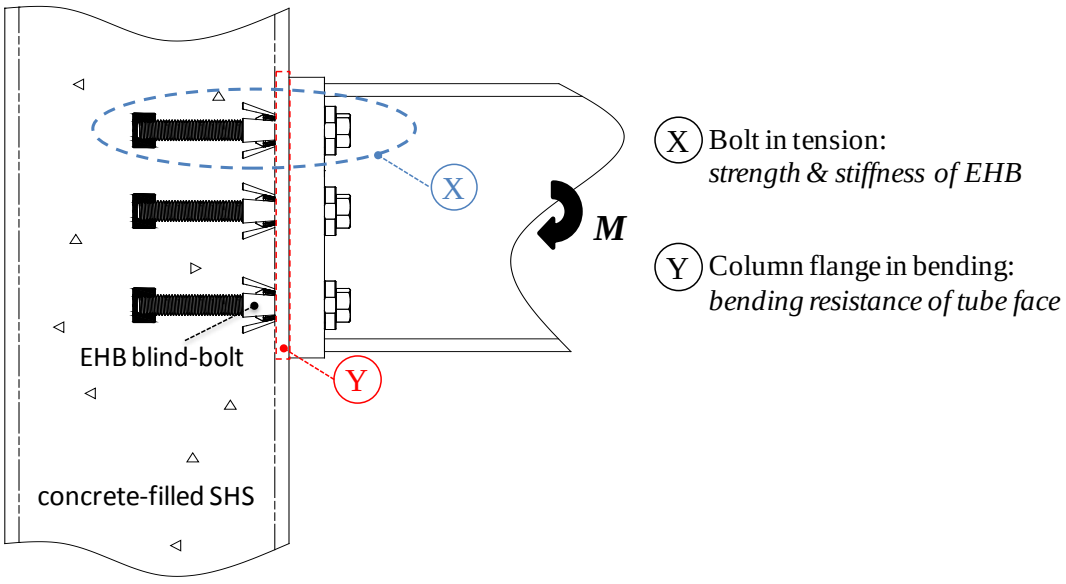

Figure 8.1 Proposed connection technology

8.3 Contribution of work

This investigation contributes to knowledge within the structural steelwork research community by providing:

- Information related to the tension zone of novel connection technology.
- The assembly of a complex fastener that is based on its individual parts.
- A new model for a novel anchored blind-bolt that can be used in a component based approach to design.
- Guidance for further investigation.

From a practical point of view, this research has enhanced the knowledge in the field of blind-bolted connections by providing:

- A step forward towards the modelling of a novel connection technology.
- A means for the possible use of a blind-bolt to enable moment-resisting connections to hollow sections.

8.4 Suggestions for future research

The majority of the work conducted in this project has been through the experimental investigation of single component testing, including pull-out and pre-load tests. The data generated from the tests have been invaluable in constructing and validating the proposed component model. But there are some areas indicated by this programme of component testing which have been shown to require some further investigation. The recommendations for future research are divided into different areas as below.

Material property related

- This project was concerned with the short-term behaviour of normal weight and normal strength concrete. The mixes that were involved in the preparation of the pull-out specimens required standard compaction procedures for the removal of the air voids, which obviously is considered an easy operation when working under laboratory conditions. But from a practical point of view, when dealing with very long columns for instance, the compaction operation would be a challenge and quality assurance would require good inspection during casting to ensure sufficient

compaction of the concrete infill. It is therefore suggested that different concrete mixes are investigated, emphasizing for practical purposes the application of self compacting concrete.

- In this thesis, the pull-out test matrix covered a range of normal strength concrete between grades of *C40* and *C60* (cube strength). The results indicated that a higher compressive strength can enhance the stiffness characteristics of the *EHB* anchored blind-bolt component. It is thus suggested to extend this tested range to confirm such observations for low ($\leqslant$ *C20*) and high (>*C60*) strength concrete mixes. It is recommended to investigate grades of *C20* and *C80*.
- The size and type of coarse aggregate could also be a subject of future research in view of investigating, whether the use of lightweight concrete could be considered as an alternative to normal weight concrete; in attempt to reduce the dead weight of the concrete infill, which can add up to a significant figure in consideration of a multi-storey structure.

Modelling

- The tri-linear idealised models for the expanding sleeves and mechanical anchorage elements of the *EHB* component have been proposed in the form of a table and a supplementary notation chart. To ease the use of the proposed component model, it is suggested that these element models are re-arranged in the form of suitable expressions; highlighting the effects of the primary parameters.
- The development of a numerical model, using the Finite Element (FE) method could also be the subject of future research to simulate the tensile stiffness of the *EHB* anchored blind-bolt. Such a model could be developed and validated with the use of the data that was generated from the experimental programme of this study. Advantageously, the FE model could then be used to conduct parametric studies to extend the rules that are currently valid for the tested range.
- To improve the proposed component model - that utilises mechanical springs which are limited to ultimate conditions - it is suggested to expand the current model to account for the effect of plasticity, and unloading. This expansion could involve the addition of viscous and/or sliding elements to capture the dissipative nature.

Structural performance study

- This project was concerned with single component pull-out testing. With reference to the design of fastenings to concrete, it is recognised that multiple pull-outs (involving a group of fasteners) could result in overlapping cones of resistance. Evidently, the *EHB* component did not exhibit any form of a concrete breakout but it is suggested that such behaviour is verified with respect to a row of components. This would require research into the influence of varying the bolt gauge and pitch.
- The pull-out testing for the *EHB* component was conducted under pure tension in this study. It is recognised that combined tension and shear testing is also required for the verification of the behaviour of the component under combined loading. It is suggested that further component pull-out tests are conducted at 30, 45 and 60 degrees to the horizontal to account for combined tension and shear effects.
- In this programme, the tension behaviour of the *EHB* connector was investigated in a manner such that the column side of the connection remained elastic. This was achieved by the employment of a rigid plate in the pull-out test setup. The test results therefore relate to Mode 3 of the classic equivalent T-stub in tension (i.e. Bolt failure). It is recognised that there is another failure mode that requires attention. That is the interaction of the tube face with the fastener in tension - which relates to Mode 2: Bolt failure with flange yielding. It is suggested to investigate and quantify the response of this interaction mode.

Cost study

- From an economic point of view, it is the author's opinion that a cost comparison study is required in order to quantify cost effectiveness of employing the *EHB* blind-bolt component within an overall structural frame; for current construction market values. The cost study could involve the construction of a three-storey frame, with semi-rigid beam-to-column joints between open profile beams and RHS columns, comparing the utilisation of the *EHB* component (involving concrete-filled RHS) with fully welded configurations (unfilled RHS) for their connections.

List of References

Abrams, D. (1913). "Tests of bond between concrete and steel." *University of Illinois at Urbana Champaign, College of Engineering. Engineering Experiment Station*, XI(15).

ACI. (2008a). "Code Requirements for Nuclear Safety-Related Concrete Structures and Commentary (ACI 349M-06)."

ACI. (2008b). "Committee 318 Building Code Requirements for Structural Concrete (ACI 318M-08) and Commentary (318R-08)."

Ahmed, K., Siddiqi, Z. A., and Yousaf, M. (2007). "Slippage of Steel in High and Normal Strength Concrete." *Pak. J. Engg. & Appl. Sci*, 1, 31-39.

Al-Mughairi, Tizani, W., and Owen, J. S. (2009). "Connection to Concrete Filled Hollow Section using Extended Hollobolt (Moment Connection Tests)." *ASCCS 9th International Conference on Steel Concrete Composite and Hybrid Structures. Leeds, UK, 8-10 July*, 599-604.

Alavi-Fard, M., and Marzouk, H. (2004). "Bond of high-strength concrete under monotonic pull-out loading." *Magazine of Concrete Research*, 56(9), 545-557.

ASTM. (2009). "A970 / A970M - 09: Standard Specification for Headed Steel Bars for Concrete Reinforcement." *American Society for Testing and Materials*.

Banks, G. (1997). "Hollobolt Joint Shear Tests Project No. S2860 " *Memo 146/RJ, British Steel Plc., Swinden Technology Centre, Rotherham*.

Barnett, T. (2001). "The behaviour of a blind bolt for moment resisting connections in hollow sections," Ph.D. Thesis, University of Nottingham, UK.

Barron, J. (1998). *Handbook of bolts and bolted joints: Computing the stiffness of a fastener*, CRC Press, Marcel Dekker, New York.

Bickford, J. H. (2008). *Introduction to the Design and Behavior of Bolted Joints , Fourth Edition , Non-Gasketed Joints*, Taylor & Francis Group.

BSI. (1993). "Structural fixings in concrete and masonry, Part 1: Method of test for tensile loading." BS 5080-1:1993, British Standards Institution, London.

BSI. (1997). "Structural use of concrete. Code of practice for design and construction ", BS 8110-1:1997, British Standards Institution, London.

BSI. (2000a). "Concrete, Part 1: Specification, performance, production and conformity." BS EN 206-1:2000, British Standards Institution.

BSI. (2000b). "Structural use of steelwork in building - Part 1: Code of practice for design - Rolled and welded sections." BS 5950-1:2000, British Standards Institution, London.

BSI. (2001a). "ISO metric precision hexagon bolts, screws and nuts - Specification." BS 3692:2001, British Standards Institution, London.

BSI. (2001b). "Metallic materials - Tensile testing - Part 1: Method of test at ambient temperature." BS EN 10002-1:2001, British Standards Institution, London.

BSI. (2005). "Fasteners -- Torque/clamp force testing." EN ISO 16047:2005, British Standards Institution, London.

BSI. (2009). "Mechanical properties of fasteners made of carbon steel and alloy steel, Part 1: Bolts, screws and studs with specified property classes - Coarse thread and fine pitch thread." BS EN ISO 898-1:2009, British Standards Institution, London.

Cairns, J., and Plizzari, G. (2003). "Towards a harmonised European bond test." *Materials and Structures*, 36(8), 498-506.

Cannon, R., Godfrey, D., and Moreadith, F. (1981). "Guide to the design of anchor bolts and other steel embedments." *Concrete International* 3(7), 28-41.

CEB. (1993). "CEB-FIP Model Code 1990: Design Code, Comité Euro-International du Béton " *Thomas Telford, London*.

CEB. (1994). "CEB Bulletin 216: Fastenings to Concrete and Masonry Structures, State of the Art Report, Comité Euro-International du Béton " *Thomas Telford, London*, 249.

CEB. (1997). "CEB Bulletin 233: Design Guide - Parts 1-3, Design of fastenings in concrete, Comité Euro-International du Béton " *Thomas Telford, London*.

CEN. (2004). "Eurocode 2: Design of concrete structures - Part 1-1: General rules and rules for buildings ", BS EN 1992-1-1:2004, British Standards Institution.

CEN. (2005). "Eurocode 3: Design of steel structures – Part 1-8: Design of joints." BS EN 1993-1-8:2005, British Standards Institution.

CEN/TS. (2009). "Design of fastenings for use in concrete - Part 4-2: Headed Fasteners." DD CEN/TS 1992-4-2:2009, British Standards Institution.

Choi, D.-U., Hong, S.-G., and Lee, C.-Y. (2002). "Test of headed reinforcement in pullout " *KCI CONCRETE JOURNAL*, 14(3), 102-110.

Chun, S., Lee, S., Thomas, H., Oh, B., and Wallace, J. (2007). "Mechanical anchorage in exterior beam-column joints subjected to cyclic loading." *ACI Structural Journal*, 104(1), 102-113.

Chun, S., Oh, B., Lee, S., and Naito, C. (2009). "Anchorage Strength and Behavior of Headed Bars in Exterior Beam-Column Joints." *ACI Structural Journal*, 106(5).

COST. (1997). "Composite steel–concrete joints in braced frames for buildings." *COST C1 report edited by Anderson D. Bruxelles, Luxembourg: European Commission*.

Da Silva, L. S. (2008). "Towards a consistent design approach for steel joints under generalized loading." *Journal of Constructional Steel Research*, 64(9), 1059-1075.

Da Silva, L. S., Santiago, A., and Vila Real, P. (2002). "Post-limit stiffness and ductility of end-plate beam-to-column steel joints." *Computers & Structures*, 80(5-6), 515-531.

Dancygier, A., Katz, A., and Wexler, U. (2009). "Bond between deformed reinforcement and normal and high-strength concrete with and without fibers." *Materials and Structures*, 1-18.

Del Savio, A. A., Nethercot, D. A., Vellasco, P. C. G. S., Andrade, S. A. L., and Martha, L. F. (2009). "Generalised component-based model for beam-to-column connections including axial versus moment interaction." *Journal of Constructional Steel Research*, 65(8-9), 1876-1895.

DeVries, R., Jirsa, J., and Bashandy, T. (1999). "Anchorage capacity in concrete of headed reinforcement with shallow embedments." *ACI Structural Journal*, 96(5).

Elghazouli, A. Y., Málaga-Chuquitaype, C., Castro, J. M., and Orton, A. H. (2009). "Experimental monotonic and cyclic behaviour of blind-bolted angle connections." *Engineering Structures*, In Press, Corrected Proof.

Eligehausen, R., Fuchs, W., and Sippel, T. M. (1998). "Anchorage to concrete." *Progress in Structural Engineering and Materials*, 1(4), 392-403.

Eligehausen, R., Popov, E., and Bertero, V. (1982). "Local bond stress-slip relationships of deformed bars under generalized excitations." *Proceedings of the 7th European Conference on Earthquake Engineering*, 4, 69-80.

Ellison, S. (2003). "Moment resisting connections to structural hollow sections." *MEng Civil Engineering Dissertation, University of Nottingham, UK*.

Ellison, S., and Tizani, W. (2004). "Behaviour of blind bolted connections to concrete filled hollow sections." *The Structural Engineer*, 82(22), 16-17.

ERICO. "Lenton terminator." www.erico.com, last accessed on 01 July 2011.

Fabbrocino, G., Verderame, G. M., and Manfredi, G. (2005). "Experimental behaviour of anchored smooth rebars in old type reinforced concrete buildings." *Engineering Structures*, 27(10), 1575-1585.

Fuchs, W., Eligehausen, R., and Breen, J. (1995). "Concrete capacity design (CCD) approach for fastening to concrete." *ACI Structural Journal*, 92(1).

Gervásio, H., Simões da Silva, L., and Borges, L. (2004). "Reliability assessment of the post-limit stiffness and ductility of steel joints." *Journal of Constructional Steel Research*, 60(3-5), 635-648.

Gomes, F., Jaspart, J. P., and Maquoi, R. (1996). "Moment capacity of beam-to-column minor axis joints." *Proc., IABSE Int.Colloquium on Semi-Rigid Structural Connections, Istanbul, Turkey*, 319-326.

HRC. "T-headed bars." www.hrc-usa.com, last accessed on 01 July 2011.

Jaspart, J. P. (2000). "General report: session on connections." *Journal of Constructional Steel Research*, 55(1-3), 69-89.

Jaspart, J. P., and Weynand, K. (2001). "Extension of the component method to joints in tubular construction." *In Puthli, R. & Herion, S. (ed), Proceedings of the Ninth International Symposium and Euroconference on Tubular Structures, Tubular structures IX, Düsseldorf 3-5 April 2001. Rotterdam*, 517-523.

Kankam, C. K. (2003). "A routine method for measuring bond stress, steel strain and slip in reinforced concrete beams at service loads." *Magazine of Concrete Research*, 55(1), 85-93.

Kuhlmann, U., Davison, J. B., and Kattner, M. (1998). "Structural systems and rotation capacity." *In: Proceedings of COST C1 conference on Control of the Semi-rigid Behaviour of Civil Engineering Structural Connections, Université de Liège, Belgium*, 167-76.

Liang, Q. Q. (2009). "Strength and ductility of high strength concrete-filled steel tubular beam-columns." *Journal of Constructional Steel Research*, 65(3), 687-698.

Lindapter. (2009). "Type HB - Hollo-Bolt." Cavity Fixings 2 Product Brochure, Lindapter International UK, 41-43.

Mason, R. L., Gunst, R. F., and Hess, J. L. (2003). *Statistical Design and Analysis of Experiments: With Applications to Engineering and Science*, John Wiley & Sons, Inc., Hoboken, NJ, USA.

Mo, Y. L., and Chan, J. (1996). "Bond and Slip of Plain Rebars in Concrete." *Journal of Materials in Civil Engineering*, 8(4), 208-211.

Motulsky, H., and Christopoulos, A. (2004). *Fitting models to biological data using linear and nonlinear regression: a practical guide to curve fitting*, Oxford University Press, USA.

Neves, L. C., and Gomes, F. (1996). "Semi-rigid behavior of beam-to-column minor axis joints." *Proc., IABSE Int. Colloquium on Semi-Rigid Structural Connections, Istanbul, Turkey*, 207-216.

Neves, L. C., Silva, L. S. d., and Vellasco, P. C. G. d. S. (2004a). "Design procedure for I-beam to concrete filled column and minor axis joints." *ECCS Technical Committee 10 "Connections"*(1).

Neves, L. C., Silva, L. S. d., and Vellasco, P. C. G. d. S. (2004b). "Experimental behaviour of end plate i-beam to concrete-filled rectangular hollow section column joints." *APPLIED MECHANICS AND ENGINEERING*, 9(1), 63-80.

Neville, A. M., and Kennedy, J. B. (1986). *Basic statistical methods for engineers and scientists*, International Textbook Co., Scranton.

Occhi, F. (1995). "Hollow Section Connections Using (Hollofast) Hollobolt Expansion Bolting." *Second Interim Report 6G-16/95, Sidercad, Italy*

Ožbolt, J., Rah, K., and Meštrovi , D. (2006). "Influence of loading rate on concrete cone failure." *International Journal of Fracture*, 139(2), 239-252.

Park, H., Yoon, Y., and Kim, Y. (2003). "The effect of head plate details on the pull-out behaviour of headed bars." *Magazine of Concrete Research*, 55(6), 485-496.

Pitrakkos, T. (2008). "Blind Bolted Connections to Structural Hollow Sections." *MEng Civil Engineering Dissertation, University of Nottingham, UK*.

RILEM/CEB/FIP. (1983). "Bond test for reinforcement steel: 2. Pull-out test. Recommendation RC 6." 6(32).

SCI/BCSA. (1995a). "Joints in steel construction: Moment Connections, Part 1." Publication 207, Steel Construction Institute (SCI) & British Constructional Steelwork Association (BCSA), Ascot.

SCI/BCSA. (1995b). "Joints in steel construction: Moment Connections, Part 2 - Capacity tables and dimensions for detailing." Publication 207, Steel Construction Institute (SCI) & British Constructional Steelwork Association (BCSA), Ascot.

SCI/BCSA. (1998). "Joints in steel construction: Composite Connections." Publication 213, Steel Construction Institute (SCI) & British Constructional Steelwork Association (BCSA), Ascot.

SCI/BCSA. (2002). "Joints in steel construction: Simple Connections." Publication 212, Steel Construction Institute (SCI) & British Constructional Steelwork Association (BCSA), Ascot.

Shapiro, S. S., and Wilk, M. B. (1965). "An analysis of variance test for normality (complete samples)." *Biometrika*, 52(3/4), 591-611.

Shima, H., Chou, L.-L., and Okamura, H. (1987). "Micro and Macro Models for Bond in Reinforced Concrete." *Journal of the Faculty of Engineering, The University of Tokyo (B)*, XXXIX(2).

Silva, L. A. P., Neves, L. F. N., and Gomes, F. C. T. (2003). "Rotational Stiffness of Rectangular Hollow Sections Composite Joints." *Journal of Structural Engineering*, 129(4), 487-494.

Swanson, J. A., and Leon, R. T. (2001). "Stiffness Modeling of Bolted T-Stub Connection Components." *Journal of Structural Engineering*, 127(5), 498-505.

Thomas, H., Sang-Su Ha, and Choi, D.-U. (2010). "Bar Pullout Tests and Seismic Tests of Small-Headed Bars in Beam-Column Joints." *ACI Structural Journal*, 107(1), 32-42.

Thompson, M., Jirsa, J., and Breen, J. (2006). "CCT Nodes Anchored by Headed Bars-Part 2: Capacity of Nodes." *ACI Structural Journal*, 103(1).

Thompson, M., Jirsa, J., Breen, J., and Klinger, R. (2002). "Anchorage Behavior of Headed Reinforcement: Literature Review." *Center for Transportation Research Report 1855-1, Austin, Texas*, 112 pp.

Thompson, M., Ziehl, M., Jirsa, J., and Breen, J. (2005). "CCT Nodes Anchored by Headed Bars-Part 1: Behavior of Nodes." *ACI Structural Journal*, 102(6).

Tizani, W., and Ridley-Ellis. (2003). "The performance of a new blind-bolt for moment-resisting connections." *JAURIETTA, M.A., ALONSO, A., CHICA, J.A., eds. Tubular structures X: Proceedings of the 10th international symposium on tubular structures*, 395-400.

Wales, M. W., and Rossow, E. C. (1983). "Coupled Moment-Axial Force Behavior in Bolted Joints." *Journal of Structural Engineering*, 109(5), 1250-1266.

Wallace, J. (1998). "Use of Mechanically Anchored Bars in exterior beam-column joints subjected to seismic loading." *Prepared for ERICO*.

Weynand, K., Busse, E., and Jaspart, J. P. (2006). "First practical implementation of the component method for joints in tubular construction." *Welding in the World*, 50(SPEC. ISS.), 126-132.

Yeomans, N. F. (1998). "Rectangular hollow section column connections using the Lindapter HolloBolt." *Tubular Structures VIII: Proceedings of the 8th International Symposium, Singapore, 26-28 August, 1998*, 559-566.

Bibliography

Al-Mughairi, A. (2009). "The Behaviour of Moment Resisting Connection to Concrete Filled Hollow Sections Using Extended Hollobolts". Ph.D. Thesis, University of Nottingham, UK.

Barnett, T., Tizani, W., and Nethercot, D. (2000). "Blind Bolted Moment Resisting Connections to Structural Hollow Sections." Connections in Steel Structures IV, Steel Connections in the New Millennium, Roanoke, Virginia, USA, 340-348.

Barnett, T., Tizani, W., and Nethercot, D. (2001). "The practice of blind bolting connections to structure hollow sections - a review." Steel and Composite Structures, 1(1), 1-16.

COST. (1997). "Composite steel–concrete joints in braced frames for buildings." COST C1 report edited by Anderson D. Bruxelles, Luxembourg: European Commission.

France, J. E. (1997). "Bolted connections between open section beams and box columns," Ph.D. Thesis, University of Sheffield, UK.

France, J. E., Buick Davison, J., and A. Kirby, P. (1999). "Moment-capacity and rotational stiffness of endplate connections to concrete-filled tubular columns with flowdrilled connectors." Journal of Constructional Steel Research, 50(1), 35-48.

France, J. E., Buick Davison, J., and A. Kirby, P. (1999). "Strength and rotational response of moment connections to tubular columns using flowdrill connectors." Journal of Constructional Steel Research, 50(1), 1-14.

France, J. E., Buick Davison, J., and Kirby, P. A. (1999). "Strength and rotational stiffness of simple connections to tubular columns using flowdrill connectors." Journal of Constructional Steel Research, 50(1), 15-34.

Gardner, A. P., and Goldsworthy, H. M. (2005). "Experimental investigation of the stiffness of critical components in a moment-resisting composite connection." Journal of Constructional Steel Research, 61(5), 709-726.

Girao Coelho, A. M., Silva, L. S. D., and Bijlaard, F. S. K. (2006). "Ductility analysis of bolted extended end plate beam-to-column connections in the framework of the component method." International Journal of Steel and Composite Structures, 6(1), 33-53.

Loh, H. Y., Uy, B., and Bradford, M. A. (2006). "The effects of partial shear connection in composite flush end plate joints Part I -- experimental study." Journal of Constructional Steel Research, 62(4), 378-390.

Loh, H. Y., Uy, B., and Bradford, M. A. (2006). "The effects of partial shear connection in composite flush end plate joints Part II--Analytical study and design appraisal." Journal of Constructional Steel Research, 62(4), 391-412.

Málaga-Chuquitaype, C., and Elghazouli, A. Y. (2010). "Component-based mechanical models for blind-bolted angle connections." Engineering Structures, 32(10), 3048-3067.

Orton, A. H. (2009). "Behaviour of semi-rigid steelwork connections of I-section beams to tubular columns." Tubular Structures XII, Proceedings of Tubular Structures XII, Shanghai, China, 201-208.

Swanson, J.A. (1999). "Characterization of the strength, stiffness and ductility behavior of T-stub connections". Ph.D. Thesis, Georgia Institute of Technology, Atlanta, USA.

Wang, J.-F., Han, L.-H., and Uy, B. (2008). "Behaviour of flush end plate joints to concrete-filled steel tubular columns." Journal of Constructional Steel Research, 65(4), 925-939.

Wang, J.-F., Han, L.-H., and Uy, B. (2009). "Hysteretic behaviour of flush end plate joints to concrete-filled steel tubular columns." Journal of Constructional Steel Research, 65(8-9), 1644-1663.

Yao, H., Goldsworthy, H., and Gad, E. (2006). "Simplified component model for curved T-stub connection to concrete-filled steel tube with blind bolts and extensions." [Proceedings] Annual Technical Conference of the Australian Earthquake Engineering Society : Earthquake Engineering in Australia, Canberra, Australian Capital Territory, 24-26 November 2006, 289-295.

Yao, H., Goldsworthy, H., and Gad, E. (2008). "Experimental and Numerical Investigation of the Tensile Behavior of Blind-Bolted T-Stub Connections to Concrete-Filled Circular Columns." Journal of Structural Engineering, 134(2), 198-208.

Yao, H., Goldsworthy, H., and Gad, E. (2009). "Parametric analysis of blind-bolted connections in a moment-resisting composite frame." Tubular Structures XII, Proceedings of Tubular Structures XII, Shanghai, China, 421-429.

Publications

PITRAKKOS, T., TIZANI, W. and WANG, Z., 2010. Pull-out behaviour of anchored blind-bolt: a component based approach. In *Computing in Civil and Building Engineering*, *Proceedings of the International Conference*, W. TIZANI (Editor), 30 June-2 July, Nottingham, UK, Nottingham University Press, Paper 255, p. 509, ISBN 978-1-907284-60-1.

PITRAKKOS, T., and TIZANI, W., 2011. Blind-bolted connections to concrete-filled sections: modelling the tensile behaviour of the anchored blind-bolt component. In *Eurosteel 2011*, *6th European Conference on Steel and Composite Structures*, 31 August-2 September, Budapest, Hungary, p.513, ISBN 978-92-9147-103-4.

Appendix A

Reinforced Concrete Design of Unconfined Test Specimen to BS 8110-1:1997

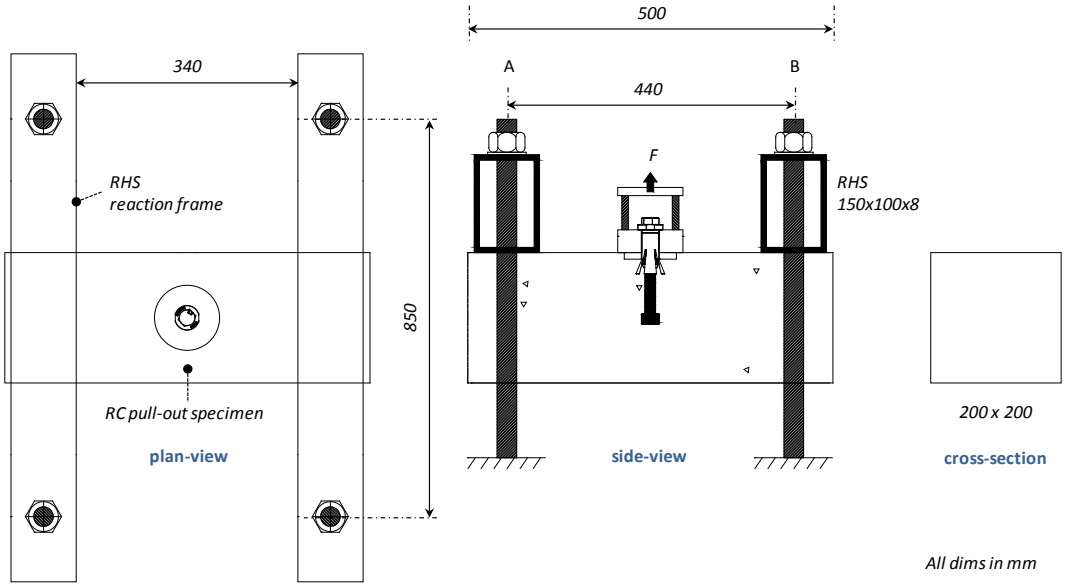

Loading

F = Maximum anticipated tensile load (Ultimate strength of the bolt) = 150kN

Material properties

f_{cu} = 40 N/mm^2 (On the day of testing)

$f_y = f_{yv}$ = 250 N/mm^2 (Mild steel) , f_y = 460 N/mm^2 (High yield steel)

Assumptions

RC pullout specimen is simply supported by the reaction frame

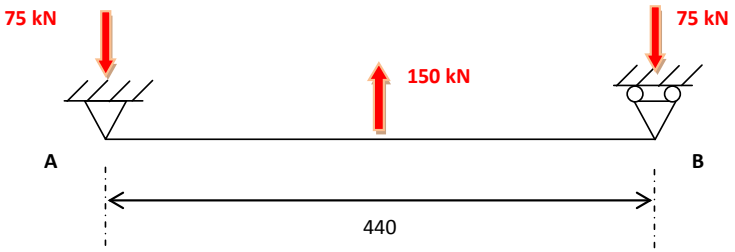

$R_A = R_B = F/2 = 75kN$

$M_{max} = FL/4 = 150 \times 0.44/4 = 16.5kNm$

BS 8110-1:1997

Cover to main reinforcement = 30mm

Assume 4T10 in top (A_s=314mm^2)

Effective depth, d = 160mm

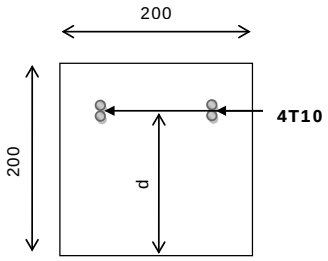

3.4.4.4 Flexure

$k = M / (f_{cu} b d^2) = (16.5 \times 10^6) / (40 \times 200 \times 160^2) = 0.080 < 0.156$

Therefore compression reinforcement not required.

$z = d [0.5 + \sqrt{(0.25 – k/0.9)}] = 0.9d = 144mm$ (<0.95d) ***OK***

$x = (d - z)/0.45 = 35mm$

$A_s = M / (0.95 f_y z) = (16.5 \times 10^6) / (0.95 \times 460 \times 144) = 262mm^2$

A_s provided > A_s required, $314 > 262mm^2$ ***OK***

3.12.6.1, Table 3.25 Minimum and Maximum Reinforcement

Tensile reinforcement:

$A_{s,max} = 0.04 A_c = 0.04 \times 200^2 = 1600mm^2 > 314$ ***OK***

$A_{s,min} = 0.0013 A_c = 52mm^2 < 314$ ***OK***

Compressive reinforcement:

$A_{s,min} = 0.002 A_c = 80mm^2$ ***Therefore use 2R8 at bottom ($A_s' = 100mm^2$)***

$A_{s,max} = 0.04 A_c = 0.04 \times 200^2 = 1600mm^2 > 100$ ***OK***

3.4.5.2 Shear

$v = V / (b_V d) = 75 / (200 \times 160) = 2.34 N/mm^2$ ($<5 N/mm^2$) ***OK***

Table 3.8

$v_c = 0.79[(100 A_s)/(b_V d)]^{1/3} [(400/d)^{1/4} / \gamma_m] (f_{cu} / 25)^{1/3} = 0.79 \times 0.99 \times 1 \times 1.17 = 0.92 N/mm^2$

Table 3.7

$v_c + 0.4 = 1.32$, $0.5v_c = 0.46$ therefore as $(v_c + 0.4) < v < 5 N/mm^2$

Area of shear reinforcement to be provided = $A_{sv} \geq b_v s_v (v – v_c) / 0.95 f_{yv} =$

$200 \times 0.75 \times 160 \times (2.34 – 0.92) / (0.95 \times 250) = 144mm^2$ (for two legs)

Therefore use R10 where s_v = maximum allowable link spacing = 0.75d = 120mm

3.12.8.23 Effective anchorage length of a hook or bend

A 90^o bend requires an anchorage length of 4 x internal radius : 12 bar diameter

Use 10 x bar diameter = 10 x 10 = 100mm for top two T10 only

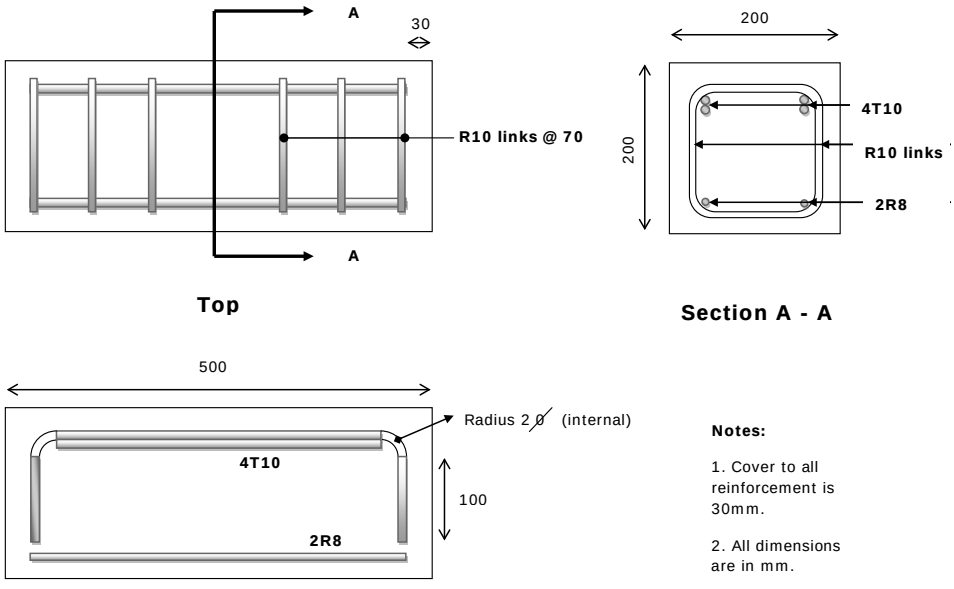

Appendix B

Pull-out test setup

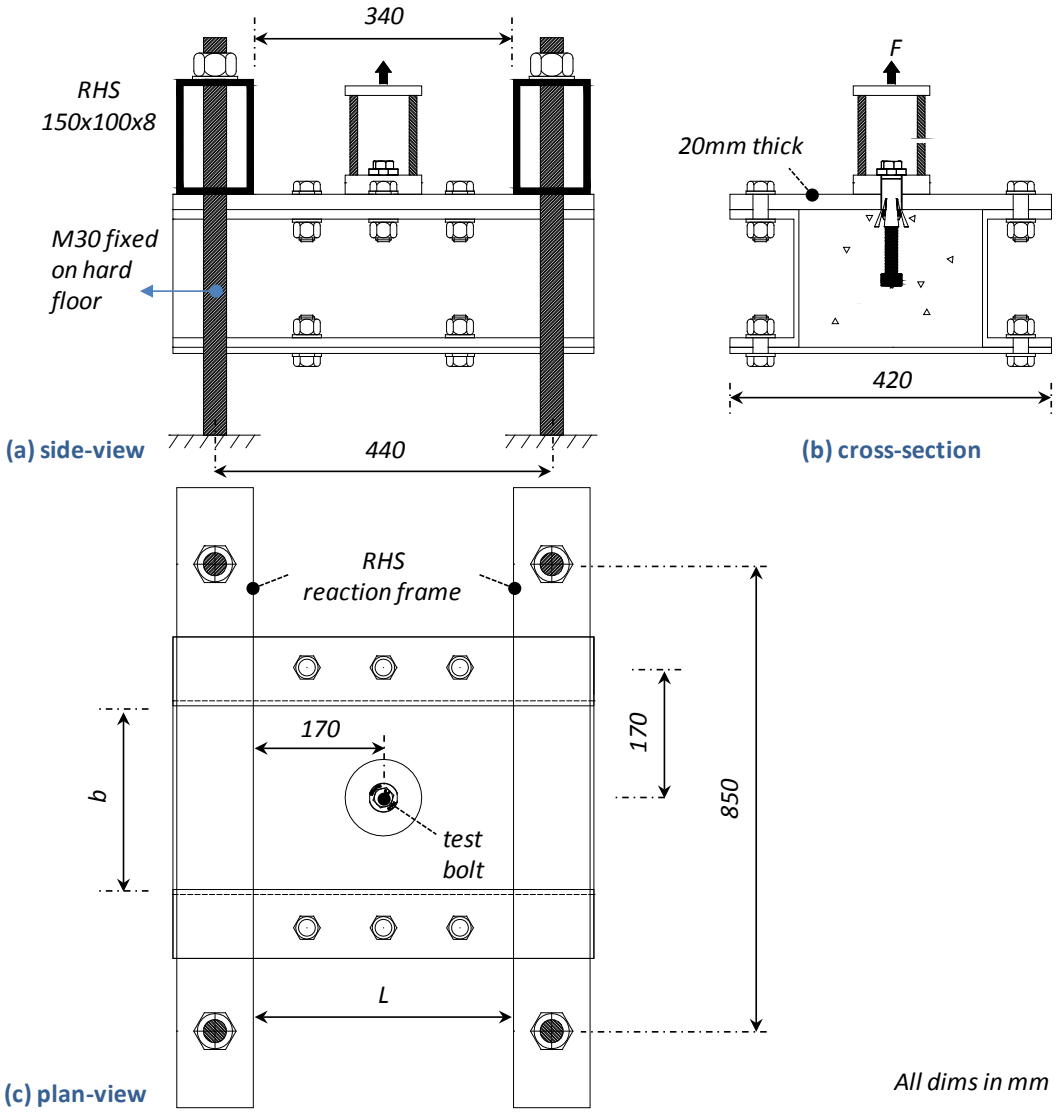

RHS frame Loading:

Maximum anticipated load *F* is uniformly distributed onto the reaction frame.

F_{max} determined by ultimate capacity of shank of test bolt.

Bolt	*Grade 8.8*	*Grade 10.9*	F_{max} *(kN)*
M16	125	163	255
M20	203	255	

Extracted from BS EN ISO 898-1:2009, Table 4 – Ultimate Tensile Loads in kN.

F = Max anticipated tensile load = Max Ultimate strength of the bolt x *FoS* =

= 255 x 1.2 = 306kN therefore *w* (UDL) = *F* / (2 x 0.42) = 364kN/m

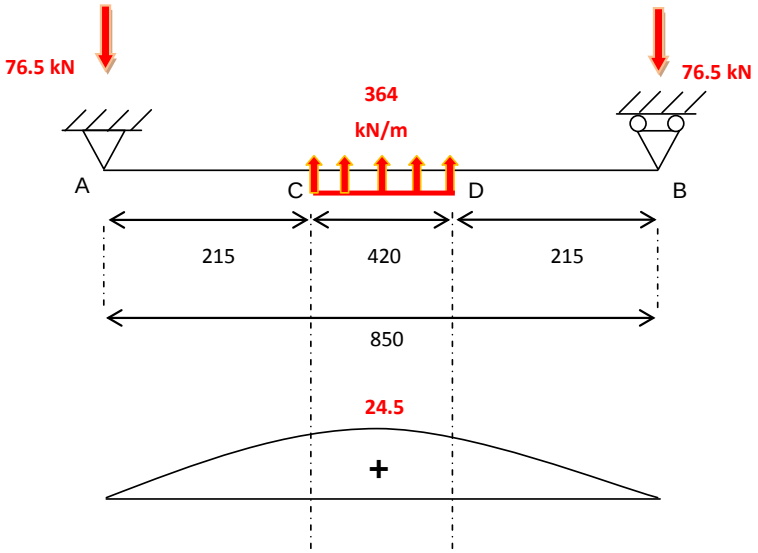

Bending moment diagram (kNm)

$$R_A = R_B = F/4 = 76.5\text{kN}$$

$$M_{max} = (R_A\, L_{AB})/2 - (w\, L_{CD}^2)/8 = (76.5 \times 0.85)/2 - (364 \times 0.42^2)/8 = 28.7\text{kNm}$$

Reaction frame capacity check:

Blue Book: *RHS* section 150x100x8 (S355) is plastic.

Moment capacity = 61.8kNm, Shear Capacity = 470kN Section is adequate

Determine required thickness (*t*) of top plate to remain elastic with minor deflection:

b (in mm)=	340
L (in mm)=	440
P (in kN)=	163
E (in GPa)=	205
f_y (in N/mm^2)=	495

Fixed end beam

δ	t	$PL/8$ M_{max}	$(Mt/2)/I_{xx}$ Bending stress	$I_{xx}/(t/2)$ Elastic modulus	f_y* elastic modulus Elastic moment capacity	
(mm)	(mm)	(kNm)	(N/mm^2)	(mm^3)	(kNm)	Elastic?
1.5	20	9	386	23231	11	YES

Use 20mm thick top plate.

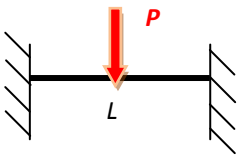

$$\delta_{max} = \frac{PL^3}{192EI} \quad where\ I = \frac{bt^3}{12} \Rightarrow \quad t = \sqrt[3]{\frac{PL^3}{16Eb\delta}}$$

Detailed drawings of rig:

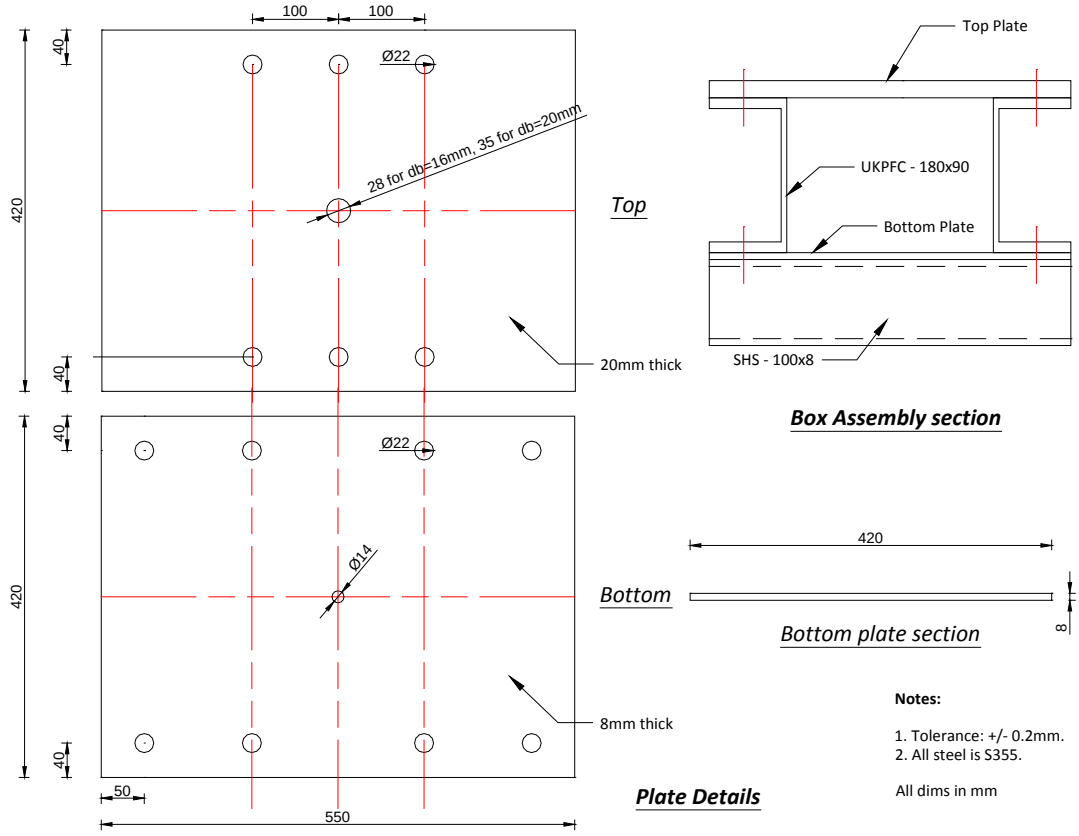

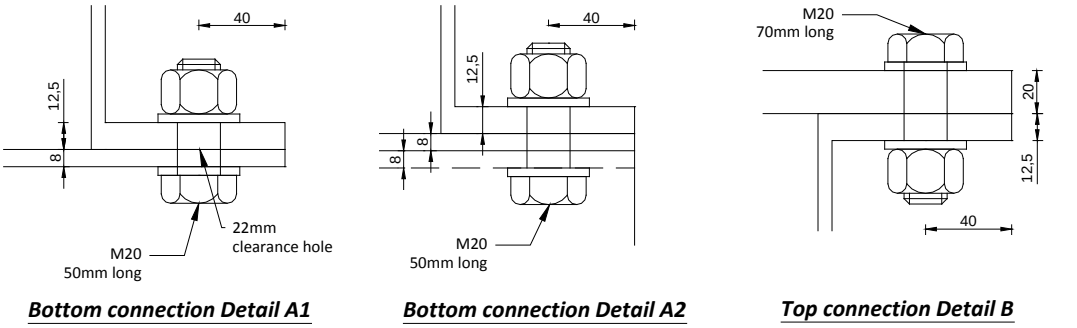

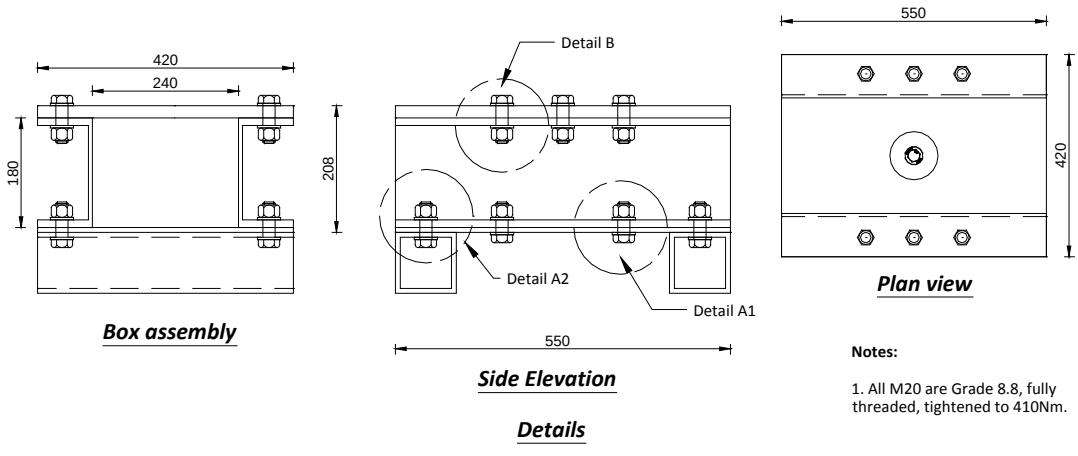

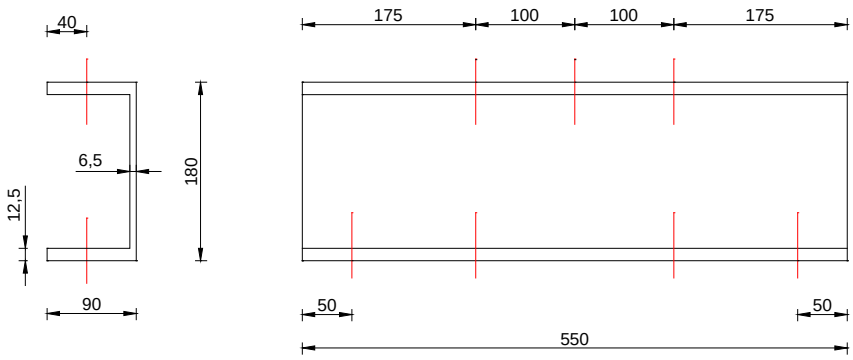

Side elevation

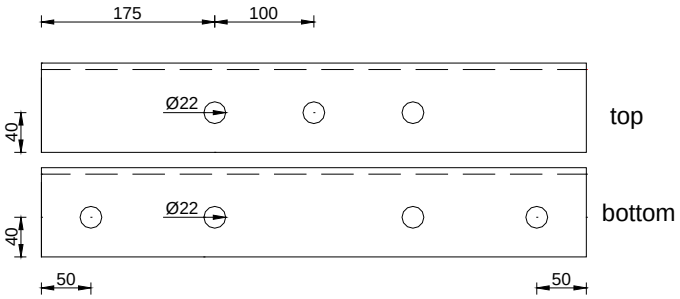

Plan view

Parallel Flange Channel section 180x90

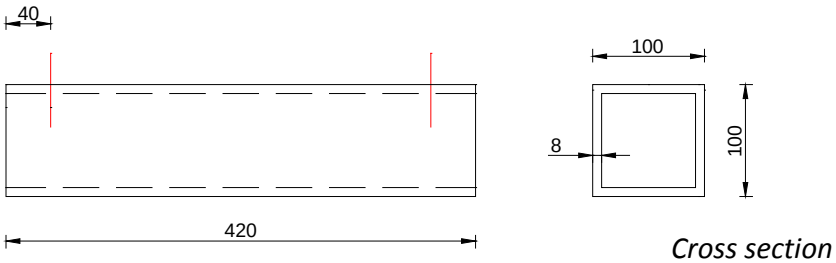

Cross section

Side elevation

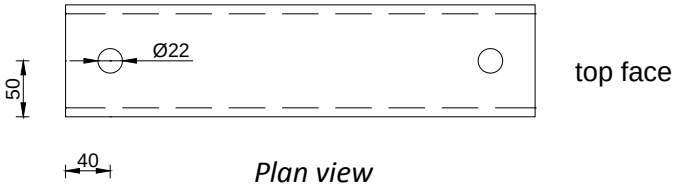

Plan view

SHS 100x8